DEVELOPMENT, CHARACTERISATION AND EVALUATION OF SUGAR GLASS MICRONEEDLES

CHRISTOPHER JOHN MARTIN

A thesis submitted to Cardiff University in accordance with the requirements for the degree of Doctor of Philosophy. Cardiff School of Pharmacy and Pharmaceutical Sciences, May 2012.

Acknowledgements

What a journey this PhD experience has been. It has been one of the most rewarding and, at times, one of the most emotional tasks that I have ever undertaken. To this end I am deeply indebted to my supervisors at the Cardiff School of Pharmacy and Pharmaceutical Sciences, Dr Birchall, Dr Allender and Dr Brain for their continual support and guidance throughout my studies. Their knowledge and advice has been invaluable throughout the entire process and I have gained a tremendous amount from their expertise.

Thanks should also be extended to my industrial sponsor 3M Healthcare Ltd. In particular I would like to thank Dr Toon for his early inspiration on this project and in the securing of funds for the research to proceed. Thanks should also be extended to Dr Hodson for supervising the project following Dr Toon's departure and in particular for his help in acquiring proprietary 3M adhesive products.

I am also extremely grateful to Professor Wess and Dr Kate Thomas from the Cardiff School of Optometry and Vision Sciences for their co-ordination of and assistance with the X-ray diffraction studies conducted in this thesis.

I would like to extend my thanks also to the rest of the Gene Delivery Research Group, Dr Coulman, Dr Pearton, Dr Bains, Miss Torrisi and Miss Chong, with whom I have worked closely with over the last 4 years. Their continual advice, support and friendship have been invaluable throughout the entire experience.

Finally I would like to express my most heartfelt wishes to my family, and in particular to my Mother, for all their love and support throughout my PhD. They have been there for me through the hardest of times and have provided me with the determination to keep going. I would finally like to acknowledge my deepest gratitude to my uncle William for proof reading my entire thesis prior to its final submission.

Publication list

Papers

Martin, C. J. et al. 2012. Low temperature fabrication of biodegradable sugar glass microneedles for transdermal drug delivery applications. *Journal of Controlled Release* 158(1), pp. 93-101.

Conference presentations

Perspectives in Percutaneous Penetration. C. J. Martin[a], C. J. Allender[a], K. R. Brain[a], D. Hodson[b], J. C. Birchall[a]. [a]Welsh School of Pharmacy, Cardiff and [b]3M Healthcare Ltd., Loughborough, UK. (1993) Biodegradable sugar glass microneedles for macromolecular drug delivery.

Conference posters

Gordon Research Conference: Barrier Function of Mammalian Skin. C. J. Martin[a], C. J. Allender[a], K. R. Brain[a], D. Hodson[b], J. C. Birchall[a]. [a]Welsh School of Pharmacy, Cardiff and [b]3M Healthcare Ltd., Loughborough, UK. (2009) Biodegradable sugar glass microneedles: the future of pain-free vaccination.

Research day presentations

Postgraduate Research Day, Cardiff School of Medicine. C. J. Martin[a], C. J. Allender[a], K. R. Brain[a], D.Hodson[b], J. C. Birchall[a]. [a]Welsh School of Pharmacy, Cardiff and [b]3M Healthcare Ltd., Loughborough, UK. (2009) Biodegradable microneedles and sugar glasses.

Postgraduate Research Day, Cardiff School of Pharmacy and Pharmaceutical Sciences. C. J. Martin[1], C. J. Allender[1], K. R. Brain[1], A. Morrissey[3], P. D. Hodson[2] and J. C. Birchall[1]. [1] Welsh School of Pharmacy, Cardiff University, Cardiff, CF10 3NB, UK, [2] 3M Health Care Limited, Loughborough, LE11 1EP, UK, [3] Biomedical Microsystems Team, Tyndall National Institute, Cork, Ireland. (2011) Low temperature fabrication of biodegradable sugar glass microneedles for transdermal drug delivery applications

Abstract

Biodegradable microneedles (MNs) are currently being developed to painlessly facilitate the effective permeation of therapeutic substances across the skin barrier. As sugar glasses are utilised in nature to protect proteins and other delicate structures upon dehydration, such materials may be an appropriate substrate for the preparation of biodegradable MNs. The aim of this work was to investigate for the first time the feasibility of preparing biodegradable MNs from sugar glasses and to test their potential utility for drug delivery applications.

Solid sugar products were fabricated from 32 different solutions containing a range of individual sugars and binary sugar combinations, utilising a low temperature dehydration methodology. Subsequently, a novel vacuum-forming micromoulding methodology was developed and optimised to produce sugar glass microneedle (SGMN) arrays from silicon master structures. The sugar materials and MN structures were characterised using a variety of microscopic, thermal and x-ray diffraction analyses. The ability of SGMNs to puncture human skin was assessed in an *in vitro* skin model, whilst SGMN facilitated drug delivery was investigated using modified static Franz-type diffusion cells. A range of model substances including methylene blue (MB) dye, ibuprofen sodium (IBU), sulforhodamine B (SRB), FITC-BSA and β-galactosidase (β-gal) were incorporated within SGMN arrays. Furthermore, novel SGMN adhesive patches containing SRB within the backing only were fabricated using silicone and acrylate adhesives. Long-term stability of SGMN arrays was assessed under a range of differing storage conditions.

Initial characterisation studies suggested that non-crystalline sugar material was formed from anhydrous trehalose and sucrose (75:25 $\%^{w}/_{w}$) sugar solutions. This finding was critical to future SGMN fabrication and incorporation of model substances within the material. Process optimisation led to fabrication of SGMNs with strong morphological fidelity to master structures, which reliably penetrated human skin to facilitate diffusion of MB dye. Furthermore, SGMNs were shown to dissolve rapidly and completely in human skin and deliver MB, IBU, SRB and FITC-BSA to the deeper skin layers. Diffusion study data suggested that SGMN arrays incorporating a range of model substances facilitated permeation across skin in a bolus delivery manner. Additionally, it was found that SGMN adhesive patches were able to control permeation of SRB, a model hydrophilic compound. Sugar glasses containing β-gal were shown to stabilise enzyme functionality at approximately 40 % of initial activity over a 3 month period when stored under desiccation. Elevated humidity and temperature storage was detrimental to SGMN morphology, with 10 % relative humidity at 20 °C being optimal for MN preservation.

Overall, this study suggests the utility of SGMNs for the stable incorporation and effective intra- or trans-dermal delivery of a range of model substances, including hydrophilic and macromolecular molecules. Furthermore, it was shown that a novel SGMN adhesive patch may provide the capability to control drug release across skin. Sugar glasses demonstrated a stabilising effect upon a functional protein cargo, although it appeared that storage conditions had a strong influence upon physical SGMN stability.

Contents

Contents

Figure list

Abbreviations

5-ALA	5-aminolevulinic acid
AC	Alternating current
ASG	Ascorbate-2-glucoside
AUC	Area under curve
BCA	Bicinchoninic acid
β-gal	Beta-galactosidase enzyme
BIO-PSA	BIO-pressure sensitive adhesive
BMD	Bone mineral density
BSA	Bovine serum albumin
CAL	Calcein
cm	Centimetre
CMC	Carboxymethylcellulose
CPEs	Chemical penetration enhancers
Da	Dalton
DDAVP	Desmopressin
dH_2O	De-ionised water
DNA	Deoxyribonucleic acid
DSC	Differential scanning calorimetry
EPO	Erythropoietin hormone
ER	Electrical resistance
FITC	Fluorescein isothiocyanate
h	Hour
HCl	Hydrochloride
HPLC	High performance liquid chromatography
IBU	Ibuprofen sodium
ID	Intradermal
IM	Intramuscular
K	Kelvin

kDa	Kilodaltons
kΩ	Kiloohm
KFA	Ketoprofen free acid
kHz	Kilohertz
LOD	Limit of detection
LogP	Logarithm of partition coefficient (octanol/water)
µL	Microlitre
µm	Micrometre
m	Month
mA	Milliampere
M	Molar
MAL	Maltose
MAN	Mannitol
MB	Methylene blue
mBar	Millibar
mg	Milligram
$MgCl_2$	Magnesium chloride
Min	Minute
mL	Millilitre
mm	Millimetre
mM	Millimolar
mmol	Millimoles
MN	Microneedle
MV	Molecular volume
MW	Molecular weight
N	Newton
NaCl	Sodium chloride
NaOH	Sodium hydroxide
ng	Nanogram
NH	Nicardipine hydrochloride
NH_4OH	Ammonium hydroxide

nm	Nanometre
ODN	Oligodeoxynucleotide
ONPG	Ortho-nitrophenyl β-D-galactopyranoside
OVA	Ovalbumin
Pa·s	Pascal-second
PB	Sodium phosphate buffer
PBS	Phosphate buffered saline
PDMS	Polydimethylsiloxane
PEG	Polyethylene glycol
PFK	Phosphofructokinase
PGA	Polyglycolic acid
PHCl	Propranolol hydrochloride
PLA	Polylactic acid
PLGA	Poly-lactide-co-glycolide
PSA	Pressure sensitive adhesive
PTFE	Polytetrafluoroethylene
PTH	Parathyroid hormone
PVA	Polyvinyl alcohol
PVP	Polyvinylpyrrolidone
Q	Cumulative amount permeated
rhGH	Recombinant human growth hormone
rPA	Recombinant protective antigen
RH	Relative humidity
RT	Room temperature
SC	Stratum corneum
S.D.	Standard deviation
SDS	Sodium dodecyl sulphate
S.E.	Standard error of mean
sec	Second
SEM	Scanning electron microscopy
SG	Sugar glass

SS	Sodium salicylate
SSA	Soft skin adhesive
SSBMS	Solid state biodegradable microstructures
SGMN	Sugar glass microneedle
SRB	Sulforhodamine B
SUC	Sucrose
TDDS	Transdermal drug delivery system
TEWL	Transepidermal water loss
Tg	Glass transition temperature
TGA	Thermogravimetric analysis
TPTD	Teriparatide
TRA	Anhydrous trehalose
TRD	Trehalose dihydrate
XYL	Xylitol

Chapter 1

General introduction

1 General introduction

1.1 Overview

Drug delivery systems that target specific body sites or provide controlled delivery have long been a goal of pharmaceutical scientists (Langer 1998). Advances in genetic engineering and biotechnology have led to the generation of potent, therapeutically-active, large molecular weight, hydrophilic molecules; many of which are peptides and proteins (Amsden and Goosen 1995). Although oral delivery of these medicaments is desirable, they tend to be extensively degraded in the liver and gastrointestinal tract if given via this route. Hence, there is a need for alternative routes of administration and suitable drug delivery systems (Brown et al. 2006). This study was motivated by the opportunity to investigate delivery of a range of model substances across skin via a novel microneedle patch drug delivery device.

Transdermal drug delivery has emerged as an attractive option to deliver medicaments to the body. Drug release can be easily controlled and systemic delivery via this route bypasses hepatic degradation (Langer 1998). However, as this chapter details, passive transdermal delivery is limited by the extraordinary resistance of human skin to the ingress of exogenous material. In an attempt to overcome the skin barrier, various enhancement techniques have been proposed, which will be discussed herein. One transdermal delivery system in particular, described as a microneedle device, has been the focus of considerable research activity over the past 10 -15 years. Since the first “microneedle patch”, introduced by Henry et al. (Henry et al. 1998), a plethora of microneedle designs and devices have been investigated. Each of these permutations has a number of advantages and limitations which will be explored in this chapter.

Amorphous sugars are utilised in nature (Potts 1994) and the pharmaceutical industry (Uritani et al. 1995) to help preserve the delicate nature of proteins and other labile biological structures during dehydration. This chapter provides an introduction to molecular glasses and their unique properties for macromolecule stabilisation. Subsequently, it was hypothesised that sugar glasses may provide a suitable material for the stable incorporation of a wide variety of molecules including peptides and proteins. A final discussion is provided in this chapter to reiterate the key aspects of this work and to rationalise the investigation of sugar glasses for biodegradable microneedle fabrication.

1.2 Human skin

1.2.1 Biological function

The integument of the human body, the skin barrier, is one of the most vital organs in determining survival. Although it appears relatively basic and homogenous, human skin is extremely complex and provides many different functions. The primary role of the skin is a physical barrier to protect the delicate internal portion of the body from its surroundings (Barry 1983). This barrier prevents the introduction of foreign substances into the body whilst preventing excessive loss of important endogenous materials, such as water (Brown et al. 2006). The protective or barrier function protects the body from a diverse range of potentially harmful external stimuli including micro-organisms, chemicals, electrical or mechanical shock, radiation and heat. Additionally, the skin serves a mechanical function to contain body fluids and therefore it is involved in the regulation of body temperature by controlling water loss through sweating. The skin is also an important site of synthesis and metabolism of compounds, such as vitamin D, an important factor in calcium regulation. Previtamin D3 is formed by photosynthesis of a cholesterol precursor in skin in the presence of sunlight (MacLaughlin et al. 1982). Subcutaneous adipose tissue is vital to the protection of internal organs from mechanical injury and also serves as an energy store for processes such as heat production (Cinti 2005). Other functions of the skin include sensation of potentially harmful external stimuli via skin receptors, including tactile (pressure), pain and heat, and the disposal of chemical wastes, such as urea, via glandular secretions (Barry 1983).

1.2.2 Structure and anatomy

Human skin covers a surface area of approximately 1.8 m^2 and constitutes 16 % of body weight (Gawkrodger 2008) making it the heaviest single organ of the body. It combines with the mucosal linings of the respiratory, digestive, and urogenital tracts to form a capsule which separates the internal body structures from the external environment (Barry 1983). To provide the functions described above, human skin comprises three distinct layers. The outer layer, termed the cellular epidermis, consists of cells which are biochemically active, stratified and avascular (Kermici et al. 1977). Beneath the epidermis lies the dermis, mainly comprised of connective tissue, and at the base of the dermis lies the fatty, subcutaneous layer (Barry 1983), Figure 1.1.

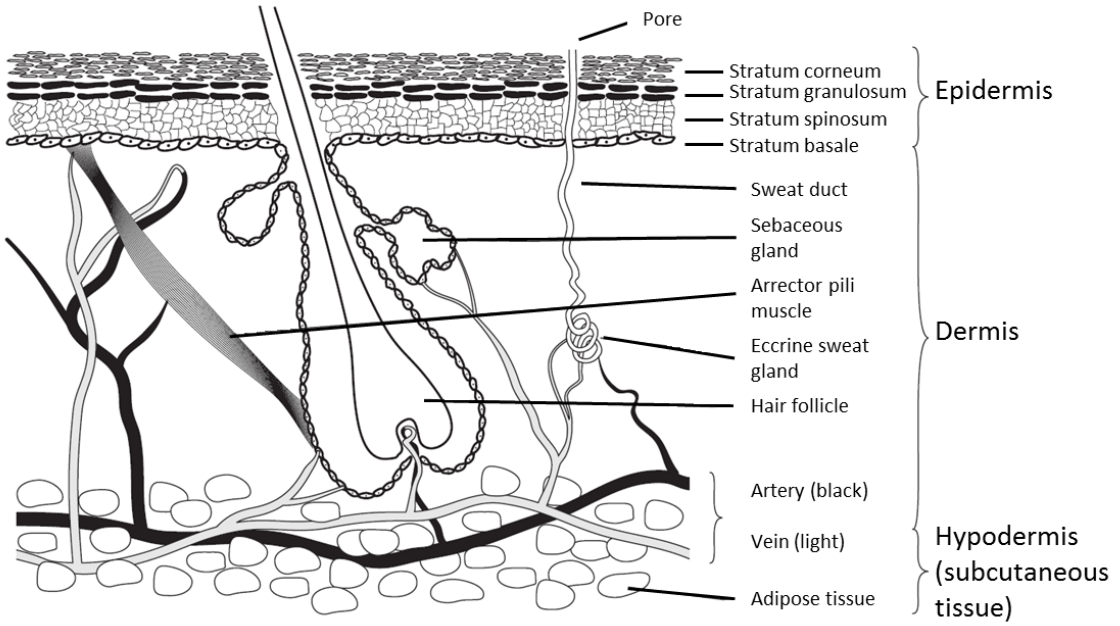

Figure 1.1 Diagrammatic cross section of human skin demonstrating layered assembly.

Adapted from source (Williams 2003).

Each of the layers in Figure 1.1 has a different role to play in skin function and hence the structure varies widely throughout the tissue. In the context of this work, skin is regarded as a barrier to cutaneous drug delivery and will be discussed in these terms. The composite structure of the skin permeability barrier is indicated by discrete skin layers; the stratum corneum (approximately 10 µm), the viable epidermis (approximately 100 µm), and the papillary dermis (approximately 100-200 µm) (Scheuplein and Blank 1971).

1.2.2.1 Epidermis

The epidermis is defined as a stratified squamous epithelium (Gawkrodger 2008). It forms a multi-layered envelope that varies in thickness, depending upon anatomical location, ranging from about 0.8 mm on the palms and the soles down to 0.06 mm on the eyelids. Cells which provide epithelial tissue, keratinocytes, differ from those of all other organs in that as they ascend from the proliferative layer of basal cells they change in an ordered fashion from metabolically active dividing cells to dense, dead, keratinized protein (Barry 1983). The epidermis is therefore further divided into several layers or strata starting with the basal layer or stratum basale just above the dermis proceeding upward through the spinous and the granular layers to the top layer, the stratum corneum (SC) (Wickett and Visscher 2006). These

four layers therefore represent the various stages of maturation of keratin by keratinocytes (Gawkrodger 2008). The process can be seen in Figure 1.2.

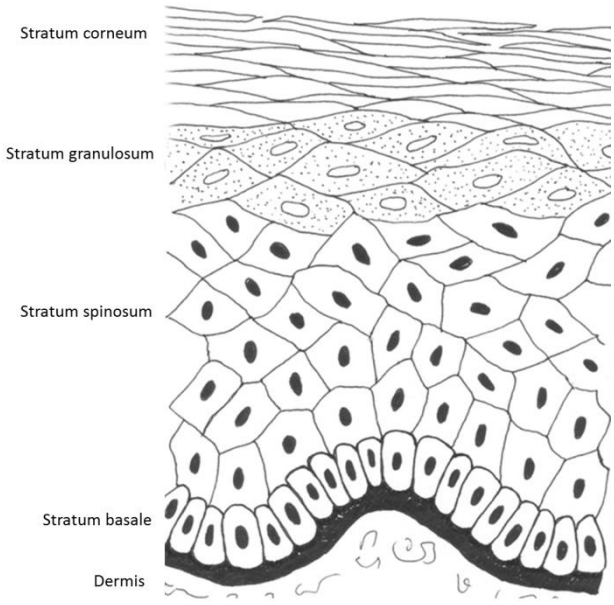

Figure 1.2 Diagrammatic representation of the epidermis showing discrete layers.

Adapted from source (Wickett and Visscher 2006).

1.2.2.2 Stratum corneum

The cells of the SC represent the terminal point in keratinocyte differentiation (Eckert 1989). This layer is formed and continuously replenished by the slow upward migration of cells from the germinative basal layer of the epidermis to the SC. This complex process includes gross dehydration and polymerisation of the intracellular material, resulting finally in keratin filled, biologically inactive, shrunken cells (Scheuplein and Blank 1971). During the transition keratinocytes lose approximately 70 % of dry weight and become flattened. Hence, the terminal corneocyte is a flattened polyhedron with a hardened and thickened cell envelope containing involucrin (Eckert 1989), and cytoplasm replaced by keratin tonofibrils in a matrix formed from keratohyalin granules (Gawkrodger 2008). Corneocytes of the SC are uniquely adapted to providing a protective barrier for the human body, before they are eventually sloughed from the skin surface (Eckert 1989) during desquamation.

During the transitional process, a change in the physical state of the tissue and a commensurate change in its diffusivity occur. A transformation occurs from an aqueous fluid medium, containing approximately 70 % water (Anderson and Cassidy 1973), characterised

approximately by liquid-state diffusion, to a dry semisolid "keratin" membrane which is characterised by a much lower fibre-type diffusivity (Scheuplein and Blank 1971). When dry, the SC is a very dense tissue, about 1.5 g cm^{-3} (Barry 1983), and provides for the mechanical strength of the epidermis through its multicellular anatomy and the overlap of adjacent cells (Scheuplein and Blank 1971).

Hence, this extremely thin layer is the ultimate stage in the epidermal differentiation process (Naik et al. 2000), forming a laminate of compressed keratin-filled corneocytes (terminally differentiated keratinocytes) anchored in a lipophilic matrix (Christophers 1971; Elias 1981; Elias 1983). Consequently, the SC is a heterogeneous membrane consisting of approximately 20 % lipids, 40 % keratinised protein and 15 – 20 % water (Anderson and Cassidy 1973). The lipids of this extracellular matrix are partly derived from membrane-coating granules (Gawkrodger 2008) and are distinctive in many respects (Gray et al. 1982). Firstly, they provide the only continuous phase (and diffusion pathway) from the skin surface to the base of the SC. Their composition (comprising ceramides, free fatty acids and cholesterol) is unique among biomembranes and particularly noteworthy is the absence of phospholipids. However, despite a deficit of polar bilayer-forming lipids, the SC lipids exist as multilamellar sheets and the predominantly saturated, long-chain hydrocarbon tails facilitate a highly ordered, interdigitated configuration. This arrangement of lipids allows formation of gel-phase membrane domains as opposed to the more usual (and more fluid and permeable) liquid crystalline membrane systems (Naik et al. 2000).

The SC architecture as a whole has been proposed to play a critical role in the barrier function of the epidermis (Potts and Francoeur 1991). The staggered corneocyte arrangement in a lipid continuum (similar to a brick and mortar assembly) (Elias 1981) is suggested to bestow a highly tortuous lipoidal diffusion pathway rendering the membrane 1000-times less permeable to water relative to most other biomembranes (Potts and Francoeur 1991). Due to its highly specialised structure, the SC is known to exhibit selective permeability and allows only relatively lipophilic compounds to diffuse into the lower layers of skin (Brown et al. 2006).

1.2.2.3 Stratum granulosum

As Figure 1.2 shows, below the SC lies the stratum granulosum. The cells in this layer contain electron-dense keratohyalin granules, to which the stratum granulosum owes its name (Eckert

1989). These granules contain profilaggrin, the high-molecular-mass precursor of the protein filaggrin, which is thought to aid in aggregation of keratin filaments (Dale et al. 1985). Also present are the lipid-filled lamellar (membrane coating) granules that eventually fuse with the plasma membrane and release their lipid contents into the extracellular space (Elias et al. 1988). This layer is often referred to as a "transitional zone" as the stratum granulosum defines a region between living cells and dead keratin (Barry 1983).

1.2.2.4 Stratum spinosum

Immediately above the basal layer is the stratum spinosum. This layer is named due to the spine-like appearance of the cell borders in histological section, which are caused by the presence of numerous desmosomes formed between adjacent cells (Obland 1958). Desmosomes are intercellular bridges that form through adherence of adjacent cytoplasmic extensions known as spines or "prickles." These links maintain the integrity of the epidermis whilst tissue fluid fills the capillary space between desmosomes to separate neighbouring cells and permit nutrients and oxygen to pass outwards (Barry 1983).

1.2.2.5 Stratum basale

The stem cell population of keratinocytes is found attached to the basal lamina, which separates the dermal layer from the epidermis (Eckert 1989). These undifferentiated cells lack the obvious biochemical and morphological markers that are expressed by cells in the upper epidermal layers. Typically stem cells are columnar and replete with keratin filaments around the nucleus. Junctions between adjacent cells, described as desmosomes, and hemidesmosomes (junctions between basal cell and basal lamina) (Eckert 1989) can be observed. Mitosis of the basal cells constantly renews the epidermis and this proliferation in healthy skin balances the loss of dead horny cells from the skin surface. The epidermis thus remains relatively constant in thickness (Eckert 1989).

Other cell types found within the basal layer include melanocytes, *Merkel* cells and dendritic cells. Melanocytes are most numerous on the face and other exposed sites and make up 5 - 10 % of the basal cell population. These cells synthesize melanin and transfer it via dendritic processes to neighbouring keratinocytes. *Merkel cells* are found infrequently in the basal layer and are closely associated with terminal filaments of cutaneous nerves, appearing to have a role in sensation (Gawkrodger 2008). The most important antigen-presenting cell of the

epidermis, formed from a dendritic cell lineage, is the Langerhans cell. These cells are vital to the immune function of the skin as they engulf exogenous material, process it into immunogenic peptides, and present it to T lymphocytes (Williams and Kupper 1996). Whilst these cells normally reside within the epidermis, upon activation during an inflammatory response, they can mobilise and migrate to the lymphatic system of the dermis and travel to regional lymph nodes (Kripke et al. 1990) to bring about a systemic immune response.

Below the basal cell layer lies the complex dermo-epidermal junction, which constitutes an anatomic functional unit (Briggaman and Wheeler 1975). The junction spans four components: (1) the basal cell plasma membrane with its specialised attachment devices, the hemidesmosomes, (2) the lamina lucida, (3) the basal lamina, and (4) the fibrous components below the basal lamina, which include anchoring fibrils, dermal microfibril bundles, and collagen fibrils. The "basement membrane" corresponds to the fibrous zone below the basal lamina (Barry 1983).

1.2.2.6 Dermis

The dermis is a tough supportive connective tissue matrix found immediately below and intimately connected with the epidermis (Gawkrodger 2008). It can be divided into two layers, the reticular (lower) and the papillary (upper) layer. The papillary layer is approximately 100-200 µm in thickness and is attached to the basal lamina (Scheuplein and Blank 1971). The dermis is typically 3-5 mm thick and hence makes up the bulk of the skin (Barry 1983). It is essentially an aqueous medium composed of a matrix of connective tissue woven from fibrous proteins (approximate composition, collagen 75 %, elastin 4 % and reticulin 0.4 %) which embed in an amorphous ground substance of mucopolysaccharide providing about 20 % of the mass (Wilkes et al. 1973). The ground substance contains a variety of lipid, protein and carbohydrate materials, with the most important being the mucopolysaccharides hyaluronic acid and dermatan sulphate (chondroitin sulphate B) (Barry 1983). Collagen and elastin fibres found throughout the dermis provide strength and elasticity to the tissue (Gawkrodger 2008). The dermal matrix supports blood vessels, nerves and lymphatics and is penetrated by skin appendages including sweat glands, apocrine glands and pilosebaceous units (Barry 1983). Sweat glands and hair follicles which extend from the dermis have been described as "shunt" pathways for transdermal drug delivery. However, these routes account for less than 0.1 % of the total surface area for passive diffusion and hence their contribution to drug delivery is negligible (Scheuplein and Blank 1971). Therefore, the barrier function of human skin is widely

thought to be a function of the SC, although it has been found that the aqueous tissues of the viable epidermis and dermis provide a residual resistance to drug transport (Potts and Guy 1992).

1.2.2.7 Hypodermis (subcutis)

The hypodermis consists of subcutaneous fat that spreads all over the majority of the body as a fibro-fatty layer. The cells manufacture and store lipids in large quantities and bundles of collagen fibres weave between the cells to provide flexible linkages between underlying structures and superficial skin layers. The subcutis provides a thermal barrier and a mechanical cushion and is a high energy depot (Barry 1983).

1.2.3 Factors governing percutaneous absorption

There is now a body of evidence which informs passive diffusion of medicaments across human skin. Permeation of small hydrophilic molecules is governed by the rate of partition into the lipid lamellae of the SC. Conversely, small hydrophobic molecules are rate controlled by partition from the SC into the aqueous environment of the viable epidermis (Brown and Langer 1988). Additionally, permeation of drugs decreases with increasing molecular size, and 500 Da is widely considered as the upper limit for passive diffusion (Brown et al. 2006). Further, because the SC is composed of metabolically inactive cells, no active transport mechanisms exist in this layer and therefore passive diffusion dictates the rate of permeation in conventional cutaneous delivery systems (Scheuplein and Blank 1971). Therefore, as equation 1 shows, drug absorption from passive transdermal systems can be described by simple diffusion mathematics (Hadgraft and Lane 2006).

$$J = \frac{KD\,(c_{app} - c_{rec})}{h} \qquad \text{(Equation 1)}$$

The rate of permeation across SC follows Fick's first law of diffusion (Flynn et al. 1974) which describes steady-state flux per unit area (J) in terms of the partition of the permeant between the applied formulation and the skin (K), its diffusion coefficient (D) in the lipid lamellae of diffusional path length (h), the applied concentration of the permeant in the vehicle (c_{app}), and the concentration of the permeant in the body, or in the case of an *in vitro* study, receptor phase (c_{rec}) (Hadgraft and Lane 2006). The partition coefficient (K) is a measure of the willingness of a permeant to leave its vehicle and partition into the SC.

Operationally, K is defined as the octanol / water partition coefficent (K_{oct}), or its logarithm, log P (Williams 2003). The greater the log P, the more lipophilic the molecule and the more readily it will partition into the SC lipids. K, D and h can be represented together as the permeability coefficient (K_p), as shown in equation 2.

$$K_p = \frac{P\,D}{h} \qquad \text{(Equation 2)}$$

Furthermore, an empirical relationship exists between K_p and molecular weight (MW) and log P as shown in equation 3 (Potts and Guy 1992).

$$\log K_p \text{ (cm sec}^{-1}) = -6.3 + 0.71 \cdot \log K_{oct} - 0.0061 \cdot MW \qquad \text{(Equation 3)}$$

From equation 3 it can be deduced that log K_p decreases with increasing MW, which generally correlates with increasing molecular volume (MV). The relationship between the D and MV is exponential (Potts and Guy 1992) and therefore it can be argued that MW decreases K_p by decreasing D and hence that permeation of larger molecules is restricted by their larger size.

In most *in vitro* transdermal diffusion studies, c_{rec} is much smaller than c_{app} and equation 1 is simplified to equation 4.

$$J = K_p\, c_{app} \qquad \text{(Equation 4)}$$

Hence, the maximum flux of a compound is achieved when c_{app} is equal to the solubility limit of drug in the applied formulation (Hadgraft and Lane 2006). Additionally, it has been shown that relatively simple processes, such as skin occlusion, lead to elevated hydration of the SC thereby facilitating permeation of model compounds including steroids (Wester and Maibach 1983). A similar effect can be achieved by physical disruption of the SC barrier, for example by adhesive tape stripping, which has been shown to increase passive transdermal drug delivery (Scheuplein 1976). Therefore, if the barrier properties of the SC are efficiently attenuated delivery of a wide range of drug molecules is theoretically feasible.

1.3 Cutaneous drug delivery

1.3.1 Scope of drug delivery approach

As discussed previously, the delivery of hydrophilic and larger MW molecules across the SC barrier is extremely limited. Consequently, a wide variety of different techniques aimed at enhancing the permeation of these substances across skin have been developed. The advent of biotechnology in the latter half of the 20th century has led to the generation of therapeutically-active, large MW (>500 Da) polar and hydrophilic molecules. Most of these macromolecules are peptides and proteins, but they also include nucleic acids, vaccines, hormones and antibodies (Brown et al. 2006). This class of materials tends to be extensively degraded by enzymes in the liver and gastrointestinal tract if given by oral delivery; hence, there is a need for alternative routes of administration and suitable drug delivery systems (Brown et al. 2006). Cutaneous delivery of these drug molecules presents a potentially attractive alternative delivery route.

1.3.2 Advantages and limitations of cutaneous delivery

For the majority of drugs the conventional route of drug delivery is via the oral route. This route of delivery is desirable as a wide range of medicaments can be formulated into tablets and capsules, it is convenient, it is easy to use, cost-effective, pain free and requires no specialist training to administer (Park et al. 2005). However, drug administration via the oral route can result in variable systemic levels of the active form of the drug, both within and among individuals, as a result of the variable absorption or release of drug from the formulation, differences in food intake, or initial entry of drug into the portal circulation (Shaw et al. 1976). In addition, degradation and metabolism in gastrointestinal fluids, which have extremely low pH (≈2), and hepatic first-pass elimination via enzymatic metabolism and biliary excretion (Benet et al. 1996) can limit oral drug delivery.

Orally inactivated molecules and macromolecules, such as proteins, are usually administered by hypodermic injection, which avoids the gastrointestinal tract but causes pain, requires medical expertise to administer (Davis et al. 2004), and introduces the risk of infection. Both oral and hypodermic routes of delivery also have added limitations as bolus delivery methods, where the full dose of drug is introduced into the body at once. To prevent irritating and potentially toxic effects of initial high doses and sub-therapeutic effects as drug concentration decays at later times, tablets and injections often need to be administered multiple times per

day or, in some cases, prolonged-release formulations can be used (Park et al. 2005). Consequently, the potential exists for developing a minimally invasive, self-administered delivery system capable of delivering a range of drug molecules, including biologically active macromolecules (Sullivan et al. 2008), where oral bioavailability is low.

Transdermal drug delivery offers the potential to address many of the aforementioned issues. Transdermal patches can be formulated to provide controlled release of the medicament across skin whilst there is an extensive underlying capillary network available for systemic drug delivery. This route of delivery also bypasses the liver and gastrointestinal tract and hence does not degrade macromolecules delivered in this manner (Bronaugh and Maibach 1999; Prausnitz 2001). However, delivery across intact skin at therapeutic rates permits transport of a very limited number of small, quite lipophilic molecules only and excludes transport of biotherapeutics, due to their large size (Sullivan et al. 2008). Proteins, in particular, being hydrophilic macromolecules, do not passively permeate across skin, and hence permeation enhancement strategies are needed to enable delivery into and across the barrier (Li et al. 2008).

The challenge of cutaneous drug delivery therefore is to formulate a device containing a hydrophilic or biological therapeutic medicament into a stable, patient acceptable form which provides controlled delivery across skin at therapeutically relevant rates.

1.4 Traditional and novel cutaneous drug delivery methods

Transdermal delivery is a term that should be restricted to the situation in which a solute diffuses through the skin and into the systemic circulation to exert a therapeutic effect. In contrast, dermal or topical delivery should only be used to define drug targeting to pathological sites within the skin, thereby ensuring minimal systemic absorption (Brown et al. 2006). To achieve these goals a number of permeation enhancement techniques have been investigated to facilitate skin drug delivery.

1.4.1 Passive methods

Passive methodologies of cutaneous drug delivery include conventional means of applying drugs to skin such as ointments, creams, gels, and "passive" patch technologies. These dosage forms have been developed and/or modified to enhance the driving force of drug diffusion (thermodynamic activity) and/or increase the permeability of the skin (Brown et al. 2006). Examples are discussed below.

1.4.1.1 Chemical penetration enhancers

Chemical penetration enhancers (CPEs) may act by one or more of three main mechanisms (Barry 1983):

1. Disruption of the highly ordered structure of SC lipid.
2. Interaction with intercellular protein.
3. Improved partitioning of the drug, co-enhancer or solvent into the SC.

Classes of penetration enhancer include, anionic surfactants, cationic surfactants, zwitterionic surfactants, non-ionic surfactants, fatty acids, fatty esters, fatty amines, azone-like compounds and sodium salts of fatty acids (Karande et al. 2005). Each enhancer acts by altering one of the three main pathways described. The key to altering the polar pathway is to cause protein conformational change or solvent swelling, whilst the fatty acid enhancers increase the fluidity of the lipid protein portion of the SC (Pathan and Setty 2009). Some enhancers act on both polar and non-polar pathways by altering the multilaminate pathway for penetration (Pathan and Setty 2009). Penetration enhancers have demonstrated efficacy in increasing systemic drug delivery both *in vitro* and *in vivo*, for example, caffeine serum concentration in rats was many times greater when Transcutol® and oleic acid were present in the topical formulation compared to an aqueous solution alone (Touitou et al. 1994).

The major drawback of CPEs is that they can be irritating to skin, and this behaviour is related to the ratio of hydrogen bonding to polar interactions. Hydrogen bonds are of significant importance in holding the proteins in their native structures and competitive bonding from CPEs can potentially alter the native hydrogen bonding in proteins leading to unfolding. Consequently, irritation potential scales directly with hydrogen bonding ability of CPEs (Karande et al. 2005).

1.4.1.2 Supersaturated systems

This technique is an attractive option as it provides the potential for enhanced penetration of drug without disturbing the lipids of the SC. Instead it relies on raising the activity of a substance within its formulation beyond that of its solubility limit (Pellett et al. 1997). For example, it has been shown that the flux of piroxicam increases linearly with the degree of saturation within a single vehicle (Pellett et al. 1994). However, due to the nature of these systems they are inherently unstable and in many instances the drug tends to crystallise out of solution (Pellett et al. 1997).

1.4.1.3 Prodrugs / metabolic approach

The use of prodrugs to facilitate transdermal drug delivery involves direct covalent bonding of a lipophilic moiety to a hydrophilic permeant via conjugation to primary and secondary amines, hydroxyls, and other functional groups of the drug to form a prodrug (Bundgaard 1992). Numerous examples are now available demonstrating enhanced delivery of hydrophilic compounds across skin due to attachment of lipophilic groups. The lipophilic groups improve partitioning of the parent compound into the SC lipids and are then cleaved *in vivo* by enzymes within the epidermis to render the drug free and active (Amsden and Goosen 1995). Specific examples include small molecules, such as 5-fluorouracil (Sasaki et al. 1990), and also certain macromolecules, for example thyrotropin-releasing hormone (Møss and Bundgaard 1990), where significantly greater permeation of prodrug was observed in comparison to the parent molecule alone. Furthermore, the lipophilic pro-moiety can preserve the functionality of the parent compound within the bloodstream prior to the drug reaching its therapeutic site of action (Møss and Bundgaard 1990). Drawbacks to this approach include limitations on molecular size, and variable enzymatic cleavage from patient to patient resulting in irreproducible bioavailability (Amsden and Goosen 1995).

1.4.1.4 Liposomes and other vesicles

Liposomes are colloidal particles, typically consisting of phospholipids and cholesterol. These lipid molecules form concentric bimolecular layers that may entrap and deliver drugs to the skin (Barry 2001). Research efforts into liposomes initially focused on their use as drug carriers to target particular organs within biological organisms (Fendler and Romero 1977; Weinstein et al. 1979). Liposomes were subsequently applied to topical drug administration (Mezei and Gulasekharam 1980). Early reports concluded that the liposomal "capsule" was able to penetrate and cross biological membranes with some selectivity (Mezei and Gulasekharam 1980); however this was later shown not to be the case in intact skin (Schreier and Bouwstra 1994; Touitou et al. 1994). Most reports cite a localising effect whereby the vesicles accumulated drugs in the SC or upper skin layers (Mezei and Gulasekharam 1980; Touitou et al. 1994). This effect is not entirely redundant however, as these systems may be used to build up a drug reservoir within the skin.

1.4.2 Active methods

To overcome the extraordinary barrier of the SC, several attempts have been made recently to develop novel strategies for delivering drugs across skin (Al-Qallaf and Das 2008). Passive methods of skin delivery have shown a number of limitations and in particular permeation enhancement is only demonstrated for solutes with a MW of approximately 500 Da (Bos and Meinardi 2000). This excludes many of the new large MW biopharmaceuticals, including peptides and proteins (Brown et al. 2006). This has led to the development of alternative active techniques. These methods of enhancement involve the use of an external energy source to act as a driving force and/or reduce the barrier nature of SC (Brown et al. 2006).

1.4.2.1 Iontophoresis

Iontophoresis involves the application of a low level electric current either directly to the skin or indirectly via the dosage form to enhance permeation of the topically applied therapeutic agent (Wang et al. 1993). A small electrical current (usually <500 microamperes cm^{-2}) is utilised to facilitate the transfer of charged drugs across skin. Charged species are repelled into and through the skin as a result of an electrical potential across the membrane; the efficiency of this process is dependent on the polarity, valency and ionic mobility of the permeant as well as on the composition of the delivery formulation and the current profile. Typically, two electrolyte chambers containing electrodes (one of which contains the ionised

therapeutic molecule of similar polarity, i.e. cationic drug in anodal chamber) are placed on the skin surface and driven by a constant current source. The magnitude of current determines the amount of charge generated in the circuit and, in turn, the number of ions transported across the skin. This method ensures a controlled and efficient form of drug delivery as the amount of compound delivered is directly proportional to the quantity of charge passed (Naik et al. 2000). Increase in drug permeation can be attributed to either one or a combination of the following mechanisms; electrorepulsion (for charged solutes), electroosmosis (for uncharged solutes) and electropertubation (for both charged and uncharged) (Brown et al. 2006). Iontophoretic systems have been approved mainly for administering drugs into the body for medical purposes and specialised uses such as diagnosis of medical conditions (e.g., cystic fibrosis) and glucose monitoring (Brown et al. 2006). In respect to therapeutic macromolecules however, delivery by iontophoresis may be limited to proteins with a maximum MW of 10 - 15 kDa (Li et al. 2008). These devices must also be designed to enhance patient compliance by utilising a patient-friendly, portable and efficient iontophoretic system (Brown et al. 2006). Further, potential drawbacks to the technology have been noted. For example, application of clinically acceptable currents, currently set at 0.5 mA cm^{-2} (Brown et al. 2008), have been shown to decrease skin electrical resistance possibly due to cell damage which is not fully reversible (Burnette and Ongpipattanakul 1988).

1.4.2.2 Electroporation

Electroporation involves the application of high voltage pulses to induce skin perturbation (Brown et al. 2006). It has been proposed that transient pores are generated during electroporation, which may account for the increase in skin permeability (Weaver et al. 1999). High voltages, typically greater than 100 volts, and short treatment durations (milliseconds) are most frequently employed in this technique. Other electrical parameters that affect delivery include pulse properties such as waveform, rate, and number (Banga et al. 1999). The technology has been used successfully to enhance the skin permeability of molecules with differing lipophilicity and size. Model compounds delivered have ranged from relatively small molecules, such as calcein (CAL) (Prausnitz et al. 1993), to macromolecules with a MW up to 40 kDa (Guy et al. 1987). Enhanced delivery of naked DNA to the skin has been achieved *in vivo* in a hairless mouse model, with a 100 - fold stimulation of gene expression compared to that obtained by intradermal injection (Zhang et al. 2002). However, *in vivo* studies have demonstrated adverse effects of the technique including erythema and oedema (Prausnitz et al. 1993) and stimulation of muscle contraction (Escobar-Chavez et al. 2009) which bring into question the long-term utility of the methodology.

1.4.2.3 Abrasion

Abrasion techniques involve the direct removal or disruption of the upper layers of the skin to facilitate the permeation of topically applied medicaments. The delivery potential of skin abrasion techniques are not restricted by the physicochemical properties of the drug (Brown et al. 2006) as the SC barrier is negated. Previous work has illustrated that such methods enhance and control the delivery of hydrophilic permeants, for example vitamin C (Lee et al. 2003), vaccines and biopharmaceuticals (Mikszta et al. 2002; Mikszta et al. 2003).

1.4.2.4 Ultrasound

Ultrasound is defined as any sound having a frequency greater than 16 kHz. Passage of these waves through skin causes compression and expansion of water resulting in pressure variations. Such variations can cause cavitation, fluid flow, mixing (which reduces the boundary layer thickness) and temperature elevation (Kost 1993). For ultrasound drug delivery to be successful, the waves must act on the SC to facilitate the permeation of macromolecular substances (Amsden and Goosen 1995). It has been found that a water-soluble tracer was located within the hydrophilic portion of the lipid lamellae of the SC following ultrasound treatment (Bommannan et al. 1992a). This suggests that the ultrasound facilitated pathway for water-soluble drugs is therefore via the extracellular route, although delivery via hair follicles and sweat ducts may also be important (Amsden and Goosen 1995). Ultrasound has been shown to increase permeation of a range of model medicaments including small MW salicylic acid (Bommannan et al. 1992b) and macromolecular insulin (Tachibana and Tachibana 1991). However, again questions have arisen over the safety and reversibility of ultrasound delivery as it has been shown that high energy depositions over prolonged periods alter epidermal morphology (Bommannan et al. 1992a). Further, due to the nature of the technique, collapse cavitation may occur as the ultrasonic intensity increases which can be damaging to cells and vesicles (May and Allen 2002). Subsequently, this process leads to an intensity and exposure time dependent increase in body tissue temperature (Lavon and Kost 2004); constituting a further risk factor.

Numerous other methodologies have been explored to circumvent the human skin barrier. These include magnetophoresis (Murthy 1999), needless injection, which involves firing of drug particles across skin at supersonic speeds (Longbridge et al. 1998), laser treatment (Lee et al. 2003) and radio frequency thermal ablation (Sintov et al. 2003). Workers have also examined combinations of active enhancement methods, for example iontophoresis and

microporation (Badkar and Banga 2002), and have shown that these approaches can be much more effective than either technique used alone (Brown et al. 2006). However, it is apparent that each of these techniques suffers from limitations and to date there is not one fully optimised system for enhancing cutaneous drug delivery.

1.5 Microfabricated microneedles

1.5.1 Definition

The concept of a microneedle (MN) array was first proposed by Gerstel and Place in the 1970s (Gerstel and Place 1976). Microneedles are perceived as a novel, hybrid cutaneous delivery approach aimed at achieving the delivery efficacy of hypodermic injections and the safety and patient compliance of the transdermal patch (Sullivan et al. 2008). Microneedles have significant advantages over other enhancement strategies as they form microconduits, or channels, across the SC, see Figure 1.3. Furthermore, they do not rely on application of a sophisticated external energy source or chemical manipulation to disrupt the skin barrier.

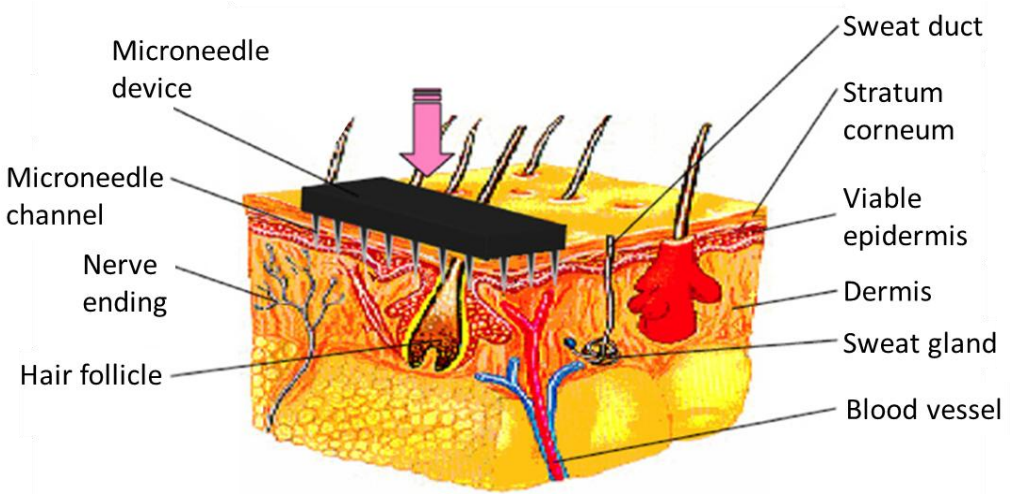

Figure 1.3 Schematic view of human skin and microneedle array.

Adapted from source (Lv et al. 2006).

The sharp tips and short length of MNs reduce the probability of encountering a nerve, and hence they provide a minimally invasive means to transport molecules with various physical and chemical properties into the intradermal layer of skin (Wu et al. 2008). Theoretically, delivering drug just under the SC causes no pain since the nerve endings appear deeper within the skin, Figure 1.3. Furthermore, it is very effective for drug delivery as the presence of a large number of capillaries within the dermal layer helps efficient absorption of drugs into the vascular system (Lv et al. 2006).

1.5.2 Microneedle permutations

1.5.2.1 Solid microneedles

Leveraging techniques from the microelectronics industry, early MN arrays were typically fabricated from silicon (Henry et al. 1998; Ji et al. 2006; McAllister et al. 2003; Moon and Lee 2005; Wilke et al. 2005; Wu et al. 2008) and metal (Gill and Prausnitz 2007; Li et al. 2010; Martanto et al. 2004). Solid MNs have been shown to increase skin permeability by orders of magnitude for a diverse range of compounds. One of the earliest reports of enhanced transdermal drug permeation following MN treatment was by Henry et al. In this study 20 x 20 conical silicon MN arrays, containing MNs with a length of 150 µm, were inserted into human epidermal membrane *in vitro* for 10 secs or 1 h. Microneedle application was shown to increase permeability of a model permeant, CAL, by four orders of magnitude compared to untreated membrane. Furthermore, it was found that enhanced permeability occurred rapidly, within 1 h, and was maintained for up to a period of 5 h (Henry et al. 1998). Additional studies conducted utilising the same silicon MN arrays were conducted by McAllister et al. In an analogous set up, permeation of model medicaments across human epidermal membrane were investigated. In these studies silicon MNs were inserted and maintained *in situ*. This was shown to increase permeability to a wide range of molecules including CAL, insulin and Texas-red labelled bovine serum albumin (BSA) by orders of magnitude. In addition, it was found that MN insertion and removal increased permeation by a further order of magnitude for all compounds and facilitated delivery of nanoparticles with a diameter of up to 50 nm (McAllister et al. 2003). Additionally, frustum tipped pyramidal silicon MNs with a length of 280 µm have been shown to facilitate diffusion of nanoparticles with a diameter of up to 150 µm across human epidermal membrane (Coulman et al. 2009).

Furthermore, *in vivo* studies have shown transdermal delivery of insulin to diabetic rats using 2 dimensional, tapered stainless steel MNs measuring 1000 µm. Due to the length of these needles, and application utilising a pneumatic insertion device, they penetrated deep into the dermal layer (Martanto et al. 2004). Once inserted, a glass chamber was fixed in place around the MN array and a commercially available solution of human insulin was placed into the chamber. Following defined time periods, MN arrays were removed from the skin and the insulin solution remained in contact with the skin for 4 h (Martanto et al. 2004). In a manner analogous to subcutaneous injection, MN insertion for 10 mins facilitated decreases in blood glucose levels up to 80 % over 8 h, with no apparent lag time, following cutaneous insulin application (Martanto et al. 2004). Additionally, it was found that a single, short MN

application (10 secs) produced the greatest decrease in blood glucose (Martanto et al. 2004). Other groups have investigated stainless steel MNs for cutaneous macromolecule delivery. For example, Lin et al. utilised MNs measuring 430 µm for the delivery of oligodeoxynucleotide (ODN) from an aqueous gel formulation (Lin et al. 2001). Pre-treatment of hairless guinea-pigs with MNs, or application of integrated MN patches, with and without iontophoretic enhancement, permitted delivery of ODN over a 24 h period at therapeutically relevant rates (Lin et al. 2001). Ding et al. investigated transcutaneous immunisation by application of diphtheria toxin and influenza subunit vaccines to the shaved abdomens of mice following MN application (Ding et al. 2009). An initial prime dose was applied followed by two booster doses and blood samples were taken at each time point. Antibodies generated to diphtheria toxin were shown to increase significantly following solid MN facilitated vaccine delivery (Ding et al. 2009). However, all these studies involved application of MN devices and the drug formulation in a multi-step process. In a clinical setting, this may lead to complication for the end-user and result in variations in the dose administered.

1.5.2.2 Coated microneedles

An approach to achieve more integrated delivery of medicaments via solid MN structures is to coat the drug formulation onto the surface of needles (Cormier et al. 2004; Han et al. 2009; Kim et al. 2011; Matriano et al. 2002; Widera et al. 2006; Zhu et al. 2009). This technique has been widely investigated for intradermal vaccination purposes, targeting immunocompetent cells within skin, such as Langerhans cells. For example, Matriano et al. found that 330 µm long titanium MNs dry-film coated with ovalbumin (OVA) produced immune responses up to 50 times greater than those observed following the same subcutaneous or intramuscular (IM) dose in a hairless guinea-pig model (Matriano et al. 2002). In another approach, Yan Jin et al. fabricated biocompatible polycarbonate MN structures with a length of 500 µm onto which they smeared a solution of OVA in PBS. These devices were applied to the shaven back areas of mice in a series of 3 injections and serum levels were found to be similar to conventional needle delivery following the third injection (Yan Jin et al. 2009). More recently, Kim et al. found that inactivated influenza virus solution dip-coated onto solid metal MNs and air-dried elicited large immunogenic responses in mice (Kim et al. 2011). Optimisation of the coating formulation for influenza virus was achieved using trehalose as an excipient. Subsequently, the virus was shown to retain reasonable activity over a period of 1 month when dried onto MNs and retained the ability to elicit significant antibody titres *in vivo* (Kim et al. 2011). Coated MNs prepared in this manner have been shown to protect animals from subsequent lethal viral challenge (Kim et al. 2011; Zhu et al. 2009). Additionally, coatings have been shown

to dissolve within minutes *in situ* (Zhu et al. 2009) to rapidly deliver drug into the skin. The success of these devices has culminated in a Phase 2 clinical trial of a titanium MN patch coated with human parathyroid hormone analogue, teriparatide (TPTD), fabricated by Zosano Pharma for the treatment of osteoporosis in postmenopausal women (Cosman et al. 2010). Injectable TPTD is currently licensed for treatment of osteoporosis in the US, but its clinical efficacy is limited by practical factors (Fraenkel et al. 2006) such as poor adherence to daily subcutaneous injection (Cosman et al. 2010). The patch in this study consisted of 1300 MNs with an average length of 190 µm coated with TPTD on their tips and an adhesive backing (Cosman et al. 2010). 165 postmenopausal women were enrolled and it was found that the MN patch significantly increased lumbar spine bone mineral density (BMD) at 6 months compared to placebo. In addition, it was shown that the patch provided a significantly greater total hip BMD compared to both placebo and subcutaneous TPTD injection (Cosman et al. 2010). The only negative aspect of this study was the lack of blinding of participants using subcutaneous injection treatment (Cosman et al. 2010).

1.5.2.3 Hollow microneedles

Hollow MNs fabricated from silicon (Stoeber and Liepmann 2000), glass (Martanto et al. 2006; McAllister et al. 2003; Wang et al. 2006) and metal (Davis et al. 2005) have allowed microinjection into skin through needle apertures. Silicon MNs with a channel diameter of 40 µm and a length of 200 µm have demonstrated fluid transport *in vitro* into chicken thigh (Stoeber and Liepmann 2000). Furthermore, microinjection experiments were performed in diabetic, hairless rats whereby insulin solution was delivered by a single hollow glass MN to the dorsal skin. In this study, MNs were applied to anaesthetised animals and penetrated to a depth of 500 – 800 µm using a circular drilling motion. Up to 32 µL of drug solution was then injected into the skin under a pressure of 10 or 14 psi for 30 mins (McAllister et al. 2003). Decreases in blood glucose levels up to 70 % over a 5 h period suggested the efficacy of microinjection (McAllister et al. 2003). Similar *in vivo* microinjection studies were performed utilising the same diabetic animal model and tapered, hollow nickel MN arrays (4 x 4 pattern) measuring 500 µm in length, with a bore of 75 µm (Davis et al. 2005). This study showed a 47 % reduction in blood glucose level over a 4 h delivery period which remained relatively stable for up to 4 h post-delivery (Davis et al. 2005). More recently, Van Damme et al. conducted a clinical trial in 180 healthy volunteers utilising 450 µm long silicon MNs to investigate intradermal (ID) influenza vaccination (Van Damme et al. 2009). This study found that there was no significant difference in geometric mean titre, a measure of humoral immune response to vaccine, between the full dose given intramuscularly compared to either

20 or 40 % of the dose given via ID MN injection (Van Damme et al. 2009). Due to the nature of the ID injection process, local reactions at the injection site, such as swelling, were significantly greater than those in the IM injection group. However, in both treatment groups these reactions were mild and generally transient (Van Damme et al. 2009). Although "prick-pain" was significantly lower in the MN treated groups, it was found that "administration-pain" was greater following MN injection. Importantly it was found that the overall mean injection pain did not vary significantly between treatment groups (Van Damme et al. 2009). Hence, this study suggested the utility and dose sparing capacity of vaccines administered intradermally via MN injection.

1.5.2.4 Biodegradable microneedles

Biodegradable MNs have emerged as an attractive alternative to solid MN arrays. The term biodegradable has been used by convention to distinguish these MNs from the solid MN permutations discussed previously. However, in the context of this work biodegradability is defined in terms of the ability of the MN material to dissolve or degrade in an aqueous, biological medium. These MNs offer advantage over those made from other materials as they can be produced from biodegradable, biocompatible materials and because they can be formed by mould based fabrication methods that lend themselves to inexpensive and robust mass production (Park et al. 2005). Furthermore, these MN devices provide the potential for incorporation of medicament within the matrix of the array, enabling increased drug loading and the opportunity for controlled release. Due to the degradable nature of these devices, a further advantage is that no sharp MN residues are left following application (Sullivan et al. 2010). This property provides potential safety benefits over solid MNs and hypodermic needles, which may be re-used following administration, and therefore generate biohazardous waste.

Initial studies involving biodegradable MNs were similar to those utilising solid MN arrays. For example, Park et al. investigated the permeation of CAL or fluorescein-conjugated BSA in aqueous solution across human epidermal membrane *in vitro*. Membranes were placed onto a tissue support and treated with solid bevelled-tip polyglycolic acid (PGA) MNs, measuring 600 µm, prior to loading into Franz diffusion cells (Park et al. 2005). In these studies it was found that PGA MNs, containing 20 or 100 needles, increased the permeation of both model compounds by a minimum of 2 orders of magnitude over 1 h (Park et al. 2005). It was

perceived that solid MNs fabricated from a biodegradable material would provide a safer alternative to silicon or metal MNs if they were to break off and remain *in situ*.

More recently, a similar approach has been utilised to assess the ability of 500 µm long maltose MNs to facilitate the delivery of a nicardipine hydrochloride (NH) across hairless rat skin. Studies were conducted both *in vitro,* using full thickness rat skin, and *in vivo* whereby skin was pre-treated with maltose MN arrays, containing 27 needles. Microneedle arrays were inserted and left *in situ* prior to application of a NH solution containing ethanol. It was determined that the MNs would dissolve rapidly upon puncture of the SC, due to the high water content of the underlying epidermal tissue (Kolli and Banga 2008). These MNs were shown to significantly increase transepidermal water loss (TEWL) following insertion and removal, analogous to hypodermic needle insertion (Kolli and Banga 2008). Furthermore, a significant increase in NH flux *in vitro* and area under the curve *in vivo* was noted following maltose MN pre-treatment of skin (Kolli and Banga 2008). In a subsequent study maltose MNs were shown to insert into rat skin *in vitro* and dissolve immediately. It was found that the microchannels remained open for 24 h when covered with a drug solution however (Li et al. 2009). Microneedles measuring 500 µm were shown to significantly enhance the permeation of large molecular weight antibody, human immunoglobulin G, from aqueous solution by orders of magnitude (Li et al. 2009). It was also observed that MNs with a length of 200 µm did not facilitate delivery to such an extent as 500 µm long needles, possibly due to ineffective skin penetration (Li et al. 2009).

One of the first reports of model drug incorporation within the structure of a biodegradable MN device was by Miyano et al. whereby small molecules ascorbate-2-glucoside (ASG), sodium salicylate (SS) and CAL were mixed into the molten maltose candy prior to MN fabrication (Miyano et al. 2005). Maltose MNs containing 5 $\%^{w}/_{w}$ ASG, measuring 500 µm in length, demonstrated sufficient structural rigidity to penetrate human skin *in vivo* and were left *in situ* to deliver drug to the deeper skin layers. This process was not associated with any significant dermatological problems (Miyano et al. 2005). More recently, Lee et al. fabricated maltose MNs containing ASG and niacinamide at concentrations of 1 % and 1.5 $\%^{w}/_{w}$ respectively. In this method an elevated temperature was again required to dissolve the powders. However, it was shown that the stability of both drugs was unaffected by the fabrication process and for up to 2 months storage (Lee et al. 2011b). These MNs were robust enough to insert into guinea-pig skin *in vivo* to bring about a localised therapeutic effect (Lee et al. 2011b). In a

separate study, Donnelly et al. added 5-aminolevulinic acid (5-ALA) and BSA powder to molten galactose before micromoulding (Donnelly et al. 2009a). Here it was found that substantial losses of both 5-ALA and BSA occurred during the fabrication process. This was attributed to a combination of chemical reaction with the disaccharide (Donnelly et al. 2009a) and direct degradation due to elevated processing temperatures (Ito et al. 2007). Similar observations were made by Park et al. following fabrication of synthetic polymer MNs encapsulating CAL or BSA. This process involved either direct encapsulation of drug within the polymer MNs, or prior encapsulation within carboxymethylcellulose (CMC) or poly-L-lactide for controlled release applications (Park et al. 2006). The polymer MNs were fabricated from synthetic poly-lactide-co-glycolide (PLGA), a polymer with a melting point of 135 ^{O}C, and it was found that the duration of elevated temperature required to form these MNs caused a time-dependent denaturation of BSA protein (Park et al. 2006).

An alternative methodology was proposed by Ito et al. whereby a hand drawing process was utilised to fabricate self-dissolving MNs from various dense glue solutions of chondroitin sulphate, dextrin and albumin containing erythropoietin hormone (EPO). These MNs were dried under desiccation at low temperature and hence EPO, a biomolecule with a MW of 34 kDa, was successfully incorporated and delivered *in vivo* (Ito et al. 2006). The same workers later prepared 500 µm long conical MNs from dense drug glues containing insulin (Ito et al. 2010), ascorbic acid (Ito Y. et al. 2010b) and EPO (Ito Y. et al. 2010a) by condensing solutions under vacuum pressure (Ito et al. 2010; Ito Y. et al. 2010b) or a nitrogen gas stream (Ito Y. et al. 2010a) and dispensing the formulations into micromoulds. These MNs were dried under the pressure of a steel plate without elevated temperature. Furthermore, MNs containing recombinant human growth hormone (rhGH) or desmopressin (DDAVP) were fabricated from drug glues in a similar manner (Fukushima et al. 2011). It was shown that all MNs in these investigations successfully penetrated *in vivo* rat skin to deliver incorporated medicaments to bring about a biological effect. In a similar study, solid state biodegradable microstructures (SSBMS) measuring 200 µm were fabricated containing up to 10 $\%^{w}/_{w}$ FITC-BSA (66 kDa) and recombinant protective antigen (rPA; 83 kDa). Solid state biodegradable microstructures were fabricated from a carbohydrate and polyvinyl alcohol (PVA) solution prepared by pressure micromoulding and drying at 32 ^{O}C (Wendorf et al. 2011). These SSBMS dissolved within minutes to successfully deliver FITC-BSA to human skin *in vitro* and elicited significantly enhanced immune responses to rPA compared to control following application to rats *in vivo* (Wendorf et al. 2011).

Further biodegradable MNs were fabricated from viscous hydrogel formulations of natural polymeric materials CMC, amylopectin and BSA. Model drugs incorporated were sulforhodamine B (SRB), BSA and lysozyme added at various final weight concentrations up to 30 $\%^{w}/_{w}$ (Lee et al. 2008). This study showed that functional macromolecule, lysozyme, retained 96 % activity within MN structures following 2 months storage at room temperature (Lee et al. 2008). Although these MNs appeared to demonstrate good stabilisation of incorporated protein, it is known that lysozyme is unusually stable (Prestrelski et al. 1993), and hence these findings may not be extrapolated to other macromolecular systems. In another approach, 600 µm long CMC MNs were fabricated containing 5 $\%^{w}/_{w}$ rhGH utilising a relatively low-temperature centrifugation casting methodology (Lee et al. 2011a). Incorporated hormone was stabilised by the addition of trehalose to the formulation and was shown to elicit a biological effect both *in vitro* and *in vivo* when administered to cell culture and hairless rat models respectively (Lee et al. 2011a). *In vivo,* rhGH pharmacokinetics were shown to be similar to conventional subcutaneous injection and MN application was found to be well tolerated causing only slight, transient erythema (Lee et al. 2011a).

In an attempt to incorporate drug substances within rapidly dissolving biodegradable polymer MNs, polyvinylpyrrolidone (PVP) was utilised as a matrix substance. Microneedles containing sulforhodamine, fluorescently labelled BSA and β-galactosidase (β-gal) were fabricated by a vacuum moulding and *in situ* photo-polymerization methodology (Sullivan et al. 2008). These 750 µm long MNs demonstrated effective delivery of BSA and functional β-gal to full thickness pig skin *in vitro* and were shown to preserve nearly 100 % β-gal activity following incorporation within PVP MN structures (Sullivan et al. 2008). Furthermore, PVP MNs incorporating lyophilised inactivated influenza virus vaccine were shown to generate robust antibody and cellular immune responses in mice providing complete protection against subsequent lethal challenge. Polyvinylpyrrolidone MN vaccination resulted in more efficient lung virus clearance and enhanced cellular recall responses compared to IM injection following viral challenge (Sullivan et al. 2010). It was also found that cellular immune responses were superior following PVP MN vaccination compared to coated metal MN delivery (Sullivan et al. 2010). Additionally, the MNs were shown to almost completely dissolve within 5 mins in *ex vivo* pig skin and by 15 mins *in vivo* in mice (Sullivan et al. 2010). Alternatively, Chu et al. investigated MN structures fabricated from blends of PVA and PVP containing SRB incorporated within the needles either in a gradient fashion or as a homogeneous mix throughout the matrix (Chu et al. 2010). Localisation of SRB within the needle tips facilitated approximately 80 % drug delivery within 10 mins in excised porcine skin, compared to 20 % with no localisation of drug (Chu et

al. 2010). Alternatively, MNs were fabricated from Gantrez™AN-139 mucoadhesive copolymer containing 1 $\%^{w}/_{w}$ theophylline. Drug-free MNs measuring 600 µm were shown to insert into human skin *in vivo* to a depth of approximately 460 µm (Donnelly et al. 2011). Loading above 1 $\%^{w}/_{w}$ had a highly plasticising effect on the polymer, making it unsuitable for MN fabrication (Donnelly et al. 2011). These MNs were shown to deliver 83 % of incorporated drug cargo across neonatal porcine skin *in vitro* (Donnelly et al. 2011). Further conical shape 600 µm long MNs were created from poly (methylvinylether maleic anhydride) containing insulin loaded at two different concentrations. Loading of MNs at both concentrations did not adversely affect MN morphology or robustness and only slight losses of insulin were incurred during fabrication (Migalska et al. 2011). *In vitro* analysis of insulin diffusion across dermatomed neonatal porcine skin demonstrated that only 40 – 55 % of the drug contained within the needles permeated the skin (Migalska et al. 2011), accounting for approximately 1 % of total drug loading. However, the effectiveness of the MNs to deliver insulin *in vivo* in diabetic rats was confirmed by a dose-dependent decrease, up to 74 %, in blood glucose level (Migalska et al. 2011).

A range of exemplar biodegradable MN structures are shown in Figure 1.4.

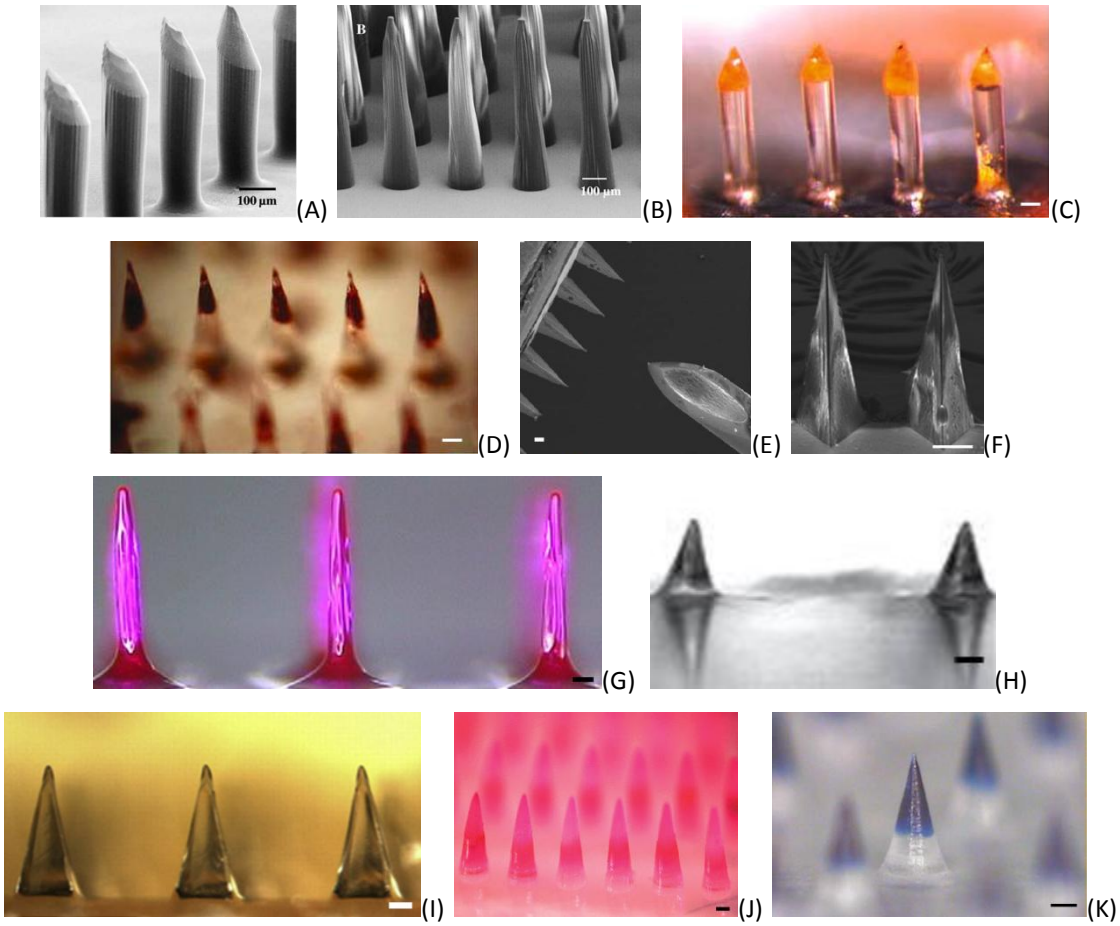

Figure 1.4 Biodegradable microneedle permutations.

(A) 600 µm bevelled-tip PGA MNs, (B) 1500 µm tapered-cone PGA MNs (Park et al. 2005), (C) 600 µm bevel-tip and (D) 750 µm tapered-cone PLGA MNs containing calcein in their tips (Park et al. 2006), (E) 500 µm tetrahedron shaped maltose MNs next to a 26 G hypodermic needle (Kolli and Banga 2008), (F) 500 µm pyramidal maltose MNs (Li et al. 2009), (G) 1200 µm tapered conical maltose MNs encapsulating sulforhodamine B (Lee et al. 2011b), (H) 270 µm pyramidal galactose MNs (Donnelly et al. 2009a), (I) 600 µm pyramidal carboxymethylcellulose MNs (Lee et al. 2008), (J) 750 µm conical polyvinyl pyrrolidone MNs encapsulating sulforhodamine (Sullivan et al. 2008) and (K) 500 µm conical chrondroitin sulfate MNs partially loaded with Evans blue dye and insulin (Ito et al. 2010). (Bar = 100 µm).

To date there have been many different approaches to MN fabrication and cutaneous drug delivery. Currently, there does not appear to be one fully optimised system however, which will be discussed in the next section.

1.5.3 Advantages and limitations of microneedle technology

The innovation of MN facilitated drug delivery offers the potential to overcome many of the issues surrounding the complex cutaneous delivery of therapeutic proteins and other hydrophilic molecules. Microneedle devices have been fabricated from a variety of materials and have demonstrated the ability to facilitate enhanced delivery of a diverse range of different compounds across skin. Furthermore, dose sparing biological responses have been noted for specific medicaments, for example intradermal vaccine delivery (Van Damme et al. 2009). Notably, there are now many reports of stable molecule and biomolecule incorporation within biodegradable MN structures which have been fabricated from a wide range of both natural and synthetic materials. It is perceived that this MN design in particular offers a number of additional advantages. Firstly, they tend to be formed by mould based fabrication methods which facilitate a low unit cost. As a corollary, biocompatible materials can be utilised which are degraded safely within the body. These materials also permit drug loading within the device matrix, potentially facilitating increased loading and stabilisation of labile medicaments. In addition, this approach lends itself to providing controlled drug release through variations in material composition and drug encapsulation prior to incorporation within the MN structure (Park et al. 2006). Furthermore, dissolving MNs offer an attractive method of delivery as they can be designed to degrade *in situ* and therefore do not leave behind sharp or hazardous waste structures. This reduces the potential for subsequent needle re-use or needle-stick injuries from contaminated needles to occur (Haq et al. 2009).

From a clinical, patient focused perspective, it has been shown that MNs circumvent many of the issues surrounding hypodermic needle delivery of medicines (Bal et al. 2008; Haq et al. 2009). Although effective, drug delivery via hypodermic needles has a number of potential drawbacks such as causing pain and apprehension for the patient (Kleinknecht 1994; Öst 1992) and the requirement of medically trained personnel to deliver the dose (Davis et al. 2004). In addition, it has been shown that hypodermic needle puncture of model membranes *in vitro* results in significantly greater microbial penetration compared to MN penetration (Donnelly et al. 2009b). Furthermore, MN insertion *in vivo* in humans appears to be generally well tolerated without causing any significant adverse effects (Van Damme et al. 2009). Hence, it is envisaged that ultimately patients will be able to safely use MN devices in their own homes and will not have to rely on visits to hospital and GP surgeries for injections.

There are however a number of potential issues over the use of MN devices. Early solid MN fabrication methods were often time consuming and expensive due to reliance on multi-step, cleanroom-intensive processes (Park et al. 2005) using complex dry and wet etch technologies. Also, if silicon or metal needles were to break off in skin, this could result in possible complications (Kolli and Banga 2008). Furthermore, solid MN devices have relied upon multi-step application processes where the drug formulation and MN device are applied separately. This process is undesirable as it makes drug delivery more complex and provides a greater chance for dosing errors to occur. Coated MNs offer the advantage of application of both the dosage formulation and the MN device in the same process. However, due to the relatively small surface area of MN arrays, total drug loading is limited to doses in the microgram range (Zhu et al. 2009) that tend to be delivered in one bolus dose. Furthermore, there is the potential for a huge loss of coated material upon MN insertion (Cormier et al. 2004; Yan Jin et al. 2009), resulting in wastage of drug formulation. To overcome these issues, biodegradable MNs have been fabricated as a safer alternative to solid MNs. However, the methodologies utilised for creating these devices have often involved melting of materials at high temperature to micromould structures (Miyano et al. 2005; Park et al. 2005). This has made incorporation of labile biological molecules within MN structures unfavourable in some instances (Donnelly et al. 2009a; Park et al. 2006). From a practical perspective, it will also be critical to evaluate microchannel duration in skin tissue *in vivo* to determine channel closure kinetics and hence stability of dose delivery. Reports generally suggest that channels close within 24 h following MN puncture (Fukushima et al. 2011; Haq et al. 2009) although it has been shown that channels will close more rapidly, unless occlusion or some other technique is employed to prolong channel opening (Banks et al. 2011; Kalluri and Banga 2011). This is a particularly pertinent issue for controlled release from dissolving MN devices aimed at providing prolonged drug release.

The focus of this project is to investigate the fabrication of biodegradable MN structures at low processing temperature for stable molecule incorporation. Sugars have been investigated by a number of researchers and present a potentially attractive material for biodegradable MN manufacture. Sugar glasses are characterised as an amorphous form of the material and are extensively utilised in nature to protect delicate biological structures (Potts 1994) during periods of water stress. Sugar glasses can be formed via a number of different methodologies, including techniques involving low temperature processes. Therefore these materials were selected as an attractive substrate for biodegradable MN fabrication.

1.6 Molecular glasses

1.6.1 Definition

The term glass is usually taken to encompass, “a wide range of inorganic substances which differ widely in chemical composition and physical properties, but which possess the essential characteristic of having been cooled from a state of fusion to become a solid without crystallisation. Glass at room temperature can be regarded as a liquid, which is of such a high viscosity that it behaves as a rigid elastic solid” (Franks 2003). It has been proposed however that this definition is too restrictive, and other authors have provided much broader definitions. A more encompassing interpretation of a glass is an amorphous solid in which the molecules form a “non-periodic and non-symmetric network.” Theoretically, the molecular mobility within these glassy state systems is many orders of magnitude lower than in liquid systems (Elliott 1990). Glasses are formed by rubber to glass transitions that can be generated by any cooling or drying processes applied to many amorphous compounds (van den Berg et al. 1995). The glass transition in amorphous systems is a temperature-, time- (or frequency), and composition-dependent, material-specific change in physical state, from a "glassy" mechanical solid to a "rubbery" viscous fluid. In terms of thermodynamics, the glass transition is operationally defined as a second order transition (Slade and Levine 1988).

In the past, the study of glasses has almost entirely been dominated by materials scientists. Hence, the considerable progress in development of novel materials has generally been confined to glasses based on metals, silicates, oxides, ceramics and polymers. The realisation that amorphous solids in general, and glasses in particular, also play an interesting and important role in technologies not necessarily related to materials science came relatively late (Franks 2003). However, it was quickly realised that glass formation had wide and varying applications, particularly in the biological and pharmaceutical sciences. This is particularly true in the study of freeze-drying formulation, and subsequent product storage, where it is now well known that amorphous sugars can stabilise biological molecules such as proteins (Schebor et al. 1997; Uritani et al. 1995), liposomes and lipoplexes (Crowe et al. 1985; Hincha et al. 2002), and even viruses (Bieganski et al. 1998; Levy and Fieldsteel 1982). Figure 1.5 shows the structure of a sucrose glass formed by freeze-drying.

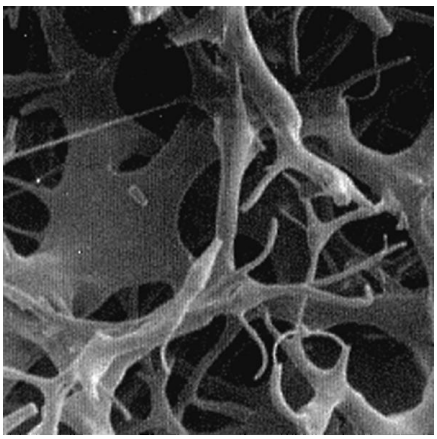

Figure 1.5 Scanning electron micrograph of a freeze concentrated aqueous sucrose solution after the sublimation of ice during freeze-drying.

The cavities denote spaces previously occupied by ice crystals. The filaments represent the glassy sucrose containing dissolved residual water (Franks 2003).

1.6.2 Natural role of sugar glasses and the glass transition temperature

Glass forming sugars have great significance in nature as they are used to protect biological tissues in the dehydrated state (Potts 1994). It has generally been accepted that cells containing sugar usually form a glassy state of sugars under extreme conditions (Seo et al. 2006). Carbohydrates play an important role in the stabilisation of biological components under water stress, which can be produced by either freezing or drying samples. Proteins and tissues mainly become damaged under such conditions due to the generation of large salt concentration gradients (Grigera and Bolzicco 2008). Although it is not known precisely how this method of protection is afforded by carbohydrates, it has been reported that the glass transition temperature (Tg) of sugars and sugar-containing materials may be linked to their cell protection abilities (Buitink et al. 2000).

It was discovered that carbohydrate glass plays a central role in anhydrobiosis many decades ago (Carpenter et al. 1987a). Anhydrobiosis is defined as the capability of an organism to survive essentially complete dehydration, commonly when over 99 % of its body water is removed, which results in dry but viable tissues containing as little as 0.1 % water. The dry organism may remain in this unique living state for decades, or perhaps even centuries under favourable conditions. When water becomes available once more, the organism rapidly swells and resumes active life (Crowe et al. 1992). It has been suggested that the ability of

anhydrobiotic organisms and plants to survive extreme dehydration is largely due to their ability to synthesize high concentrations of disaccharides. These sugars, for example sucrose or trehalose, serve to protect sensitive biological structures, for example, proteins, membranes, or even whole cells *in vitro* (Guo et al. 2000; Leslie et al. 1995) via a synergistic mechanism involving direct interactions with biomolecules and glass formation (Buitink and Leprince 2004; Crowe et al. 1998). Intrinsic characteristics of a hydrophilic glass that are important to protein stabilisation appear to include its amorphous nature and retarded dynamics of the protein, relative to physiological conditions, within the matrix (Cicerone and Soles 2004). The amorphous sugar appears to replace water molecules which surround the protein in the physiological state. Subsequently, this process seems to cause stabilisation of the native structure of the protein in the dehydrated state (Allison et al. 1999). It has been found that intimate contact is necessary for effective hydrogen bonding to occur, and this is only made possible by the amorphous nature of the glass (Cicerone and Soles 2004). It seems likely that spatial constraints imposed by the crystalline phase do not allow this, as evidenced by the observation that proteins are not stabilised in the crystalline phase of an otherwise effective preservant (Izutsu et al. 1994).

1.6.3 Material properties of vitrified glasses

Glasses formed by the rapid cooling of a melt are thermodynamically unstable systems in a higher energy state relative to both the crystalline state and the meta-stable supercooled liquid state, (Zhou et al. 2007). This is represented diagrammatically in Figure 1.6.

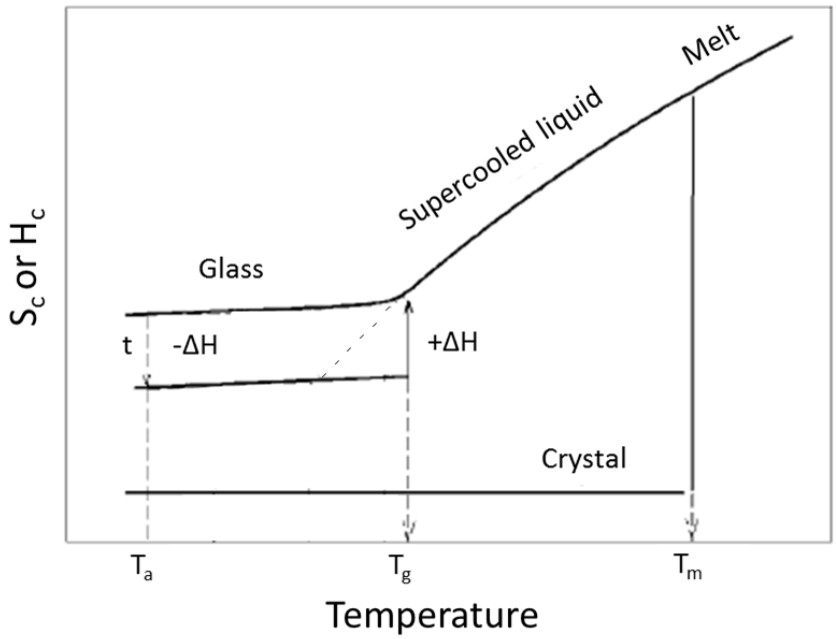

Figure 1.6 Phase diagram of an amorphous phase showing glass annealed at Ta for duration t.

Tm and Tg are the melting and glass transition temperatures, respectively. Sc and Hc are configurational entropy and enthalpy, respectively. ΔH is the enthalpy lost during annealing and the dotted line represents the meta-stable supercooled liquid state. Adapted from source (Zhou et al. 2007).

The meta-stable nature of amorphous solids means that they often exhibit decreased physical and chemical stability (Aso et al. 2001; Pikal et al. 1978) due to their higher free energy, enthalpy and entropy (Zhou et al. 2007) in comparison to the crystalline state. In general molecular mobility has been discussed as a critical factor for dictating physical stability of amorphous substances (Hancock et al. 1995), but it is not the sole predictor (Zhou et al. 2007). Therefore, it is still relatively difficult to predict the stability of amorphous dosage forms compared to solutions (Zhou et al. 2007). In many pharmaceutical systems a correlation has been demonstrated between molecular mobility and chemical stability (Shamblin et al. 2006), protein aggregation (Yoshioka et al. 2003) and crystallisation (Bhugra et al. 2006) in the amorphous state; although not all systems exhibit similar behaviour (Luthra et al. 2008). Zhou et al. developed this further and stipulated that molecular mobility and also configurational entropy are important in determining the crystallisation tendency in the rubbery state (Zhou et

al. 2007). Therefore, at temperatures above Tg, it has been postulated that crystallisation would be governed by (1) the configurational entropy, because this is a measure of the probability of molecules being in the appropriate conformation, and (2) mobility, because this is related to the number of collisions per unit time (Zhou et al. 2007). Water can also affect the chemical stability of solid protein formulations, and it does this in at least three ways: (1) as a solvent, (2) as a reactant in a reaction such as hydrolysis, and/or (3) as a plasticising agent. Water acts as a plasticiser of amorphous solids inducing a physical transition from a brittle, dynamically constrained glassy state to a more mobile, rubbery state with decreased viscosity (Hageman 1992) and lowers Tg (Nowakowski and Hartel 2002; Roos and Karel 1991b).

The stabilising effect of amorphous sugar glass has been explained by the formation of a sugar matrix which acts as a physical barrier between particles (particle isolation) (Allison et al. 2000) and strongly reduces diffusion and molecular mobility (vitrification) (Leopold et al. 1994). Both the physical barrier and the lack of mobility provided by the glassy matrix, prevent aggregation and degradation of the dried material. Under dry conditions, the glass is maintained as long as the temperature is kept below the characteristic Tg of the stabilising sugar used (de Jonge et al. 2007). Vitrification at Tg effectively locks the liquid structure into an amorphous solid matrix due to the densification process which occurs during cooling or drying. The rate of densification is related to the structural relaxation time of the material (Noel et al. 2005). When glass is stored below Tg, a non-equilibrium state exists, and this, coupled with mobility over a longer time scale, leads to the so-called “physical aging” phenomena. Physical aging, or annealing, refers to structural relaxation of the non-equilibrium glass toward the meta-stable equilibrium or supercooled liquid state, that is the ideal glass, Figure 1.6 (Zhou et al. 2007). Physical aging relates also to a change in material properties including compliance, stiffness and brittleness (Struik 1978) which slowly evolve with time due to the densification process (Noel et al. 2005). Above the Tg, the glass moves toward the rubber state, which has a higher degree of mobility (de Jonge et al. 2007), and hence proteins and other biological molecules begin to lose preservation of their native state within the glass. If annealed properly, as the excess enthalpy and entropy of the non-equilibrium glass decrease, the molecular mobility within the glass should also decrease. The rate and extent of this decrease may be important to chemical and physical stability within the glass (Zhou et al. 2007).

In nature the disaccharide trehalose is widely utilised in anhydrobiotic organisms and is generally thought of as having the best biopreservative abilities *in vitro* (Curtis et al. 2006). Trehalose, (α-D-glucopyranosyl-α-D-glucopyranoside) is shown in Figure 1.7.

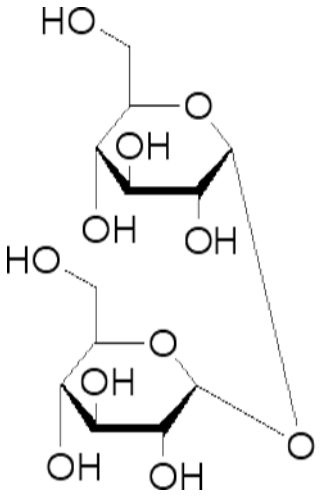

Figure 1.7 Molecular structure of trehalose.

Trehalose is a non-reducing sugar as the two glucose subunits are joined through their anomeric centres. Adapted from source (www.sigmaaldrich.com, accessed 03/10/2011).

Trehalose is a non-reducing disaccharide whose glassy amorphous state can easily be produced by the rapid quench of its liquid phase and also by rapid dehydration of its dihydrate form (T_{2H2O}) (Willart et al. 2001). It has been suggested that unique preservative properties of amorphous trehalose include those that invoke either the inclusion (Belton and Gil 1994) or exclusion (Carpenter and Crowe 1989) of water from the surface of proteins, direct interaction of trehalose by adhering to the protein (Cordone et al. 1999), and intrinsic viscosity effects of the glass alone (Sampedro and Uribe 2004). The uniquely high Tg of trehalose (Green and Angell 1989) has been ascribed to the latter mechanism of protection and therefore it is claimed to be responsible for the preservation of functional proteins in the glassy state (Curtis et al. 2006). The inherently slow relaxation dynamics of the polyhydroxyl glass is expected to retard motions and reactions, both intrinsic and extrinsic to the protein that lead to degraded protein function (Cicerone and Soles 2004).

Sucrose is a further glass forming disaccharide that is found widely in nature to protect biological entities. For example, seeds commonly contain a large amount of sucrose, together with a high proportion of oligo- and poly-saccharides, a combination that has been found to

elevate the Tg and maintain seed viability for long-term storage (Koster and Leopold 1988). This property of sucrose has been realised for some time, and the disaccharide has been utilised more extensively in the pharmaceutical industry than trehalose, despite the Tg of trehalose being over 40 °C higher than that of sucrose (Green and Angell 1989). The structure of sucrose (β-D-fructofuranosyl-α-D-glucopyranoside) is similar to trehalose, as shown in Figure 1.8. Sucrose is a non-reducing sugar and consists of a molecule of glucose linked to a molecule of fructose.

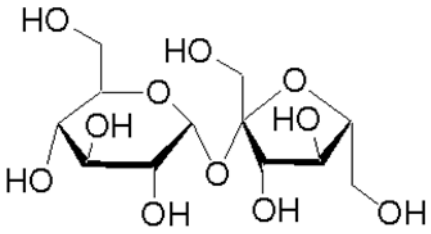

Figure 1.8 Molecular structure of sucrose.

Adapted from source (www.sigmaaldrich.com, accessed 03/10/2011).

The benefits of one of these excipients over the other appear to be equivocal, dependent upon the system under investigation. For example, sucrose has been found to be more effective in preserving the native structure of lysozyme during lyophilisation (Allison et al. 1999) and freeze-dried monoclonal antibody stored at 5 °C (Duddu and DalMonte 1997), when compared to trehalose. In addition, it has been demonstrated that carbohydrate glasses formed from combinations of sugars can effectively inhibit crystallisation of the material (Roos and Karel 1991a).

Subsequently, a strong focus of this work was to explore the material properties of both of these disaccharides and to determine their suitability for forming sugar glass microneedles (SGMNs). It is envisaged that SGMN arrays containing an incorporated drug cargo may facilitate effective transdermal drug delivery.

1.7 Thesis aim and objectives

Due to the unstable and delicate nature of biotechnology derived pharmaceuticals, such as proteins, peptides and nucleic acids, they present significant challenges for stable production and effective and reliable delivery (Brown et al. 2006). These medicaments have typically been administered via hypodermic needle directly into the systemic circulation. Although an effective means of delivery, this route presents a number of issues and is often not a preferred method of drug administration by patients (Öst 1992). Due to their small size MNs offer the potential to alleviate the pain and blood vessel trauma associated with hypodermic needle insertion (Haq et al. 2009) and may address some of the current limitations and inadequacies in the delivery of many of the newer biologically active therapeutics on the market.

To date, MNs have been formed from a variety of materials and a number of different permutations have been investigated for transdermal drug delivery applications. To address limitations of early solid devices, MNs formed from biodegradable materials, whereby drug can be incorporated within the MN matrix, have emerged as an attractive alternative. The aim of this approach is to stably incorporate medicaments within MN structures using materials and processes that do not adversely affect the drug cargo.

Sugar glasses are amorphous forms of sugars which have been utilised widely in the pharmaceutical industry as excipients to aid in preservation of delicate macromolecules during preparation and storage (Schebor et al. 1997). Furthermore, there are now many reports of biodegradable MN fabrication utilising carbohydrate substrates (Lee et al. 2008; Miyano et al. 2005). Therefore, it was hypothesised that sugar glass material presented an attractive substrate for biodegradable MN fabrication and incorporation of model therapeutic molecules for transdermal drug delivery.

1.7.1 Aim

The aim of this thesis was to fabricate and characterise sugar glass material utilising low temperature processing and to investigate the feasibility of micromoulding biodegradable sugar glass microneedle devices. The capability of these devices to incorporate a range of model substances, including macromolecules, and to deliver them across human skin *in vitro* was a key focus.

1.7.2 Objectives

1. Develop a low processing temperature methodology to form amorphous sugar glass materials.
2. Characterise sugar glass materials using a range of different techniques, including thermal and x-ray analyses, to determine material properties.
3. Quantitatively assess the stability of model macromolecule contained within sugar glass material.
4. Investigate and optimise fabrication of biodegradable SGMN structures from sugar glasses utilising a micromoulding methodology.
5. Investigate the capacity to incorporate a range of model substances with differing physicochemical properties within SGMNs.
6. Qualitatively and quantitatively assess the ability of SGMNs to penetrate human skin barrier to deliver incorporated substances.
7. Assess long-term stability of sugar glasses under different conditions to investigate optimal storage conditions for SGMNs.
8. Quantitative assessment of *in vitro* drug delivery potential of SGMN arrays containing a small molecule across heat separated epidermal membrane.
9. Quantitative assessment of *in vitro* drug delivery potential of SGMN arrays containing larger molecular weight moieties across heat separated epidermal membrane.
10. Investigate *in vitro* drug delivery potential of integrated SGMN array transdermal patches containing model drug substance across heat separated epidermal membrane.
11. Assess dissolution of SGMN arrays *in situ* in full thickness human skin *in vitro*.

Chapter 2

Characterisation of sugar glasses

2 Characterisation of sugar glasses

2.1 Introduction

In the past, a number of different methods have been investigated to form amorphous sugar glass (SG) materials. Classically, glasses are prepared by the rapid cooling of a melt, which bypasses crystallisation (Willart and Descamps 2008). Below the melting temperature (T_m) the liquid becomes metastable and the chance of forming a glass strongly depends upon the persistence of the metastable liquid during the quenching process (El Adib et al. 1989). This is shown schematically in Figure 2.1 where the time taken for a given amount of crystalline phase to evolve is plotted as a function of temperature for a typical undercooled melt system (Willart and Descamps 2008).

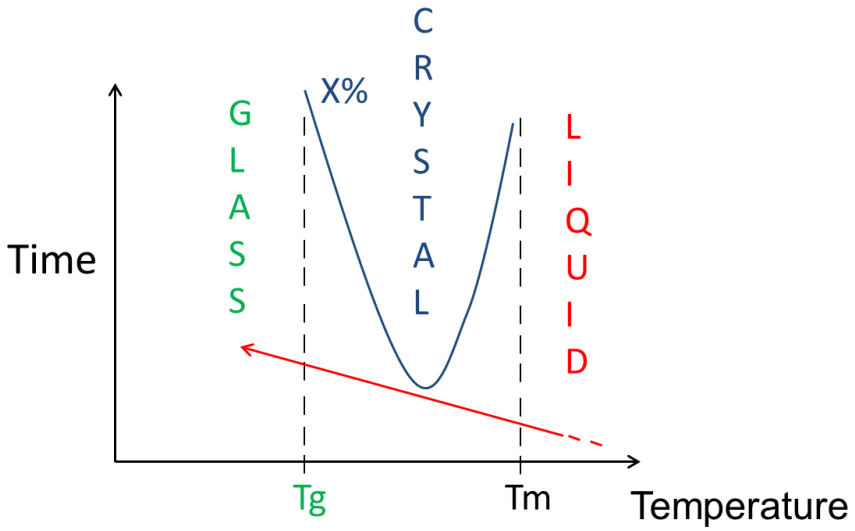

Figure 2.1 Schematic time-temperature transformation diagram for crystallisation during conventional vitrification.

(Tg = glass transition temperature, Tm = melting temperature). Adapted from source (Willart and Descamps 2008).

At the glass transition temperature (Tg) the liquid falls out of equilibrium, which is denoted during differential scanning calorimetry as a fall in heat capacity during the scan (Willart and Descamps 2008). The random disordered state of the liquid phase is frozen within the glassy matrix, at least to a great extent, and the atoms within the glass vibrate about these new frozen points. Hence, a characteristic of glassy phases is an absence of any identifiable structural pattern detectable by X-ray scattering (Willart and Descamps 2008). This conventional route to glass formation is demonstrated by pathway (1) in Figure 2.2. During

formation, the glass is trapped within a local minimum of the potential energy landscape distribution whose arrangement subsequently dictates the structure of the amorphous phase. Therefore, the physical state of the glass may vary with the history of the sample, such as preparation process and subsequent aging. For example, annealing a glass below its Tg or modifying the cooling rate will affect the relaxation times within the system and have a strong impact on stabilisation capabilities (Willart and Descamps 2008).

As stated, a glass can be regarded as a liquid which is of such a high viscosity that it has the properties of a rigid elastic solid material (Franks 2003). The viscosity of such liquids in their glassy state is usually determined as 10^{13} poises (Kauzmann 1948). Importantly in the context of this work, it has been shown that this state may be achieved via a number of alternative techniques to the quench of the melt method. Other methods include spray-drying, lyophilisation and direct milling of solid crystal, as shown in Figure 2.2 pathway (2) (Willart and Descamps 2008). However, regardless of formation technique, as the Gibbs energy diagram in Figure 2.2 shows, glassy systems tend to have greater free energy in relation to crystal and liquid (stable and undercooled) states, and hence demonstrate reduced physical stability (Willart and Descamps 2008).

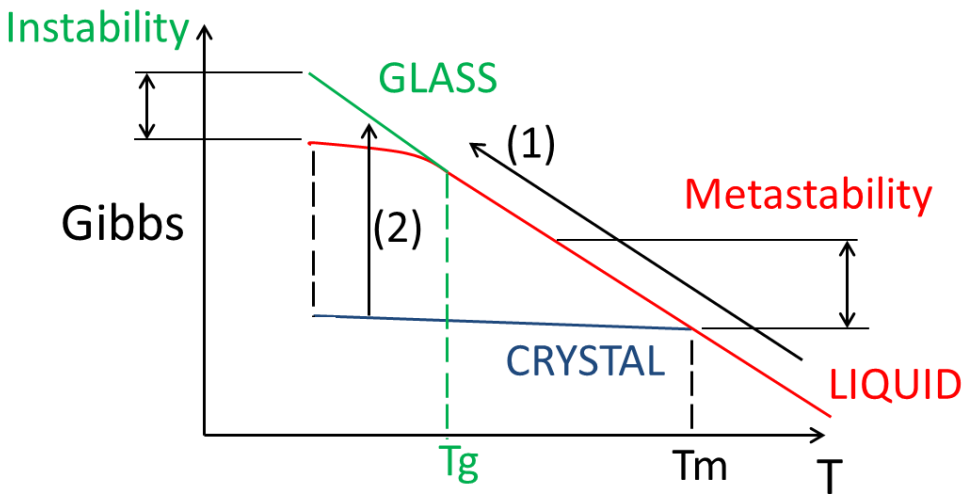

Figure 2.2 Gibbs free enthalpy curve for crystal, liquid and glass.

Paths (1) and (2) correspond to conventional and solid state vitrification pathways respectively. Adapted from source (Willart and Descamps 2008).

As Figure 2.2 shows, the amorphous product is in a higher energy state relative to the metastable supercooled liquid state. Therefore, under usual conditions, the glassy form of a material is more soluble than any crystalline form of the same compound at a given

temperature. Hence, solid compounds may either be crystalline or glassy with each state possessing differing consequential properties (Shamblin et al. 2000), such as reactivity (Liu et al. 2002), solubility, hygroscopicity, and mechanical properties (Noel et al. 2005).

As stated previously, glasses can be formed by rubber to glass transitions generated by any cooling or drying processes applied to many amorphous compounds (van den Berg et al. 1995). Polyhydroxyl compounds, such as sugars, generally fulfil the requirements of very slow crystallisation combined with a specific rheology and chemistry. As water is removed from a dilute solution of the sugar, the viscosity of the resulting supersaturated residue increases towards the critical 10^{12} - 10^{14} Pa·s required for vitrification. However, the vitrified solid may still contain up to 50 $\%^{w}/_{w}$ water in this state and this depends upon the dehydration method and chemical properties of the solute under investigation (Franks 1997). Figure 2.3 demonstrates a variety of different methods for the preparation of amorphous pharmaceutical systems (Surana et al. 2004).

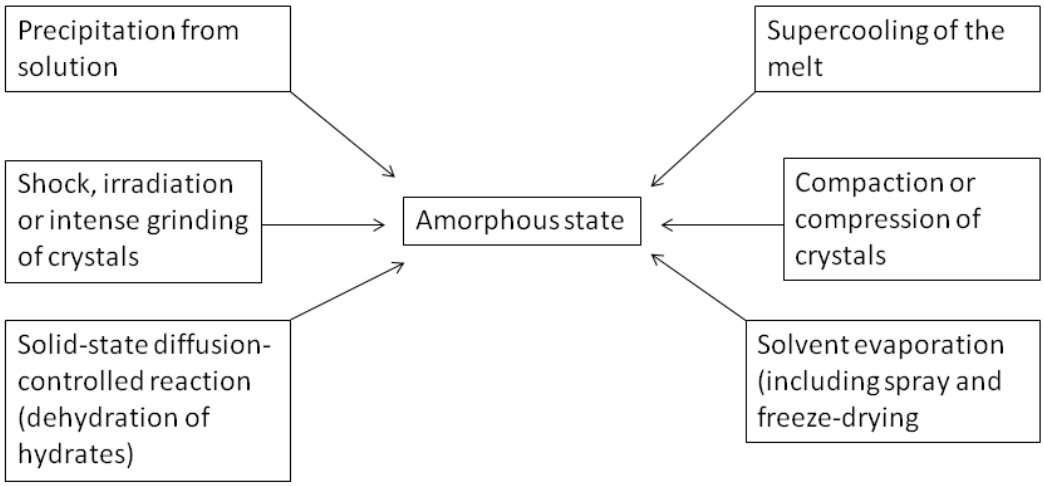

Figure 2.3 Some common methods of inducing amorphous character in pharmaceutical systems.

Adapted from source (Surana et al. 2004).

As Figure 2.3 shows, there are many different routes to the formation of an amorphous solid. The common feature of all these routes is that they form a disordered solid state (Surana et al. 2004). However, it has frequently been reported that there is a local or short-range order within the material, despite the absence of long-range crystalline order (Shalaev and Zografi 2002). It has been proposed that the method of production of the amorphous material is one of the most important determinants of the order within the structure (Surana et al. 2004) and hence the tendency for nucleation and crystal growth (Shalaev and Zografi 2002).

An aim of this current work was to form amorphous sugar materials without using excessive temperature or mechanical force. This dictated that a mild processing methodology should be used to form a glassy sugar system. Therefore, the most attractive route to the production of an amorphous sugar was via dehydration of a sugar solution. However, in amorphous systems both the surrounding temperature and the substance determine the rate of spontaneous crystallisation. Crystallisation is governed by two independent steps: firstly nuclei must form and then these nuclei must grow to form crystals (Kauzmann 1948). It has been shown that slow dehydration of pure sugar solutions at low or ambient temperatures often promotes nucleation and crystallisation (Wright et al. 2002). To circumvent this problem, workers have reported that slow evaporation of 1/1 mixtures of trehalose and sucrose sugar solutions at low or ambient temperatures appear to result in the formation of a sugar glass (Wright et al. 2002; Wright et al. 2003). This approach was an appealing way to attempt production of solid sugar glasses for micromoulding into the geometry of a biodegradable microneedle array.

2.2 Chapter objectives

1. Explore and optimise formation of amorphous sugar glasses via a low temperature dehydration technique.

2. Screen dehydration properties of a number of individual sugar and binary sugar combination solutions for reliable sugar glass formation.

3. Explore the residual water content of sugar glasses formed.

4. Characterise dehydrated sugar products using a number of different techniques including visual, microscopic, thermal and X-ray based analyses.

5. Determine optimal sugar glass forming material for biodegradable microneedle fabrication.

2.3 Materials and methods

2.3.1 Materials

All reagents were obtained from Fisher Scientific Ltd. (Loughborough, UK) and were of analytical grade unless stated otherwise.

2.3.2 Methods

2.3.2.1 Preparation of sugar glasses

Dehydrated sugar formulations were prepared using trehalose anhydrous (TRA) (30987-0250, 99 %, varied batches), trehalose dihydrate (TRD) (18255-0250, 99 % min., A0251934), sucrose (SUC) (17714-0010, 99.7 %, A0240570), maltose monohydrate (MAL) (M/1450/48, >90 %, 0600669), mannitol (MAN) (M/2405/53, 99+ %, A0242017) and xylitol (XYL) (22598-0250, 99+ %, A0264195). Briefly, 400 mg of sugar (either individual sugars or binary mixtures of 25, 50 and 75 $\%^{w}/_{w}$) was dissolved in 2 mL of deionised water yielding a 16.7 $\%^{w}/_{v}$ solution. Each solution was introduced into a 100 mL beaker and allowed to dehydrate in a fume cupboard, flow rate 0.53 m/s, at room temperature for 24 h followed by 24 h at 50 °C (Fraenkel et al. 2006). Sugar glasses were examined visually and photographed using a digital camera, (Nikon, Coolpix 5600, Japan), to confirm whether a uniform glass had been created.

2.3.2.2 Determination of residual water content of sugar glasses

Three sugar solutions, (TRA/SUC 75:25 $\%^{w}/_{w}$, TRD/SUC 75:25 $\%^{w}/_{w}$, MAL/TRA 75:25 $\%^{w}/_{w}$) were formed as in section 2.3.2.1 and dehydrated for 24 h in a fume cupboard at room temperature followed by 24 h at either 50 or 60 °C. Changes in sample weight were recorded to determine water loss during dehydration. Following the initial 48 h of drying, samples were maintained at 50 or 60 °C until no further weight change was recorded. Once dehydrated to dry weight, samples were placed under ambient conditions and stored up to 360 h (Fraenkel et al. 2006).

2.3.2.3 Preparation and scanning electron microscopy of sugar glass films

Polydimethylsiloxane (PDMS) pre-polymer, in the form of Sylgard® 184 silicone encapsulant (R W Greeff, Glasgow, UK), and curing agent were combined in a 10:1 ratio, mixed and degassed for 30 mins under 900 mBar vacuum at room temperature (RT). A PDMS mould of a glass slide was prepared by covering the slide with PDMS solution, degassing under vacuum (RT 30 mins

900 mBar), and curing at 100 °C for 1 h. This formed a PDMS well of approximately 1 x 25 x 75 mm into which sugar solutions were pipetted and dehydrated for 48 h to form sheets of sugar glass. Samples were stored under vacuum in a desiccation chamber before analysis. The samples were manually sectioned transversely and sputter coated with gold prior to visualisation using scanning electron microscopy (SEM; Philips XL-20, Philips, Eindhoven, The Netherlands) (Fraenkel et al. 2006).

2.3.2.4 Thermal characterisation of sugars

Unprocessed sugars and solid sugar films of 100 % TRA, 100 % SUC and TRA/SUC 75:25 $\%^{w}/_{w}$ (prepared as described in section 2.3.2.3) were analysed by differential scanning calorimetry (DSC; Perkin-Elmer Series 7). Samples (approximately 10 mg) in crimped aluminium pans were heated between 20 and 220 °C at a rate of 10 °C min^{-1}. Samples of 5 mg were further analysed by thermogravimetric analysis (TGA; Perkin-Elmer Series 7) in a platinum pan between 20 and 220 °C at a heating rate of 10 °C min^{-1} (Fraenkel et al. 2006). The content of water within each sample was inferred by measuring the percentage weight loss of the sample at the end of the heating sequence.

2.3.2.5 Powdered X-ray diffraction analysis of sugars

Sugar films were prepared, as described in section 2.3.2.3 and stored in sealed centrifuge tubes under desiccation until analysis. Samples were ground using a pestle and mortar to produce a powder and mounted into a sample cell. The sample cell was placed inside the vacuum chamber of a Nanostar™ (Bruker AXS, Germany) and an X-ray beam was produced by a Kristalloflex 760 X-ray generator (Bruker AXS, Germany). The beam was focussed using two cross-coupled Göbel mirrors and then reduced in size via a series of three pinholes to produce an X-ray beam of 0.4 x 0.8 mm, with a wavelength of 0.154 nm. Each sample was analysed at two different sample to detector path lengths, 4 and 22 cm, and the main X-ray beam was passed through each sample cell for 6 h. The X-ray scatter pattern from the sample was collected using a HiStar gas filled detector and an air background image was also collected.

2.3.2.6 Single crystal X-ray diffraction analysis of sugars

Unprocessed sugars and solid sugar films of 100 % TRA, 100 % SUC and TRA/SUC 75:25 $\%^{w}/_{w}$ (prepared as described in section 2.3.2.3) and then filtered through a 0.2 µm filter, were

analysed by single crystal X-ray diffraction. Unprocessed sugars were mounted onto wire loops and placed onto metal stubs for analysis. Sections of sugar film were mounted directly onto the metal stubs using molten wax. Data from the samples were measured on a Rigaku R-Axis IV image plate mounted on a Rigaku Ru300 rotating anode generator (wide-focus, 50 kV, 100 mA) using graphite-monochromated CuKα radiation (1.54 angstrom wavelength) with Osmic mirrors.

2.4 Results and discussion

2.4.1 Sugar glass fabrication

The formation of sugar glasses has been well described and there are a variety of methods for producing these materials. A number of different methodologies were considered for amorphous sugar glass production, and various different methods were explored. In the chosen method, a simple low temperature dehydration technique was utilised to form solid sugar glasses. The rationale behind using this methodology, described in section 2.3.2.1, was that the amorphous material would be required to fill an inverse micromould. Therefore, an amorphous sugar produced by an energetic process, for example crystalline melting or ball milling, would not be suitable for filling such a mould. Creating a sugar solution and dehydrating it to create an amorphous glass, as described by Wright et al. (Wright et al. 2002), was seen as an attractive option for filling these moulds.

Solutions of individual sugars and sugar alcohols, and binary combinations of these, were dehydrated to determine those that formed solid sugar glasses and those that crystallised, as shown in Figure 2.4.

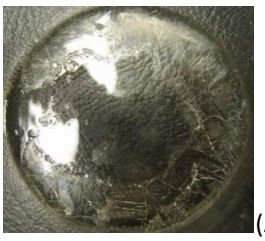 (A)
 (B)
 (C)
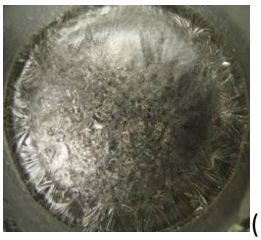 (D)
 (E)
 (F)
 (G)
 (H)
 (I)
 (J)
 (K)
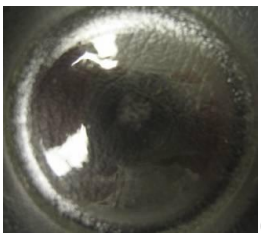 (L)
 (M)
 (N)
 (O)

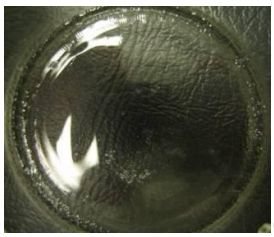 (P)  (Q) 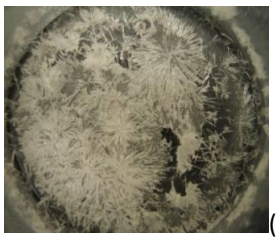 (R)

 (S)

Figure 2.4 Images of dehydrated solid sugar products.

Macro photographic images of sugars following dehydration. (A) D - trehalose anhydrous (TRA), (B) D (+) - trehalose dihydrate (TRD), (C) D - mannitol (MAN), (D) D (+) - sucrose (SUC), (E) TRA/MAN 25:75 $\%^{w}/_{w,}$ (F) TRA/MAN 50:50 $\%^{w}/_{w,}$ (G) TRA/MAN 75:25 $\%^{w}/_{w,}$ (H) TRD/MAN 25:75 $\%^{w}/_{w,}$ (I) TRD/MAN 50:50 $\%^{w}/_{w}$, (J) TRD/MAN 75:25 $\%^{w}/_{w}$, (K) TRA/SUC 25:75 $\%^{w}/_{w,}$ (L) TRA/SUC 50:50 $\%^{w}/_{w,}$ (M) TRA/SUC 75:25 $\%^{w}/_{w,}$ (N) TRD/SUC 25:75 $\%^{w}/_{w,}$ (O) TRD/SUC 50:50 $\%^{w}/_{w,}$ (P) TRD/SUC 75:25 $\%^{w}/_{w,}$ (Q) SUC/MAN 25:75 $\%^{w}/_{w,}$ (R) SUC/MAN 50:50 $\%^{w}/_{w,}$ (S) SUC/MAN 75:25 $\%^{w}/_{w}$.

Each of the solutions containing single sugars crystallised upon dehydration, as shown in Figures 2.4 (A) – (D). This was unsurprising given that crystallisation occurs when sugar solutions of pure sugars are evaporated slowly at low or ambient temperatures (Wright et al. 2002). Where a sugar combination consisted of two sugar molecules of approximately the same molecular weight however, for example two disaccharides, a stable solid sugar glass could be formed (Fraenkel et al. 2006) (see Appendix 2); TRA/SUC 75:25 $\%^{w}/_{w}$, Figure 2.4 (M), TRD/SUC 75:25 $\%^{w}/_{w}$, Figure 2.4 (P), and TRA/SUC 50:50 $\%^{w}/_{w}$, Figure 2.4 (L). Similar observations have been noted by Wright et al. who reported that using a mixture of disaccharides circumvented crystallisation of sugar solutions during evaporation (Wright et al. 2002; Wright et al. 2003). It was speculated that sugar combinations containing molecules of different relative molecular size, for example a disaccharide and a hexose, such as TRA/MAN 50:50 $\%^{w}/_{w}$, Figure 2.4 (F), did not interact during dehydration and therefore co-crystallised (Fraenkel et al. 2006). For example, mixtures containing disaccharides and sugar alcohols failed to form sugar glasses under the same processing conditions. It was speculated that the low Tg of MAN and XYL, 303 and 247 K respectively, hindered the formation of a solid glass under these conditions (Fraenkel et al. 2006). The Tg of these two sugar alcohols is close to ambient temperature and therefore sugar combinations containing these sugars will have lower Tgs (Willart et al. 2006) and hence are less likely to form a stable amorphous state under ambient conditions. Further, sugar combinations containing xylitol, a pentose, did not form a

stable solid product by the end of the dehydration period. This behaviour was attributed to the hygroscopic nature and extremely low Tg of xylitol making the glass unstable at room temperature and humidity (Fraenkel et al. 2006).

As disaccharides appeared to be good candidates for amorphous glass formation, another disaccharide, maltose, was investigated. Solutions of maltose, and combinations with other sugars, were dehydrated to observe the glass forming propensity of this sugar.

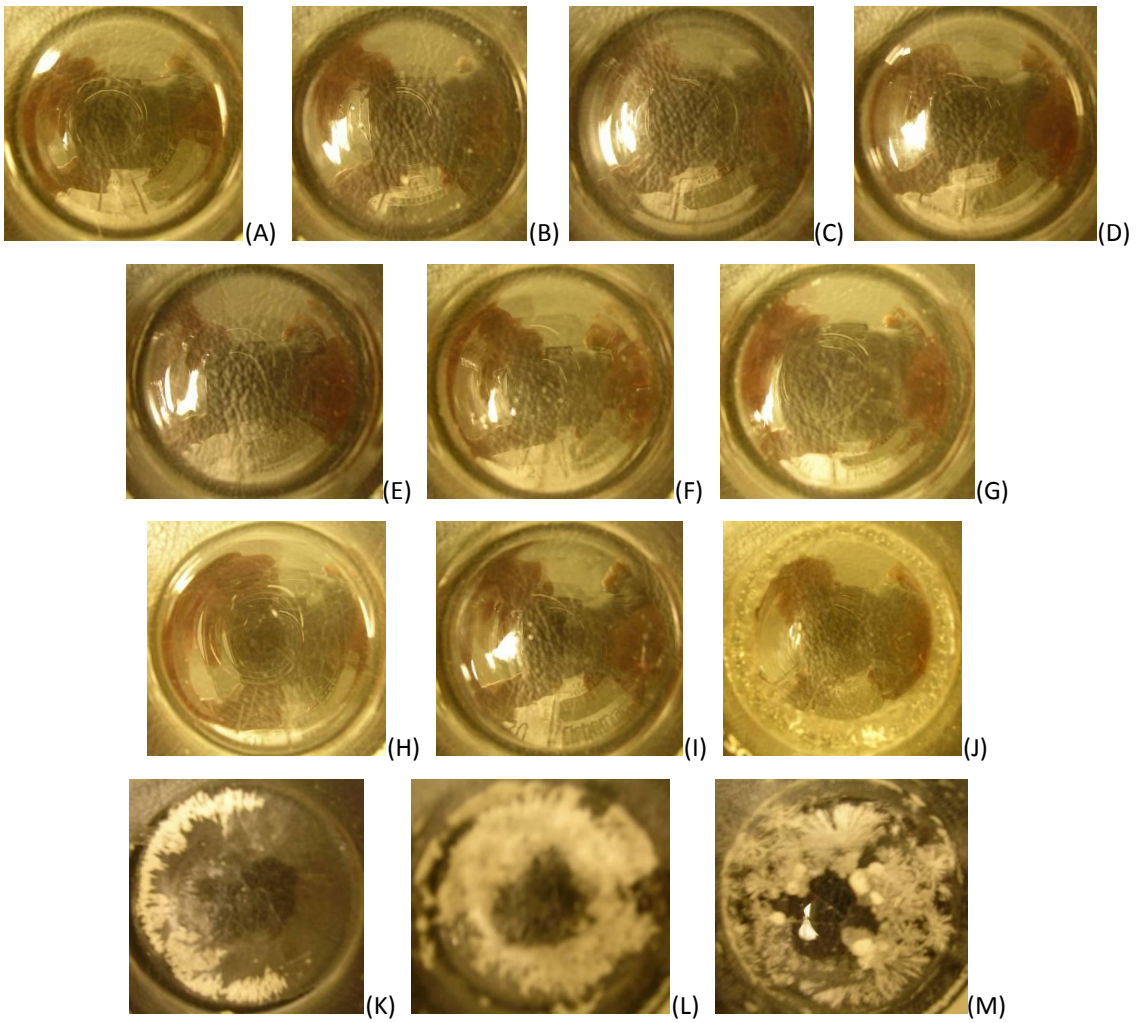

Figure 2.5 Images of dehydrated solid sugar products.

Macro photographic images of sugars following dehydration. (A) D (+)- maltose (MAL), (B) MAL/TRD 75:25 $\%^{w}/_{w}$, (C) MAL/TRD 50:50 $\%^{w}/_{w}$, (D) MAL/TRD 25:75 $\%^{w}/_{w}$, (E) MAL/TRA 75:25 $\%^{w}/_{w}$, (F) MAL/TRA 50:50 $\%^{w}/_{w}$, (G) MAL/TRA 25:75 $\%^{w}/_{w}$, (H) MAL/SUC 75:25 $\%^{w}/_{w}$, (I) MAL/SUC 50:50 $\%^{w}/_{w}$, (J) MAL/SUC 25:75 $\%^{w}/_{w}$, (K) MAL/MAN 75:25 $\%^{w}/_{w}$, (L) MAL/MAN 50:50 $\%^{w}/_{w}$, (M) MAL/MAN 25:75 $\%^{w}/_{w}$.

As shown in Figure 2.5 (B) – (I), the majority of sugar combinations containing MAL, and even pure MAL, Figure 2.5 (A), appeared to form a solid amorphous product following dehydration. Once more, sugar combinations containing MAL and a sugar alcohol did not form a glassy product, Figure 2.5 (K) – (M). This supported the data shown in Figure 2.4, and further suggested that only certain combinations of disaccharides would form amorphous phases following this method of sugar glass formation.

2.4.2 Determination of residual water content of sugar glasses

To maintain optimal functionality of macromolecular cargo contained within the matrix of a SG, processing temperatures should be kept low. Prior to the formation of a vitrified glass, heat labile medicaments will not be adequately protected, which is particularly critical for many proteins whose functionality is dependent upon the working temperature that they are exposed to. For example, enzymes will, at certain processing temperatures, denature and lose their three dimensional conformation and hence their functionality. For example, β-galactosidase has been shown to be stable up to 55 °C (Yoshioka et al. 2003) whilst it denatures at temperatures over 70 °C (Ladero et al. 2006; Yoshioka et al. 2003). Therefore, it was hypothesised that such an enzyme would be more stable in a sugar glass formed at 50 °C rather than at 60 °C.

As the water content of sugar glasses is a key parameter governing the structure and stability of the material, this study compared the residual quantity of water remaining within sugar glasses created at both 50 and 60 °C.

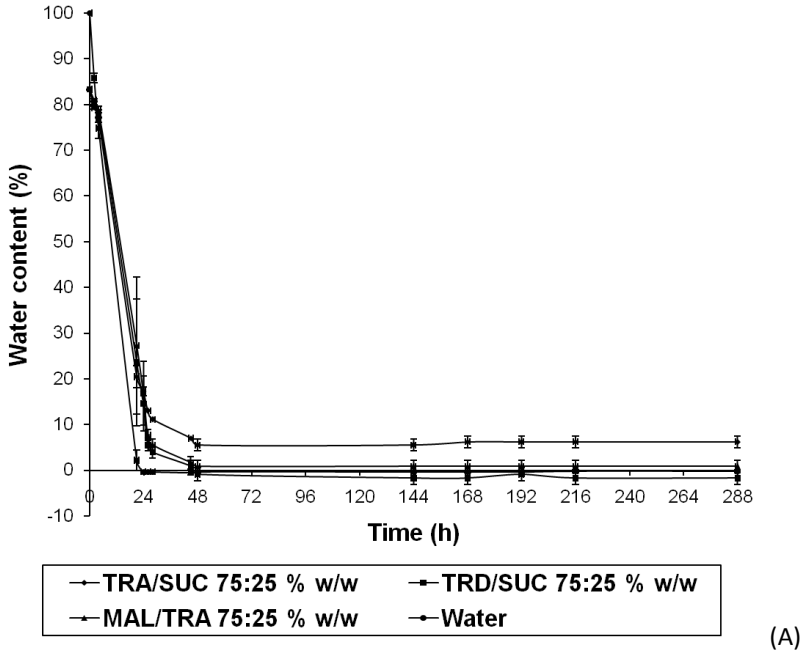

(A)

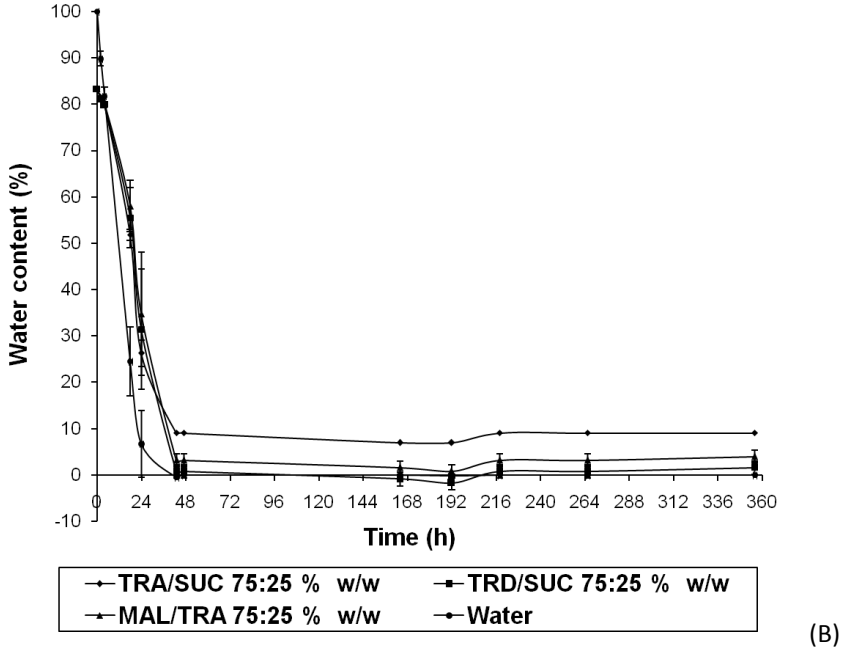

(B)

Figure 2.6 Analysis of water content in sugar solutions.

Sugar solutions were dehydrated at ambient temperature for 24 h then at, (A) 60 °C until 144 h or (B) 50 °C until 192 h. After 144 or 192 h, solid sugar glasses were maintained under ambient conditions until 288 or 356 h respectively. Changes in sample weight upon dehydration and storage were used to determine water content. Data presented as mean ± standard deviation (S.D.) (n=3).

Figure 2.6 shows the change in water content of three different sugar solutions with dehydration time, at both 50 and 60 °C. For all sugar solutions the majority of water loss occurred during the first 24 h. A further 24 h of dehydration at elevated temperature removed

the remaining water to leave a solid glass. This was the case for sugar solutions dehydrated at both 60 °C, Figure 2.6 (A), and 50 °C, Figure 2.6 (B). However, the weight of all the sugar glasses decreased slightly between 48 and 192 h whilst maintained at 50 °C, Figure 2.6 (B). This was not observed to such an extent in the sugar glass solutions treated at 60 °C, where the minimum water content was achieved by 24 h in the heated oven, Figure 2.6 (A). Following re-introduction into ambient conditions, the weight of each of the sugar glasses increased marginally, returning to the levels observed at 48 h (Fraenkel et al. 2006). This was expected as sugar glasses have a hygroscopic nature (Dittmar 1935).

It was deduced that any residual water remaining within the glass at this point must be intrinsically associated with the material and therefore not able to be removed. Under both conditions explored, it was apparent that the TRA/SUC 75:25 $\%^{w}/_{w}$ sugar glass retained approximately 9 $\%^{w}/_{w}$ water in its structure at 48 h. In comparison, the TRD/SUC 75:25 $\%^{w}/_{w}$ and MAL/TRA 75:25 $\%^{w}/_{w}$ glasses both contained negligible quantities of water in the solid glass state. It was speculated that the additional water retained in the TRA/SUC 75:25 $\%^{w}/_{w}$ sugar glass was due to the association of 2 moles of water to each TRA molecule to form the dihydrate sugar. This weight increase was not observed in the TRD/SUC 75:25 $\%^{w}/_{w}$ glass as the trehalose molecule was fully hydrated before dissolution (Fraenkel et al. 2006).

It was not obvious why the sugar solutions would behave differently during storage following production at either 50 or 60 °C. One possible explanation could have been that the residual water content of the sugar glasses formed at 50 °C was marginally greater than the residual water content of the sugar glasses formed at 60 °C. It is known that water can affect the stability of amorphous materials, for example, it has been shown to have a plasticising effect on glasses, (Lai et al. 1999). Therefore, the increased quantity of water within each of the glasses formed at 50 °C could have increased the propensity of the glass to adsorb water following removal from the oven and subsequent storage under ambient conditions. Importantly, however, even though the water content was seen to increase in these glasses, the macroscopic structure of the glasses remained the same. There was no obvious crystallisation of the sugars, or a change towards the rubbery state of the material, and so it was concluded that the two different production temperatures did not have a significant effect on the overall properties of the glasses formed.

2.4.3 Scanning electron microscopy of sugar glass films

To support the data obtained in Figures 2.4 and 2.5 the solid sugar products were further examined under SEM, Figure 2.7.

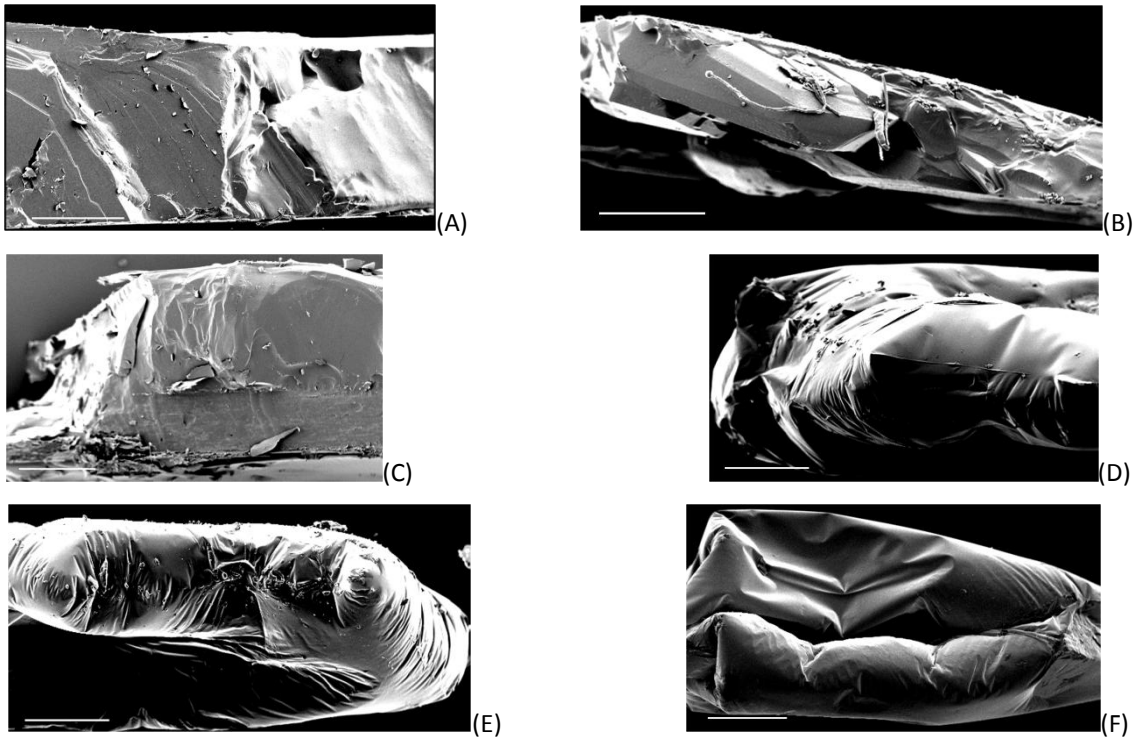

Figure 2.7 Scanning electron micrographs of transverse sections of dehydrated sugar films.

(A) 100 % TRA, (B) 100 % SUC, (C) 100 % TRD, (D) 100 % MAL, (E) TRA/SUC 75:25 $\%^{w}/_{w}$, (F) TRD/SUC 75:25 $\%^{w}/_{w}$ (Bar = 500 µm) (n = 1).

The solid mass formed from dehydrated single sugars TRA, SUC and TRD suggested an ordered structure of crystalline nature when transversely sectioned, Figures 2.7 (A) – (C) (Fraenkel et al. 2006). In contrast, SEM images of solid sugar transverse sections formed from pure MAL and combination sugars TRA/SUC 75:25 $\%^{w}/_{w}$ and TRD/SUC 75:25 $\%^{w}/_{w}$, Figures 2.7 (D), (E) and (F) respectively, were shown to form a non-crystalline mass providing no evidence of order. It was interesting to note that pure MAL, Figure 2.7 (D), appeared to have a structure more closely related to that of the combination sugars, Figure 2.7 (E) and (F), than the other single sugar samples. This data supported earlier visual studies where pure MAL solution appeared to form an amorphous sugar glass following dehydration, Figure 2.5 (A), following dehydration. It was not obvious why pure MAL should behave in this way, but this data began to suggest a correlation between the visual appearance of a sugar product following dehydration, and its physical properties. If a sugar product appeared to be glassy and transparent following dehydration, then under SEM the product looked distinctly different to a solid crystalline mass and hence this suggested an amorphous nature of the material. However, what was not clear

was whether the materials formed by the sugar combinations and MAL were less ordered through their amorphous structure or were more prone to melting under the electron beam. Nevertheless, these data support the utility of this simple dehydration methodology to form sugar glasses from selected sugar solutions (Fraenkel et al. 2006).

2.4.4 Thermal characterisation of sugars

To probe the nature of pure sugar and promising sugar glass forming combinations, the materials were further analysed by differential scanning calorimetry (DSC) and thermogravimetric analysis (TGA). The DSC scan of a pure TRA dehydrated film is characterised by two sharp endotherms with peaks at 101 and 214 °C with a third more poorly defined endothermic region between 130 and 150 °C, Figure 2.8 (A). The weight loss profile with temperature (TGA) for the same material is superimposed in Figure 2.8 (A) and shows a total weight loss of approximately 10 $\%^{w}/_{w}$ over the heating range. It was observed that the water loss was greatest over the temperature range 90 – 140 °C and hence the endothermic peaks observed over this range correspond to dehydration of the dihydrate crystal. Once water was removed from the sample this left the anhydrous sugar which melted at approximately 214 °C, correlating with literature values for the melting point of the anhydrous trehalose crystal at 210.5 °C (Higashiyama 2002). This suggested that the hydrated form of the sugar was formed during the process and that residual water remained within the glass following dehydration (Fraenkel et al. 2006). We speculate that this residual water was bound to the trehalose molecule within the amorphous structure and hence would not be available for reaction. This concept is supported by the work of Surana et al. where they suggest that amorphous trehalose prepared by dehydration may possess residual structural history of the hydrate from which it was formed (Surana et al. 2004).

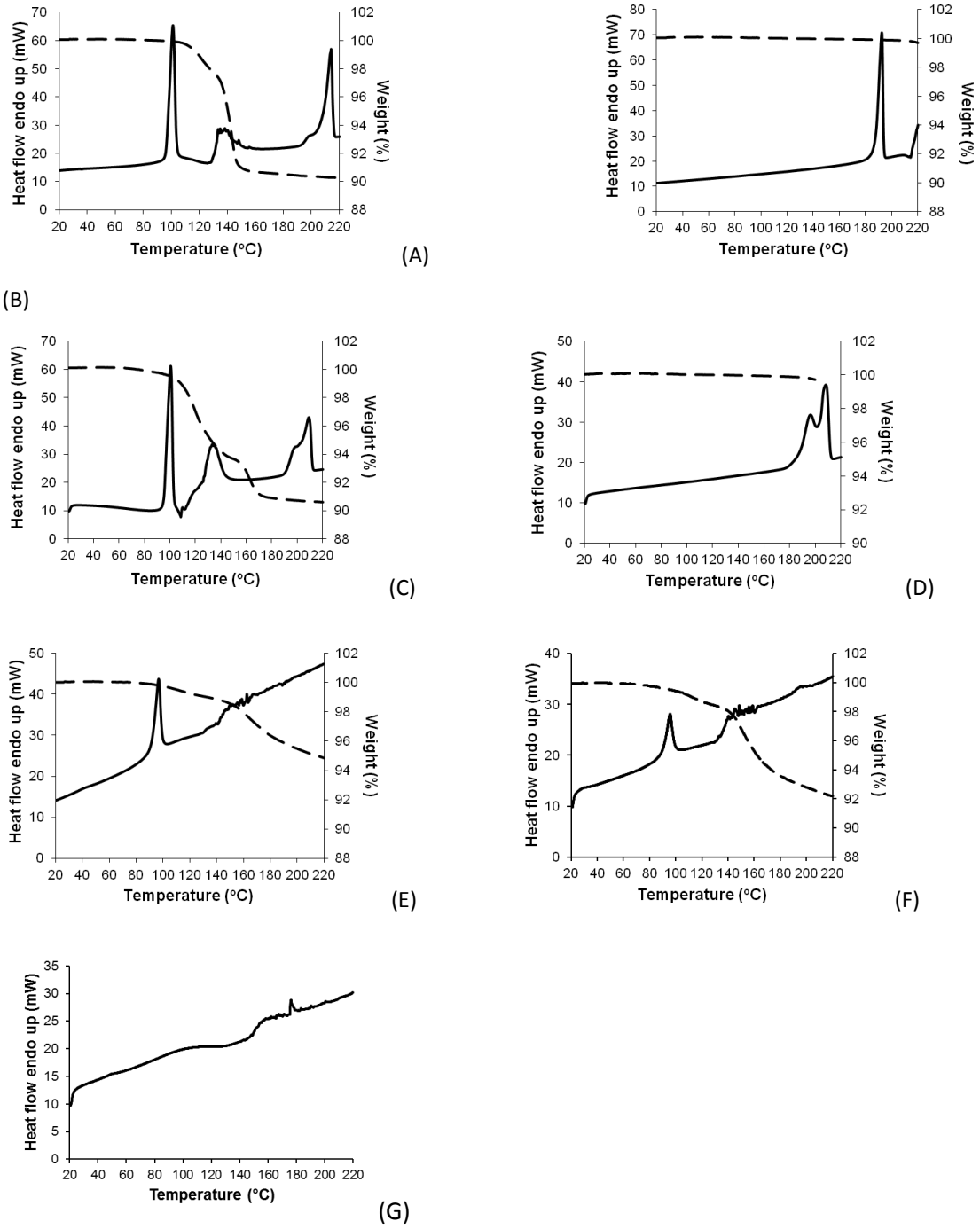

Figure 2.8 Thermal characterisation of solid sugar films.

DSC (solid line) and TGA (dashed line) profiles of unprocessed and dehydrated sugars. (A) 100 % TRA dehydrated sugar film, (B) 100 % SUC dehydrated sugar film, (C) unprocessed TRD, (D) unprocessed TRA, (E) TRA/SUC 75:25 % $^{w}/_{w}$, (F) TRD/SUC 75:25 % $^{w}/_{w}$, (G) TRA/SUC 75:25 % $^{w}/_{w}$ (following 1 month desiccated storage) dehydrated sugar films.

The profiles shown in Figure 2.8 (C) and (D) show the DSC and TGA scans of unprocessed TRD and TRA powder respectively. Unprocessed TRA, Figure 2.8 (D), showed a distinctly different thermal profile to the dehydrated TRA film, Figure 2.8 (A), which showed only a single melting

endotherm at approximately 200 °C, corresponding to melting of the trehalose crystal. As a corollary, no weight loss was observed through the temperature range, indicating that no water was present in the sample. Unprocessed TRD, Figure 2.8 (C), however, displayed endothermic peaks and respective weight losses at approximately the same temperatures as the dehydrated TRA film, further indicating that TRD was formed following dehydration of aqueous TRA solution (Fraenkel et al. 2006; Surana et al. 2004). The thermal profile of pure SUC dehydrated film, Figure 2.8 (B) suggested that no residual water content was contained within the structure. This was demonstrated by the single endothermic peak observed at 191 °C, attributed to melting of pure SUC crystal, and no evidence of weight loss by TGA (Fraenkel et al. 2006). Figure 2.8 (E) shows DSC and TGA scans of TRA/SUC 75:25 $\%^{w}/_{w}$ dehydrated film. This film appeared to have a more complex nature than the individual sugar films. A sharp endothermic peak was observed at 97 °C, corresponding with the loss of water from the sample, but no other discrete thermal events were observed. A poorly defined endothermic region was shown between 130 and 170 °C and a gradual weight loss of the sample was observed from approximately 80 to 220 °C. The thermal behaviour of the TRD/SUC 75:25 $\%^{w}/_{w}$ dehydrated film, Figure 2.8 (F) was shown to be very similar to the TRA/SUC 75:25 $\%^{w}/_{w}$ dehydrated film, Figure 2.8 (E) (Fraenkel et al. 2006), supporting the similar apparent nature of the dehydrated products (see Appendix 2). Although there was no evidence of a distinct endothermic step in the heat flow, indicative of a glass transition (Franks 2003), as there were no obvious endothermic peaks at elevated temperatures, it was deduced that these samples were likely to be non-crystalline in nature. In replicate samples, the endothermic peak at 97 °C was not always observed, Figure 2.8 (G), correlating with the duration of storage under desiccation following formation of the glass. However, the key feature in all replicate samples was the absence of endothermic peaks at elevated temperature (Fraenkel et al. 2006).

2.4.5 Powdered X-ray diffraction analysis

To explore the nature of dehydrated sugar glass films further, samples were analysed by powdered X-ray diffraction analysis, Figure 2.9. In this analysis, samples that demonstrated areas of crystallinity showed distinct dark spots within the diffraction pattern, for example, Figure 2.9 (B). As a camera length of 22 cm was used this method detected the presence of longer range order within the material, from 0.22 to 300 nm.

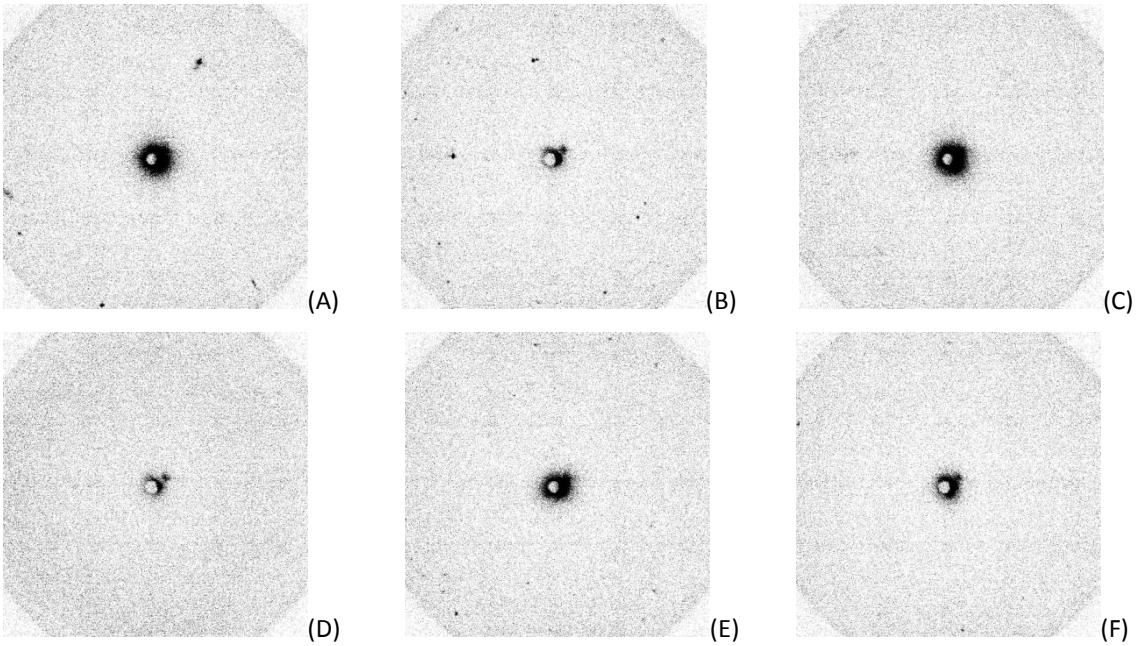

Figure 2.9 Powdered X-ray diffraction analysis of dehydrated sugar films using a 22 cm camera.

(A) 100 % TRA, (B) 100 % SUC, (C) 100 % TRD, (D) 100 % MAL, (E) TRA/SUC 75:25 % $^{w}/_{w}$, (F) TRD/SUC 75:25 % $^{w}/_{w}$ (n = 1).

As shown in Figure 2.9 the pure sugar dehydrated films TRA and SUC appeared to show distinct areas of crystallinity in their structure, Figures 2.9 (A) and (B) respectively. This supported previous findings suggesting that individual sugars formed solid crystalline masses following dehydration, Figures 2.4, 2.7 and 2.8. However, in this study pure TRD dehydrated film, Figure 2.9 (C), did not appear to demonstrate a crystalline nature. This was in contrast to previous findings, Figures 2.4 (B) and 2.7 (C), which appeared to show that the TRD film had a crystal structure.

In support of previous studies, the pure MAL dehydrated film, Figure 2.9 (D), appeared to have a non-crystalline nature, denoted by the absence of dark spots in the diffraction pattern. This behaviour was partly observed within the TRA/SUC 75:25 %$^{w}/_{w}$ and TRD/SUC 75:25 %$^{w}/_{w}$

dehydrated films, Figures 2.9 (E) and (F) respectively, where a blank diffraction pattern was generally observed. However, in both Figures 2.9 (E) and (F) there was evidence of some small dark spots within each diffraction pattern. This suggested that these combination sugar films had some evidence of crystallinity within their structure. In a similar manner to the pure TRD film, this result was in contrast to prior studies, Figures 2.4, 2.7 and 2.8. Where dehydrated films formed from sugar combination solutions appeared to form an amorphous solid with no evidence of crystallinity.

To investigate the short range order, up to 0.22 nm, within these materials they were viewed at a sample to camera length of 4 cm, Figure 2.10. From these scatter patterns it appeared that over shorter ranges of measurement pure TRA, TRD and TRA/SUC 75:25 $\%^{w}/_{w}$ dehydrated films were X-ray amorphous, Figures 2.10 (A), (C) and (E) respectively. In this analysis, it appeared once more that pure TRD film, Figure 2.10 (C), and in this case only pure TRA dehydrated film, Figure 2.10 (A), demonstrated an absence of crystallinity which was in contrast to previous findings. Interestingly, the diffraction patterns of pure MAL and TRD/SUC 75:25 $\%^{w}/_{w}$ dehydrated films suggested order within the material over a shorter range. Once again this behaviour had not been indicated by previous studies conducted on these materials.

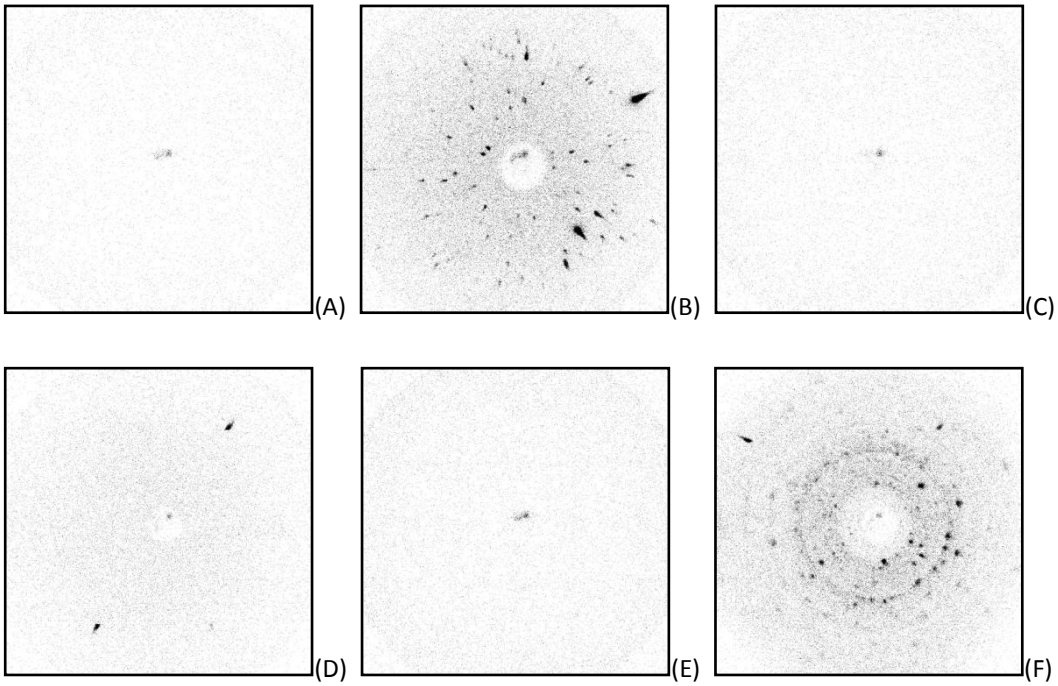

Figure 2.10 Powdered X-ray diffraction analysis of dehydrated sugar films using a 4 cm camera.

(A) 100 % TRA, (B) 100 % SUC, (C) 100 % TRD, (D) 100 % MAL, (E) TRA/SUC 75:25 % $^{w}/_{w}$, (F) TRD/SUC 75:25 % $^{w}/_{w}$ (n = 1).

As discovered during thermal analysis studies, it appeared that the nature of these dehydrated sugar materials was not straightforward. As stated in section 2.1, both the formation methodology and subsequent storage conditions can affect the nature of amorphous materials (Willart and Descamps 2008). Therefore, the contrasting data obtained in this study could be explained by a number of factors including the duration between sugar film formation and preparation of the sample for analysis. Samples were sent away for analysis and storage instructions were given. However, the exact conditions and duration of storage of these samples prior to analysis were unknown; hence this may have had an effect on the results obtained. For example, if samples had been exposed to humid or elevated temperature storage conditions prior to analysis, this may have induced crystallinity within samples. Conversely, it is known that powdering or milling a sample can induce amorphous behaviour (Nagahama and Suga 2002) within a sample due to the shear forces involved. This may have been a factor within the pure TRD sample, for example, where the sample appeared to be amorphous in these X-ray studies.

2.4.6 Single crystal X-ray diffraction analysis

To develop and explore the powder X-ray diffraction analysis in section 2.4.5, samples were analysed by single crystal X-ray diffraction analysis. In this methodology no powdering of the sample was required before analysis. The diffraction patterns of various different sugars are shown in Figure 2.11.

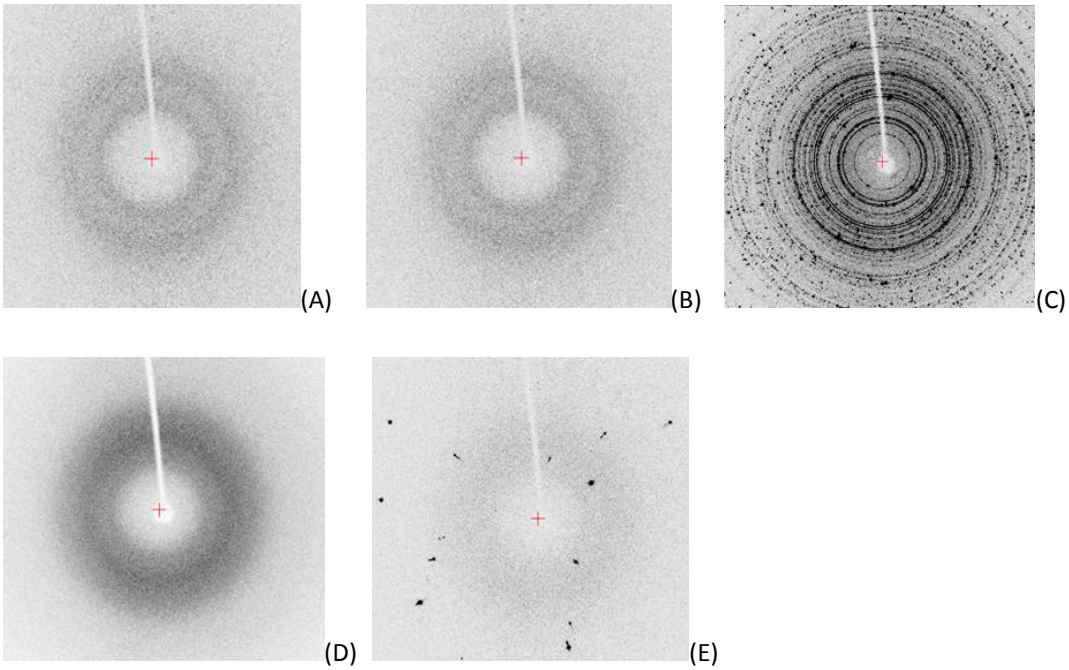

Figure 2.11 Single crystal X-ray diffraction analysis of sugar samples.

(A) 100 % SUC dehydrated film, (B) 100 % SUC solution, (C) 100 % SUC powder, (D) TRA/SUC 75:25 % $^{w}/_{w}$ dehydrated film (glass like part), (E) TRA/SUC 75:25 % $^{w}/_{w}$ film (crystal part), (n = 1).

As an altered method was used in this experiment, specifically the filtering of sugar solutions via a 0.2 µm filter before dehydration, it appeared that an amorphous pure sucrose material was produced, Figure 2.11 (A). It was speculated that the filtering process removed any particulates that may have acted as nucleation agents for crystallisation. This was confirmed by the control solution of pure SUC solution, Figure 2.11 (B), which showed a similar "amorphous" structure to the SUC dehydrated film. In contrast, pure SUC powder, Figure 2.11 (C), demonstrated a purely crystalline scattering pattern. However, the diffraction pattern obtained from the TRA/SUC 75:25 %$^{w}/_{w}$ sugar film showed two distinctly different profiles in this experiment. From visual observations, it was noted that within this sugar film there were two distinct areas within the sample. The majority of the sample was optically transparent and appeared to be amorphous however there was one area where discrete crystals were observed. By orientating the sample within the X-ray beam it was possible to

analyse both areas of the material. As Figure 2.11 (D) shows, where the transparent part of the material was analysed, the structure of the material appeared to be amorphous. However, when the crystalline portion was analysed, Figure 2.11 (E), the scattering pattern confirmed that this section of the material contained order within its structure.

These observations were encouraging as they confirmed that previous conclusions drawn from early visual data obtained in Figures 2.4 and 2.5 were likely to be correct. If a sugar combination appeared to be glassy and transparent, then it was likely to be amorphous, whereas if crystals were observed in the dehydrated product then it was likely to be crystalline.

2.5 Conclusion

The aim of this first chapter of work was to produce amorphous sugar glass materials via a low-temperature fabrication technique. Hence, certain routes to amorphisation were not applicable, for example, quenching of the crystalline melt. The rationale for this was twofold. Firstly, it was speculated that a low temperature methodology would produce sugar glasses that would be capable of incorporating heat labile medicaments and delicate macromolecules within their structure. Secondly, it was necessary for the amorphous material to conform into the geometry of a microneedle array. Therefore, the dehydration of a solution method to achieve amorphisation was appealing as it provided the possibility to address both these issues.

It appeared from early studies that a combination of two disaccharides in solution would be optimal to produce an amorphous material via this slow dehydration method. However, it appeared that particulate matter in solution could still act as a nucleation agent and cause regions of crystallisation during dehydration. Amorphous sugar glasses formed by this technique were shown to have a complex nature and they did not appear to demonstrate all the classical features of a glassy system. However, it was found that where a particular dehydrated sugar product appeared to be transparent and amorphous the system displayed an absence of crystal melting or X-ray scattering behaviour; both characteristics of an amorphous phase. This suggested that such systems may be suitable for future incorporation of unstable compounds and fabrication of biodegradable microneedle structures.

Chapter 3

Optimisation of micromoulding technique for biodegradable sugar glass microneedle array fabrication

3 Optimisation of micromoulding technique for biodegradable sugar glass microneedle array fabrication

3.1 Introduction

3.1.1 Development of micromould fabrication approaches

Arrays of solid MNs have demonstrated effectiveness at enhancing delivery of model compounds across the skin barrier. However, their usage poses a number of potential problems. Silicon is not an FDA-approved biomaterial and therefore may cause regulatory and safety concerns. Furthermore, broken silicon or metal MNs could cause skin problems if left *in situ* in the body. Solid non-coated MNs also require a two-step application process whereby MNs are applied in a separate process to the dosage form, which is undesirable. Finally, accurate coating of MNs is not straightforward and these devices only deliver a very small amount of drug as a bolus dose (Prausnitz 2004). Therefore, micromoulding has become a commonplace methodology to prepare biodegradable MN structures with three dimensional structures. Some of the earliest reports of micromoulding processes by McAllister et al. include those utilising silicon, metal and polymer micromoulds. Briefly, silicon moulds were made by direct etching of silicon wafers to produce cylindrical holes within the wafer. Metal micromoulds were prepared by electroplating onto solid silicon MN master structures before removal of the master by reactive ion etching (McAllister et al. 2003). Polymer moulds were produced by coating a layer of PDMS over silicon or polymer master structures and curing. This later technique is a low-cost, repeatable methodology which is now widely used by many workers (Gittard et al. 2009; McAllister et al. 2003; Park et al. 2005, 2006; Sullivan et al. 2008; Xueqiu et al. 2010). A similar approach has been adopted subsequently where a female master micromould is etched from SU-8 epoxy photoresist by UV exposure before a male MN master is fabricated from PDMS. The male master structure is then sputter coated with a thin layer of gold before a second layer of PDMS is coated onto the surface to form an inverse mould (Chu et al. 2010; Lee et al. 2008; Park et al. 2007). Alternatively, other groups have fabricated metal micromoulds by etching the inverse shape of an array of MNs into a solid metal casting mould (Kolli and Banga 2008; Miyano et al. 2005). More recently, a silicone micromould has been reported whereby micromould templates were prepared on the surface of silicone sheets using a galvanometer-based laser-machine tool. Computer-aided design files were employed to control the laser milling process and therefore invaginations with varying base diameter, height and interspacing could be produced (Donnelly et al. 2011). This sophisticated process allows much greater control over the geometry of the resulting MN structures produced. However, the most straightforward and commonly utilised methodology

for creating inverse micromoulds for biodegradable MN manufacture remains the formation of a PDMS micromould from a solid master structure. In this context, it was determined that generation of PDMS against silicon MN master structures would be employed to fabricate SGMN arrays.

3.1.2 Micromoulding of microstructures

Once a micromould has been formed it is filled with the desired material to form replicate MN structures. Various groups have explored different techniques to prepare and fill such moulds. Metal MNs formed by McAllister et al. were prepared by an electrodeposition methodology whereby a nickel layer was deposited onto polymer or silicon micromoulds (McAllister et al. 2003). Synthetic slow-degrading polymer MNs have been prepared by melting polyglycolic acid (PGA), polylactic acid (PLA) or poly-lactide-co-glycolide (PLGA) and using vacuum to draw the melt into the mould (Chu et al. 2010; McAllister et al. 2003; Park et al. 2005, 2006) whilst Takano et al. fabricated polyethylene glycol (PEG) MNs by melting powdered PEG into a micromachined die (Takano et al. 2009). A similar methodology has been utilised to form natural silk fibroin MNs. Here a heat pre-treated fibroin solution was poured into the PDMS micromould, degassed under vacuum, and fan-dried for 24 h at room temperature to form solid MNs (Xueqiu et al. 2010). Alternatively, Park et al. utilised synthetic polymer microparticles, with and without drug encapsulated, to fill micromoulds. The microparticles were packed into the mould and either heated or ultrasonically welded to fuse the particles into MN geometries (Park et al. 2007). This technique permitted greater control over MN design, and allowed fabrication of structures with a complex geometry created from multiple materials using milder processing conditions (Park et al. 2007).

Another approach to forming polymeric MNs is to use centrifugal force to aid filling of the inverse micromould with a viscous material (Donnelly et al. 2011; Donnelly et al. 2009a; Lee et al. 2008). For example, Lee et al. utilised concentrated hydrogels of ultra-low viscosity carboxymethylcellulose (CMC), amylopectin and bovine serum albumin (BSA) deposited onto female micromoulds and placed into a 45 ° angled rotor at an elevated temperature. This process formed the hydrogel mixture into the mould, whilst removing residual solvent from the formulation, to form a solid MN array containing conical or pyramidal MN arrays (Lee et al. 2008). Chu et al. used a combination of vacuum at room temperature followed by centrifugation to prepare MNs formed from 30, 40 and 50 $\%^{w}/_{w}$ blends of polyvinyl alcohol (PVA) and polyvinylpyrrolidone (PVP) (Chu et al. 2010).

A number of workers have fabricated natural polymer MNs by creating dense "glue" solutions. These solutions contain a drug, including both small and large molecular weight moieties, and a polymer, such as chondroitin sulphate or dextran, which is compressed and dried into a micromould under the pressure of a steel plate (Fukushima et al. 2011; Ito Y. et al. 2010a; Ito Y. et al. 2010b). In a similar manner, solid state biodegradable microstructures have been formed by mixing drug powders into polymer / excipient solutions containing PVA, trehalose, maltitol and hydroxypropyl-β-cyclodextrin in PBS. These solutions were spread over the surface of a silicone female micromould and briefly pressurised before drying at slightly elevated temperature for 1 h. A backing layer consisting of Eudragit® E PO solution in alcohol was pipetted on top of the dried drug formulations before final pressurising and drying at elevated temperature (Wendorf et al. 2011).

Alternative approaches include polymerisation of polymers within the micromould itself. For example, Sullivan et al. used a liquid monomer of vinyl pyrrolidone and the free-radical initiator azobisisobutyronitrile applied to the mould surface. Vacuum pressure was used to draw the solution into the mould before UV light was employed to photo-polymerise the polymer *in situ* (Sullivan et al. 2008). A similar methodology was utilised by Gittard et al. where a monomer of eShell 200 polymer was used as the starting material (Gittard et al. 2009). Solid maltose MNs have been fabricated by forming a maltose candy and casting the material into metal micromoulds at elevated temperature (Kolli and Banga 2008; Miyano et al. 2005). Finally, Lee et al. recently proposed a sophisticated methodology of forming solid maltose MNs whereby a stepwise controlled drawing lithography of a viscous solution of melted maltose monohydrate yielded tapered conical shape MNs with varying lengths (Lee et al. 2011b).

As stated, there are now a number of different approaches to forming biodegradable MN structures using a variety of methodologies. Accordingly, the main focus of this chapter of work was to investigate and optimise a robust micromoulding technique to reliably fabricate SGMN arrays using the low temperature method developed in Chapter 2.

3.1.3 Advantages and disadvantages of biodegradable microneedle fabrication techniques

As discussed above, there are now many different approaches to forming replicate MN devices from master structures. Each approach has its own benefits and drawbacks and therefore

different micromoulding techniques are used for different applications. For example, earlier methodologies employing high temperature melting of synthetic polymers (Park et al. 2005) and powdered maltose (Miyano et al. 2005) into a micromould were found to produce robust MN structures. However, neither group attempted incorporation of labile medicaments within the matrices of the arrays. More recently, workers found that incorporation of both small molecular weight drug and macromolecular protein during melt processing of galactose powder to form MNs involved substantial drug losses due to temperature elevation (Donnelly et al. 2009a).

Therefore, many attempts have been made to form biodegradable MN structures using methodologies involving lower processing temperatures. An increasingly popular technique is the use of centrifugation to fill micromoulds with a viscous polymeric material (Chu et al. 2010; Donnelly et al. 2011; Donnelly et al. 2009a; Lee et al. 2008). This methodology provides the potential for drug incorporation within different portions of the MN array, to facilitate bolus or sustained release. However, elevated temperatures are often still required for the initial formation of viscous solutions and removal of residual solvent which may potentially damage incorporated drug cargo. It has also been found that polymeric CMC MNs having the same dimensions as master silicon or metal MNs do not possess sufficient mechanical properties for skin insertion and therefore require a reduction in needle aspect ratio (Lee et al. 2008). A critical objective of this chapter was to investigate the skin insertion capabilities of SGMNs with the same geometry as the silicon MN master structures.

To try and address these fabrication issues, novel approaches have included the photopolymerisation of liquid monomers *in situ* within the micromould itself (Gittard et al. 2009; Sullivan et al. 2008). These systems easily lend themselves to segregation of the base and MNs for drug incorporation within different portions of the array. This approach allows flexibility over drug loading and therefore facilitates bolus and / or controlled release depending upon the appropriate indication. As these MNs are formed from synthetic materials, copolymers can be utilised which confer other advantageous properties, for example an increase in mechanical strength (Sullivan et al. 2008). It has also been shown that biological activity of incorporated macromolecules is maintained within these systems (Sullivan et al. 2008). However, there are safety concerns over some larger molecular weight synthetic polymers, such as polyvinyl pyrrolidone, relating to clearance and kidney damage. It has also

been shown that not all the small scale features within MN arrays, such as MN tips, form perfectly (Gittard et al. 2009).

Other workers have investigated single MNs, of millimetre dimensions, formed from thread-forming polymers produced from viscous solutions at ambient temperature (Ito et al. 2006). These MN devices have shown effective delivery of large molecular weight hormone *in vivo*, however they are formed by hand which is a poorly controlled and non-manufacturable process (Sullivan et al. 2008). More recent methodologies utilising a steel plate to dry polymer solutions into micromoulds have permitted the stable incorporation and delivery of macromolecular medicaments *in vivo* (Ito et al. 2010; Ito Y. et al. 2010a). One of the latest references to biodegradable MN fabrication is the formation of PLGA MNs incorporating drug loaded hydrogel particles. When left *in situ* in skin, hydration of the hydrogel particles cause disruption of the MN matrix and controlled release of drug (Kim et al. 2012). This is an attractive approach, but one which still requires further optimisation to eliminate issues of hydrogel toxicity and elevated processing temperatures. As described, each biodegradable MN fabrication technique has its own merits and some methodologies now look very promising, however to date there is not one fully optimised system. Consequently, a novel vacuum-forming methodology will be explored in this chapter to attempt reliable SGMN fabrication.

3.2 Chapter objectives

1. Develop a reliable methodology for forming micromoulds against silicon MN master structures for SGMN fabrication.

2. Investigation of MN fabrication from alternative substrates and potential for generation of micromoulds against these MNs.

3. Investigation of different techniques including vacuum-formation, centrifugation, ultrasonication and compression to micromould biodegradable SGMN arrays.

4. Optimisation of a micromoulding technique for reliable SGMN array fabrication.

5. Qualitative and quantitative assessment and visualisation of the capacity of SGMN arrays generated to penetrate human skin barrier.

3.3 Materials and methods

3.3.1 Materials

All reagents were obtained from Fisher Scientific Ltd. (Loughborough, UK) and were of analytical grade unless stated otherwise.

The silicon MN arrays used in this study were supplied by Tyndall National Institute, Cork, Ireland. Pyramidal MNs were fabricated using wet-etching in potassium hydroxide and subsequent coating with a 0.3 μm layer of platinum (Wilke et al. 2005).

Human breast skin was obtained from the Aneurin Bevan Health Board Royal Gwent Hospital (Newport, Wales, UK) following mastectomy or breast reduction surgery with full ethical committee approval and informed patient consent.

3.3.2 Methods

3.3.2.1 Characterisation of silicon microneedle master arrays

The master MN structures utilised in this study were octagonal pyramid in morphology being approximately 250 μm in length and 200 μm at base width. Arrays were cross illuminated and viewed under light microscope (Olympus BX50, Japan) to confirm uniformity and integrity of the needles. When required, arrays were mounted onto aluminium stubs using adhesive carbon discs and imaged under SEM as described in section 2.3.2.3.

3.3.2.2 Polydimethylsiloxane micromoulding

Polydimethylsiloxane micromoulds were created from master silicon MNs. Silicon arrays were cleaned by ultrasonication in methanol for 10 mins followed by rinsing in fresh methanol and air drying for 10 mins. Pre-mixed, degassed PDMS was added to a well containing the master array, prior to degassing for 30 mins and curing, as described in section 2.3.2.3, to form the mould. The master array was subsequently removed to yield the MN mould. To visualise channels within the micromould, the mould was sectioned transversely and cross illuminated for viewing under light microscope (Olympus BX50, Japan).

3.3.2.3 Initial fabrication of sugar glass microneedle arrays

A 16.7 $\%^{w}/_{v}$ solution of TRA/SUC 75:25 $\%^{w}/_{w}$ was prepared as described in section 2.3.2.1 and 150 μL was pipetted onto the surface of a PDMS micromould. The mould was dehydrated in a

fume cupboard for 24 h at ambient temperature followed by 24 h at 60 °C. The mould was cooled to room temperature and the MN array was removed by hand. The array was viewed under light microscopy (Olympus BH-2, Japan) and then mounted onto an aluminium stub, sputter coated with gold and imaged under SEM as described in section 2.3.2.3.

3.3.2.4 Investigation of standard deposition fabrication methodology

A 16.7 $\%^{w}/_{v}$ solution of TRA/SUC 75:25 $\%^{w}/_{w}$ was prepared as described in section 2.3.2.1. Methylene blue (MB) powder was incorporated at 5 $\%^{w}/_{w}$ of final sugar glass weight. 200 µL of a sugar solution containing 5 $\%^{w}/_{w}$ MB was pipetted onto the surface of a micromould and viewed by digital camera, (Nikon, Coolpix 5600, Japan), and light microscope (Olympus BH-2, Japan). The micromould was then placed into a vacuum oven at 300 mBar for 60 mins to form MNs. The solution was dehydrated, as described in section 2.3.2.1, and the mould was viewed with time to investigate MN formation. Once formed, sugar glass arrays were removed by hand and stored in a vacuum desiccator at room temperature (Fraenkel et al. 2006).

3.3.2.5 Optimisation of novel vacuum deposition methodology

Sugar glass MN arrays were fabricated using an improved vacuum-loading methodology. A micromould was placed into a 100 mL conical vacuum flask. The flask was sealed and held under a vacuum of approximately 100 mBar for various time periods. 200 µL of a 20 $\%^{w}/_{v}$ solution of TRA/SUC 75:25 $\%^{w}/_{w}$ was injected onto the mould surface and the vacuum was then released immediately. The micromould was removed from the vacuum chamber and dehydrated as described in section 2.3.2.1. Once formed, SGMN arrays were removed by hand and stored in a vacuum desiccator at room temperature. When required, arrays were mounted onto aluminium stubs, sputter coated with gold and imaged under SEM as described in section 2.3.2.3.

3.3.2.6 Fabrication of sugar microneedle arrays

Sugar MNs were fabricated from 200 µL aliquots of 20 $\%^{w}/_{v}$ solutions of pure TRA and SUC sugars utilising the vacuum deposition methodology described in section 3.3.2.5.

3.3.2.7 Investigation and comparison of novel sugar glass microneedle array fabrication techniques

A 20 $\%^{w}/_{v}$ solution of TRA and SUC 75:25 $\%^{w}/_{w}$ was prepared and MB powder was incorporated at 2 $\%^{w}/_{w}$ of final sugar glass weight. The solution was filled into PDMS micromoulds using one of three methodologies:-

A) Vacuum deposition method (section 3.3.2.5). The vacuum was held for 10 mins prior to sugar solution injection onto mould, as shown in Figure 3.1.

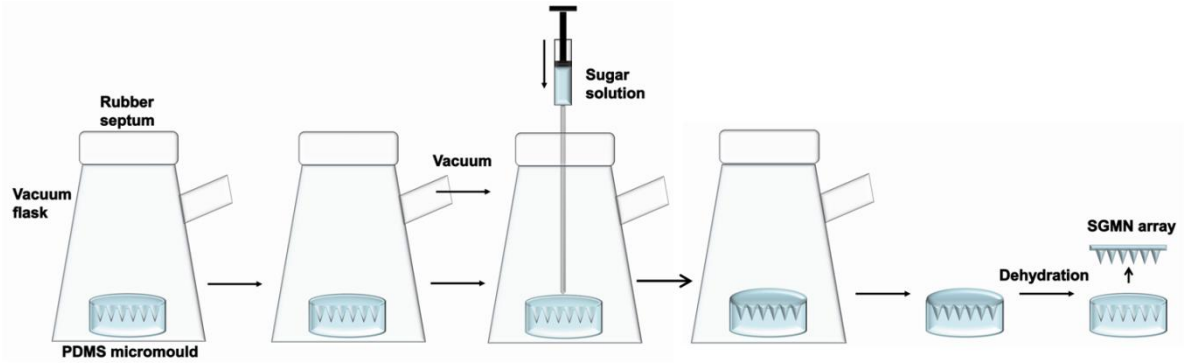

Figure 3.1 Schematic of vacuum deposition methodology.

Reproduced from source (Fraenkel et al. 2006).

B) Buchner funnel vacuum-forming method. A PDMS micromould was placed into the base of a narrow neck Buchner funnel attached to a vacuum pump. 100 µL of sugar solution was pipetted onto the surface of the micromould and a vacuum was drawn through the funnel for 10 mins. Following this period, the vacuum was released and a further 100 µL sugar solution was pipetted onto the mould surface, as shown in Figure 3.2.

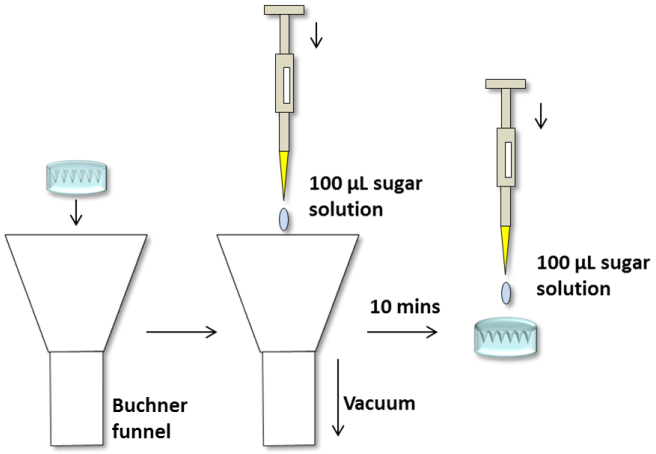

Figure 3.2 Schematic of Buchner funnel deposition methodology.

C) 100 µL of sugar solution was pipetted onto the micromould surface and the mould was placed into a petri dish within an ultrasonication bath for 10 mins. Following this period, a further 100 µL sugar solution was pipetted onto the mould surface.

Following formation, all micromoulds were dehydrated as described in section 2.3.2.1 before removal of SGMN arrays by hand.

3.3.2.8 Fabrication of alternative master microneedle arrays

A variety of potential MN substrates were analysed by light microscope (Olympus BX50, Japan) to investigate the suitability of each for the fabrication of master MN structures. The following substrates were considered:-

A) BD Microfine™ needles (21, 23 and 25 G)

B) Dermaroller™ needles (length 500 µm)

C) generic sewing needles

D) Monoject™ lancets (Sherwood Medical)

Microneedles of various geometries and length (500 - 1000 µm) were created by inserting a line of five individual needles through a base plate material. Base materials included flat PDMS sheets, Araldite® fixative and various plastic sheets**.** MN length was controlled by inserting the tip of each substrate into various layers of folded Parafilm®. Once inserted, MNs were secured in place using Araldite® fixative and cured for 12 hours. Following formation, PDMS was prepared and formed over the MN arrays to form inverse micromoulds as described in section 2.3.2.3. SGMNs containing 1 $\%^{w}/_{w}$ MB powder were created against the master MN arrays using the ultrasonication methodology described in section 3.3.2.7 (C).

3.3.2.9 Sugar glass microneedle penetration of human skin

A previously frozen full-thickness skin sample was defrosted for 60 mins. Subcutaneous fat was removed by blunt dissection and the sample was pinned onto a semi-circular cork board. The skin surface was patted dry with tissue paper. Sugar glass and silicon MN arrays were mounted onto flattened 2.0 mL syringe plungers using double-sided adhesive tape. Plungers were applied to the skin in a rolling fashion with downward pressure being applied for 10 secs and the array being rolled off in the same direction as the application. Following application, the MNs were viewed under light microscopy (Zeiss Stemi 2000-C, Hertfordshire, UK) to observe structural integrity. 10 µL of a 2 $\%^{w}/_{v}$ MB staining solution was pipetted onto the

treated skin area and left to air dry for 10 mins. Excess dye was removed with tissue paper soaked in ethanol prior to viewing under light microscopy (Fraenkel et al. 2006).

3.3.2.10 Measurement of transepidermal water loss

Transepidermal water loss (TEWL) readings were taken immediately prior to and following MN array application to skin using a Dermalab® open chamber TEWL apparatus (Cortex Technology, Hadsund, DK). A one-way ANOVA with Dunnett's multiple comparison *post hoc* test was performed on the experimental data using the GraphPad Prism 5 software package. In all cases, statistical significance was determined by a value of $P < 0.05$ (Fraenkel et al. 2006).

3.3.2.11 Human skin sectioning and staining

Samples of MN treated skin were mounted transversely onto cork sections and covered with OCT embedding media (RA Lamb, Thermo Fisher Scientific, UK) before snap freezing in hexane and storage at -80 °C. Skin samples were removed from the freezer and maintained on dry ice before cryosectioning (Leica CM3050s**,** Wolf Laboratories Limited, York, UK). Sections (10 µm) were mounted onto glass slides, rinsed in phosphate buffered saline and fixed in acetone. Slides were stained with eosin and counterstained with hematoxylin prior to rapid dehydration in an ethanol gradient and then xylene before permanent mounting in Histomount™ (National Diagnostics, Atlanta, GA, USA) (Fraenkel et al. 2006).

3.3.2.12 Dissolution of sugar glass microneedles *in situ*

Ex vivo human skin was defrosted and prepared as described in section 3.3.2.9. SGMN arrays containing 2 $\%^{w}/_{w}$ MB powder were mounted onto syringe plungers and rolled onto the skin. The plunger was pressed down for 10 secs before being secured in place with Fastaid adhesive plaster (Robinson Healthcare, Nottinghamshire, UK). The arrays were left *in situ*, under ambient conditions, for time periods up to 5 h before removal. Arrays were viewed before and after application under light microscopy (Olympus BH-2, Japan). Residual MB was removed (section 3.3.2.9) prior to visualisation of the skin under light microscopy (Fraenkel et al. 2006).

3.4 Results and discussion

3.4.1 Characterisation of silicon microneedle master arrays and polydimethylsiloxane micromoulds

To determine the precise geometry of silicon MN master structures, they were visualised under light and scanning electron microscopy, Figure 3.3.

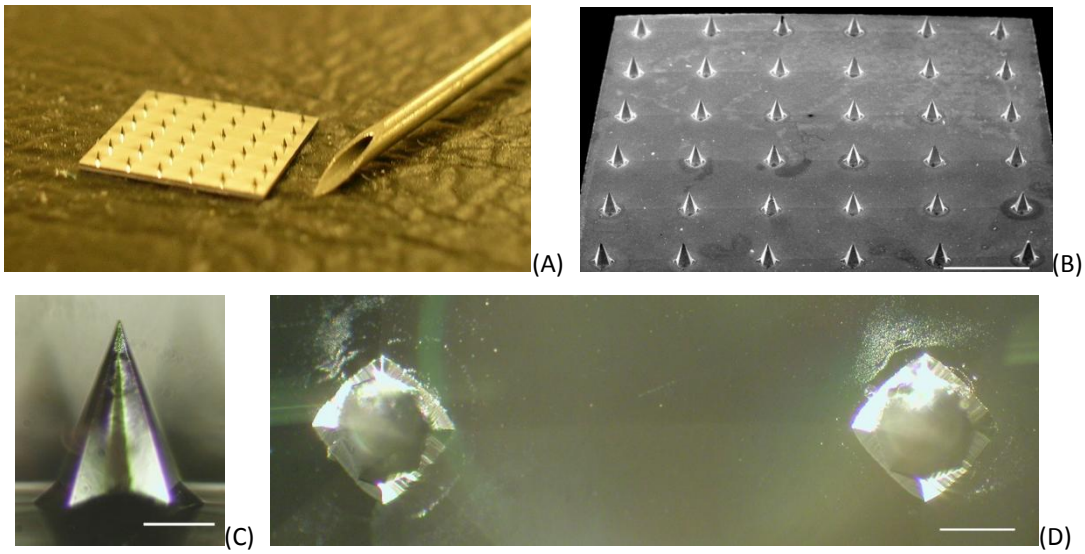

Figure 3.3 Characterisation of silicon MN array master structure.

(A) Macro image of array compared to a 26 G hypodermic needle and (B) scanning electron micrograph of (A) (Bar = 1000 µm). (C) and (D) light photomicrographs of master array from (B) showing (C) transverse angle and (D) *en face* view (Bar = 100 µm).

The images in Figure 3.3 (A) and (B) show a silicon master array prepared at Tyndall National Institute by wet-etch fabrication. Silicon MNs are shown in Figure 3.3 (C) and (D) displaying the octagonal pyramidal geometry of the master structure with base width of approximately 200 µm and needle length of approximately 250 µm (Fraenkel et al. 2006) providing an aspect ratio of 1.25.

To form a micromould, pre-polymerised PDMS was poured over the surface of the MN array. Due to the low surface tension of the polymer (Roe 1968) it easily conformed to the low aspect ratio structure of the master arrays producing inverse micromoulds of the master array that had a strong correlation to the geometry of the master array, Figure 3.4 (A); an example of a single channel created within the PDMS micromould is shown in Figure 3.4 (B)(Fraenkel et al. 2006).

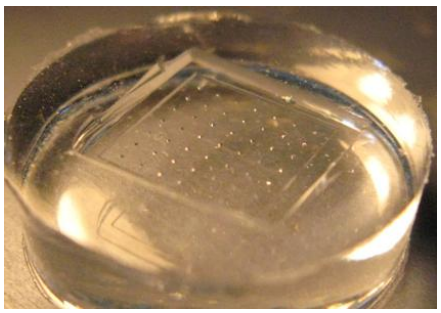
(A)
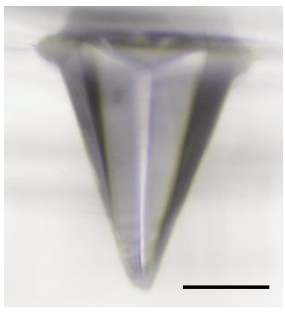
(B)

Figure 3.4 Characterisation of PDMS micromould.

(A) macro image of cross-illuminated micromould and (B) light photomicrograph of transverse section through the micromould showing an individual mould channel (Bar = 100 µm).

The data shown in Figure 3.4 confirmed the utility of the PDMS micromoulding methodology to fabricate precise moulds of master MN structures for future replication studies.

3.4.2 Initial fabrication of sugar glass microneedle arrays

A number of different methodologies were attempted to investigate production of SGMN arrays. These included methods based upon vacuum formation, compression and centrifugation of sugar material into micromoulds (data not shown). Ultimately, it appeared that a relatively simple methodology could be utilised to attempt SGMN array formation. Sugar solution was pipetted onto the micromould surface and dehydrated for 48 h, as described previously for sugar glass formation. The aim of this experiment was to observe whether the sugar solution would naturally flow into the invaginations of the mould.

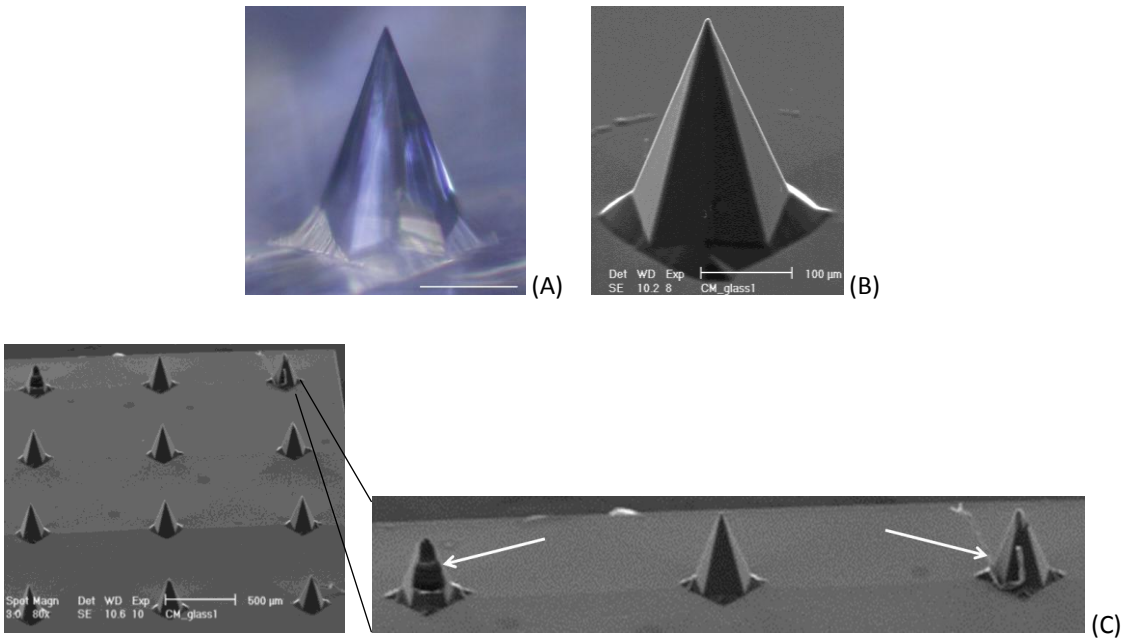

Figure 3.5 Characterisation of initial SGMN arrays.

(A) light photomicrograph of individual cross-illuminated SGMN (Bar = 100 µm) and (B) and (C) scanning electron micrographs of array (arrows indicate incompletely formed SGMNs).

As Figure 3.5 (A) and (B) show, the SGMNs that did form during this experiment generally formed very well and had strong morphological fidelity to silicon MN master structures, Figure 3.3 (C). This was encouraging as it suggested the utility of PDMS micromoulds to form SGMN structures via a simple dehydration procedure. However, certain areas of the MN array did not form well, correlating with where air bubbles remained entrapped within the micromould. Therefore, solution was unable to enter those portions of the mould. It was noted that 100 µL of sugar solution was sufficient to produce an array of MNs, but it was speculated that the moulds could be loaded with an increased volume of sugar solution in future to reliably ensure complete filling of the micromould. Importantly, it was also noted that a number of MNs within the array did not form completely, as shown in Figure 3.5 (C). It was reasoned that poor MN formation could have been due to small air bubbles remaining entrapped within the PDMS micromould invaginations, for example the top right-hand MN, Figure 3.5 (C). Alternatively, poor MN formation could have been due to damage upon removal from the array; this appeared likely with the top left-hand needle in Figure 3.5 (C).

3.4.3 Investigation of standard deposition fabrication methodology

To attempt improvement and reproducibility of the SGMN fabrication technique discussed in section 3.4.2, a number of iterations of the micromoulding methodology were investigated. Initially, this was based on the work of Park et al. where a vacuum pressure of 300 mBar was applied for 10-20 mins to form PLGA MNs into a PDMS micromould (Park et al. 2005). Following a number of small optimisation studies (data not shown) a similar methodology to Park et al. was utilised, section 3.3.2.4, and the SGMN array shown in Figure 3.6 was produced.

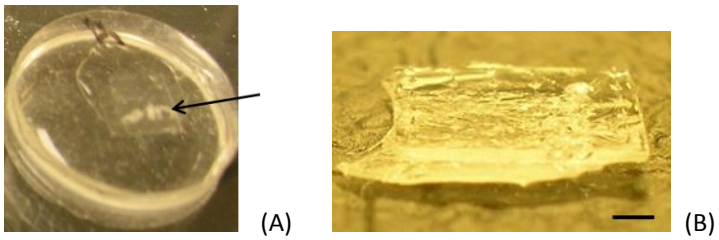

Figure 3.6 SGMN array fabricated by the standard vacuum forming methodology.

(A) PDMS micromould containing array (arrow indicates residual air bubbles remaining within array base) and (B) SGMN array (Bar = 1000 μm).

As Figure 3.6 (B) suggests, generally when SGMNs formed utilising this vacuum methodology they formed well. However, residual air bubbles (black arrow) remained within the base of the array, Figure 3.6 (A). To explore reasons for this further, the initial stages involved in SGMN manufacture were studied using MNs incorporating MB dye. When the sugar solution was placed onto the mould it initially remained on the mould surface forming a large droplet with a high contact angle, Figure 3.7 (A). It appeared that none of the micromould invaginations contained any solution at this stage. This was expected as PDMS is a hydrophobic material and because the sugar solution had a high surface tension. After the moulds had been placed under vacuum for 1 h the sugar solution was observed to have begun filling the micromould invaginations, Figure 3.7 (B). The height and contact angle of the solution droplet had also decreased following vacuum exposure. However, it is apparent from Figure 3.7 (B) that not all of the invaginations were filled with sugar solution (black arrow) at this stage. Following 48 h dehydration however the sugar glass material appeared to have filled the micromould more completely as confirmed by light microscopy, Figure 3.7 (C)(Fraenkel et al. 2006).

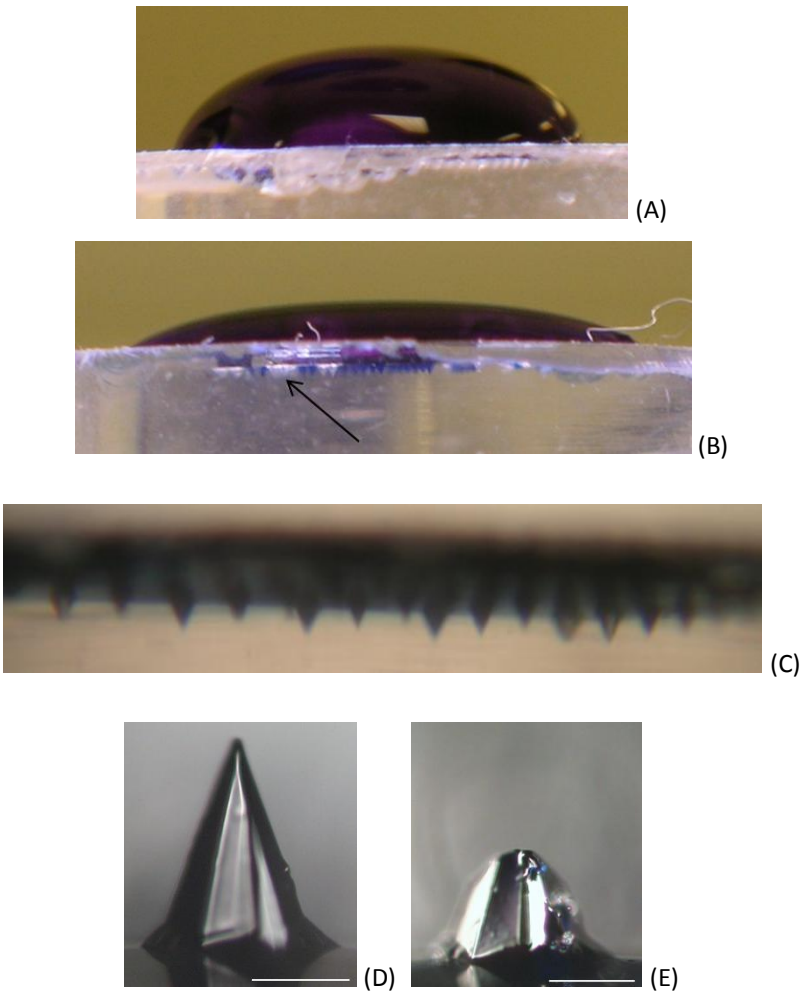

Figure 3.7 Investigation of standard deposition process of SGMN fabrication.

Macro images of a PDMS micromould showing (A) sugar solution containing 5 $\%^{w}/_{w}$ MB powder on mould surface (prior to vacuum), (B) mould following processing under 300 mBar vacuum for 60 mins (arrow indicates empty mould invaginations), (C) light photomicrograph of a SGMN array within the micromould following 48 h dehydration. (D) and (E) representative light photomicrographs of two 'MNs' formed by this process (Bar = 100 µm).

To confirm successful formation of SGMNs, newly formed MN arrays were removed from the PDMS moulds and individual MNs were viewed by light microscopy. Figure 3.7 (D) shows that SGMNs that were fully formed had strong morphological fidelity to the master structure, shown in Figure 3.3 (C). However, it was noted that only 22 SGMNs were exact replicas of the 36 silicon MN master needles with the remainder being incompletely formed, Figure 3.7 (E). This result appeared to be reproducible in subsequent studies and SGMN arrays formed by this methodology never formed full arrays of 36 needles. It was speculated that the vacuum applied to the micromould in this method was insufficient to release all of the air trapped beneath the sugar solution, or that the duration of vacuum applied was insufficient to remove

all the air from within the indentations. This process represented the completion of a number of studies aimed at optimising this vacuum-forming technique and hence it was determined that this methodology could be improved no further (Fraenkel et al. 2006).

3.4.4 Optimisation of novel vacuum deposition methodology

To improve filling of the micromould and to overcome the deficiencies in formation of a complete biodegradable SGMN array a novel vacuum-forming methodology was developed, Figure 3.1. In the original vacuum oven method (section 3.3.2.4) vacuum pressure was applied after the sugar solution was placed onto the mould surface. Consequently when the sugar solution was applied, it appeared that air bubbles remained entrapped within the micromould invaginations. Following a number of small methodological optimisation studies (data not shown), a fabrication method (section 3.3.2.5) was developed whereby a vacuum was produced within an enclosed chamber before sugar solution was applied to the mould surface, Figure 3.1 (Fraenkel et al. 2006).

To explore an optimal SGMN array fabrication technique utilising this methodology a number of different conditions were investigated. In the first instance, a vacuum was drawn within the flask and the sugar solution was injected onto the mould surface immediately. The vacuum was released immediately, and following dehydration this method produced SGMN arrays as shown in Figure 3.8 (A). In another technique, the same processes were applied again, except that the micromoulds were placed into an ultrasonication bath for 10 mins following vacuum deposition, producing SGMNs as shown in Figure 3.8 (B). In the final method, a vacuum was drawn within the flask for 10 mins prior to injection of solution onto the mould. The vacuum was released immediately and following dehydration the SGMN array in Figure 3.8 (C) was produced.

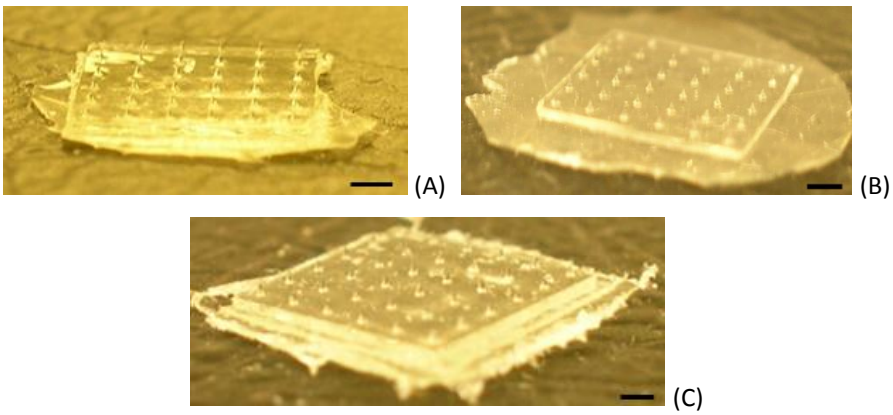

Figure 3.8 Macro images of SGMN arrays formed by novel vacuum deposition techniques.

The following methodologies were utilised, (A) immediate injection, (B) immediate injection plus ultrasonication and (C) 10 min chamber evacuation before injection (Bar = 1000 µm).

As Figure 3.8 shows, all of the SGMN arrays produced utilising the novel vacuum deposition methodology had strong morphological fidelity to the silicon MN master array, Figure 3.3 (A). These results demonstrated the utility of the new miniature vacuum chamber to form SGMN arrays. As a corollary it appeared that no air was entrapped within the micromould during application of the sugar solution (Fraenkel et al. 2006). Again, the individual SGMNs formed using this improved methodology, Figure 3.9, had identical morphological fidelity to the master structure, Figure 3.3 (C).

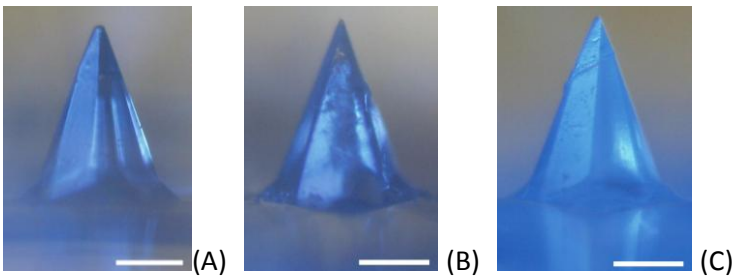

Figure 3.9 Representative light photomicrographs of individual SGMNs formed by novel vacuum deposition techniques.

The following methodologies were utilised, (A) immediate injection, (B) immediate injection plus ultrasonication and (C) 10 min chamber evacuation before injection (Bar = 100µm).

The data presented in Figures 3.8 and 3.9 appeared to show little difference between the SGMN arrays produced by each of the methodologies investigated. It appeared that ultrasonication did not improve MN array formation significantly, Figure 3.8 (B), but it was

noted that the MNs formed following a prolonged period of vacuum chamber evacuation, Figure 3.9 (C), did appear to have a closer morphological fidelity to master silicon MNs. Most importantly however, this process development enabled the precise fabrication of entire SGMN arrays, i.e. 36 out of 36 replicate structures, Figure 3.10. The novel methodology of chamber evacuation and vacuum maintenance during loading of sugar solution onto the mould reliably formed complete SGMN arrays of 36 needles that did not contain any entrapped air, as observed in initial studies. Therefore, this method was chosen as the process to take forward for all future studies (Fraenkel et al. 2006).

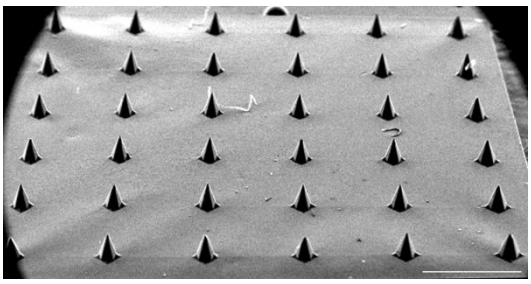

Figure 3.10 Scanning electron micrograph of SGMN array formed by the novel vacuum deposition method.

(Bar = 1000 μm).

3.4.5 Fabrication of sugar microneedle arrays

As a control, MN arrays were formed from solutions of the individual sugars SUC and TRA using the optimised vacuum methodology described in section 3.4.4. The aim of this study was to compare the SGMN arrays formed in section 3.4.4 with MN arrays formed from the component sugars, Figure 3.11.

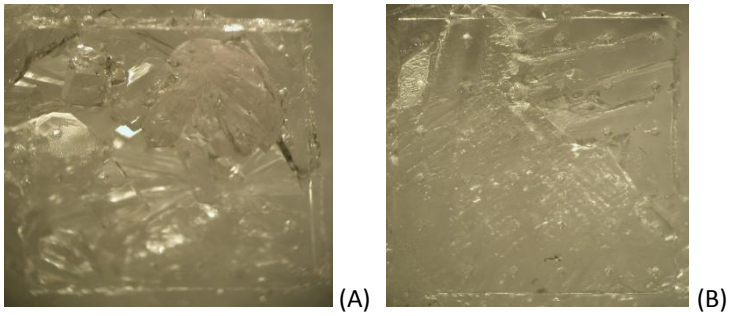

(A) (B)

Figure 3.11 Representative macro *en face* images of sugar MN arrays within micromoulds.

Arrays were formed from (A) 100 % SUC and (B) 100 % TRA (representative of n=3).

As Figure 3.11 shows, all the arrays formed from both individual sugar solutions appeared to crystallise upon dehydration (n=3). This behaviour correlated with previous data regarding dehydration of sugar solutions, section 2.4.1. However, even though the sugar solutions were shown to crystallise, it appeared that some MN structures did form within the PDMS micromoulds, Figure 3.12.

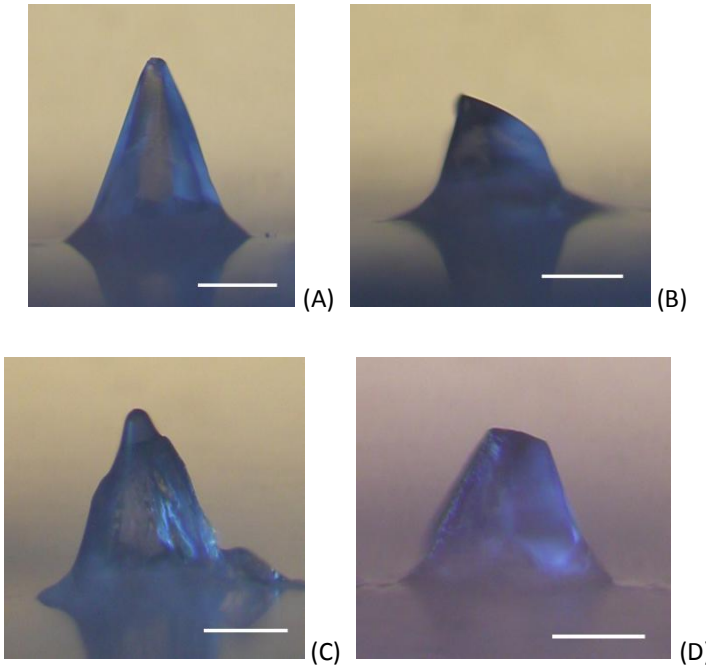

Figure 3.12 Representative light photomicrographs of sugar MNs formed.

Arrays were formed from (A) and (B) 100 % SUC and (C) and (D) 100 % TRA (Bar = 100 µm) (representative of n=3).

As shown, 36 "micro-structures" were formed on the arrays fabricated from each of the individual sugar solutions. These structures appeared to have some morphological similarity to the silicon master MNs, Figure 3.3 (C). However, it was apparent that none of the MNs formed from 100 % SUC or TRA formed with the same morphological fidelity as the SGMNs formed in section 3.4.4. It was speculated that this result was due to crystallisation of the sugar solutions within the PDMS micromould and therefore incomplete filling of the invaginations within the mould during dehydration. This study further supported the use of a TRA/SUC 75:25 $\%^{w}/_{w}$ sugar solution to enable fabrication of sugar MNs with precise replication of silicon master structures.

3.4.6 Investigation and comparison of novel sugar glass microneedle array fabrication techniques

To explore and validate the optimised novel vacuum deposition methodology described in section 3.4.4 the technique was compared to two other novel micromoulding methods, as described in section 3.3.2.7. Ultrasonication processing had shown potential for SGMN manufacture, section 3.4.4, and it was speculated that the use of a Buchner funnel may provide a more simplistic method for vacuum-forming SGMNs. Micromoulding involving the Buchner funnel was attempted to evaluate whether vacuum force could be utilised to produce SGMN arrays without a vacuum chamber. This method relied heavily on the assumption that the PDMS polymer had some porosity and hence that a vacuum could be drawn through the micromould. Examples of MN arrays formed by each of the techniques are shown in Figure 3.13.

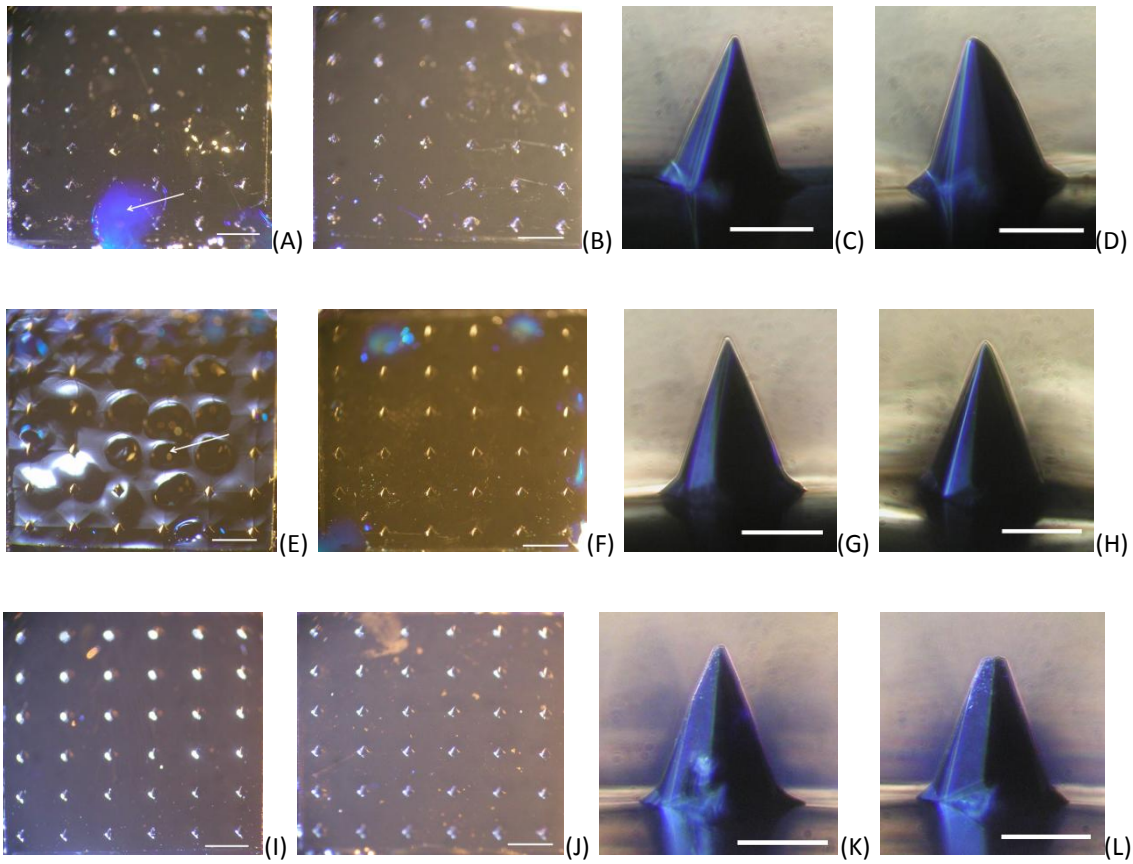

Figure 3.13 Representative light photomicrographs of SGMN arrays formed by novel fabrication techniques.

Arrays were formed by (A – B) Buchner funnel, (E – F) ultrasonication and (I - J) vacuum deposition methodologies (Bar = 1000 µm) (representative of n=3). Representative light photomicrographs of individual SGMNs formed by (C – D) Buchner funnel, (G – H) ultrasonication bath and (K - L) vacuum deposition methodologies (Bar = 100 µm). Arrows indicate residual air bubbles remaining within SGMN arrays.

As Figure 3.13 shows, generally all of the individual MNs formed by each of the methodologies had strong morphological fidelity to the silicon master structure, Figure 3.3 (C). However, a number of MNs were found to be incompletely formed on each of the arrays.

The data in Figure 3.14 show the number of whole MN structures produced using each of the methodologies.

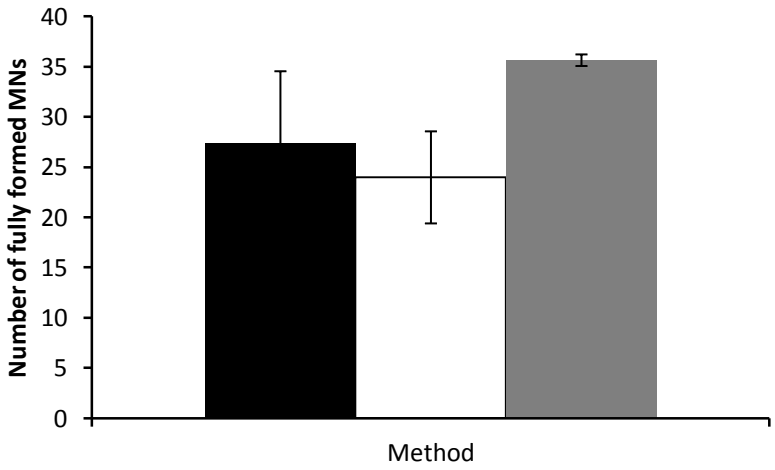

Figure 3.14 Comparison of SGMN fabrication techniques and MN formation.

Bars demonstrate the number of MN structures formed using ultrasonication (black), Buchner funnel (white) and vacuum deposition (grey) methodologies. Data presented as mean ± standard deviation (S.D.) (n=3).

In combination, the data presented in Figure 3.13 and 3.14, suggested that the vacuum chamber forming methodology produced the most reproducible SGMN arrays. As shown in Figure 3.13 (A) and (E), SGMN arrays fabricated using the Buchner funnel and ultrasonication methodologies did not always produce complete MN arrays. Air bubbles were observed within the structures of some arrays produced using both these techniques. This meant that the number of individual MNs formed using each method was consistently lower in comparison with the vacuum-forming methodology, Figure 3.14. Although not all of the MNs formed perfectly using the vacuum-forming methodology, for example Figure 3.13 (L), the MN arrays produced by this technique were the most reproducible. This study further suggested the utility of the novel vacuum methodology described in section 3.3.2.7 for robust SGMN array fabrication.

3.4.7 Fabrication of alternative master microneedle arrays

In an attempt to achieve greater flexibility over the morphology and dimensions of SGMNs, attempts were made to produce MN arrays from alternative substrates. Workers have previously utilised commercially available hypodermal needles (Verbaan et al. 2008; Verbaan et al. 2007) and sharpened stainless steel wire (Verbaan et al. 2008) to fabricate MN arrays. Therefore, a range of potential MN master substrates were investigated in this study, as shown in Figure 3.15.

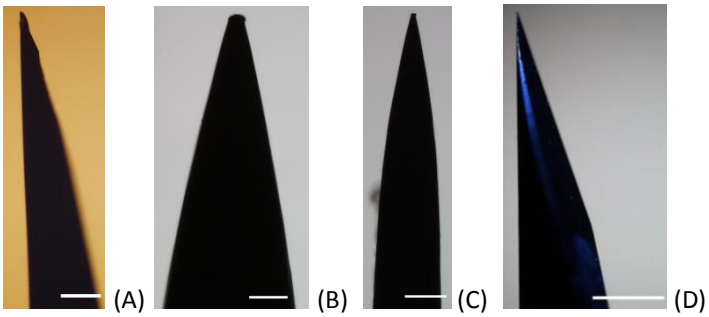

Figure 3.15 Representative light photomicrographs of potential MN substrates.

Materials examined included (A) 25 G BD Microfine™ needle, (B) sewing needle, (C) Dermaroller™ needle and (D) Monoject™ lancet needle (Bar = 100 µm).

Three different gauges of BD Microfine™ needle were investigated and it was observed that they all had exactly the same tip dimension, Figure 3.15 (A). The only variation between each needle was the bore size of the needle shaft. However, this substrate was discounted as although the needle tips were precisely machined, a needle that had a bore in the centre would be no use for PDMS micromoulding. Commercial sewing needles, Figure 3.15 (B), were found to be poorly machined, and the needle tip geometry was found to vary widely from needle to needle, Figure 3.16 (A) and (C). Hence, these needles were discarded from further analysis. The Dermaroller™ and Monoject™ lancet needles showed more potential for MN production however. Both types of needle were observed to be manufactured to a much higher level of uniformity and precision with very fine tip diameters, as shown in Figure 3.15 (C) and (D) respectively.

To form MN arrays, a range of base plate materials were explored, including flat PDMS sheets, Araldite® fixative and various plastics, to observe which was the most effective for the creation of arrays. Examples of MNs formed from these substrates are shown in Figure 3.16.

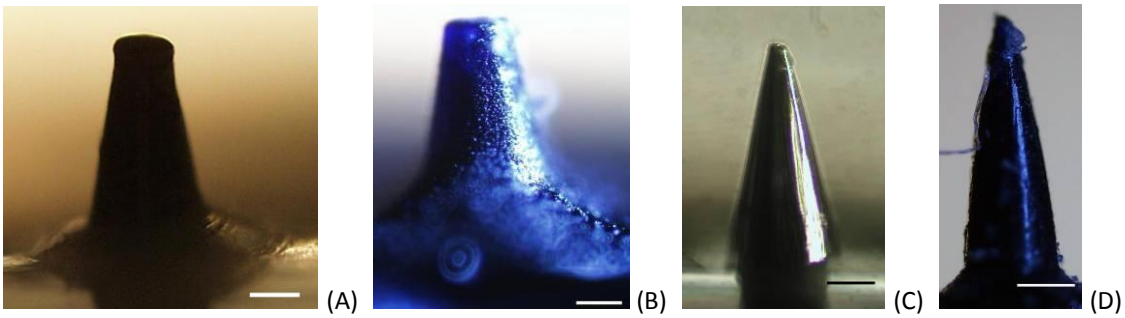

Figure 3.16 Representative light photomicrographs of alternative geometry MNs and SGMNs formed by ultrasonication.

Images depict (A) sewing needle inserted through PDMS base, (B) SGMN replica of (A), and (C) sewing needle with Araldite® base, (D) SGMN replica of (C) (representative of n=5).

As shown in Figure 3.16 (B) and (D), it was possible to form replica SGMN structures, containing 1 $\%^{w}/_{w}$ MB, of the "microneedles" fabricated in this study. Following this initial optimisation process, it was concluded that neither PDMS nor Araldite® was an optimal base material. It was speculated that a solid plastic base material may be a better substrate for MN production as it would be more straightforward to machine and provide easier control of MN length.

Combining the preliminary findings of this section, an array of 5 in plane MNs was fabricated from Monoject™ lancet needles using a rigid plastic base material. Female PDMS micromoulds were formed against the MN master structures and used to fabricate replica SGMN structures. Examples of SGMNs formed by this process are shown in Figure 3.17.

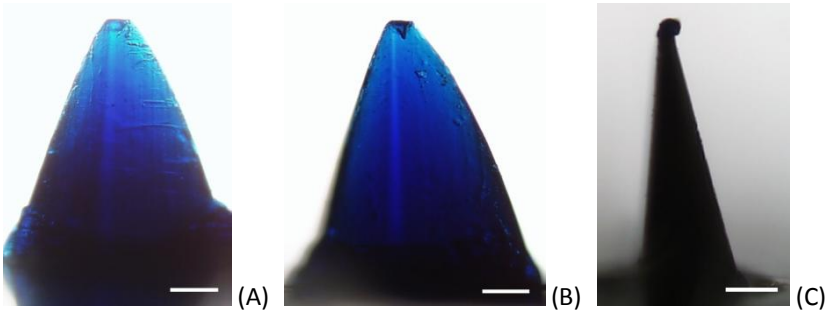

Figure 3.17 Representative light photomicrographs of SGMNs formed from Monoject™ lancet needles.

Images depict (A) and (B) *en face* view of SGMNs containing 1 $\%^{w}/_{w}$ MB and (C) 90 ° angle view of SGMN (representative of n=5).

As the images in Figure 3.17 demonstrate it was possible to produce SGMNs with alternative dimensions to the MNs produced utilising silicon MN master structures. As shown, these SGMNs had a very different geometry and aspect ratio to the pyramidal based SGMNs produced previously. Although these structures had a rigid glassy structure, it was often observed that the MNs appeared to "bend over" at the tip, Figure 3.17 (B) and (C). The reason for this observation was not clear, but it was speculated that due to the increased depth of the micromould the SG material may not have fully dehydrated at the needle tips by 48 h. Therefore, upon removal from the mould, the tips may not have had the structural rigidity to maintain their lancet shape and hence collapsed.

In summary, it appeared that it would be possible to form biodegradable SGMNs with different geometries to the master silicon MNs. However, production of these arrays, and inverse PDMS micromoulds, were not trivial and it was concluded that silicon MN shaped SGMNs would be utilised for all future studies.

3.4.8 Sugar glass microneedle penetration of human skin

To investigate the structural rigidity and skin puncture performance of SGMNs of these dimensions the arrays were inserted into excised human skin. It has been stated that an inappropriate pitch, or spacing, between individual MNs with three-dimensional geometries will prohibit skin penetration. For example, if the pitch is too short neighbouring needles will hinder each other from insertion (Miyano et al. 2005). It has also been found that MNs formed from CMC and amylopectin having the same dimensions as master silicon MNs do not possess

sufficient structural rigidity to penetrate human skin (Lee et al. 2008). Other workers have stated that MNs with a length shorter than 300 µm are ineffective as shorter needles do not pierce the skin (Bal et al. 2008). Therefore, it was an important aim of this work to ascertain the skin penetration capabilities of pyramidal SGMNs.

Methylene blue post-staining of the microchannels generated in skin following MN array application for 10 seconds showed that SGMNs, Figure 3.18 (B), appeared to penetrate human skin with the same efficacy as silicon MNs, Figure 3.18 (A). This demonstrated that SGMNs of these dimensions possess suitable structural rigidity and sharpness to effectively puncture the SC of human skin (Fraenkel et al. 2006). Transverse skin sections further confirmed that SGMNs efficiently circumvented the SC to facilitate diffusion of MB dye, applied post-application, into the epidermal layer, Figure 3.18 (D), in a manner analogous to silicon MNs, Figure 3.18 (C). Whilst master silicon MNs were largely unaffected by the skin application process, Figure 3.18 (E), Figure 3.18 (F) shows that SGMNs were physically altered following 10 secs insertion into human skin (Fraenkel et al. 2006). It was not obvious from this study whether SGMNs were damaged due to the relatively brittle nature of the material, or partially dissolved during the application process, but it rendered their re-use for skin puncturing purposes unlikely (Fraenkel et al. 2006).

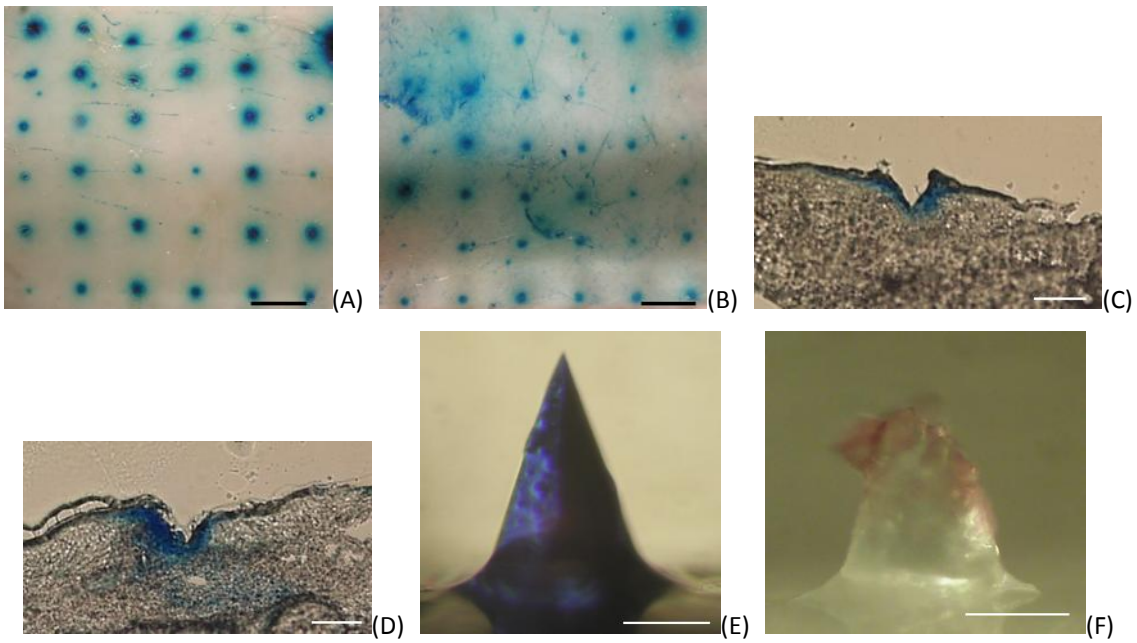

Figure 3.18 Human skin penetration capability of SGMNs.

MNs were inserted into excised human skin and removed prior to staining with 2 $\%^{w}/_{v}$ MB dye. *En face* images of microchannels following insertion of (A) silicon and (B) SGMN arrays (Bar = 1 mm). Light photomicrographs of transverse skin sections taken from skin shown in (A) (silicon MNs, panel C) and (B) (SGMNs, panel D) respectively (Bar = 100 µm). Light photomicrographs of representative silicon (E) and sugar glass (F) MNs following rapid (10 seconds) skin insertion (Bar = 100 µm).

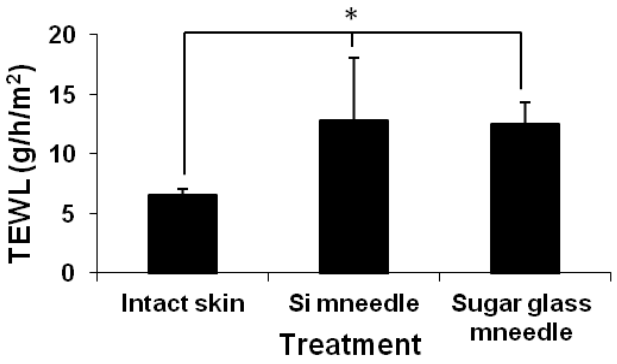

Figure 3.19 Transepidermal water loss measurement across human skin following MN treatment.

Both sugar glass (n=3) and silicon MN treatments (n=4) were shown to significantly increase TEWL versus intact skin (n=3). Data presented as mean ± standard error of mean (S.E.). * denotes statistical significance at $p<0.05$.

Skin puncture performance of MN devices was further assessed by measurement of TEWL from skin following application. TEWL data confirmed that human skin insertion of both silicon

and sugar glass MNs significantly ($p < 0.05$) increased water loss over that of intact non-treated skin, Figure 3.19 (Fraenkel et al. 2006).

This data demonstrated that pyramidal SGMN with a length of 250 µm and an inter-needle spacing of 1 mm were capable of successfully inserting into full thickness human skin. This indicated that MNs formed from sugar glass material were of a sufficient structural rigidity to penetrate the SC barrier to a similar extent as master silicon MNs. This finding is in contrast to work carried out by others utilising dissolvable carbohydrate materials for MN manufacture (Lee et al. 2008). Following skin insertion however, it was apparent that silicon and sugar glass MNs behaved quite differently. Sugar glass MNs were shown to degrade rapidly and it was speculated that this may be due to the hygroscopic and / or brittle nature of the material. Rapid dissolution of natural biodegradable MNs *in vitro*, on the timescale of seconds, have been noted by other workers (Lee et al. 2008; Xueqiu et al. 2010) and therefore it appears that sugar glass MNs have similar degradation kinetics.

3.4.9 Dissolution of sugar glass microneedles *in situ*

Due to the material properties of sugar glass, it was hypothesised that SGMNs would dissolve rapidly and completely within skin to deposit incorporated model drug cargo. To test this, SGMN arrays incorporating 2 $\%^{w}/_{w}$ MB powder were inserted into *ex vivo* human skin and left *in situ* for various time periods. Figure 3.20 shows the dissolution status of the MNs, with complete dissolution being evident between 10 mins, Figure 3.20 (B), and 20 mins, Figure 3.20 (C), following skin insertion (Fraenkel et al. 2006). This data correlates closely with reports from other workers where biodegradable MNs fabricated from natural substances have been shown to dissolve over similar time scales both *in vivo* (Fukushima et al. 2011; Lee et al. 2011b; Miyano et al. 2005) and *in vitro* (Lee et al. 2008; Xueqiu et al. 2010).

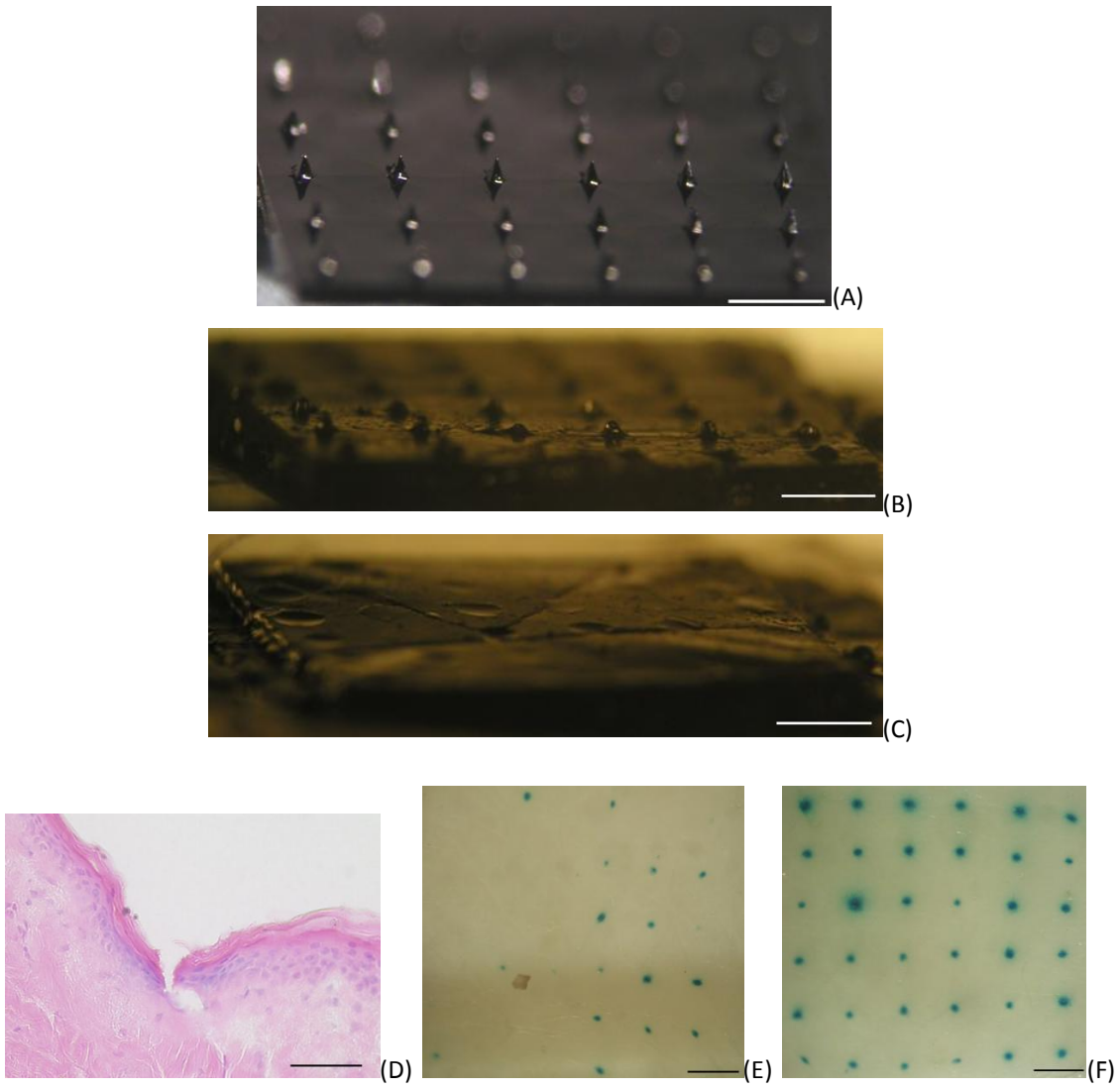

Figure 3.20 *In situ* dissolution of SGMNs incorporating 2 %$^{w}/_{w}$ methylene blue.

Representative light photomicrographs of SGMNs: (A) after formation, (B) following 10 mins insertion into *ex vivo* human skin and (C) following 20 mins insertion into *ex vivo* human skin (representative of n = 4) (Bar = 1 mm). (D) 10 µm hematoxylin and eosin stained transverse tissue section of skin showing a single MN puncture site following 20 mins insertion (Bar = 100 µm). *En face* images of skin after removal of SGMNs incorporating dye at 10 mins (E) and 20 mins (F) insertion time (Bar = 1 mm).

The SGMNs fabricated in this study were shown to penetrate the SC of human skin, Figure 3.20 (D) and to dissolve *in situ*. Figures 3.20 (E) and (F) show the degree of skin staining arising from dissolution of MNs containing MB within the needle structure at 10 and 20 mins respectively. These images generally support the SGMN array dissolution kinetics detailed in Figure 3.20 (A) – (C) and further confirm the utility of these MNs for creating microchannels within skin and releasing material incorporated within the matrix of the array leaving behind no hazardous waste (Fraenkel et al. 2006).

3.5 Conclusion

The focus of this chapter was to establish a robust micromoulding methodology to fabricate biodegradable SGMN arrays. It was demonstrated that PDMS micromoulds generated against silicon MN master structures had strong morphological fidelity to the master structures. This suggested the utility of the moulds for creating replicate MN structures. Various different techniques have been reported for filling micromoulds to form biodegradable MN structures. Here it was shown that modifications to the classical vacuum oven based micromoulding methodology utilised by other workers facilitated the reliable fabrication of SGMN arrays against silicon MN masters at a low temperature. A number of different master MN permutations were fabricated in this chapter and inverse micromoulds were successfully produced against them. Although these MNs and moulds allowed greater flexibility over MN length and geometry, it was found that micromoulds produced from silicon MN masters permitted fabrication of the most reliable SGMN structures. It was demonstrated that these MN structures had sufficient strength and tip sharpness to effectively puncture human SC barrier creating microchannels into the deeper skin layers. The SGMNs were shown to dissolve rapidly *in situ* to facilitate delivery of an incorporated dye into the epidermis. However, as these studies were investigated *in vitro*, it may be that the actual degradation of SGMNs *in vivo* is considerably faster. This study suggests the utility of SGMN arrays for the transdermal delivery of potent therapeutics, potentially including hydrophilic macromolecules.

Chapter 4

Stability and incorporation of model substances within sugar glass microneedles

4 Stability and incorporation of model substances within sugar glass microneedles

4.1 Introduction

4.1.1 Incorporation of model substances within biodegradable microneedles

A wide variety of biodegradable MN permutations have been reported to investigate the cutaneous delivery of a range of model substances. Studies have explored both local and systemic delivery of compounds and medicaments via biodegradable MNs utilising both *in vitro* and *in vivo* models. In Chapter 3 it was shown that SGMN arrays could penetrate human skin to facilitate permeation of dye into deeper skin layers. One of the potential benefits of biodegradable MNs is that drug can be incorporated within the device thereby facilitating increased drug loading. Accordingly, it was important to establish the characteristics and limitations of loading within SGMN arrays.

As mentioned previously, other workers have investigated incorporation of model compounds within the structure of biodegradable MN devices. Miyano et al. incorporated the small molecules ascorbate-2-glucoside (ASG), sodium salicylate (SS) and calcein (CAL) within molten maltose candy at concentrations of 5, 10 and 10 $\%^{w}/_{w}$, respectively. This was found to be the upper limit of concentration attainable, as exceeding this quantity decreased the mechanical strength of the MNs so that they would no longer insert into skin (Miyano et al. 2005). More recently, Lee et al. fabricated maltose MNs containing the small molecules ASG and niacinamide at concentrations of 1 % and 1.5 $\%^{w}/_{w}$ respectively. In a similar manner to that reported by Miyano et al., this process utilised elevated temperature to dissolve the powders; although it was found that the stability of these compounds was unaffected by the fabrication process and for up to 2 months when stored at ambient temperature and relative humidity (Lee et al. 2011b).

Utilising a fabrication methodology analogous to Miyano et al., Donnelly et al. added 5-aminolevulinic acid (5-ALA) and BSA powder to molten galactose before micromoulding (Donnelly et al. 2009a). In this study it was found that substantial losses of both 5-ALA and BSA, approximately 30 and 100 % respectively, occurred during the fabrication process. Similar observations were made by Park et al. following fabrication of synthetic polymer MNs encapsulating CAL or BSA. Drug was either directly encapsulated within poly-lactide-co-

glycolide (PLGA) MNs, or first encapsulated within CMC or poly-L-lactide for controlled release applications (Park et al. 2006). Due to the high melting point of PLGA, and the duration of elevated temperature required to form these MNs, a time-dependent denaturation of BSA protein was observed (Park et al. 2006). Mechanics of MN insertion were assessed and it was found that MNs containing 2 $\%^{w}/_{w}$ CAL remained strong enough to insert into skin, whereas those containing 10 $\%^{w}/_{w}$ decreased below the failure force required for skin penetration (Park et al. 2006). As reliable skin penetration is essential to the utility of MN devices, this was an important finding and suggested that there may be limitations to drug loading within biodegradable MNs.

Accordingly, it was envisaged that the low temperature SGMN fabrication process developed in Chapter 3 may facilitate the stable incorporation of a wide range of model substances. In support of this concept, there have been a growing number of reports of low temperature micromoulding methodologies for biodegradable MNs. Ito et al. proposed a process to fabricate self-dissolving MNs from various dense glue solutions of chondroitin sulphate, dextrin and albumin containing erythropoietin hormone (EPO). These MNs were dried under desiccating conditions at low temperature and hence the biomolecule EPO was successfully incorporated and retained its structure when delivered *in vivo* (Ito et al. 2006). The same workers later prepared MNs from dense drug glues containing insulin (Ito et al. 2010), ascorbic acid (Ito Y. et al. 2010b) and EPO (Ito Y. et al. 2010a) by condensing solutions and micromoulding utilising low temperature processes. All these MNs delivered functional drug substances capable of producing biological effects *in vivo*. Furthermore, MNs containing 12 or 22 % recombinant human growth hormone (rhGH) or 4 % desmopressin (DDAVP) were fabricated from drug glues in a similar manner (Fukushima et al. 2011). These model substances were shown to be almost completely stable within MN structures for 1 month when stored at either -80 or 4 °C (Fukushima et al. 2011). Solid state biodegradable microstructures (SSBMS) containing 5 and 10 $\%^{w}/_{w}$ FITC-BSA (66 kDa) and 2, 5 and 10 $\%^{w}/_{w}$ recombinant protective antigen (rPA; 83 kDa) in a carbohydrate and polyvinyl alcohol (PVA) excipient solution were prepared by pressure micromoulding and drying at 32 °C (Wendorf et al. 2011). These SSBMS stably incorporated both proteins for successful transdermal delivery (Wendorf et al. 2011).

To fabricate biodegradable MNs from natural polymeric materials CMC, amylopectin and BSA, viscous hydrogel formulations were fabricated and model drug was added by hand. The model

substances investigated were sulforhodamine B (SRB), BSA and lysozyme added at final weight concentrations of 0.15 – 30 %, 20 % and 5 % respectively (Lee et al. 2008). In contrast to previous reports, this study found that the addition of 20 % BSA to CMC MNs increased the mechanical strength of the needles in comparison to pure CMC MNs; however, the authors acknowledged that this may not be the case with other model drugs (Lee et al. 2008). Furthermore, lysozyme retained almost 100 % activity within MN structures following 2 months storage at room temperature (Lee et al. 2008). Alternatively, CMC MNs were fabricated containing rhGH at 5 $\%^{w}/_{w}$ utilising a relatively low temperature casting methodology (Lee et al. 2011a). When stored in air under ambient conditions, rhGH contained within the needles was shown to be stable over a 3 month period maintaining biological activity (Lee et al. 2011a).

Further reports describe MNs fabricated from other synthetic polymeric materials. Polyvinylpyrrolidone (PVP) MNs formed by *in situ* photo polymerisation at ambient temperature demonstrated effective incorporation and delivery of BSA and functional β-gal *in vitro* and were shown to protect nearly 100 % β-gal activity following incorporation within MN structures (Sullivan et al. 2008). This suggested that macromolecular drug incorporation within these MNs would be favourable. Chu et al. investigated MN structures created from blends of PVA and PVP containing SRB incorporated within the needles either in a gradient fashion or as a homogeneous mix throughout the matrix (Chu et al. 2010). The MNs contained 2 – 8 % drug and were shown to reliably insert into excised porcine skin (Chu et al. 2010). Alternatively, MNs were fabricated from Gantrez® AN-139 polymer containing 1 $\%^{w}/_{w}$ theophylline. It was found that loading above this concentration led to a highly flexible material that was unsuitable for MN manufacture (Donnelly et al. 2011). However, at 1 $\%^{w}/_{w}$ loading, MNs possessed similar mechanical properties to their non-drug-loaded counterparts and were shown to successfully deliver drug across porcine skin *in vitro* (Donnelly et al. 2011). Further MNs were created from poly (methylvinylether maleic anhydride) containing insulin loaded at 2.5 and 10 mg per device. Loading of MNs at both concentrations did not adversely affect MN morphology or robustness and only slight losses of insulin were incurred during fabrication (Migalska et al. 2011). These studies suggested that if formulated correctly biodegradable MN structures could be produced to stably encapsulate a range of both small and large molecular weight substances.

As described, there are many different approaches to biodegradable MN fabrication and incorporation of model compounds. In this chapter the incorporation of a range of model substances will be investigated to determine the loading capacity and stability of SGMN arrays.

4.1.2 Macromolecule incorporation within sugar glasses

As described, glass forming sugars have great significance in nature as they are used to protect delicate biological tissues in the dehydrated state (Potts 1994). Pharmaceutical processes such as heating, freeze-thawing and freeze-drying can potentially denature proteins (Uritani et al. 1995) through stresses involved in removal of its hydration shell (Prestrelski et al. 1993). Subsequently, it has been shown that certain disaccharides, for example trehalose, maltose and sucrose protect these molecules in the dehydrated state (Carpenter and Crowe 1988). It has been suggested that water molecules that surround polar residues within labile macromolecular assemblies, such as membranes and proteins, in the natural state are replaced by sugars. Hence this maintains stability when the hydration shell is removed (Crowe and Clegg 1973). It has been proposed that the mode of action of these sugars is to encourage the retention of the native structure of the protein and prevent unfolding in the dried state (Prestrelski et al. 1993). Accordingly, it was hypothesised that these materials may be suitable for biodegradable MN fabrication and stable macromolecule incorporation.

Although many workers have investigated carbohydrates for biodegradable MN manufacture, there are only a few instances of stable macromolecule incorporation within these structures. Limitations of this approach appear to be the utilisation of elevated temperatures to fabricate these structures. However, as described in Chapter 2, sugar glasses can be produced by a variety of different techniques, which do not always require elevated temperature or force to cause vitrification. A prominent area where the protective capacity of sugars has been explored is in the study of freeze-drying formulation and subsequent product storage. For example, addition of trehalose or maltose to phosphofructokinase solution prior to freeze-drying was shown to stabilise the enzyme to a minimum of 80 % of its original level (Carpenter et al. 1987a). However, in the context of this work it was realised that freeze-drying would not be appropriate for filling micromoulds. It was hypothesised that the low temperature dehydration process developed in Chapters 2 and 3 would be more appropriate to producing SGMNs containing model substances, which was the focus of this chapter.

4.2 Chapter objectives

1. Incorporate a range of model substances within SGMN arrays and investigate limitations of the system.

2. Assess the stability of model macromolecule contained within sugar glass material formed by low temperature dehydration.

3. Investigate the long-term physical stability of sugar glasses (SGs) and SGMN arrays under varying storage conditions.

4. Investigate the long-term stability of SGs containing model macromolecule under varying storage conditions.

5. Investigate cutaneous delivery of model macromolecule by SGMN arrays.

4.3 Materials and methods

4.3.1 Materials

All reagents were obtained from Fisher Scientific Ltd. (Loughborough, UK) and were of analytical grade unless stated otherwise.

β-galactosidase, product code G-6008, was obtained from Sigma - Aldrich (Poole, UK).

Human breast skin was obtained from the Aneurin Bevan Health Board Royal Gwent Hospital (Newport, Wales, UK) following mastectomy or breast reduction surgery with full ethical committee approval and informed patient consent.

4.3.2 Methods

4.3.2.1 Incorporation of model drugs within sugar glass microneedle arrays

A 20 $\%^{w}/_{v}$ solution of TRA/SUC 75:25 $\%^{w}/_{w}$ in dH_2O was prepared. Model drugs ibuprofen sodium (IBU), propranolol hydrochloride (PHCl), bovine serum albumin (BSA), FITC-BSA and sulforhodamine B sodium (SRB) (Sigma - Aldrich, Poole, UK) were incorporated at 5, 1 – 10, 1 – 10, 5 and 5 $\%^{w}/_{w}$ respectively, of final sugar glass weight. Sugar solution containing drug was magnetically stirred to dissolve the powders. Additionally, to dissolve 10 $\%^{w}/_{w}$ PHCl, solutions were heated to 50 °C for 10 mins. Once formed, solutions were filtered through a cellulose acetate 0.2 µm filter and vacuum formed in PDMS micromoulds as described in section 3.3.2.5. All arrays were viewed under light microscopy (Olympus BH-2, Japan). A one-way ANOVA with Dunnett's multiple comparison *post hoc* test was performed on the experimental data using the GraphPad Prism 5 software package. In all cases, statistical significance was determined by a value of $P < 0.05$

4.3.2.2 Incorporation of model macromolecule within sugar glass microneedle arrays

A 16.7 $\%^{w}/_{v}$ solution of TRA/SUC 75:25 $\%^{w}/_{w}$ was prepared by dissolving the sugars in 100 mM sodium phosphate buffer (PB) (Sigma - Aldrich, Poole, UK). A stock solution of β-gal was made up in PB solution at a concentration of 1 U/µL. Stock solution was further diluted with PB to form a 5 U/10 µL solution. 10 µL of sugar PB solution was removed from a 1 mL aliquot and replaced with 10 µL of diluted β-gal stock solution, to form a solution with a final enzyme concentration of 5 U/mL. 200 µL of the solution was vacuum formed into a PDMS micromould,

as described in section 3.3.2.5. Following 48 h dehydration, SGMN arrays were stored in a vacuum desiccator prior to use.

4.3.2.3 Theoretical calculation of microneedle volume

The theoretical volume of the MNs within a 6 x 6 SGMN array was calculated as follows to determine the potential drug loading within the MNs alone. The geometry of the silicon MN master structures used in this work were approximated to a square based pyramid. The volume of individual SGMNs fabricated in this study were calculated using Equation 1.

$$\text{Pyramid volume } (\mu L) = \text{base area } (\mu m) \times \text{height } (\mu m) \times 1/3 \qquad (1)$$

Utilising the volume calculated in (1) the mass of sugar contained within the SGMNs of the array was calculated as shown in equation 2.

$$\text{SGMN volume} \times \text{Sugar density} \times 36 \qquad (2)$$

The theoretical amount of drug contained within SGMNs was then calculated based on percentage incorporation.

4.3.2.4 Formation of X-gal staining solution for qualitative β-galactosidase assay

X-gal powder was dissolved in N,N-dimethylformamide at a concentration of 40 mg/mL. 2.42 g tris-hydrochloride buffer (Sigma - Aldrich, Poole, UK) was dissolved in 8 mL dH_2O. The pH was adjusted to pH 8.5 by adding hydrochloric acid (0.5 M) in a drop-wise manner. The solution was then made up to a final volume of 100 mL using dH_2O.

Approximately 5 mL of X-gal staining solution was created using the following formula:

X-gal solution	250µL
K^+ ferricyanide (III)	42µL
K^+ hexacyanoferrate	42µL
1 M $MgCl_2$ solution	10µL
Tris-HCl buffer	2.5mL
dH_2O	2.15mL

4.3.2.5 Delivery of β-galactosidase to human skin via SGMN arrays

A previously frozen full thickness human skin sample was defrosted and prepared as described in 3.3.2.9. SGMN arrays containing β-gal, section 4.3.2.2, were mounted onto the flattened end of a syringe plunger and applied to defrosted human skin, as described in section 3.3.2.9. The arrays were left *in situ* for 30 mins before being removed. Upon removal, treated skin sections were maintained at the air-liquid interface using a "Trowell-type" organ culture setup placed into an incubator at 37 °C for 1 h. Following incubation, the samples were removed and rinsed in PBS containing 4 mmol $MgCl_2$ before fixation in chilled 2 $\%^{w}/_{v}$ glutaraldehyde in PBS / $MgCl_2$ solution for 2 h. Once fixed, skin sections were rinsed twice in PBS / $MgCl_2$ solution for 15 mins and transferred into X-gal staining solution. Samples were maintained in an incubator at 37 °C for 18 h before removal and visualisation of the insoluble blue X-gal product.

4.3.2.6 Quantitative ortho-nitrophenyl β-D-galactopyranoside assay for β-galactosidase

β-gal activity was quantified by adding 100 µL of sample or standard enzyme solution to a reaction vessel, equilibrated to 37 °C, containing:-

Ortho-nitrophenyl β-D-galactopyranoside (ONPG)	100 µL
30 mM $MgCl_2$ solution	100 µL
3.36 M 2-mercaptoethanol solution	100 µL
100 mM PB	2.6 mL

Blanks for each sample contained the same reaction components including ONPG substrate, but no enzyme. Samples were incubated in a water bath at 37 °C for 90 mins. The reaction was stopped with 1.5 mL sodium carbonate solution (1 M) and 100 µL of enzyme sample was added to each blank solution. 300 µL aliquots of each sample were analysed by UV spectrophotometer (Fluostar Optima™, BMG Labtech, Aylesbury, UK), with absorbance at 405 nm. Residual enzyme activity was estimated by linear regression and correlation analysis of the calibration curve generated. A one-way ANOVA with Bonferroni's multiple comparison *post hoc* test was performed on the experimental data using the GraphPad Prism 5 software package. In all cases, statistical significance was determined by a value of $P < 0.05$

4.3.2.7 Effect of dehydration surface area on enzyme stability

A 20 $\%^{w}/_{v}$ sugar solution TRA/SUC 75:25 $\%^{w}/_{w}$ was created by dissolving the sugars in PB before filtering through a cellulose acetate 0.2 µm filter. Stock solutions of 10^{-3} U/µL β-gal in PB and

sugar PB were created by diluting stock β-gal solution, section 4.3.2.2, in further PB. Samples of 300 µL were pipetted into 96, 24 and 6 well plates (Fisher Scientific Ltd, Loughborough, UK) and dehydrated as described in section 2.3.2.1. Dehydrated products were then re-hydrated with 300 µL dH_2O and left for 10 mins to dissolve. Samples were stirred with a 200 µL pipette tip and the remaining enzyme activity was quantified by ONPG assay, as described in section 4.3.2.6. All plates were weighed throughout the 48 h dehydration period using a balance (Sartorius, Goettingen, Germany). Changes in sample weight were recorded and residual water content was inferred by subtracting the initial powder mass from sample weight.

4.3.2.8 Investigation of β-galactosidase enzyme stability within sugar glasses

A 16.7 $\%^{w}/_{v}$ solution of TRA/SUC 75:25 $\%^{w}/_{w}$ was prepared as described in section 4.3.2.2. Solutions of PB and sugar PB containing 10^{-3} U/µL β-gal were created, as described in section 4.3.2.7. To form sugar glasses, 200 µL samples of solution were dehydrated within 24 well plates. Samples were dehydrated as described in section 2.3.2.1, and negative controls were dehydrated for 24 h at ambient temperature followed by a further 24 h at 90 °C. Control solution samples were pipetted into Eppendorf tubes and sealed to prevent evaporation. Following dehydration, samples were re-hydrated with 200 µL dH_2O and assayed as described in section 4.3.2.7. The enzyme was quantified by ONPG assay, section 4.3.2.6.

4.3.2.9 Initial stability study of sugar glass formulation

A 20 $\%^{w}/_{v}$ solution of TRA/SUC 75:25 $\%^{w}/_{w}$ was created by dissolving sugars in PB. The solution was filtered through a cellulose acetate 0.2 µm filter. Solutions of PB and sugar PB containing 10^{-3} U/µL β-gal enzyme were created and 300 µL samples were pipetted into 24 well plates (Fisher Scientific Ltd, Loughborough, UK). The solutions were dehydrated to form a solid as described in section 2.3.2.1. SGMN arrays were fabricated from a 20 $\%^{w}/_{v}$ solution of TRA/SUC 75:25 $\%^{w}/_{w}$, as described in section 3.3.2.5. Dehydrated samples and SGMN arrays were stored for a period of 3 months under the following storage conditions:-

1. At room temperature (20 ± 2 °C) under vacuum desiccation (silica gel)
2. In a desiccator (silica gel) under refrigeration (4 ± 2 °C)
3. At room temperature under 60 ± 5 % relative humidity (RH)
4. At 40 ± 2 °C under 75 ± 5 % RH
5. Under refrigeration (4 ± 2 °C)

Following time points 7 days, 28 days and 3 months solid products were re-hydrated with 300 µL dH_2O and assayed as described in section 4.3.2.7. SGMN arrays were viewed at all time points under light microscopy to examine needle integrity.

4.3.2.10 Long-term assessment of β-galactosidase stability within sugar glasses

A 16.7 $\%^w/_v$ solution of TRA/SUC 75:25 $\%^w/_w$ was prepared by dissolving the sugars in PB and a stock solution of β-gal enzyme was prepared as described in section 4.2.2.2. To form sugar glasses, 300 µL samples were pipetted into 24 well plates (Fisher Scientific Ltd, Loughborough, UK). The solutions were then dehydrated to form a solid as described in section 2.3.2.1. Following dehydration, samples were re-hydrated with 300 µL dH_2O and assayed as described in section 4.3.2.7. Further samples were stored under vacuum desiccation utilising Sorbsil® Chameleon® desiccant (VWR International Ltd, Leicestershire, UK) at 20 ± 2 °C or desiccation (Sorbsil® Chameleon®) at 4 ± 2 °C for up to 3 months. Samples were re-hydrated as stated previously and residual enzyme activity was quantified at 7, 35 and 95 days following sugar glass formation.

4.3.2.11 Sugar glass microneedle stability study

SGMN arrays were formed from a filtered 20 $\%^w/_v$ solution of TRA/SUC 75:25 $\%^w/_w$, as described in section 3.3.2.5. Blank sections of SG material were formed by pipetting 200 µL sugar solution onto flat sections of PDMS and dehydrating as described in section 2.3.2.1. Once fabricated, arrays and SGs were stored under one of the following conditions:-

1. At room temperature (20 ± 2 °C) under vacuum desiccation (Sorbsil® Chameleon®)
2. In a desiccator (Sorbsil® Chameleon®) under refrigeration (4 ± 2 °C)
3. At room temperature under 5.5 % RH
4. At room temperature under 10 % RH
5. At room temperature under 15 % RH
6. At 37 °C under 10 % RH.

Sugar glass MN arrays were viewed under light microscopy (Olympus BH-2, Japan) following 7 days, 28 days and 3 months storage. The water content of SGs were analysed by thermogravimetric analysis (TGA) (section 2.3.2.4) at the same time points.

4.4 Results and discussion

4.4.1 Incorporation of model drugs within sugar glass microneedle arrays

Previous data in Chapter 3 had shown that MB powder could be incorporated within SGMNs as a model drug compound. Other workers have incorporated this compound within biodegradable MN structures as a model medicament (Xueqiu et al. 2010). It was found that incorporation of this substance at a concentration of 2 $\%^{w}/_{w}$ dry weight had little effect on the structural integrity of SGMN arrays formed. However, when incorporated at a concentration of 5 $\%^{w}/_{w}$ it was observed that SG material properties changed significantly and lost robustness (data not shown). Sugar glass MN arrays became very difficult to remove from PDMS micromoulds and often cracked during the process. To probe this behaviour further model substances with widely differing physicochemical properties were incorporated into SGMNs. Propranolol hydrochloride (PHCl) is a relatively small molecule, molecular weight (MW) approximately 296, whilst bovine serum albumin (BSA) is a large MW protein, approximately 66 kDa in size, as shown in Figure 4.1.

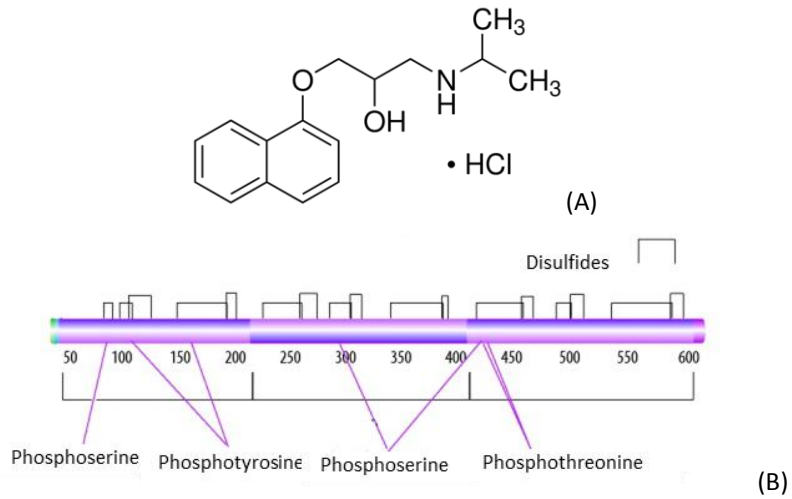

Figure 4.1 Structure of model drugs incorporated within SGMNs.

Models incorporated included (A) propranolol hydrochloride and (B) bovine serum albumin. Adapted from source, http://www.sigmaaldrich.com/catalog/ProductDetail. Accessed 17/01/2012.

Each model drug was incorporated into model sugar solution before being vacuum-formed into solid SGMN arrays.

SGMN arrays containing PHCl are shown in Figure 4.2. Visually, it was observed that there was little difference between each of the MN arrays formed. Generally all of the SGMNs formed

had strong morphological fidelity to the silicon master MNs and increasing the content of PHCl appeared to have little effect on MN structure.


(A)


(B)


(C)

Figure 4.2 Representative light photomicrographs of SGMN arrays containing propranolol hydrochloride.

Arrays contain (A) 1 $\%^{w}/_{w}$, (B) 5 $\%^{w}/_{w}$ and (C) 10 $\%^{w}/_{w}$ drug. Images cross illuminated for visualisation (Bar = 100 µm) (representative of n=3).

Although all individual MNs containing PHCl formed well, upon removal of arrays from the PDMS moulds it was found that SGMNs incorporating 10 $\%^{w}/_{w}$ PHCl were weaker than the arrays containing smaller quantities of PHCl. It was observed that two thirds of the SGMN arrays incorporating 10 $\%^{w}/_{w}$ PHCl fractured during removal from the moulds, whereas none of the other arrays were affected during removal. This behaviour was similar to the results obtained from SGMN arrays incorporating 5 $\%^{w}/_{w}$ MB powder. Although these were only small datasets, it was reasoned that incorporation of 5 to 10 $\%^{w}/_{w}$ of a small MW model substance caused loss of gross structural integrity. This correlated closely with previous findings by others where incorporation up to 10 $\%^{w}/_{w}$ within biodegradable MNs was feasible (Miyano et al. 2005; Park et al. 2006).

In a similar manner, all SGMNs containing up to 10 $\%^{w}/_{w}$ BSA, Figure 4.3, appeared to have good morphological correlation to silicon MN master structures.

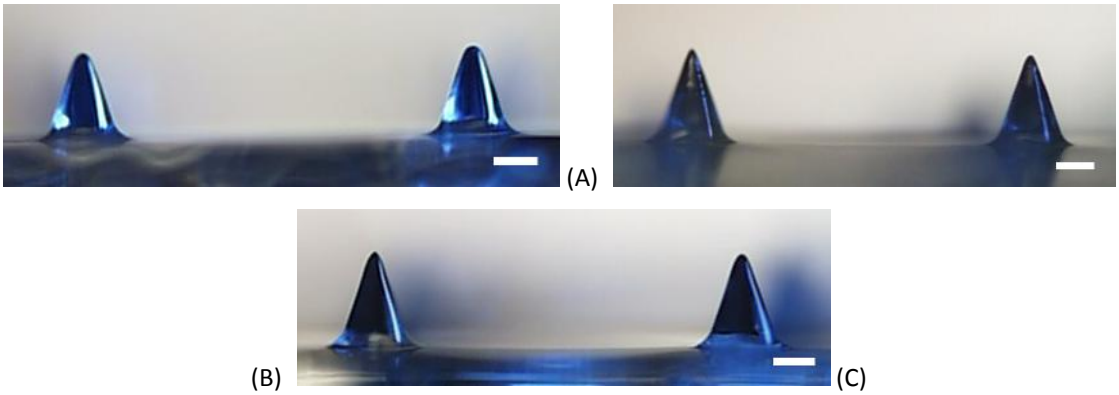

Figure 4.3 Representative light photomicrographs of SGMN arrays containing bovine serum albumin.

Arrays contain (A) 1 $\%^{w}/_{w}$, (B) 5 $\%^{w}/_{w}$ and (C) 10 $\%^{w}/_{w}$ protein. Images cross illuminated for visualisation (Bar = 100 μm) (representative of n=3).

To further assess differences between the loaded SGMN arrays formed, the number of individual MNs formed on each of the arrays was counted, Figure 4.4.

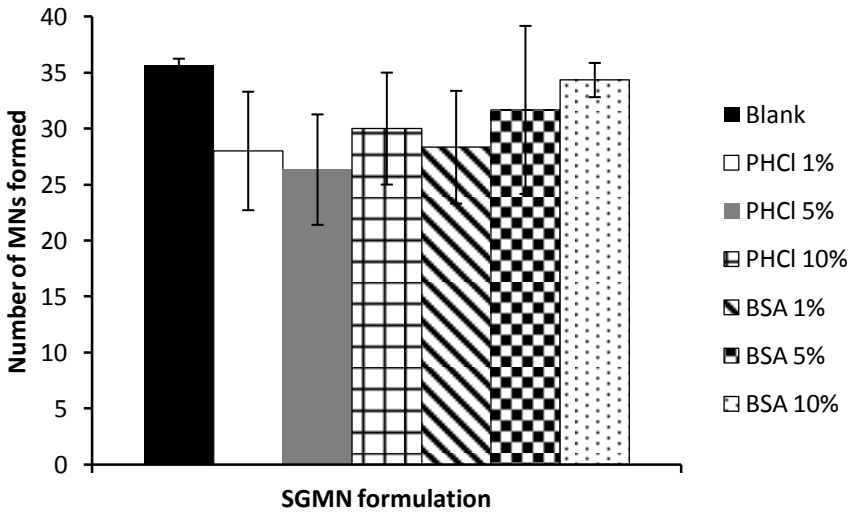

Figure 4.4 Comparison of the number of MNs fully formed on SGMN arrays containing model drugs.

Data presented as mean ± S.D.

As Figure 4.4 shows, there was no statistical difference (P=0.24) in MN formation between loaded SGMN arrays and control. This correlated with the similarities in MN structure, regardless of substance loading, visualised previously (Figures 4.2 and 4.3). Further, it appeared that incorporation of model fluorescent compounds at 5 $\%^{w}/_{w}$ had a negligible effect on SGMN structure, as Figure 4.5 shows.

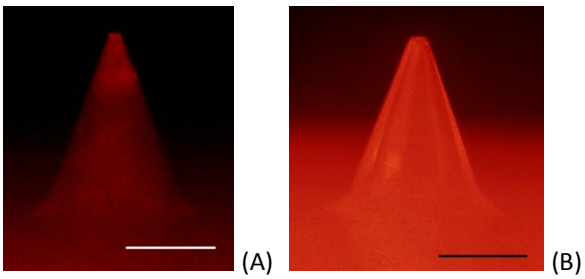

Figure 4.5 Fluorescent photomicrographs of SGMN arrays containing fluorescent model substances.

Arrays contained 5 $\%^{w}/_{w}$ loading of (A) sulforhodamine B, and (B) FITC-BSA (Bar = 100 µm).

Therefore, to maintain SGMN array integrity, a maximum of 5 $\%^{w}/_{w}$ model drug was incorporated within arrays in all future studies.

4.4.2 Theoretical calculation of sugar glass microneedle volume

Due to the relatively small dimensions of the SGMNs fabricated in this work, it was important to calculate the quantity of drug that could theoretically be loaded into the MNs alone. Based upon MN dimensions of 200 µm base width and 250 µm height, the total volume occupied by 36 SGMNs (Equation 1) was 0.12 µL. The densities of trehalose and sucrose are approximately 1.58 g/cm^3 and hence using Equation 2, 36 SGMNs contain approximately 0.19 mg of sugar. If drug were incorporated uniformly within these MNs at a concentration of 5 $\%^{w}/_{w}$, theoretically 9.5 µg drug would be contained within the needles. If this were extrapolated to a patch measuring 50 x 50 mm containing 2500 SGMNs then the amount of drug contained within the MNs at 5 $\%^{w}/_{w}$ loading would be 650 µg.

Others have calculated that a MN patch containing 100 – 1000 bevel-tip or tapered-cone needles, each with an individual mass of 10 µg, containing 10 $\%^{w}/_{w}$ drug could theoretically deliver 100 – 1000 µg (Park et al. 2006). Further, Lee et al. calculated that 600 µm long pyramidal MNs formed from various natural polymeric materials contained 25 - 60 µg matrix material per needle (Lee et al. 2008). Due to restrictions in the concentration of drug that could be incorporated within the matrix, the authors calculated that doses up to 1000 µg could be contained within a patch of a few hundred MNs. This dose could be increased to between 10 and 100 mg by loading drug throughout the entirety of the MN device however (Lee et al. 2008). Hence, this constrains the number of treatment applications for biodegradable MNs, but doses up to 1000 µg are appropriate for a number of drugs on the market. These include

interferon α-2A for hepatitis C, interferon β-1A for multiple sclerosis and EPO for anaemia which have doses of 33 μg/week, 132 μg/week and 100 μg/day, respectively (PDR 2005). Thus controlled release of drug would allow treatment for 30 weeks, 7 weeks and 10 days, respectively (Park et al. 2006). Vaccine delivery presents another very attractive option, for example, hepatitis B vaccine and influenza vaccine require antigen doses of only 10 and 45 μg, respectively (Park et al. 2006). Therefore, the SGMNs fabricated in this study could find utility in transdermal delivery of a number of medicaments.

4.4.3 Delivery of β-galactosidase to human skin via SGMN arrays

A model macromolecule, β-gal, was incorporated into sodium phosphate buffer (PB) solution containing TRA and SUC 75:25 $\%^{w}/_{w}$. The solution was vacuum-formed into a PDMS micromould and dehydrated to form a solid SGMN array containing enzyme, as described in section 4.3.2.2. Sugar glass MN arrays containing β-gal were shown to have strong morphological fidelity to silicon MN master structures, as shown in Figure 4.6.

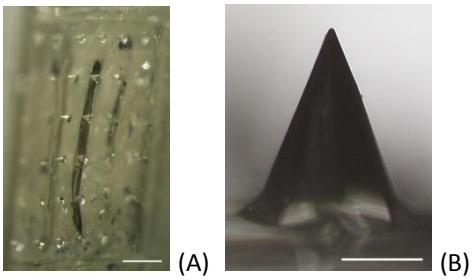

Figure 4.6 Representative light photomicrographs of SGMN array containing β-galactosidase.

(A) Entire array (Bar = 1000 μm) and (B) individual SGMN within array (Bar = 100 μm) (representative of n=3).

The SGMN arrays shown in Figure 4.6 were mounted onto syringe plunger applicators, as described section 3.3.2.9, and inserted into human skin. The arrays were maintained under an occluded environment throughout the experiment to aid dissolution and degradation. Upon removal of the arrays and X-gal staining of treated skin sections, the following data were obtained, Figure 4.7.

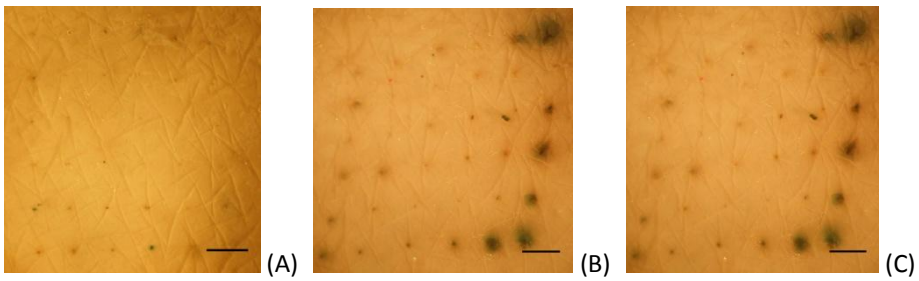

Figure 4.7 *En face* light photomicrographs of human skin following β-galactosidase delivery via SGMN and X-gal post-staining.

(Bar = 1000 μm) (n=3).

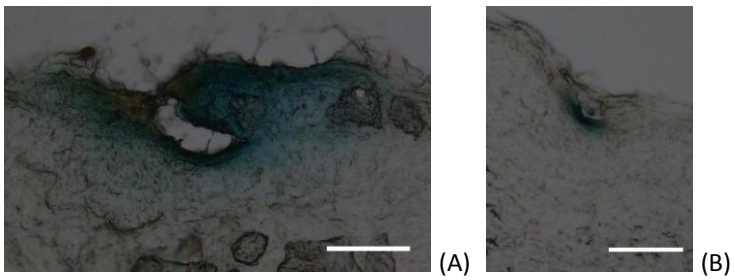

Figure 4.8 Representative light photomicrographs of human skin sectioned transversely following β-galactosidase delivery via SGMNs.

(Bar = 100μm).

As shown in Figure 4.7, each of the SGMN arrays containing β-gal punctured human stratum corneum (SC) to facilitate the delivery and deposition of enzyme within deeper skin layers. This was confirmed by the presence of oxidised blue X-gal staining product surrounding SGMN channels, Figure 4.8. However, deposition of enzyme was not uniform in each case, for example, as Figure 4.8 (B) shows it appeared that a considerably smaller amount of enzyme was delivered into this MN channel compared to the channel in Figure 4.8 (A). Although all SGMN arrays did penetrate human skin to deliver β-gal, under these conditions deposition of enzyme appeared to vary between individual treatments. It was reasoned that the variations observed could be due to a number of issues. Firstly, skin penetration by each array may not have been uniform which may have led to uneven protein deposition within the epidermis. Furthermore, the MN channels created may have re-sealed or become blocked during subsequent processing. Consequently, there may have been variations in penetration of X-gal staining solution into the tissue for reaction and post-staining of the enzyme. All these factors may have contributed to the variations in apparent β-gal activity observed.

Figure 4.9 Representative light photomicrograph of SGMN array containing β-galactosidase following insertion into human skin.

All needles were observed to have completely dissolved on each array following 30 mins (Bar = 1000 μm) (representative of n=3).

In contrast to Figure 4.6, it was visually apparent that all of the MNs on each of the SGMN arrays had dissolved by the end of the study, as shown in Figure 4.9. Subsequently it appeared logical that any viable enzyme contained within the MNs will have been deposited into the skin, providing that SC penetration occurred in each case. Therefore, this further suggested an issue with enzyme post-staining within the skin tissue. However, this experiment did demonstrate that β-gal remained viable in the sugar glass material throughout the process of SGMN array fabrication.

4.4.4 Effect of dehydration surface area on enzyme stability

Qualitative results utilising X-gal staining solution had demonstrated that β-gal was stable within SGMN arrays when maintained under vacuum desiccation (section 4.4.3). However, quantitative assessment of β-gal dehydrated within PB and sugar PB solutions appeared to show that the enzyme lost significant activity under certain conditions, even when maintained within a sugar glass (SG), Figure 4.10.

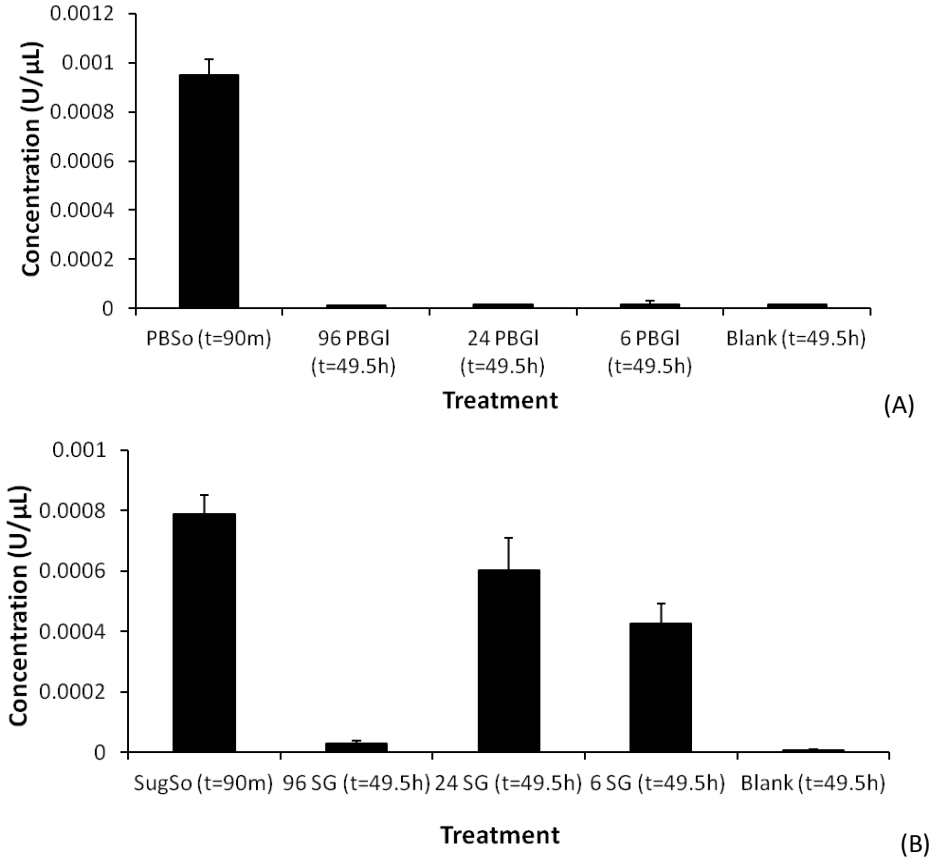

Figure 4.10 Residual enzyme activity following solution dehydration within wells with differing volumes.

Fresh enzyme solutions (t=90m) contained (A) β-gal in sodium phosphate buffer solution (PBSo) and (B) β-gal in sugar buffer solution (SugSo) dehydrated within 96, 24 and 6 well plates for 48 h (t=49.5 h) to form PB solid (PBGl) or sugar glass (SG). Data presented as mean ± S.D. (n=3).

Initially, enzyme solutions were dehydrated within 96 well plates and the enzyme was almost completely denatured under standard dehydration processing conditions, Figure 4.10. This appeared to contradict previous qualitative data and it was hypothesised that the surface area to volume ratio of the well plates used for dehydration of enzyme solutions was a key determinant in residual enzyme activity. This hypothesis was supported by data shown in Figure 4.10 (B) where the enzyme appeared to be more stable in plates with larger well dimensions. It was reasoned that this may be due to the larger surface area provided for water evaporation. This is likely to have facilitated more rapid water loss during the first 24 h, leading to enhanced protein stabilisation within a sugar matrix during the second 24 h dehydration at elevated temperature.

The data in Figure 4.10 (A) demonstrated that enzyme dehydrated in PB solution alone retained no residual activity following dehydration, regardless of well surface area. This was expected as phosphate buffer solution alone is not known to protect biomolecules in the liquid (Leslie et al. 1995) or dehydrated state (Carpenter et al. 1987a). During dehydration under elevated temperature conditions, enzymes, such as β-gal, can become deactivated by processes such as denaturation (unfolding) and thermal aggregation (Yoshioka et al. 2003). Thermal denaturation is defined as a first-order phase transition during which the native folded conformation of the protein is altered (Cordone et al. 1999), leading to inactivation. However, when the enzyme was dehydrated in the presence of sugars, Figure 4.10 (B), the volume of the wells appeared to play an important role in enzyme stabilisation. As stated, when a 96 well plate was utilised the enzyme retained little activity following dehydration. Conversely, when the enzyme was dehydrated in sugar PB in 24 or 6 well plates the sugar provided significant protection and the enzyme retained 76 % and 54 % residual activity, respectively. Similar levels of protein recovery following dehydration in the presence of amorphous stabilising mediums have been noted in other model systems, for example phosphofructokinase (Carpenter et al. 1987a; Carpenter et al. 1987b) and invertase (Schebor et al. 1996).

It was speculated that the increased surface area provided by the wells in the 24 and 6 well plates permitted faster evaporation of the solution and hence a solid SG was formed more rapidly to stabilise the enzyme. Surprisingly, the enzyme appeared to be slightly less stable when dehydrated within 6 well plates, the plate with the largest surface area, compared to 24 well plates. In all cases 300 µL of enzyme solution was used, and it was observed that only the 6 well plates had a large enough surface area for the solution to form a distinct droplet in the centre of the well. However, the reason for decreased protection afforded by SGs in these wells was not obvious. Consequently, it appeared that the 24 well plates provided the optimal surface area to volume ratio for solution evaporation and enzyme stabilisation and hence were used in all future studies.

To examine water evaporation kinetics, changes in enzyme solution weight were recorded throughout the experiment. In comparison to the 24 and 6 well plates, it was found that there was considerably more water present in enzyme formulations contained within 96 well plates following the first 24 h of dehydration. It was observed that approximately 60-70 % water remained within 96 well plates at 24 h, regardless of whether sugar was present or not.

Conversely, formulations dehydrated in 24 and 6 well plates contained much lower quantities of water at 24 h. As more water was present within the 96 well plate formulations at 24 h, it was speculated that the enzyme was less likely to have been stabilised during subsequent temperature elevation. This may have led to denaturation of the protein within 96 well plates, Figure 4.10.

4.4.5 Investigation of β-galactosidase stability within sugar glasses

To further explore the capacity of SG material to stabilise a functional macromolecule, β-gal was incorporated within PB and sugar PB solutions. These solutions were exposed to the processing conditions developed to fabricate solid SGs with dehydration at ambient temperature for 24 h followed by dehydration at an elevated temperature of 50 °C for a further 24 h. Enzyme activity at all time points was estimated by linear regression analysis of standard β-gal concentrations, as Figure 4.11 shows.

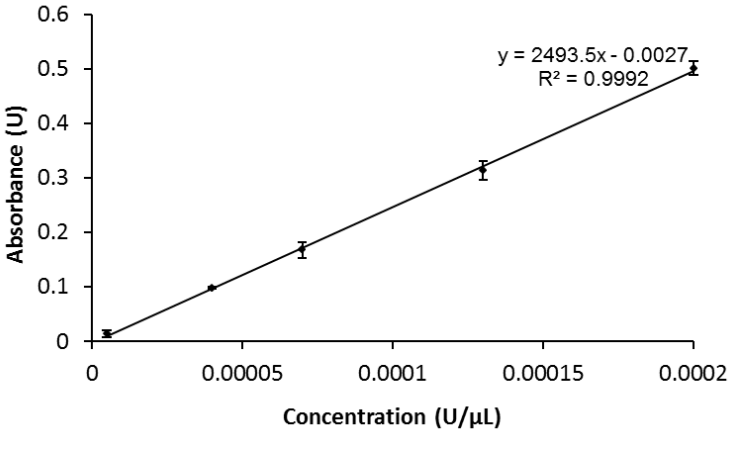

(A)

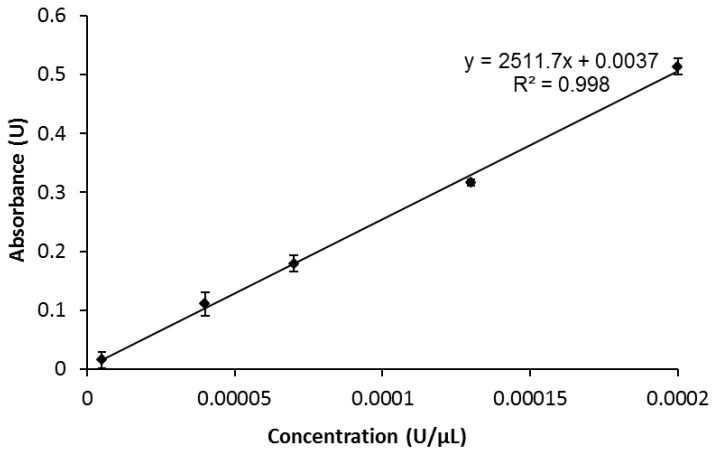

(B)

Figure 4.11 Exemplar standard curves used in quantitative determination of β-galactosidase.

Curves represent (A) β-gal in PB solution and (B) β-gal in sugar PB solution. Data presented as mean ± S.D. (n=3).

It was found that the activity of β-gal was very similar regardless of whether it was formulated into a solution containing sugar or not. This was indicated by the similarity in the slopes obtained for the calibration curves generated in Figure 4.11. Utilising these curves sample enzyme concentrations were estimated following 48 h processing. As stated, sample solutions were dehydrated over a 48 h period under standard dehydration conditions. Control solutions were either maintained in sealed vials to prevent solvent evaporation or heated to 90 °C; a temperature known to denature β-gal (Ladero et al. 2006; Leslie et al. 1995). The stability of the enzyme following processing is shown in Figure 4.12.

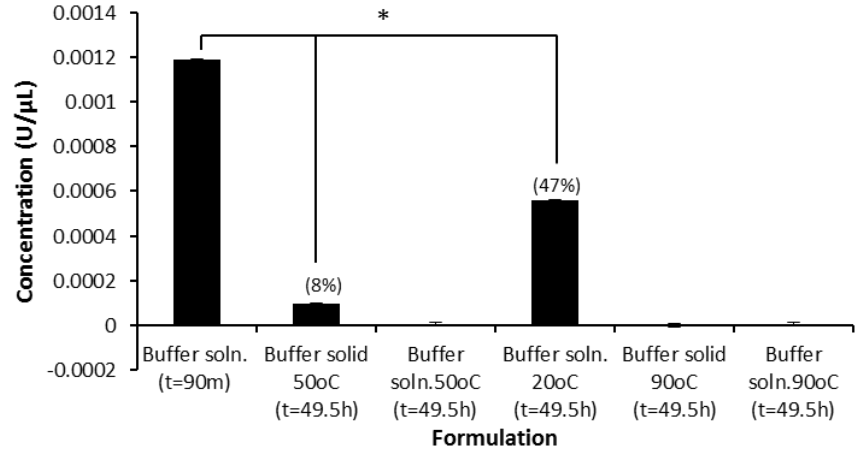

(A)

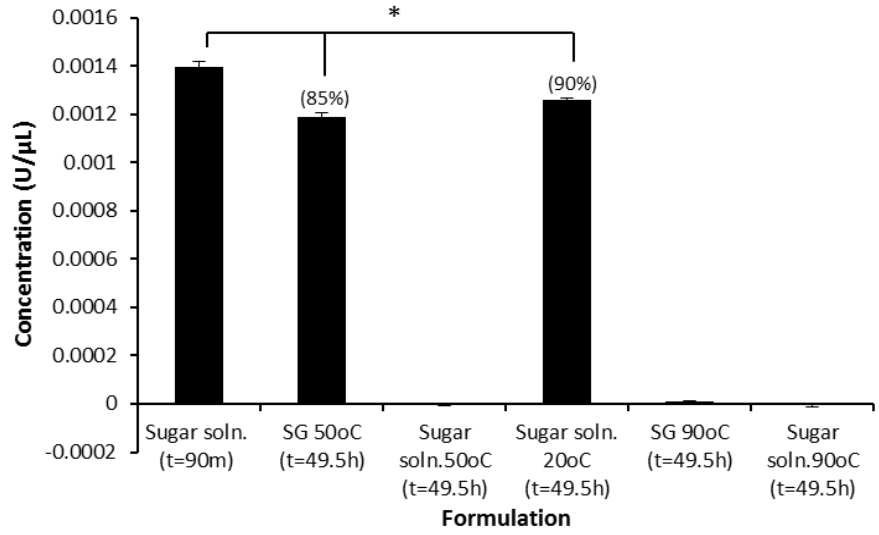

(B)

Figure 4.12 Stability of β-galactosidase during dehydration processing and sugar glass formation.

Treatments were as follows; fresh enzyme (t=90 m) in (A) phosphate buffer solution and (B) sugar buffer solution. Enzyme in (A) phosphate buffer and (B) sugar buffer solution dehydrated under standard conditions (ambient temperature for 24 h followed by 24 h at 50 °C); Buffer solid 50oC and SG 50oC (t=49.5 h), respectively. Enzyme in (A) phosphate buffer and (B) sugar buffer solutions maintained under standard conditions; Buffer soln. 50oC and Sugar soln. 50oC (t=49.5 h), respectively. Enzyme in (A) phosphate buffer and (B) sugar buffer solution stored at ambient temperature (20 °C) for 48 h; Buffer soln. 20oC and Sugar soln. 20oC (t=49.5 h), respectively. Enzyme in identical formulations as stated under standard conditions except with dehydration at 90 °C for 24 h; suffix 90oC. Data presented as mean ± S.D. (n=3), * denotes statistical significance at $P<0.05$.

As Figure 4.12 shows, β-gal was denatured in all treatments processed at 90 °C. This was expected as 90 °C is known to denature β-gal and because it is unlikely that a solid SG will have formed completely by 24 h to stabilise the enzyme prior to temperature elevation. This temperature is also close to the Tg of TRA and SUC and hence they will have afforded little protection to the enzyme at this temperature (de Jonge et al. 2007). Formation of a solid dehydrated product appeared to be critical to enzyme protection. This was demonstrated by the samples heated to 50 °C, where the enzyme was completely denatured when maintained in PB (Buffer soln. 50oC) and sugar PB (Sugar soln. 50oC) solutions. Similar observations were made by Mazzobre et al. where β-gal was denatured rapidly at 45 – 55 °C when maintained in liquid phosphate buffer (Leslie et al. 1995). However, in the corresponding samples where a solid product was formed, Buffer solid 50oC and SG 50oC respectively, the enzyme retained residual activity following processing, Figure 4.12. It was apparent that the residual enzyme activity remaining within the SG 50 °C product was significantly greater than that of the Buffer solid 50 °C product though. It has been stated that during drying, the major stress that a protein must overcome is loss of its hydration shell. This effect can cause irreversible inactivation upon rehydration (Carpenter and Crowe 1989) unless a carbohydrate is present (Carpenter et al. 1987a; Carpenter et al. 1987b; Prestrelski et al. 1993). Accordingly, it was surprising that the enzyme retained any activity following dehydration within PB alone.

It was speculated that the enhanced residual enzyme activity within the SG was due to replacement of evaporated water through hydrogen bonding of sugar to the protein to prevent dehydration-induced denaturation and inactivation (Carpenter and Crowe 1988, 1989). Additionally, there were only small decreases in enzyme activity between freshly prepared sugar PB solution (Sugar soln.) and enzyme left at ambient temperature for 48 h in sugar solution (Sugar soln. 20oC) or incorporated within SG at 50 °C. These data together demonstrate the protective functionality of solid TRA/SUC 75:25 $\%^{w}/_{w}$ SG on β-gal when processed below the denaturation temperature of the enzyme.

Furthermore, solutions maintained at ambient temperature for 48 h showed significantly greater enzyme stability in sugar PB solution compared to PB alone. This result was unexpected as solid SG had not been formed. However, similar effects have been noted by others where it has been shown that solutes in solution have a protective effect on proteins undergoing stresses, such as freezing (Koster and Leopold 1988). In conclusion, it appeared that the enzyme was stable during dehydration processing when incorporated into the matrix

of a SG. Although the quantity of enzyme that remained within the glass decreased slightly compared to the initial concentration, it appeared that the enzyme was protected to a far greater extent when sugar was present in the formulation. This data demonstrated the utility of solid SGs to maintain β-gal viability during air-drying dehydration processes.

4.4.6 Initial stability study of sugar glass formulation

During the initial 7 days of the study it appeared that SGMNs maintained under refrigeration, elevated temperature and relative humidity (RH) conditions, as stated in section 4.3.2.9, were completely unstable. Upon visual examination of SGMN arrays it was apparent that these devices would not be stable unless maintained in a low moisture environment. Amorphous materials are known to be unstable under high humidity (Hageman 1992; Lai et al. 1999; Nowakowski and Hartel 2002) and elevated temperature environments (de Jonge et al. 2007; Hageman 1992) and the results observed here support these findings. Further, maltose MNs were shown to be unstable when stored at a RH of 50 % and dissolved within hours (Miyano et al. 2005). Additionally, galactose MNs were found to dissolve within 1 h at a RH of 75 % and within 6 h at a RH of 43 % (Donnelly et al. 2009a). In a similar manner, the arrays stored at 4 °C, Figure 4.13 (C), and at 60 %RH, Figure 4.13 (A), in this study were both found to be viscous semi-solids whilst the array stored at 75 %RH and elevated temperature had completely re-crystallised, Figure 4.13 (B).

Figure 4.13 Light photomicrographs of SGMN arrays within micromoulds following 7 days storage.

Arrays were stored under (A) 20 ± 2 °C and 60 ± 5 %RH, (B) 40 ± 2 °C and 75 ± 5 %RH and (C) 4 ± 2 °C. Arrows indicate example areas of crystallisation (Bar = 1000 μm).

It was hypothesised that the results observed in Figure 4.13 were due to moisture absorption from the environment by the SGMN arrays. It was speculated that this may be due to the hygroscopic nature (Dittmar 1935) of the SG material being examined. Additionally, the result observed with elevated temperature storage, Figure 4.13 (B), could have been due to

increased molecular mobility within the material (de Jonge et al. 2007) as these conditions were closer to the glass transition temperatures of the sugars studied. As none of the storage conditions in Figure 4.13 yielded viable SGMN arrays following 7 days storage, these treatment groups were discontinued. It was rationalised that β-gal was unlikely to be stable within the SG material under these conditions, as it has been shown that enzyme activity is significantly reduced upon sugar crystallisation at elevated humidity (Cardona et al. 1997). It is likely that spatial constraints within the crystalline phase reduce the effectiveness of hydrogen bonding between protein and sugar leading to reduced stabilisation (Izutsu et al. 1994). Furthermore, if MN structure could not be maintained then it would be impossible to deliver the protein across skin.

In contrast, SGMN arrays maintained under a desiccated environment appeared to retain their amorphous structure at 7 days, as Figure 4.14 shows.

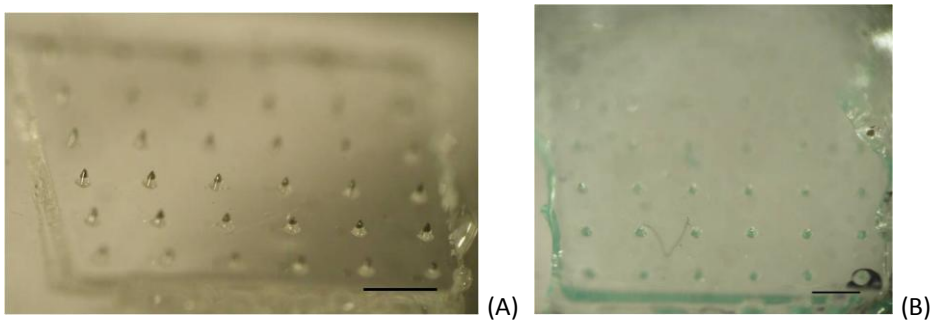
(A) (B)

Figure 4.14 Light photomicrographs of SGMN arrays following 7 days storage.

Arrays were stored under (A) 20 ± 2 °C and vacuum desiccation and (B) 4 ± 2 °C and desiccation (Bar = 1000 μm).

It appeared that under desiccated storage environments at both 4 and 20 °C, SGMN arrays maintained their gross structure throughout the study duration. Once more, this is supported by the work of Miyano et al. where it was found that maltose MNs maintained under an environment of less than 40 %RH retained their morphology over a 3 month period (Miyano et al. 2005). Donnelly et al. made similar findings and observed that the morphology of galactose MNs stored at 0 %RH did not change throughout 3 weeks storage (Donnelly et al. 2009a). However, in this study there were differences noted between individual MNs within the arrays stored under each of the desiccated conditions. This is shown in Figure 4.15.

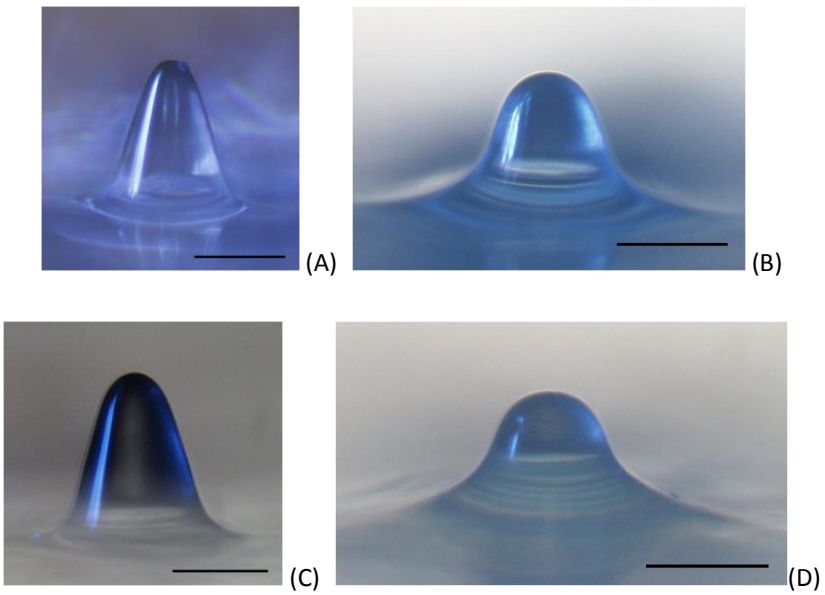

Figure 4.15 Representative light photomicrographs of SGMNs following desiccated storage.

Arrays were stored for 5 weeks under (A) 20 ± 2 °C and vacuum desiccation and (B) 4 ± 2 °C and desiccation, and (C) and (D) 3 months under the storage conditions stated in (A) and (B) respectively. Images cross illuminated for visualisation (Bar = 100 µm).

As Figure 4.15 shows, SGMNs maintained under both desiccated storage conditions lost their pyramidal structure during the study duration. It appeared that SGMNs maintained under 20 ± 2 °C and vacuum desiccation, Figure 4.15 (A) and (C), retained their morphology to a greater extent than MNs stored under 4 ± 2 °C and desiccation, Figure 4.15 (B) and (D) however. This study suggested that neither storage condition was optimal for maintaining SGMN geometry over a 3 month storage period. The images in Figure 4.15 appeared to suggest that the SG material had flowed during the storage period. Microneedles maintained under both conditions appeared to be more rounded and smooth than freshly prepared MNs. A similar phenomenon had been observed with the first SGMN array formed in Chapter 3. This array was mounted onto a metallic stub and sputter coated with a thin layer of gold, for SEM viewing, before being left under ambient conditions for a period of 12 months. The array was mounted at a 90 ° angle and, as Figure 4.16 shows, following this period the glassy material appeared to have flowed under the force of gravity in a similar manner to a liquid droplet. From these data, it was speculated that this phenomenon may have been due to the relatively unstable amorphous nature of SGs deforming during storage.

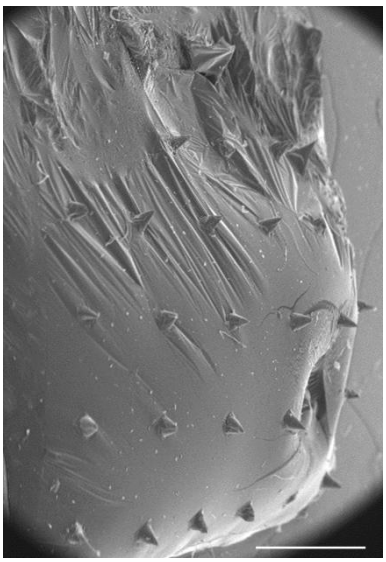

Figure 4.16 First SGMN array fabricated.

Array was sputter coated with gold for SEM viewing and left under ambient conditions for 12 months at a 90 ° angle (Bar = 1000 μm).

4.4.7 Assessment of β-galactosidase stability within sugar glasses

To quantitatively explore the stability afforded by SGs a model macromolecule, β-gal, was incorporated into the matrix and its activity was assayed over a 3 month period. In this study 24 well plates were used as these had been shown to provide the most effective surface area to volume ratio for dehydration and stabilisation of enzyme in SGs (section 4.4.4). The data presented in Figure 4.17 shows the residual enzyme activity remaining within dehydrated samples throughout the study.

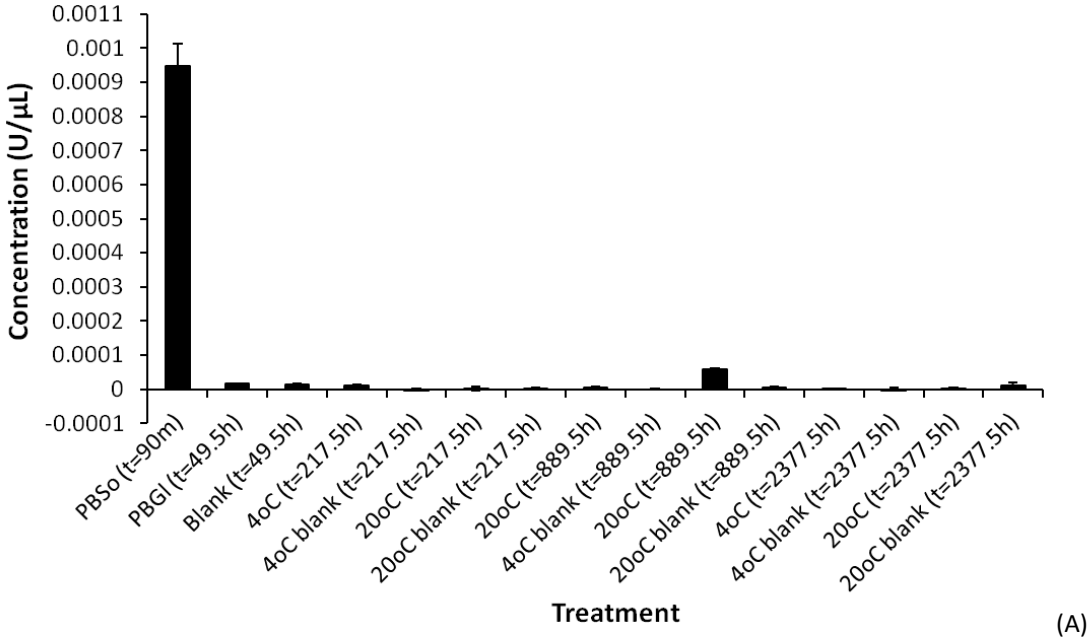

(A)

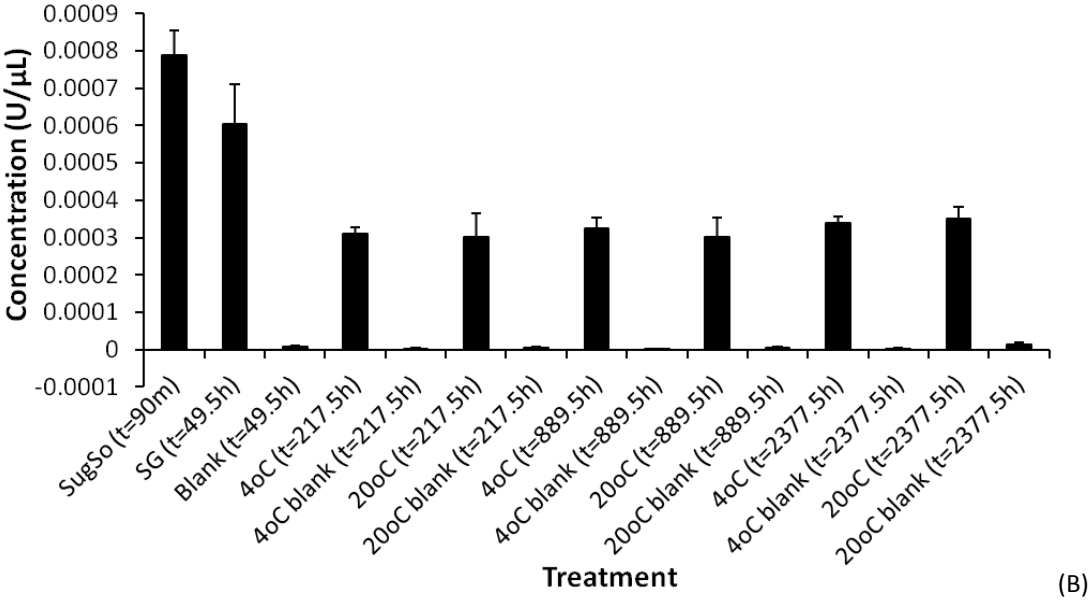

(B)

Figure 4.17 Stability of β-galactosidase in dehydrated formulations stored over 3 months.

Treatments were as follows; fresh enzyme (t=90 m) in (A) phosphate buffer solution (PBSo) and (B) sugar buffer solution (SugSo) and enzyme maintained within (A) dehydrated PB solid (PBGl) and (B) sugar glass (SG) stored under 4 ± 2 °C or 20 ± 2 °C and desiccation; 4oC and 20oC, respectively. Enzyme activity was quantified in fresh solutions and in dehydrated formulations (t=49.5 h) and then at 7 days (t=217.5 h), 5 weeks (t=889.5 h) and 3 months (t=2377.5 h) following dehydration. Data presented as mean ± S.D. (n=3).

As Figure 4.17 (A) shows, β-gal was denatured when dehydrated slowly within PB alone. This supported previous findings where the enzyme lost activity when dehydrated within buffer solution only, Figure 4.12. In contrast, to maintain enzyme activity in commercial formulations

the enzyme is supplied as a lyophilised powder containing Tris buffer salts and magnesium chloride (http://www.sigmaaldrich.com/catalog/product/sigma/g6008?lang=en&region=GB. Accessed 27/03/12) to maintain β-gal activity. As hypothesised, when the enzyme was contained within a SG material, Figure 4.17 (B), the enzyme retained residual activity throughout the study duration. During SG formation (t=49.5 h) there was a small but significant decrease in initial enzyme activity. This correlated with previous data showing that dehydration processing in 24 well plates decreased enzyme activity to approximately 76 % of the freshly prepared stock solution, Figure 4.10. Enzyme activity then decreased further during the first week of storage (up to 217.5 h). This behaviour is not uncommon as it is known that chemical deterioration processes can still occur in SG systems stored below Tg, but at a reduced rate (Streefland et al. 1998). Further, it was speculated that the reduction in β-gal activity during the first week of storage may have been due to annealing of the sugar glass. This process alters the material properties towards a lower energy state which is under meta-stable equilibrium (Zhou et al. 2007). From one week storage onwards, enzyme activity appeared to remain stable within the glass when maintained under vacuum or refrigeration desiccation, which supports this hypothesis. This data indicated that as long as the SG material was maintained under a desiccated environment the amorphous material would be stable and protect the enzyme incorporated within the matrix (Fraenkel et al. 2006). In this work β-gal enzyme was chosen as a model protein due to its ease of assay. It seems likely that the protective SG effects observed here may be extrapolated to other proteins however. β-galactosidase is prone to loss of activity through increase in apparent size which may be due to covalent bond formation between molecules, aggregation without covalent bond formation or protein denaturation and unfolding (Guyot and Fawaz 2000). Other proteins such as interferon, basic fibroblast growth factor, lactalbumin, and casein are known to undergo similar conformational changes during dehydration which leads to inactivation (Prestrelski et al. 1993). It has been postulated that these changes maximise the intra- and inter-chain hydrogen bonds between polypeptides to replace those bonds lost to water (Prestrelski et al. 1993). Furthermore, lactate dehydrogenase in buffer solution was completely inactivated following freeze-drying, whereas it maintained approximately 100 % activity when dried in the presence of sucrose and various other sugars (Prestrelski et al. 1993). Similarly, Lee et al. recently demonstrated only a 15 % loss of recombinant human growth hormone activity contained within CMC MNs stored under ambient conditions (Lee et al. 2011a). This suggests that a number of proteins may behave in a similar manner to β-gal and hence further optimisation of the fabrication conditions of SGMN arrays may be required for enhanced macromolecule stabilisation.

4.4.8 Sugar glass microneedle stability study

Previous findings had shown that SGMN arrays were physically unstable when stored under high RH conditions, under refrigeration or at elevated temperature (section 4.4.6). To investigate the optimal storage conditions for SGMN arrays further, arrays were stored under the following conditions, vacuum desiccation at 20 °C, desiccation at 4 °C, 15 %RH at 20 °C, 10 %RH at 20 °C, 5.5 %RH at 20 °C and 10 %RH at 37 °C. Examples of SGMNs formed at the beginning of the study are shown in Figure 4.18.

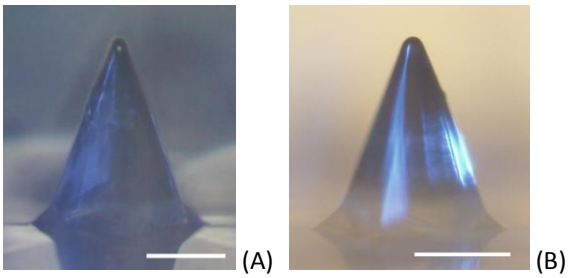

Figure 4.18 Representative light photomicrographs of freshly formed SGMNs.

Images cross illuminated for visualisation (Bar = 100 µm).

As Figure 4.18 demonstrates, SGMNs formed initially had a strong morphological correlation to silicon MN master structures. This was important to establish as all SGMNs would be compared to these initial structures throughout the duration of the study. Following storage of SGMNs for 7 days the arrays were viewed once more under light microscopy. It was observed that SGMNs stored at ambient temperature under 5.5 %RH and 10 %RH or 37 °C and 10 %RH were unstable and no MN structures remained on these arrays at 7 days (data not shown). However, SGMN arrays stored under desiccation at 4 or 20 °C and 15 %RH at 20 °C did appear to be stable, Figure 4.19.

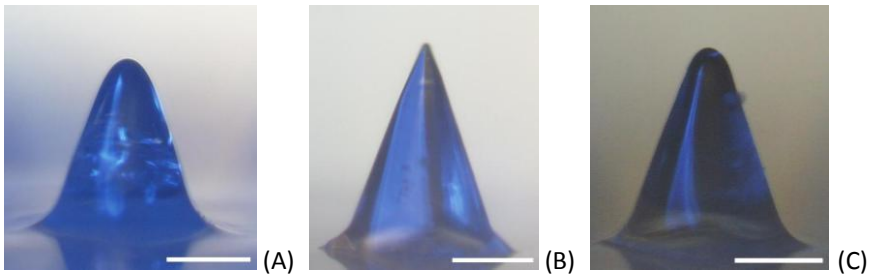

Figure 4.19 Representative light photomicrographs of SGMNs stored for 7 days.

Arrays were stored under (A) 4 ± 2 °C and desiccation (B) 20 ± 2 °C and 15 %RH, (C) 20 ± 2 °C and vacuum desiccation. Images cross illuminated for visualisation (Bar = 100 µm).

It was apparent from the data presented in Figure 4.19 that the different storage conditions had distinctive effects on SGMN structure. It appeared that the optimal storage condition at this time point was 15 %RH at 20 °C, Figure 4.19 (B), as the MNs within this array retained the strongest morphological fidelity to the master structures. In support of previous findings, Figure 4.15, it appeared that SGMNs stored under a desiccated environment, Figure 4.19 (A) and (C), began to lose their initial morphology within 7 days. It was speculated that there was an equilibrium relationship established between the moisture in the storage chamber and the residual water remaining within the SGMNs. Furthermore, it has been shown that storage RH does not equate to moisture content of amorphous sugars maintained within the environment at equilibrium (Nowakowski and Hartel 2002). For example, corn syrup and sucrose glasses with high surface to volume ratios equilibrated to 80 %RH for one week contained approximately 9 % total moisture (Nowakowski and Hartel 2002). Therefore, it may have been that 15 %RH, which corresponds to an absolute humidity of 2 g/kg at 20 °C (Margetts and Sawyer 2007), provided the optimal storage humidity for stabilisation of the SGMN structure. When the environment contained a lower mass of water vapour at 5.5 or 10 %RH, this appeared to cause rapid MN degradation, and conversely when excess water was present in the environment this caused rapid water sorption and destabilisation of the amorphous glass, Figure 4.13.

To assess the water content of SG material maintained under these conditions, TGA was performed on the glasses, Figure 4.20.

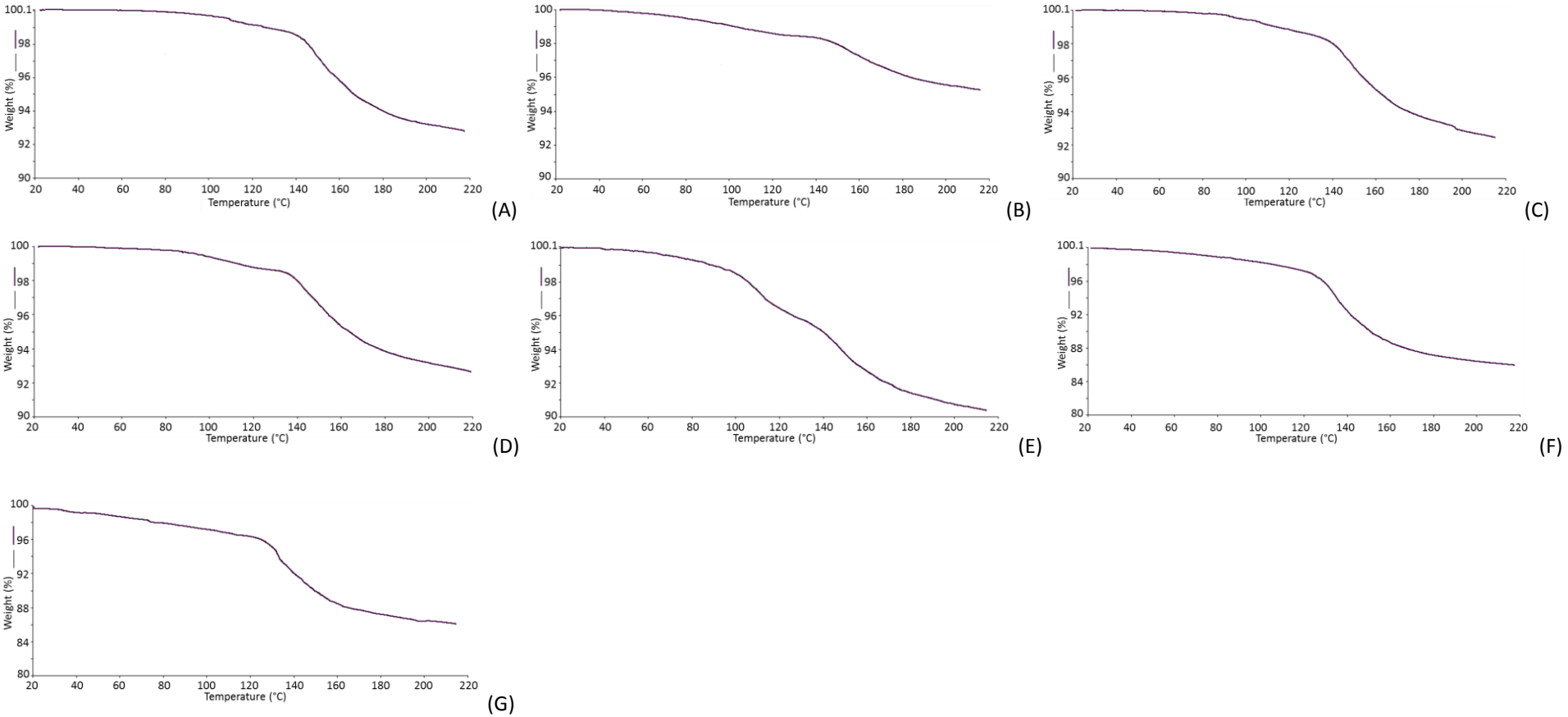

Figure 4.20 Thermogravimetric analysis of sugar glasses under various storage conditions.

Profiles indicate water content of SGs (A) at formation, and then following storage under (B) 4 ± 2 °C and desiccation, (C) 20 ± 2 °C and 15 %RH, (D) 20 ± 2 °C and vacuum desiccation, (E) 20 ± 2 °C and 5.5 %RH, (F) 20 ± 2 °C and 10 %RH, (G) 37 °C and 10 %RH.

As shown in Figure 4.20 (A), the SGs formed initially contained approximately 7 $\%^{w}/_{w}$ water. This correlated with previous findings in section 2.4.4, where combination SGs were shown to contain approximately 5 - 8 $\%^{w}/_{w}$ water. However, once introduced into environments with differing RH the water content of the SGs appeared to change. Variation in water content was not large under any of the storage conditions, but it may have had an effect on the subsequent stability of the SGMN arrays. As stated, SGMNs appeared to be completely unstable following storage under ambient temperature at 5.5 %RH and 10 %RH or 37 °C and 10 %RH. The profiles in Figures 4.20 (F) and (G) showed that both glasses maintained under 10 %RH showed an increase in water content following 7 days storage and a slight increase in water content was shown following storage at ambient temperature and 5.5 %RH, Figure 4.20 (E). It was not apparent why these glasses may have increased in water content, and as the increases were only small, the differences may have been due to experimental variation. Importantly, none of these storage conditions appeared to stabilise the SGMN structure and hence were disregarded.

In contrast, it appeared that SGMN arrays remained stable when maintained under desiccation or 15 %RH at ambient temperature. Sugar glasses maintained under ambient temperature and vacuum desiccation or 15 %RH, Figures 4.20 (C) and (D), appeared to show thermal profiles very similar to the initially fabricated SG, Figure 4.20 (A). This data suggested that the material was stable under these environments and supported visual observations of SGMN stability, Figure 4.19. The SG maintained at 4 °C under desiccation showed a slight decrease in water content following 7 days storage however. Similar observations had been made previously, section 2.4.4, where it appeared that the water content of SGs had decreased following periods of desiccated storage. This decrease in water content did not appear to be completely detrimental to the SGMN structure, Figure 4.19 (A), but the array was noted to have changed from being transparent to opaque. It was speculated that this effect may have been due to the desiccated environment utilised and further removal of water from the SG structure. From these data it was concluded that the nature and stability of SGMNs formed by low temperature dehydration was not straightforward. Fabrication technique and thermal history are known to influence amorphous sugar properties (Surana et al. 2004) and hence it was speculated that the process developed for SGMN production may have led to the unusual material properties observed.

To observe how storage conditions affected SGMN properties over extended periods, arrays were maintained under these conditions for 3 months. The images in Figure 4.21 depict SGMNs following 28 days storage. As shown, the geometry of each of the SGMNs stored under each of the environments studied appeared to have changed little in comparison to 7 days storage. It was observed that all MNs on each of the arrays appeared to have taken on a more rounded appearance, but that they generally resembled the SGMNs shown in Figure 4.19. Once more, this supported previous findings following 5 weeks storage, Figure 4.15.

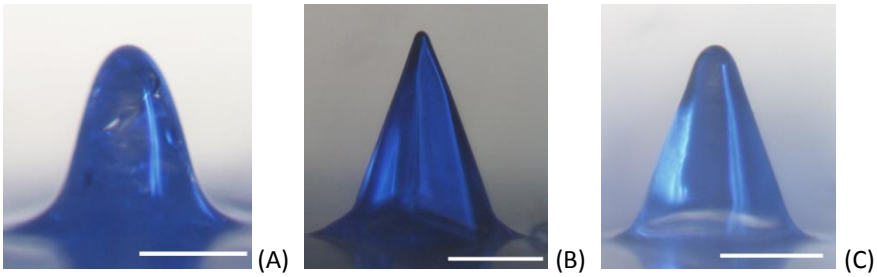

Figure 4.21 Representative light photomicrographs of SGMNs following 28 days storage.

Arrays were stored under (A) 4 ± 2 °C and desiccation (B) 20 ± 2 °C and 15 %RH, (C) 20 ± 2 °C and vacuum desiccation. Images cross illuminated for visualisation (Bar = 100 µm).

Further sections of SG were examined to determine water content at this time point, Figure 4.22. Again, it appeared that the water content of these glasses closely resembled those obtained at 7 days, Figure 4.19 (B) – (D). However, it was noted that the content of the SG maintained at 4 °C under desiccation appeared to have decreased marginally once more, Figure 4.22 (A). This is likely to have been due to the desiccated environment and further water loss over this period.

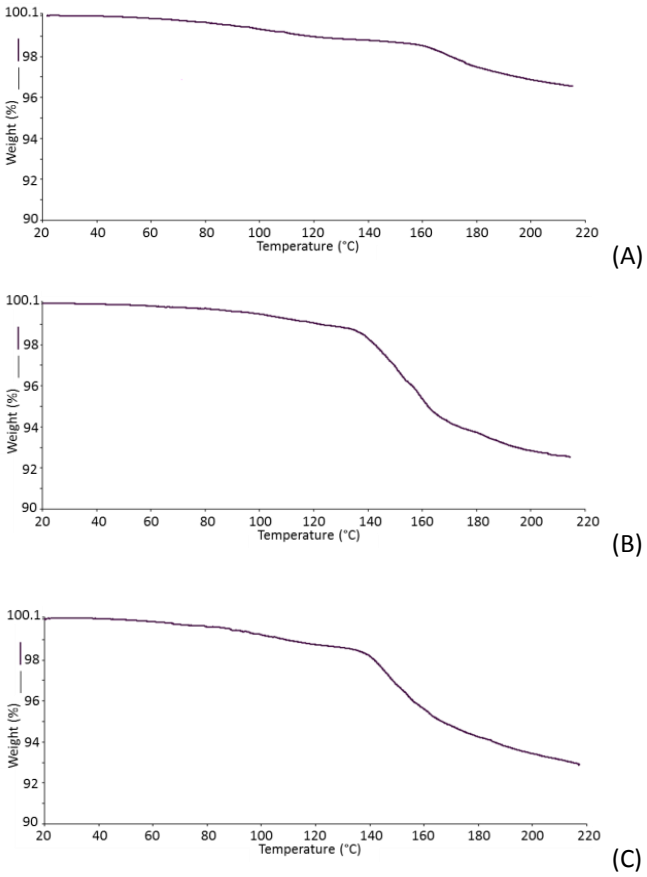

Figure 4.22 Thermogravimetric analysis of sugar glasses following 28 days storage.

Profiles indicate water content of SGs following storage under (A) 4 ± 2 °C and desiccation, (B) 20 ± 2 °C and 15 % RH, (C) 20 ± 2 °C and vacuum desiccation.

The data obtained following 3 months storage was disrupted prior to SGMN array visualisation. As Figure 4.23 shows, all of the arrays viewed at this time point retained no MN structures. It was noted that each of the arrays had developed a "lustrous" appearance, and the surfaces had become viscous in nature. According to reports on the day of assessment and visualisation, the ambient temperature was approximately 25 °C whilst the RH was 94 %. As RH is a measure of the degree of water vapour saturation of air (Margetts and Sawyer 2007), and as it was a warm day, the air will have contained a relatively large mass of water vapour. From the results observed, it was speculated that due to the hygroscopic nature of SG material (Dittmar 1935) SGMN arrays had adsorbed and absorbed water from the environment prior to visualisation. Moisture sorption processes are likely to have caused the rapid dissolution and change in material properties (Nowakowski and Hartel 2002) of the SGMNs observed.

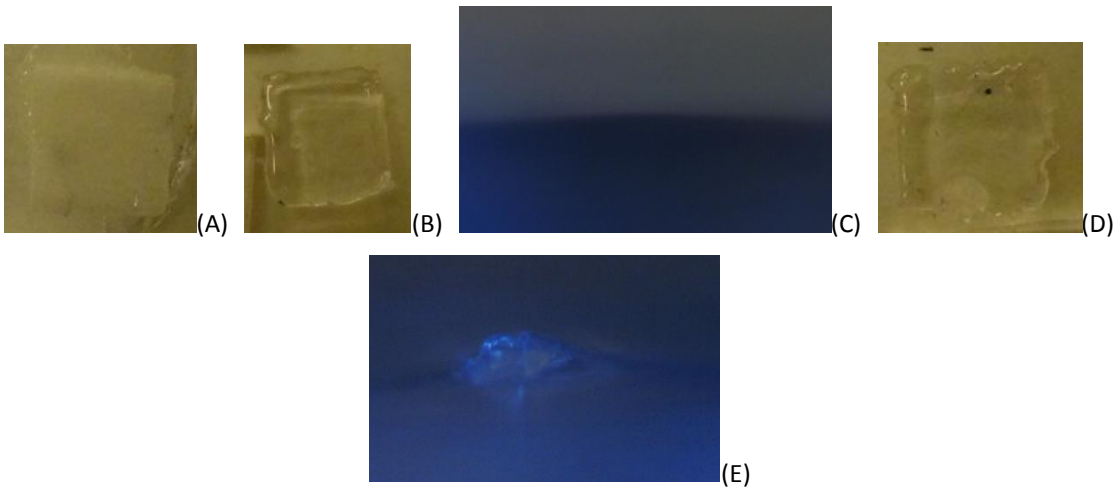

Figure 4.23 Representative examples of SGMN arrays stored for 3 months.

Macro images of arrays stored under (A) 4 ± 2 °C and desiccation (B) 20 ± 2 °C and 15 % RH, (D) 20 ± 2 °C and vacuum desiccation prior to visualisation(Bar = 100 µm). (C) and (E) light photomicrographs of the surface of arrays (B) and (D), respectively, demonstrating the absence of discrete microneedle structures. Images cross illuminated for visualisation purposes.

Due to the suspected adverse effects of the ambient conditions on SGMN arrays, measures were taken to protect SG material from these conditions prior to thermal analysis. As the profiles in Figure 4.24 show, there was little difference in water content noted at 3 months in comparison to samples examined at 28 days, Figure 4.22. This suggested that the material was stable for up to 3 months under desiccation at 4 and 20 °C and at 20 °C under 15 %RH. The small decrease in water content noted in samples stored under desiccation at 4 °C was speculated to be due to the mass of desiccant utilised. As the quantity of desiccant was not standardised between different storage conditions this may have accounted for the decrease in water content observed in refrigerated samples only.

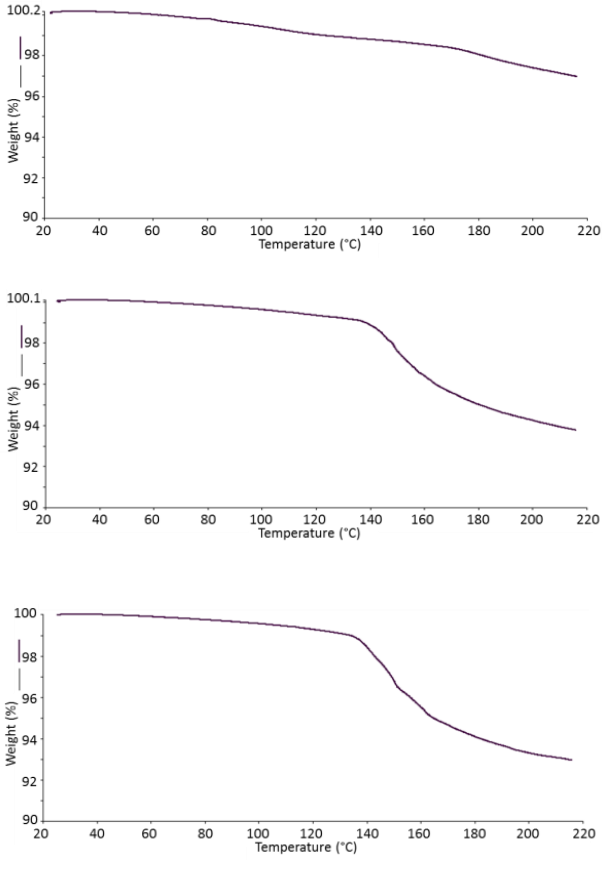

Figure 4.24 Thermogravimetric analysis of sugar glasses following 3 months storage.

Profiles indicate water content of SGs following storage under (A) 4 ± 2 °C and desiccation, (B) 20 ± 2 °C and 15 % RH, (C) 20 ± 2 °C and vacuum desiccation.

4.5 Conclusion

It was an important focus of this chapter to investigate incorporation of model substances within the structure of SGMN arrays. In line with previous reports, loading of a range of different model molecules with varying physicochemical properties did not appear to affect MN stability up to approximately 5 $\%^{w}/_{w}$. Drug loading at a greater concentration than this, especially with small molecules, appeared to decrease SGMN array integrity however. The activity of a functional model macromolecule, β-galactosidase, following incorporation within SGMNs was shown to be stable following vacuum processing and dehydration. Sugar glass MNs containing enzyme demonstrated sufficient structural rigidity to puncture the human skin barrier to facilitate delivery of protein into deeper skin layers. This finding was essential to the future utility of these devices to facilitate transdermal drug delivery of macromolecular drug substances.

Furthermore, the enzyme was shown to retain activity when maintained within sugar glass material following storage at ambient or refrigerated temperature under desiccation over a period of months. Storage conditions were shown to be critical to the physical stability of SGMN structure however. Elevated temperature and humidity appeared to be extremely detrimental to MN morphology; although conversely a completely desiccated environment did not appear to be optimal either. Preliminary studies indicated that a storage environment with a low relative humidity at ambient temperature may be optimal for prolonged SGMN stability.

Chapter 5

Optimisation of in vitro assays to assess sugar glass microneedle drug delivery

5 Optimisation of in vitro assays to assess sugar glass microneedle drug delivery

5.1 Introduction

5.1.1 *In vitro* transdermal drug delivery

The gold standard for assessing the drug delivery capacity of any novel transdermal delivery device would be to evaluate its efficacy in human subjects. However, there are many drawbacks to this form of investigation including cost, ethical approval and the potential for harm to be caused to the subject. Therefore, a number of *in vitro* and *in vivo* techniques have been developed to estimate the drug delivery efficiency of transdermal formulations in model systems.

In vitro methods are particularly interesting as they remove the necessity to use a living organism to assess transdermal drug delivery properties. Typically, diffusion cells are used to assess potentially suitable transdermal formulations and devices. In this set up a model membrane is sandwiched between the flanges of the donor and receptor chambers of the diffusion cell and a formulation is applied to the donor phase. Different representative barriers are used in these experiments, each with their own advantages and disadvantages. One approach is to use a synthetic membrane that is not of animal origin, but one which retains certain characteristics of the human skin barrier. For example, medical grade non-porous Silastic® (polydimethylsiloxane) sheeting has been compared to heat separated human epidermal membranes in the assessment of oestradiol diffusion from saturated and supersaturated solutions of drug in various co-solvent systems (Megrab et al. 1995). The rationale for the use of such a model is that the material represents a simple and inert membrane to investigate the permeation of drug from an unstable formulation. Skin represents a heterogeneous and variable membrane in comparison to Silastic® and therefore the polymer provides a more predictable barrier in such permeation studies (Donnelly et al. 2009a; Megrab et al. 1995). It has also been shown previously that the permeability of silicone rubber membrane to a small molecular weight drug, such as salicylic acid, is comparable to that of human skin (Nakano and Patel 1970). Other synthetic model membranes that have been investigated include hydrophilic, microporous polyethylene membrane for hormone drug release studies from transdermal patches (Schulz et al. 2010). Once again, this material provides a more homogenous barrier for assessing drug release kinetics from a formulation.

Another model barrier that has been used is excised skin tissue of animal origin. For example, Wang et al. investigated the iontophoretic delivery of hydrocortisone across full thickness hairless mouse skin (Wang et al. 1993). Similarly, full thickness porcine skin was utilised by Karande et al. to assess the effect of chemical penetration enhancers on the permeation of inulin (Karande et al. 2005). These are good models for transdermal permeation as all the various layers of the skin are present and have not been through harsh processing conditions. However, the precise skin structure of humans and animals does vary, for example the SC of mouse skin is much thinner, 5.8 ± 0.3 μm compared to 16.8 ± 0.7 μm (Bronaugh et al. 1982), and contains considerably more hair follicles, 658 ± 38 compared to 11 ± 1 (Bronaugh et al. 1982) for human skin, and therefore it may be hard to extrapolate findings.

It is apparent that both these model barriers bear no relation to the physiology and anatomy of genuine human skin. The mechanical, hydration and overall barrier properties of all of the models discussed so far will never be precisely the same as those of human tissue. This is particularly critical when assessing mechanical methods for disrupting the skin barrier to facilitate drug delivery. Therefore, many workers have examined either split thickness human skin, where the epidermis and a portion of the dermis are utilised, or fully separated epidermal membrane as a model barrier for transdermal drug delivery studies (Akomeah et al. 2009; Prausnitz et al. 1993). The rationale behind the use of these barriers is that the SC provides the primary barrier to drug transport (Brown and Langer 1988), in particular to hydrophilic and large molecular weight substances, and because the dermis provides an artefactual reservoir and binding site for drugs which have crossed the epidermal barrier and would be removed by capillaries found within the dermal-epidermal layer *in vivo* (Amsden and Goosen 1995). Accordingly, it was an important focus of this chapter to investigate a robust *in vitro* human skin model to predict SGMN facilitated drug delivery across skin.

5.1.2 Establishment of skin barrier integrity by electrical resistance measurement

A critical aspect of assessing drug delivery across human skin *in vitro* is to determine initial barrier functionality. Removal and processing of tissue prior to experimentation may all have damaging effects on barrier function and therefore it is vital to establish integrity prior to study initiation.

As stated in section 1.2.2.2 the SC barrier consists of protein rich corneocytes stacked within lipid bilayers. The barrier characteristics of the SC have previously been studied by a number of methods including determination of the rate of tritiated water permeation (Dugard et al. 1984; Scott et al. 1991) and measurement of transepidermal water loss (Heylings et al. 2003; Zhao and Singh 1999). An alternative technique that has been receiving increasing interest is measurement and variation in electrical properties of the barrier. The ordered structure and low permeability of SC lipids are responsible for the high electrical impedance or resistance of the SC as it forms a relatively non-conductive, semi-permeable membrane to ions (Lackermeier et al. 1999). Therefore, electrical impedance measurement across skin is strongly related to its barrier function (Karande et al. 2006). As a corollary, damage to the lipids of the SC, for example from chemical irritants, will enable an electrical current to pass through the skin barrier more easily (Heylings et al. 2003). Hence, skin impedance in the context of this work was used in its simplest form, by measuring the resistance of electrons to move from the donor to the receptor compartment in the presence of an AC current (Karande et al. 2006).

It has been shown previously that the electrical resistance (ER) of intact epidermal barriers from various biological organisms vary. For example, a value of 5 - 20 kΩ for full thickness mouse skin (Heylings et al. 2003) represented the normal range for this skin type and a similar range of 6 - 20 kΩ was observed for rat epidermal skin (Oliver et al. 1988). Other workers have examined human skin samples from various anatomical sites and found that ER greater than 20 kΩ/cm^2 was indicative of an intact barrier (Chilcott et al. 1996; Lawrence 1997). However, Davies et al. found that human whole and epidermal membranes both had mean resistance values of approximately 10 kΩ (Davies et al. 2004) and Fasano et al. found that epidermal membrane values ranged from 12 - 62 kΩ (Fasano et al. 2002). The differences reported are likely to be due in part to variations in experimental methodology and setup, for example it has been shown that ER decreases with an increase in cell area (Fasano et al. 2002) and ion concentration in skin (Oh et al. 1993). What has been suggested is that ER measurement is a suitable and robust methodology for evaluating skin integrity; there being a strong association between high water flux and low ER across different species (Davies et al. 2004; Fasano et al. 2002; Oliver et al. 1988). Importantly, skin storage conditions can be a potential issue when investigating barrier properties of skin membranes, especially following storage under frozen conditions. However, it is generally accepted that the integrity of both full thickness human skin and epidermal membranes is unaffected by storage at -20 ^{o}C for up to one year (Davies et al. 2004).

The broad aim of this chapter of work was to establish and validate a robust *in vitro* methodology for the estimation of percutaneous drug delivery from SGMN array devices. Selection of the most appropriate barrier, and establishment of barrier integrity, were critical factors in assessing the utility of this methodology.

5.1.3 Transdermal drug delivery systems

The transdermal drug delivery system (TDDS), or patch, is an attractive, non-invasive option (Sullivan et al. 2008) for delivering small molecular weight, lipophilic drugs at low flux rates (Langer 1998) through the skin for systemic therapeutic effect (Brown and Langer 1988). There are numerous advantages associated with transdermal delivery. These include controlled release of drug into the patient, thus potentially enabling a steady blood-level profile resulting in reduced systemic adverse effects, and the possibility of improved efficacy over other dosage forms (Chong and Fung 1989). Importantly, drugs administered via this route are not subject to hepatic first-pass metabolism. Improved patient compliance arises from the convenience of application and dose flexibility (Audet et al. 2001). Examples of drugs currently delivered transdermally include nicotine, fentanyl, ethinylestradiol, norethisterone acetate, testosterone, clonidine, scopolamine, buprenorphine, norelgestromin and oxybutynin (Hadgraft and Lane 2006). However, most drugs investigated for transdermal drug delivery do not cross the skin at therapeutically relevant rates (Guyot and Fawaz 2000) due to the extraordinary barrier function of the SC.

Transdermal patches have broadly been developed into three different categories, namely the reservoir system, matrix diffusion-controlled system, and multiple polymer system. The reservoir system is a diffusion-controlled system that contains a drug reservoir with a rate-controlling polymer membrane (Margetts and Sawyer 2007). In this device, the membrane that lies between the drug reservoir and the skin controls the rate of release from the drug reservoir to the skin surface and zero order drug release is achievable (Hadgraft and Lane 2006). Conversely, in matrix diffusion-controlled systems the active drug is contained within an adhesive polymer matrix and the drug is released at a rate governed by the components in the matrix (Margetts and Sawyer 2007). However, matrix patches in themselves are not designed to provide true zero-order release because as the drug closest to the skin is released, the drug deeper within the patch must travel a longer distance to reach the skin. The longer diffusional path slows the rate of absorption from the patch over time. For most well designed matrix patches this is not an issue as the decrease in release rate is so small that it does not

significantly affect the rate of drug absorption (Hadgraft and Lane 2006). Inter-patient variability in drug absorption in both patch systems is minimised by a slow rate of release from the patch; either by the rate controlling membrane or the adhesive matrix (Margetts and Sawyer 2007). However, in conventional drug-in-adhesive patches, the dual functionality of the adhesive and reservoir may pose a problem for patch size. A small patch needs high drug concentrations, but loading the polymer adhesive with drug can compromise its adhesive properties (Hadgraft and Lane 2006) and lead to drug crystallisation.

Conventional drug delivery from passive diffusion controlled TDDSs remains limited because the barrier properties of the skin are not fundamentally changed. The SC barrier remains intact and therefore permits diffusion of only specific exogenous materials with appropriate properties. For example, patch-type transdermal products on the market are employed to deliver only a small number of drugs, as mentioned previously. These drugs tend to have similar physicochemical properties including a molecular weight less than 500 Da, sufficient aqueous and lipid solubility (LogP between 1 - 3) and high potency, for example, 10 - 30 ng/mL for nicotine. Although patch systems do not overcome the physicochemical restrictions discussed, they offer an improvement in dose control, patient acceptance, and compliance compared with semisolid formulations (Brown et al. 2006).

It was hypothesised that SGMNs could be integrated into an adhesive patch system to provide controlled release of model substances. In Chapter 3 it had was found that SGMNs dissolve rapidly *in situ* in skin and therefore it was unlikely that control of drug release would be feasible in these systems. It was envisaged that an integrated SGMN adhesive patch may provide controlled delivery of relatively impermeable molecules across skin.

5.2 Chapter objectives

1. Investigate the potential for model hydrophilic compound incorporation within adhesive patch systems.

2. Fabricate integrated transdermal adhesive SGMN array patches for percutaneous drug delivery applications.

3. Assess the stability of SGMN arrays attached to a range of adhesive backing layers.

4. Develop the classical static type Franz diffusion cell set up for MN penetration and diffusion studies.

5. Explore the percutaneous drug delivery efficacy of MN arrays across a number of different model barriers utilising Franz diffusion cells.

6. Assessment and validation of ER measurement as a determinant of human skin barrier integrity.

5.3 Materials and methods

5.3.1 Materials

All reagents were obtained from Fisher Scientific Ltd. (Loughborough, UK) and were of analytical grade unless stated otherwise.

All films and adhesive films were kindly obtained from 3M Drug Delivery Systems (St Paul, MN, USA).

Acrylate adhesives were generously supplied by Henkel Limited (Berkshire, UK).

Silicone adhesives were generously supplied by Dow Corning (MI, USA).

Human breast skin was obtained from the Aneurin Bevan Health Board Royal Gwent Hospital (Newport, Wales, UK) following mastectomy or breast reduction surgery with full ethical committee approval and informed patient consent.

5.3.2 Methods

5.3.2.1 Fabrication and stability assessment of SGMN arrays with adhesive backings

A 20 $\%^{w}/_{v}$ solution of TRA and SUC 75:25 $\%^{w}/_{w}$ was prepared and MB powder was incorporated at 1 $\%^{w}/_{w}$ of final sugar glass weight. The solution was filtered using a 0.2 µm filter and vacuum formed into PDMS micromoulds. 200 µL of sugar solution was injected onto the mould surface under vacuum using the methodology described in section 3.3.2.7 (A). Upon removal from the vacuum chamber, 170 - 180 µL of the solution was pipetted off the surface of the mould and the solution was dehydrated for 48 h as described in section 2.3.2.1 to form SGMN arrays with a thin backing layer. Once dried, SGMN arrays were removed using a cuboidal shaped rod, dimensions 5 x 5 x 100 mm, with double-sided adhesive tape attached to the square end. A variety of SGMN backing materials were attached to the adhesive tape including:-

- fabric plaster
- waterproof plaster
- Micropore™ tape
- CoTran™ 9699
- foam 9733
- polyurethane 9832F

The SGMN array adhesive patches were viewed under light microscope to observe patch and needle integrity prior to storage under vacuum desiccation.

5.3.2.2 Fabrication and optimisation of drug loaded adhesive patches

Silicone soft skin adhesive (SSA; MG 7-9800) and amine compatible silicone BIO-pressure sensitive adhesive (BIO-PSA 7-4302) were used to create 500 mg samples of blank adhesives and adhesives containing 1 $\%^{w}/_{w}$ ketoprofen (KFA) and propranolol hydrochloride (PHCl). To create drug loaded adhesives two approaches were used:-

a) KFA was dissolved in acetone or ethyl acetate and mixed by hand into part A of the adhesive kit for 60 secs

b) KFA or PHCl powder was mixed by hand into part A for 60 secs.

An equal mass of part B was added to the mixtures and thoroughly mixed by hand for another 3 mins. Blank adhesives were fabricated by adding equal quantities of part A and B and mixing thoroughly for 3 mins. All adhesive mixtures were mixed on Scotchpak™ 1022 release liner in a square base dish (approximately 5 x 5 cm). Once mixed, SSAs were cured at 95 ^{o}C for 1 h and BIO-PSAs were placed into a fume hood at ambient temperature for 2 h.

5.3.2.3 Fabrication of integrated sugar glass microneedle transdermal patches containing sulforhodamine B

Sulforhodamine B sodium salt (SRB) was loaded into the adhesives Duro-Tak® 87202-A (acrylate adhesive) and BIO-PSA® 7-4302 (silicone adhesive) at a concentraion of 5 $\%^{w}/_{w}$. A known amount of dry adhesive was dissolved in ethyl acetate and the drug powder was added. The resulting suspension was magnetically stirred for 30 mins to uniformly disperse the drug. Once dispersed, the formulation was pipetted onto Scotchpak™ 1022 release liner and placed on a flat bed shaker overnight (18 h) to evaporate the solvent. To ensure removal of residual solvent, the adhesive was then dried for 1 h in an oven at 60 ^{o}C (Schulz et al. 2010). Once the adhesive layer had formed, Scotchpak™ 9733 backing layer was placed onto the adhesive and pressure was applied in a rolling motion. Patches were formed using a biopsy punch with a diameter of 0.8 cm. This technique yielded patches containing approximately 5 mg of adhesive and 250 μg SRB.

SGMN arrays with a thin backing layer (formed from 40 µL of 20 $\%^{w}/_{v}$ TRA:SUC 75:25 $\%^{w}/_{w}$ solution) were formed as described in section 5.3.2.1. Release liner was removed from the adhesive patches and they were placed adhesive side down onto the PDMS moulds. SGMN arrays were removed using a cuboid shaped rod as described in section 5.3.2.1.

5.3.2.4 Investigation of model membranes to assess microneedle facilitated drug delivery capabilities

Silastic® (Dow Corning, MI, USA) and plasticised PVC film membranes (Saran™ premium wrap) were mounted onto semi-circular cork board wrapped in tissue paper and treated with a single silicon MN array application. Membranes were then mounted between the greased donor and receptor chambers of static Franz type diffusion cells of known receptor volume (mean volume 3.58 mL) and internal diffusional area (diameter approximately 1 cm). The receptor compartment was filled with degassed de-ionised water (dH_2O) for PHCl studies or phosphate buffered saline (pH 7.4) (PBS) (Sigma - Aldrich, Poole, UK) for IBU studies. Positive control cells in both experiments were treated with a single hypodermic needle (26 G) application. To assess Silastic® as a model membrane barrier, 0.5 mL of a solution of PHCl 0.5 mg/mL dissolved in dH_2O (1.7 mM) (Coulman et al. 2009) was applied to the donor compartment of each cell and occluded with a section of Parafilm®.

Blank sugar glasses (SGs) and SGs containing 5 $\%^{w}/_{w}$ IBU were prepared by pipetting 150 µL sugar or drug-sugar solutions, respectively, onto a flat sheet of PDMS and dehydrating as described in section 2.3.2.1. To assess model plasticised PVC film barrier, blank or drug loaded SGs were applied to the donor compartment of each cell and occluded with intact plasticised PVC film. Cells were placed on top of a multipoint magnetic stirrer in a water bath and equilibrated to 37 ^{o}C for at least 30 mins. A small magnetic follower was added to each cell providing a membrane surface temperature of approximately 32 ^{o}C and continuous agitation of the receptor solution (Chabri et al. 2004). 200 µL samples were removed from the receptor phase at time points 1, 2, 4, 6, 12 and 24 h and the receptor compartment was replenished with an equal volume of dH_2O or PBS pre-equilibrated to 37 ^{o}C; a dilution factor which was accounted for in subsequent data analysis. Samples were stored at -20 ^{o}C until required for high performance liquid chromatography (HPLC) analysis.

For comparisons of multiple treatment groups, a one-way ANOVA with Bonferroni's multiple comparison *post hoc* test was performed on the experimental data using the GraphPad Prism 5 software package. In all cases, statistical significance was determined by a value of $P \leq 0.05$.

5.3.2.5 Investigation of heat separated epidermal membrane to assess microneedle facilitated drug delivery

A saturated solution of IBU (1871.8 mM) was created by adding excess IBU to continuously agitated dH_2O heated to 37 ^{o}C. A 20 $\%^{w}/_{v}$ solution of TRA and SUC 75:25 $\%^{w}/_{w}$ was prepared and IBU powder was incorporated at 5 $\%^{w}/_{w}$ of final sugar glass weight. Previously frozen full thickness human skin from a female donor, age 58 years, was defrosted at room temperature for approximately 1 h before underlying subcutaneous fat was removed by blunt dissection. The epidermis was isolated by immersion into a water bath at 60 ^{o}C for 55 secs followed by membrane removal with forceps. Samples were stored at -20 ^{o}C until required and used within 2 months of preparation. Before use, membranes were defrosted for up to 20 mins, and mounted dermal side down between the greased donor and receptor chambers of static Franz type diffusion cells. The receptor compartment was filled with degassed PBS and equilibrated to 37 ^{o}C in a water bath. Treated membranes were punctured with a single hypodermic needle (26 G) application and 0.5 mL of IBU saturated solution was applied to the donor compartment of each cell and occluded with Parafilm® to prevent evaporation. In a separate experiment, epidermal membranes isolated from female donors aged 47 and 80 years, were mounted dermal side down onto a section of Whatman no. 1 filter paper (1.5 x 1.5 cm). Membranes were mounted in Franz cells and treated with a single silicon MN array puncture before 150 µL of the 5 $\%^{w}/_{w}$ IBU sugar solution was applied to the donor compartment. Cells were placed into a water bath and 200 µL samples were removed from the receptor phase at defined time points, as described in section 5.3.2.4 and stored at -20 ^{o}C until required for HPLC analysis.

5.3.2.6 Quantitative analysis of small molecule model drug substances

Samples containing the analyte PHCl were analysed by fluorescence spectrophotometry (Fluostar Optima™, BMG Labtech, Aylesbury, UK) using a 96 well plate methodology with excitation and emission filters set at 280 and 330 nm respectively. Drug quantities were estimated by linear regression and correlation analysis of the calibration curve generated with a LOD of 1 x 10^{-3} mM. IBU sample analysis was performed using reversed-phase HPLC apparatus with the following instrumentation: SCM 1000, pump P2000 and auto-sampler

AS3000 equipped with a UV2000 detector (Spectra System®, Thermo Fisher Scientific, Hertfordshire, UK). The GraceSmart™ RP C18 5 µ column (250 x 4.6 mm) and an isocratic eluent (pH 3.4) of 75 % methanol, 24 % water and 1 % glacial acetic acid were used in this study. The flow rate was set at 1.5 mL/min and 20 µL samples were injected onto the column. The elution time was set for 6 mins and absorbance detection was at a wavelength of 272 nm. Drug quantities were estimated by linear regression and correlation analysis of the calibration curve generated with a LOD of 5 x 10^{-3} mM. Error bars shown on permeation profiles in all studies relate to the standard error of the mean to take into account sample size.

5.3.2.7 Development and optimisation of static type Franz diffusion cells for microneedle facilitated penetration / permeation studies

SGMN arrays were fabricated from a 20 $\%^{w}/_{v}$ solution of TRA and SUC 75:25 $\%^{w}/_{w}$ as described in section 3.3.2.5. The following modifications were made to the classical setup of the Franz diffusion cell to assess optimal membrane penetration capabilities of SGMN arrays.

5.3.2.7.1 Inverted method

A cylindrical shaped metal rod with diameter approximately 1 cm was placed into an upturned donor chamber. SGMN arrays were placed with their needles facing upwards onto a circular section (1 cm diameter) of plasticised PVC film and placed onto the end of the rod. A section of epidermal membrane, mounted dermal side down onto a section of Whatman no. 1 filter paper (1.5 x 1.5 cm) was then placed SC side down on top of the SGMN array. Pressure was applied to the membrane for 10 secs using a syringe plunger covered with a section of foam 9773 tape. The receptor compartment was filled with degassed PBS and the donor compartment and SGMN assembly were clamped in place, as shown in Figure 5.1.

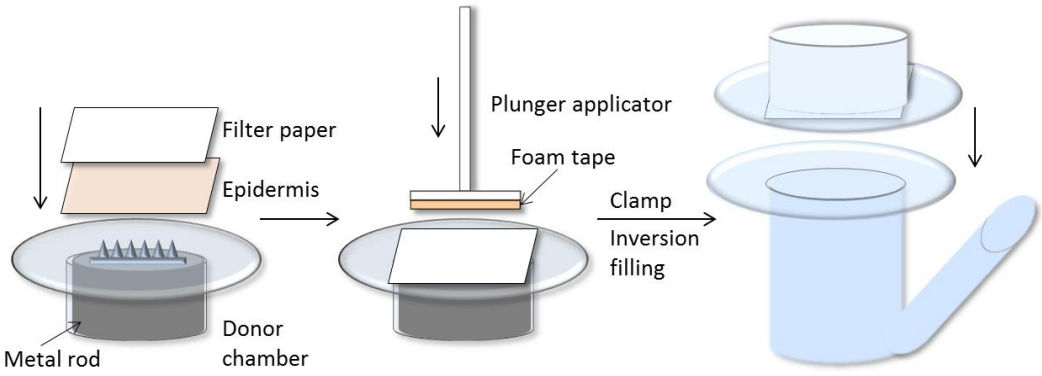

Figure 5.1 Schematic of inverted SGMN application methodology.

Finally, cells were inverted to displace any residual water bubbles beneath the membrane.

5.3.2.7.2 Gauze method

A Franz cell was assembled with a disc of polytetrafluoroethylene (PTFE) material, (approximately 2 cm diameter, 0.4 cm depth), between the flanges of the donor and receptor chambers. A circular hole of 1 cm diameter was punched in the centre of the disc with a slightly larger hole on one side only to create a step. A section of stainless steel gauze (Goodfellow Cambridge Ltd., Huntingdon, UK) with a nominal aperture of 0.38 mm, was fashioned to fit inside the stepped hole. A section of filter paper was placed on top of the gauze and the epidermal membrane was placed dermal side down onto the filter paper. The donor chamber was clamped in place and the receptor was filled with degassed PBS. A SGMN array was mounted onto the flattened end of a syringe plunger and inserted into the donor compartment and pressed down for 10 secs into the membrane, as shown in Figure 5.2.

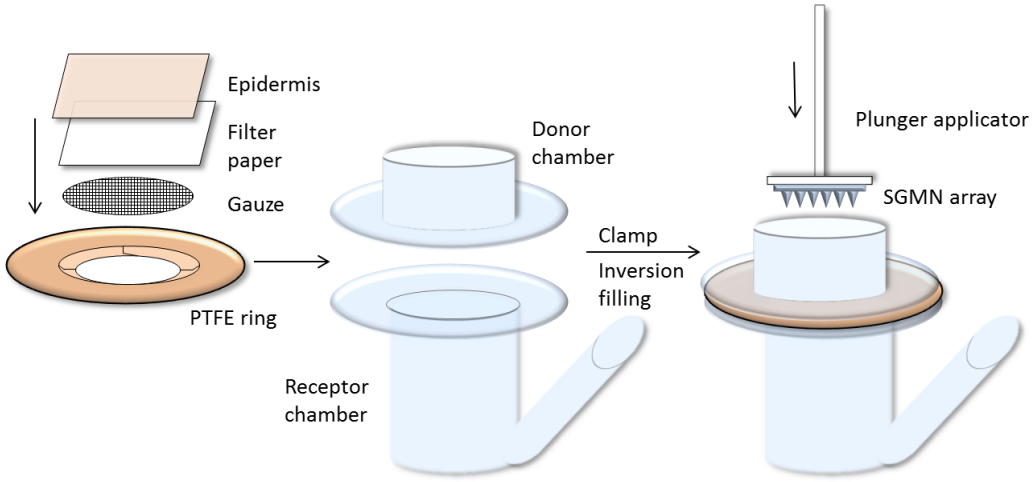

Figure 5.2 Schematic of SGMN application methodology utilising gauze Franz cell insert.

Once inserted, a 1 cm disc of plasticised PVC film was placed on top of the array.

5.3.2.7.3 PTFE disc method

The same assembly as in 5.3.2.7 (2) was utilised, except that the PTFE disc had 4 holes, diameter 2 mm, drilled into the centre rather than a section of gauze material.

All membranes were observed by light microscope, Leica Zoom 2000 (Leica, Scotts Valley, CA, USA) prior to and following SGMN insertion to determine the penetration profile for each method.

5.3.2.8 Assessment and validation of electrical resistance as a measure of epidermal barrier integrity

Modified static type Franz diffusion cells were assembled with a PTFE ring containing gauze insert as described in section 5.3.2.7 (2). Heat separated epidermis was prepared as described in section 5.3.2.5 and mounted onto the modified cells. The donor chamber was secured, and the receptor and donor compartments were filled with physiological saline (0.9 % NaCl in water) pre-equilibrated to 37 ^{o}C. Once assembled, the electrical resistance (ER) of each membrane was measured with an Agilent U1731A™ dual display handheld LCR meter (Agilent Technologies UK Ltd, Edinburgh, UK) using a testing frequency of 1 kHz. Measurements were taken by inserting the stainless steel cathode probe into the side arm of the receptor chamber and then inserting the anode probe into the donor chamber, taking care not to touch the membrane. Following stabilisation of the reading, the resistance value was recorded for each cell. Once the ER assessment for each cell had been completed the contents of the donor and receptor compartments was discarded and the skin allowed to air dry (Heylings et al. 2003).

5.4 Results and discussion

5.4.1 Fabrication of SGMN arrays with alternative backings

As described in section 3.4.9, SGMN arrays dissolved rapidly *in situ* in *ex vivo* human skin. Therefore, it was concluded that they were unlikely to be suitable as controlled release drug delivery devices. The solid SGMN array bases had also demonstrated poor structural rigidity upon skin insertion and it was envisaged that end-user application of arrays may be difficult. Using a traditional transdermal patch device as a template, it was hypothesised that SGMNs could be attached to a different base material. This material would be a completely different material to rigid sugar glass that may confer desirable properties upon the SGMN arrays. It was envisaged that possible benefits may include increased drug loading within the backing layer, potential for controlled release of medicament and ease of application for end-user. However, to fabricate stable SGMN arrays with flexible adhesive backings, it was critical to find a patch system that would not adversely affect SGMNs attached to it.

A variety of base materials were investigated including generic fabric plaster and waterproof plaster, Micropore™ tape and various 3M adhesive films. Each material was chosen for its adhesive properties and proven compatibility with human skin.

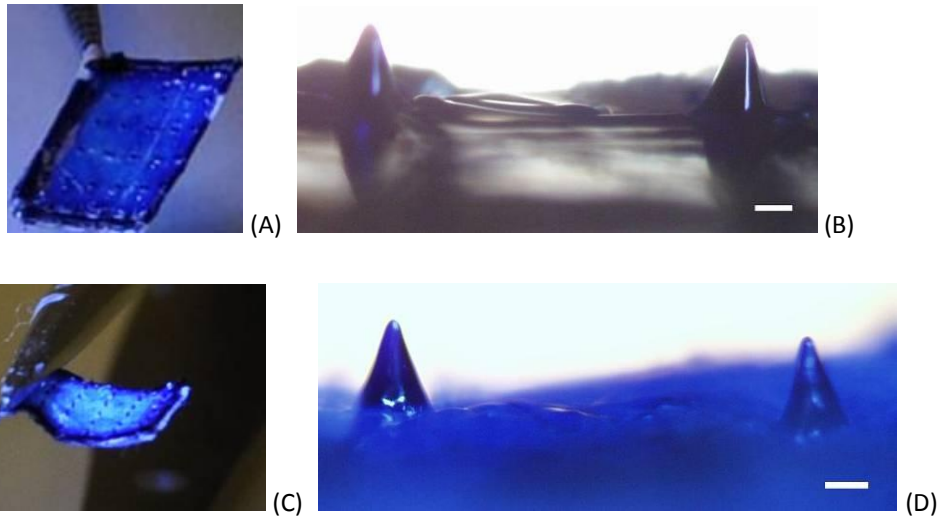

Figure 5.3 SGMN arrays with alternative backings.

Digital images of SGMNs incorporating 1 $\%^{w}/_{w}$ MB attached to (A) waterproof plaster and (C) Micropore™ tape backings. (B) and (D) light photomicrographs of SGMNs depicted in (A) and (C) respectively (Bar = 100 µm).

Although SGMNs were successfully attached to a fabric plaster backing the plaster did not have the desired properties of a SGMN base. It was envisaged that the base material would be flexible, with a smooth and flat adhesive side that would not adversely affect the morphology of the SGMN array. The fabric plaster fulfilled some of these criteria, but critically the material was not smooth enough and MNs were observed to be positioned at many different angles (data not shown). It was hypothesised that such an array would not be effective at penetrating human SC. As shown in Figure 5.3 however, SGMN arrays with flexible backings made from waterproof plaster and Micropore™ tape fulfilled the above criteria to a much greater extent. Both backing materials were much smoother than the fabric plaster and hence individual MNs were orientated in approximately the same direction. However, the waterproof plaster backing appeared to cause rapid degradation of the SGMN morphology. Within 15 mins of creation, the MNs were observed to have changed shape and become rounder and less pyramidal, as shown in Figure 5.4.

Figure 5.4 Light photomicrograph of SGMNs with a waterproof plaster backing.

Image shows the rapid alteration in MN morphology observed.

The rapid alteration in SGMN morphology was attributed to the waterproof nature of the plaster and it was speculated that it may be causing hydration and degradation of the needles. In contrast, SGMN arrays attached to Micropore™ tape appeared to be much more stable and SGMNs attached to this backing, Figure 5.3 (D), retained a much closer morphology to the silicon master structure.

Another factor that became apparent through this study was that SGMN arrays fabricated from 20 µL of sugar solution did not always contain a sufficient quantity of material to form a continuous base layer once dehydrated. Micromould invaginations were full of sugar glass material, but this did not extend to the entire surface of the mould. It was found that removal of all 36 MNs formed became problematic, as shown in Figure 5.5 (A).

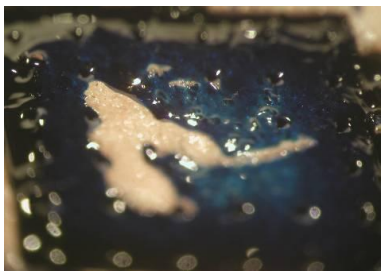
(A)
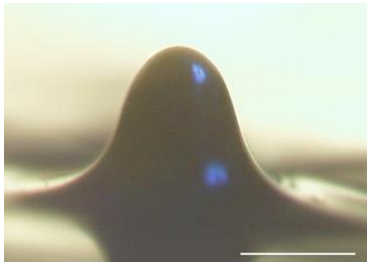
(B)
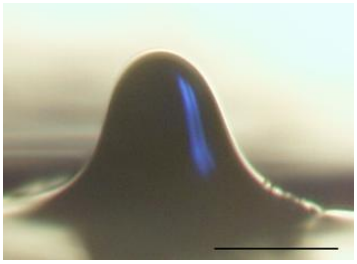
(C)

Figure 5.5 Light photomicrographs of SGMN array with a CoTran™ 9699 backing.

(A) E*n face* of entire SGMN array and, (B and C) individual SGMNs contained within array (Bar = 100 μm).

As shown in Figure 5.5 (A) a number of MNs near the centre of the array were not removed by the adhesive backing layer. This data appeared to suggest that a residual continuous base layer was required for successful removal of all SGMNs from the PDMS micromould. Further, this study highlighted that CoTran™ 9699 adhesive tape was not an ideal backing material. As shown in Figure 5.5 (B) and (C), SGMNs degraded when attached to this adhesive, and this process happened rapidly, within 14 days of fabrication and subsequent storage under vacuum desiccation.

Figures 5.6 (A) and 5.7 (A) support Figure 5.5 (A) indicating that a continuous base layer was required for successful SGMN array attachment. In both examples, very few of the SGMNs formed were removed by the backing layer adhesive. However, the individual MNs remaining appeared to be stable on each of the adhesive backings, Figure 5.6 (C) and 5.7 (E).

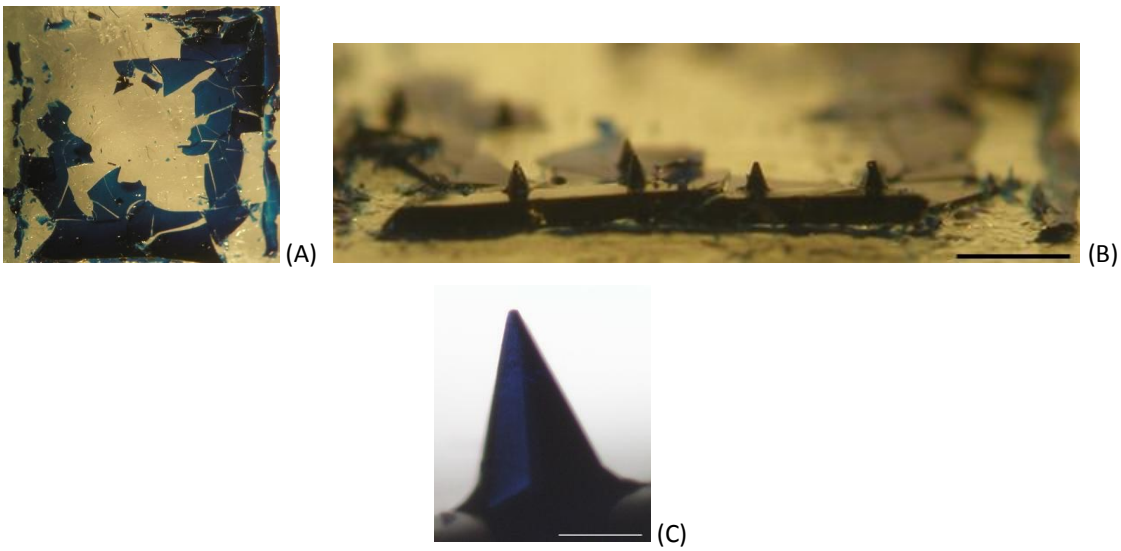

Figure 5.6 Light photomicrographs of SGMN array with a polyurethane 9832F backing.

(A) *En face* view of SGMN array and (B) transverse view of SGMNs (Bar = 1000 µm) and (C) individual SGMN contained within array (Bar = 100 µm).

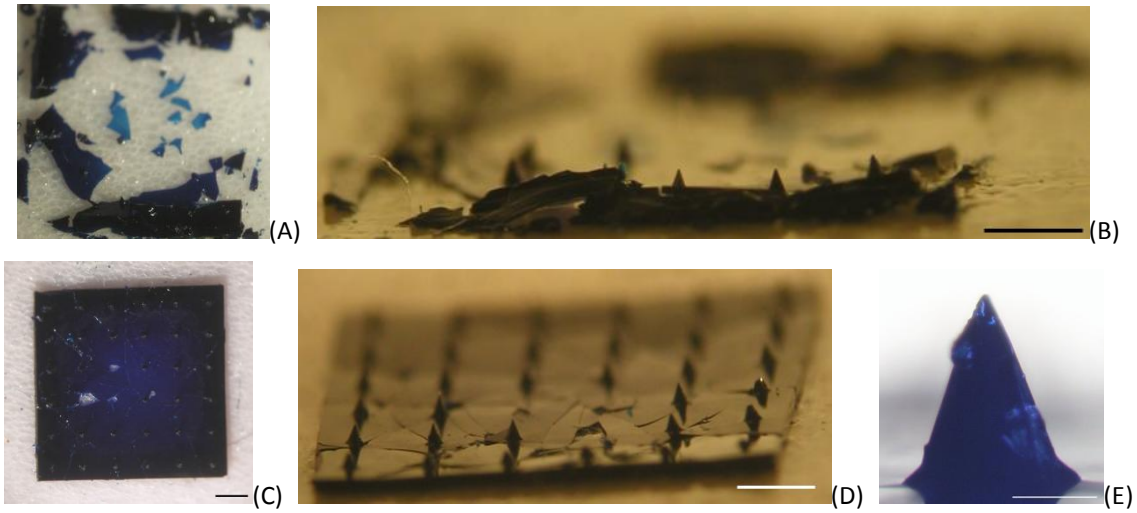

Figure 5.7 Light photomicrographs of SGMN array with a foam 9773 backing.

(A) and (C) *en face* view of SGMN array, (B) and (D) transverse view of SGMNs (Bar = 1000 µm), (E) individual SGMN contained within array (Bar = 100 µm).

This data appeared to show that SGMNs could be successfully attached to the correct adhesive backing layer and that they would remain stable under desiccated storage conditions, Figure 5.7 (D) and (E). To overcome the issue of incomplete SGMN array removal from micromoulds, the process was adapted and 30 µL rather than 20 µL was left on the mould surface before

dehydration. This quantity of material generally formed an array with a complete base, and facilitated removal of all MNs from the mould, as shown in Figure 5.8.

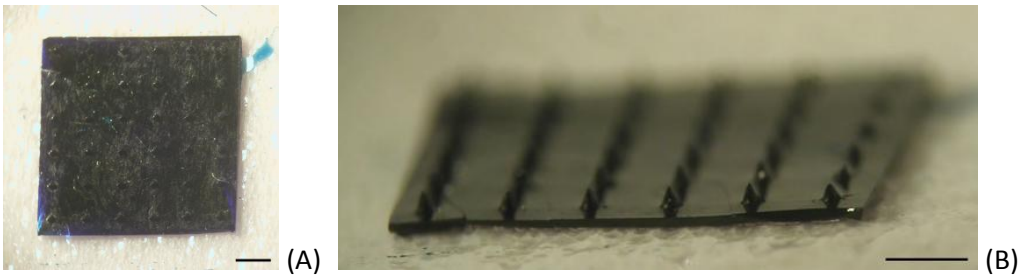

Figure 5.8 Light photomicrographs of SGMN array with a foam 9773 backing.

(A) E*n face* view of SGMN array and (B) transverse view of SGMNs (Bar = 1000 µm).

From this study, it appeared that SGMN arrays formed from at least 30 µL of sugar solution could reliably and stably be attached to 3M polyolefin foam 9773 tape to form SGMN arrays with an alternative flexible backing.

In conclusion, it was determined that the stability of SGMN arrays mounted onto a flexible backing would be a critical issue. The utility of such a device would depend on the ability to successfully attach a plurality of SGMNs onto an adhesive backing layer that would not adversely affect the delicate and hygroscopic nature of the sugar glass material. These pilot studies indicated that this concept may be feasible with the correct backing material and they led the way for further studies to optimise the system by fabrication of transdermal patches from basic principles, as detailed in section 5.4.3.

5.4.2 Fabrication and optimisation of drug loaded adhesive patches

Soft skin adhesives (SSAs) are intended for adhesion to skin and include a range of products such as over-the-counter bandages and scar therapies (Van Damme et al. 2009). Conversely, BIO-pressure sensitive adhesives (PSAs) are intended for transdermal drug delivery products owing to good chemical stability of the adhesive in the presence of amine-functional drugs, excipients and enhancers (Laurent et al. 2007). Two model drugs, with differing physicochemical properties, were incorporated into the two different adhesives at a concentration of 1 $\%^{w}/_{w}$. When KFA was incorporated within the SSA and heated to cure at 100 ^{o}C, dishes containing the adhesive dissolved and the adhesive did not cure fully (data not

shown). This led to modification of the initial processing conditions and the use of a lower curing temperature of 95 ^{o}C.

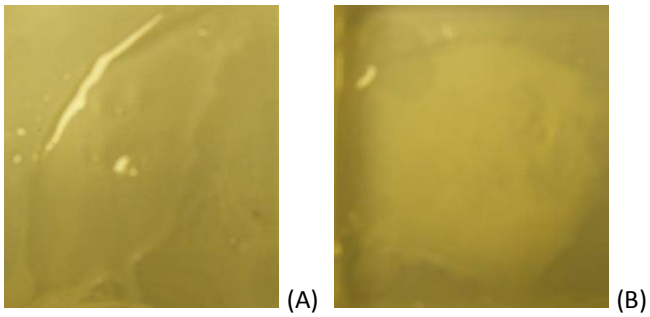

Figure 5.9 Images of soft skin adhesives.

(A) Blank adhesive and (B) 1 $\%^{w}/_{w}$ PHCl powder loaded SSA.

As shown in Figure 5.9 (A), blank SSA formed a uniform transparent adhesive once cured. When PHCl powder was incorporated at 1 $\%^{w}/_{w}$, the drug initially appeared to dissolve within the adhesive. Upon curing of the adhesive however, the drug appeared to re-crystallise and an adhesive was formed that had an opaque nature, Figure 5.9 (B). This was expected as PHCl is a water soluble salt of a basic drug and SSA does not contain amine compatible functionality in its structure.

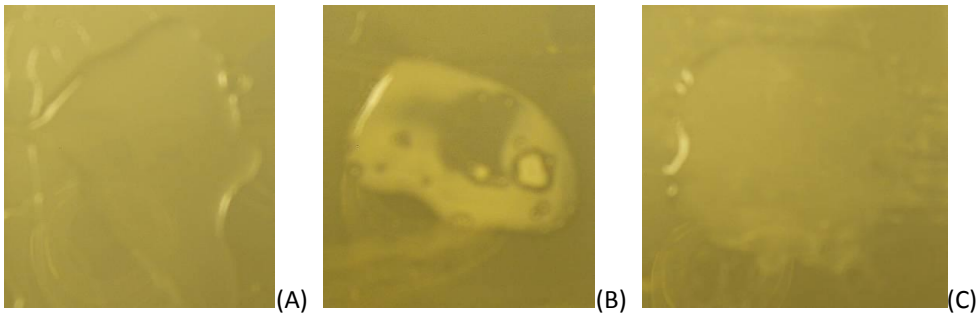

Figure 5.10 Images of BIO-pressure sensitive adhesives.

(A) Blank adhesive, (B) 1 $\%^{w}/_{w}$ KFA and (C) 1 $\%^{w}/_{w}$ PHCl loaded adhesive samples.

Blank BIO-PSA adhesive, like blank SSA, formed a transparent adhesive once cured, Figure 5.10 (A). The properties of the two adhesives varied significantly however, and the BIO-PSA adhesive formed a much more rigid material than the SSA. The BIO-PSA had a lower tack than the SSA also and this made it easier to handle once cured. It was hypothesised that this property may be useful in future applications when attaching SGMN arrays to the adhesives. As shown in Figure 5.10 (B), when 1 $\%^{w}/_{w}$ KFA was incorporated within the adhesive the drug

did not mix well within the matrix and re-crystallised rapidly as the solvent evaporated. Again this was expected as KFA is a weak acid and contains no amine functionality. It was rationalised that the PHCl may integrate better within the BIO-PSA matrix due to its basic nature. This outcome was partially observed, as shown in Figure 5.10 (C), where no obvious crystallisation appeared in the adhesive; in contrast to the KFA adhesive, Figure 5.10 (B). However, it appeared that the drug remained in a suspended state, as shown by the opaque nature of this adhesive.

The aim of these preliminary studies was to investigate the suitability of various commercial adhesives for incorporation of model medicaments. These studies suggested that although drug appeared to crystallise within the cured adhesives, regardless of the physicochemical nature of the medicament, it may be possible in future work to incorporate a variety of model drug substances within these adhesives. It was shown that thin adhesive layers containing medicament could be fabricated and it was hypothesised that these could be utilised as the basis of an integrated adhesive backed SGMN array patch. This approach would potentially allow increased drug loading of the patch system and facilitate controlled drug release and skin adhesion.

5.4.3 Fabrication of integrated sugar glass microneedle transdermal patches containing sulforhodamine B

Sulforhodamine B (SRB) was chosen as a model compound to assess SGMN facilitated transdermal drug delivery. This molecule has a MW of approximately 600 and a LogP of -0.45 (Kushner et al. 2007) and is widely used as a model hydrophilic permeant when assessing active enhancement methods of drug delivery across the SC (Kushner et al. 2007; Sullivan et al. 2008). As demonstrated in section 4.4.1, SRB can successfully be incorporated within the matrix of SGMN arrays. Therefore, it was chosen as an ideal model compound for comparison with SGMN adhesive patches in terms of transdermal drug delivery potential. A loading concentration of 5 $\%^{w}/_{w}$ was chosen as percutaneous drug delivery systems are often formulated containing 5 – 10 $\%^{w}/_{w}$ drug. It had also been shown that 5 $\%^{w}/_{w}$ was an appropriate concentration of drug to incorporate within the matrix of SGMN arrays, section 4.4.1, and therefore it seemed a logical concentration to work with. The images in Figure 5.11 show the nature of the novel integrated SGMN transdermal patch.

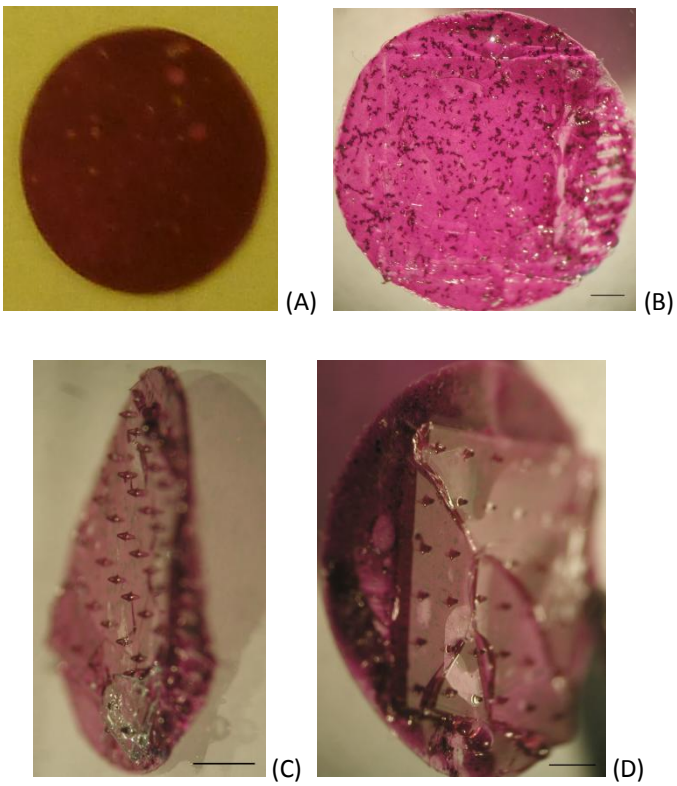

Figure 5.11 Images of novel integrated SGMN transdermal patch.

(A) Blank Duro-Tak® 87202-A adhesive patch incorporating 5 $\%^{w}/_{w}$ SRB. Light photomicrographs of (B) *en face* view and (C) transverse view of SGMN patch, (D) transverse view of SGMN patch following 6 days storage under vacuum desiccation (Bar = 1000 µm).

The dimensions of the patch, 0.8 cm diameter, were chosen for two reasons. Firstly, the adhesive backing required a greater surface area than the square 6 x 6 mm dimensions of the SGMN attached to it. Secondly, the patch had to be small enough to be applied to the donor phase of a Franz diffusion cell with a nominal diffusional surface area of 1 cm. As shown in Figure 5.11 (B) the SGMN array sat well in the centre of the adhesive backing layer leaving a small area of unoccluded adhesive for skin adhesion. Figure 5.11 (B) shows that the SRB formed discrete particles within the adhesive layer once formed. This suggested that the solubility of SRB within the adhesive was low and it was speculated that this may provide a higher thermodynamic potential for transdermal drug delivery from the patch (Higuchi 1960).

As Figure 5.11 (C) shows, SGMN arrays adhered to acrylate adhesive patches and appeared to retain their morphological structure. This was expected as acrylate adhesives are hydrophobic materials and because the SGMN arrays were formed from 40 µL solution. Therefore, the arrays had a slightly thicker base layer which may have improved the stability of the SGMNs

attached. The SGMNs also appeared to be relatively stable under vacuum desiccation storage, Figure 5.11 (D). Due to the flexible nature of the backing material and adhesive layer, the base of the SGMN array was often observed to crack in places, Figure 5.11 (C) and (D), but this did not appear to adversely affect the structure of individual MNs. This data suggested the utility of this adhesive to formulate an integrated SGMN transdermal patch system.

5.4.4 Investigation of different model membranes to assess microneedle facilitated drug delivery

Various different methodologies for assessing the transdermal drug delivery potential of topical formulations have been described in the literature. The Franz diffusion cell is a commonly used tool for assessing such parameters and a number of different model skin membranes have been utilised. The aim of this section of work was to determine the most appropriate model membrane for examining the drug delivery potential of MN arrays.

As shown in Figure 5.12 there was no significant difference (P=0.08) between untreated Silastic® membrane and membrane punctured with a hypodermic needle or silicon MN array. It appeared that penetrating the membrane decreased barrier integrity initially, as demonstrated by the absence of a lag phase in these treatment groups. However, by the end of the study it was apparent that even Silastic® membrane treated with a hypodermic needle demonstrated little enhancement on total PHCl permeation compared to control. There was also large variation in PHCl flux across the membrane, particularly following silicon MN treatment. This result was not unexpected as although the MNs were applied to the membrane in the same manner each time, and visually inspected to observe membrane puncture, it may have been possible that not all of the MNs on the array fully punctured the membrane each time. Also, as Silastic® membrane was used, any channels made within the membrane could potentially have closed up during the study.

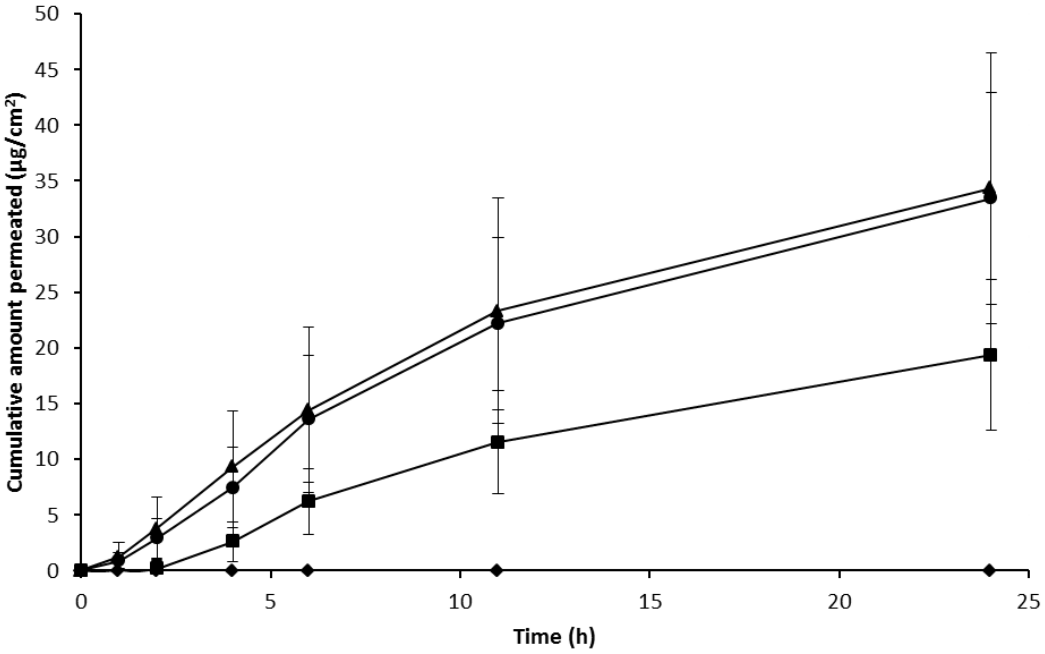

Figure 5.12 Cumulative permeation of PHCl across Silastic® membrane.

The square denotes data obtained following no membrane treatment (n=4), the triangle denotes data from hypodermic needle (26 G) treatment (n=4) and the circle from silicon MN treatment (n=4), the diamond denotes data from dH_2O (n=3) application. Data presented as mean ± S.D.

To further investigate this membrane, a follow up study was performed in which Silastic® membranes were treated with one, five or ten hypodermic needle (26 G) punctures, Figure 5.13. As shown, there was no significant difference between each treatment group compared to untreated membrane. From these studies, it appeared that puncturing Silastic® membrane had little effect on diffusion of the small molecule PHCl across the membrane. Therefore, it was concluded that this model membrane would not be optimal for assessing MN facilitated drug delivery.

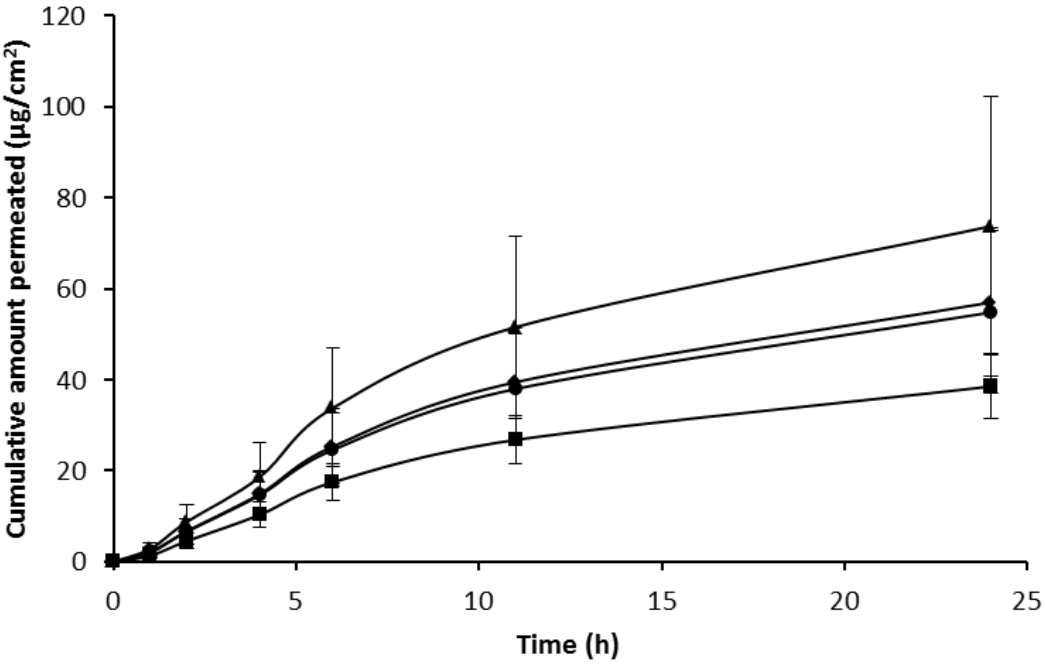

Figure 5.13 Permeation profiles of PHCl across hypodermic needle treated Silastic® membrane.

The data represent permeation following no membrane treatment (diamonds) and after hypodermic needle (26 G) puncture 1x (squares), 5x (triangles) and 10x (circles). Data presented as mean ± S.D. (n=4).

Initial penetration studies suggested that Silastic® membrane may not be appropriate for assessing MN facilitated drug delivery. Instead another synthetic model barrier, plasticised PVC film, was investigated. In comparison, this membrane displayed quite different properties to Silastic®, as shown in Figure 5.15. This set of experiments utilised an alternative water soluble analyte, IBU, and analysis was performed by HPLC. A model standard curve is shown in Figure 5.14.

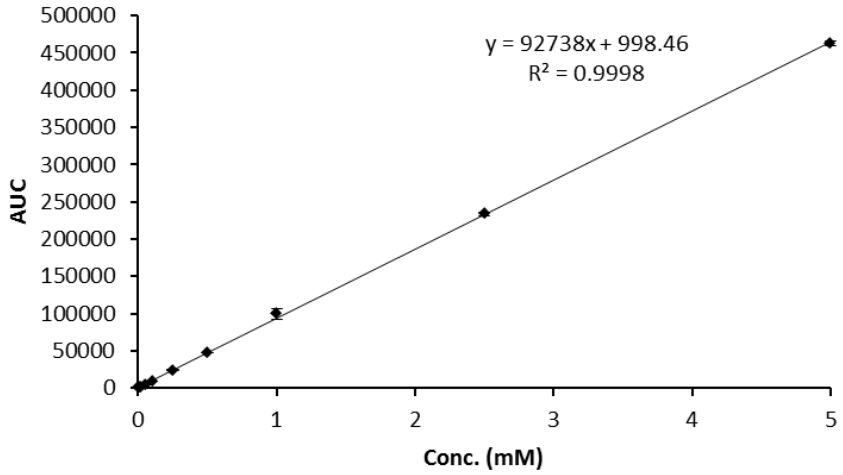

Figure 5.14 Exemplar standard curve used in quantitative determination of ibuprofen sodium flux across model barrier.

Data presented as mean ± S.D. (n=3).

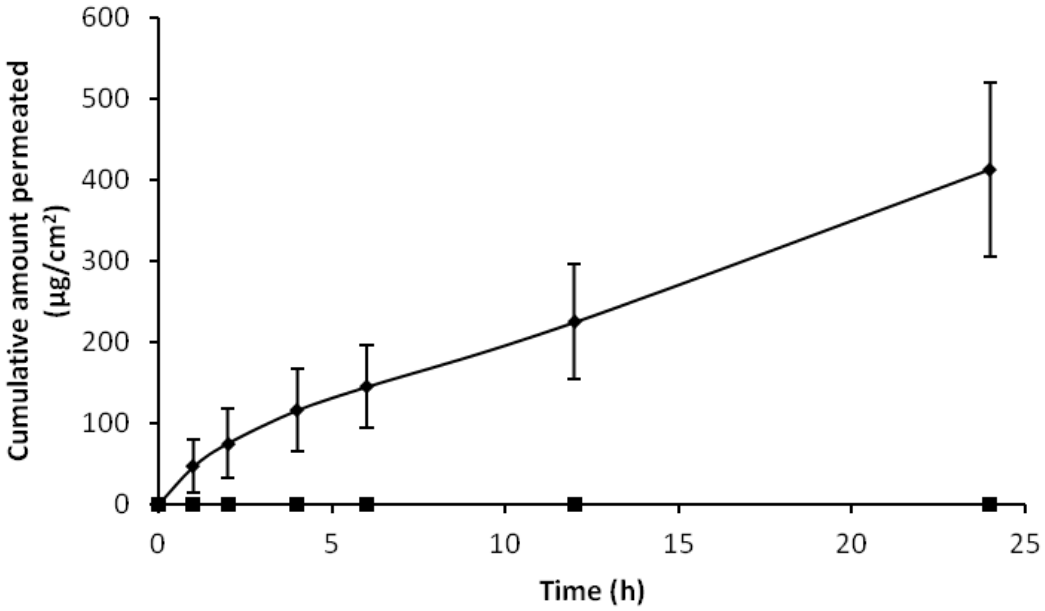

Figure 5.15 Permeation profile of ibuprofen from 5 $\%^{w}/_{w}$ sugar glasses across plasticised PVC film.

The square denotes data obtained following no membrane treatment and the diamond denotes data following silicon MN array application. Data presented as mean ± S.E. (n=10).

As shown in Figures 5.12 and 5.15, it appeared that treatment of model membranes with a silicon MN array was not always reproducible. This was shown by the relatively large standard error values of ibuprofen flux across the membranes following MN treatment. From this

study, it was speculated that the plasticised PVC membrane may suffer from the same penetration and resealing issues as the Silastic® membrane used in previous studies.

This study did show however, that intact plasticised PVC film formed an impenetrable barrier to the permeation of ibuprofen from SGs. By 24 h significantly more ibuprofen had diffused across the membrane treated with a MN array in comparison to untreated membrane. As a positive control plasticised PVC membranes were punctured with a single 26 G hypodermic needle puncture, Figure 5.16. As shown, following both hypodermic and silicon MN treatments, there was an initial lag phase up to 1 h, before ibuprofen began to diffuse across the punctured membranes. By 4 h however, significantly more ibuprofen had permeated across the hypodermic treated membrane containing the IBU loaded SG, Figure 5.16, compared to the silicon MN treated membrane, Figure 5.15.

Interestingly, it appeared that there was no significant difference in permeation between drug loaded SG formulation compared to sugar solution containing the same drug concentration, Figure 5.16. This behaviour was not unexpected as it is known that amorphous systems are in a higher energy state relative to crystalline materials (Zhou et al. 2007) and hence that they demonstrate similar properties to a liquid phase.

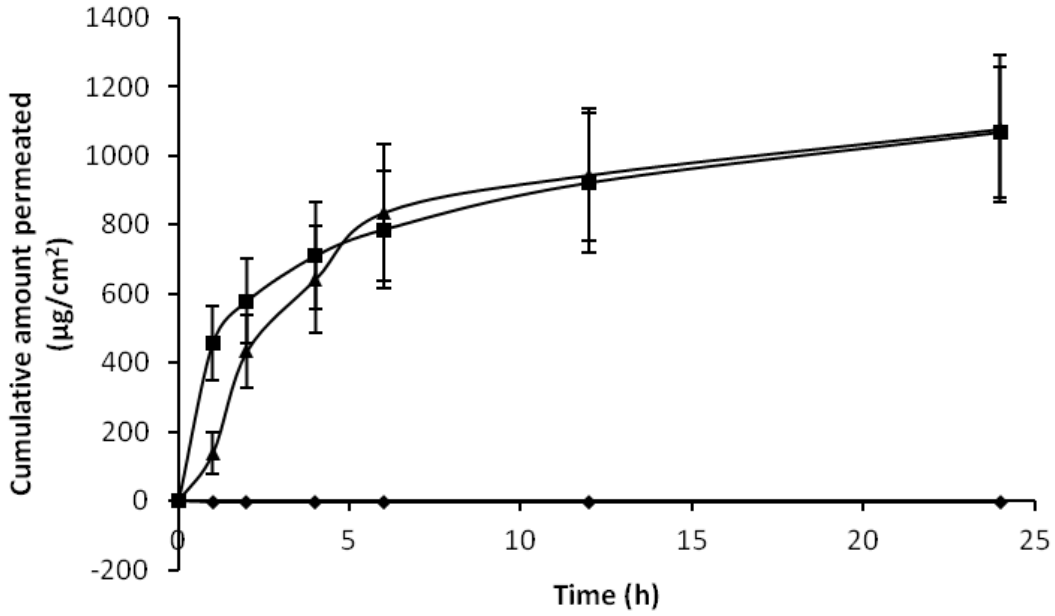

Figure 5.16 Permeation profile of ibuprofen across plasticised PVC film treated with a single hypodermic needle (26 G) puncture.

The square denotes data obtained following application of 5 $\%^{w}/_{w}$ SGs to the donor chamber. Controls were a blank SG (diamond) and stock IBU sugar solution used to create 5 $\%^{w}/_{w}$ SGs (triangles). Data presented as mean ± S.E. (n=10).

The final model barrier system investigated was heat separated human epidermis. It had been shown that neither Silastic® or plasticised PVC membranes were ideal models for assessing penetration and delivery studies, and therefore it was hypothesised that epidermal membrane would be the most appropriate model for this investigation.

As shown in Figure 5.17, after an initial lag phase of approximately 1 h, ibuprofen began to permeate the epidermal membrane from a saturated solution. By 12 h a mean cumulative total of 864.4 µg ibuprofen had diffused across the membrane, providing a mean maximal flux rate of approximately 104 µg / cm^2 / h by 24 h. This correlated with previous literature values for permeation of ibuprofen from saturated aqueous solutions across human epidermis of approximately 35 – 332 µg / cm^2 / h (Al-Saidan 2004) and 11.8 µg / cm^2 / h (Stott et al. 1998); in the latter paper the SC had been fully hydrated prior to study initiation.

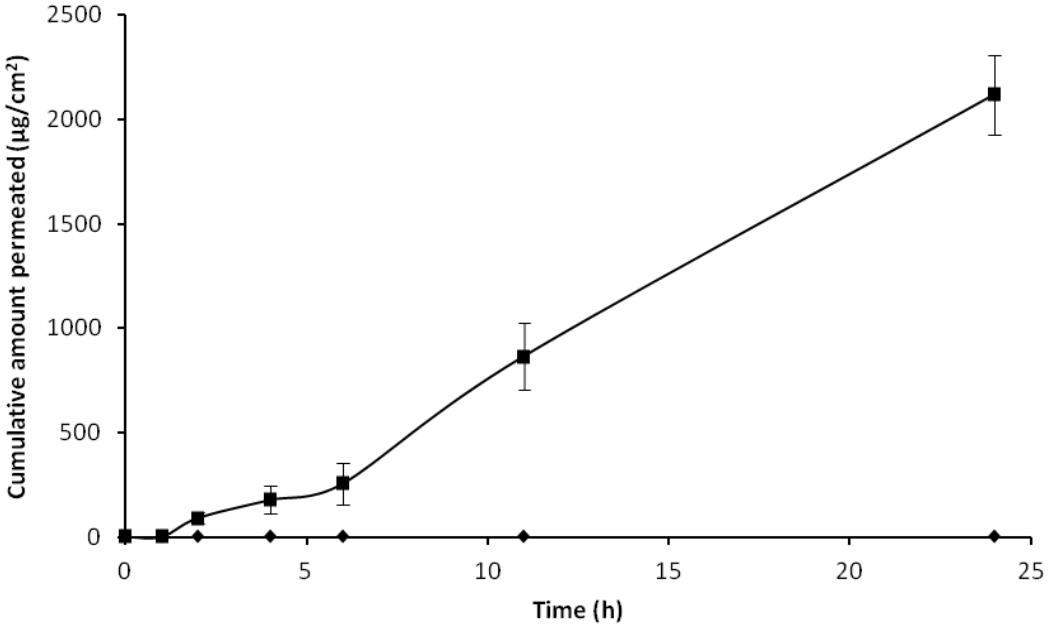

Mean flux (µg / cm^2 / h) ± S.D.	Permeability coefficient (cm / h) ± S.D.	Mean cumulative amount permeated at 6 h (Q_6) (µg / cm^2) ± S.E.	Lag time (L_t) (h)	Percentage formulation permeated at Q_6 (%) ± S.E.
104 ± 11.4	5.4 x 10^{-4} ± 0.6	254.3 ± 99.0	1.4	0.13 ± 0.05

Figure 5.17 Permeation profile of ibuprofen across epidermal membrane.

The square denotes data obtained after application of a saturated IBU solution and the diamond denotes data for blank dH_2O. Data presented as mean ± S.E. (n=4).

To observe the effect of membrane penetration, other sections of membrane were treated with a single hypodermic puncture and a saturated solution was applied to the donor chamber. As shown in Figure 5.18, significantly more ($P<0.0001$) ibuprofen permeated across epidermal membranes treated with a hypodermic needle compared to intact membranes. This was demonstrated by a mean Q_6 of approximately 84435 µg / cm^2 (Figure 5.18) compared to approximately 254 µg / cm^2 for untreated membrane (Figure 5.17). Unlike Silastic®

membranes, it appeared that penetrating epidermal membrane would lead to a significant increase in drug permeation, confirming the utility of this membrane for future MN penetration studies. A plateau in ibuprofen permeation was noted from 12 h onwards which correlated with depletion of the donor formulation (containing approximately 192,000 µg IBU). Furthermore, although the solubility of ibuprofen in aqueous solution is low (0.12 mg / mL) (Iervolino et al. 2000), ibuprofen sodium salt has been incorporated at 16 % $^{w}/_{v}$ (160 mg / mL) within water-in-oil liquid microemulsions (Sintov and Botner 2006). Therefore, sink conditions (<10 % of saturation concentration) (Ng et al. 2010) were violated within this study, which may also account for the plateau in permeation observed.

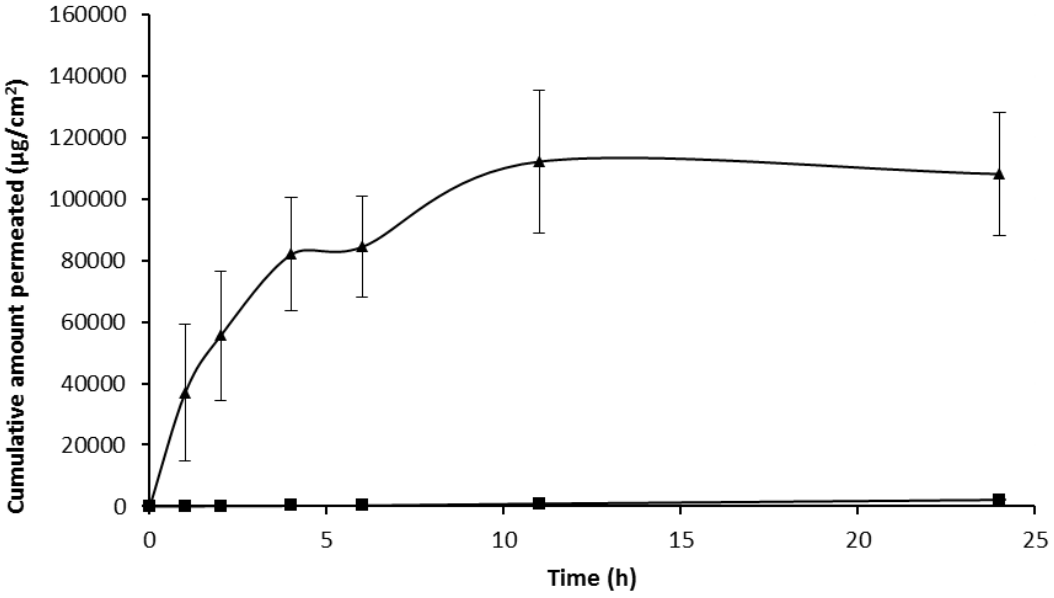

Treatment	Mean Q_6 (µg / cm^2) ± S.E.	Percentage formulation permeated at Q_6 (%) ± S.E.
Hypodermic needle	84434.9 ± 16521.1	43.8 ± 8.6

Figure 5.18 Permeation profile of ibuprofen from saturated solution across epidermal membrane.

The triangle denotes data following hypodermic needle (26 G) treatment and the square denotes data obtained for no membrane treatment (patient age 58 years). Data presented as mean ± S.E. (n=4).

However, when a finite dose and silicon MN array penetration was used as a positive control treatment to enhance ibuprofen flux, the results deviated from hypothesis. As Figure 5.19 shows, there was no significant difference (P=0.29) at 24 h in the quantity of ibuprofen permeation across intact and silicon MN treated membranes.

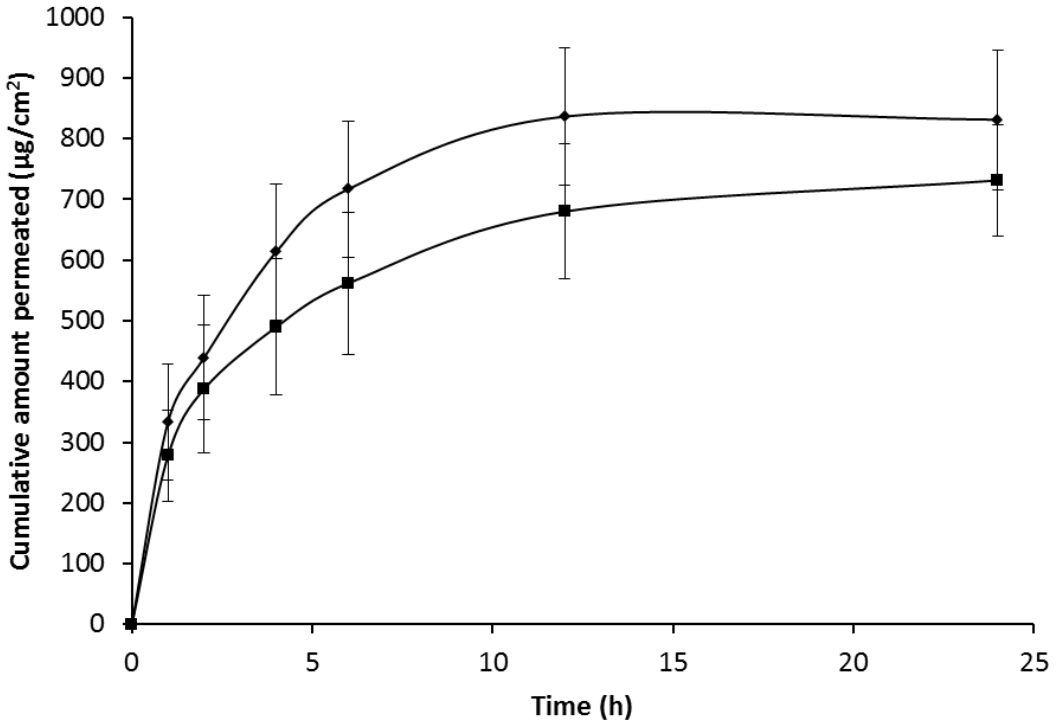

Treatment	Mean Q_6 (µg / cm^2) ± S.E.	Percentage formulation permeated at Q_6 (%) ± S.E.
Silicon MN array	561.9 ± 116.8	37.5 ± 7.8
Untreated membrane	716.9 ± 112.4	47.8 ± 7.5

Figure 5.19 Permeation profile of ibuprofen from 5 $\%^{w}/_{w}$ IBU loaded stock sugar solution across epidermal membrane.

The square denotes data following silicon MN treatment and the diamond denotes data obtained for no membrane treatment (patient ages 47 and 80 years). Data represented as mean ± S.E. (n=6).

This result was not expected, and suggested that either the classical Franz cell experimental setup or the model permeant may not be optimal for assessing MN facilitated drug delivery. If the silicon MNs did not reliably penetrate the membrane this may account for the similarities in drug flux observed. Alternatively, the membrane could have been compromised prior to the beginning of the study, possibly due to prolonged periods under frozen storage conditions. Finally, due to favourable physicochemical properties, it may have been that ibuprofen permeated the membrane easily without physical disruption of the epidermal barrier (Stott et al. 1998). Furthermore, as noted previously in Figure 5.18, as the donor concentration became depleted, permeation of ibuprofen decreased and a plateau in delivery was observed.

It also became apparent that standardisation of the initial epidermal barrier properties was essential to permeation studies. As Figure 5.20 (B) shows, even though silicon MNs decreased ER of the epidermal barrier by appearing to penetrate the membrane, Figure 5.20 (D), impedance measurement of the untreated epidermal membranes in each treatment group varied significantly (P=0.03). It is known that if skin integrity is compromised prior to *in vitro* percutaneous absorption studies this will affect the permeability of the membrane to test substances (Scott et al. 1991). Therefore, to make comparisons between treatment groups, baseline ER measurements would need to be established to ensure standardisation of barrier integrity.

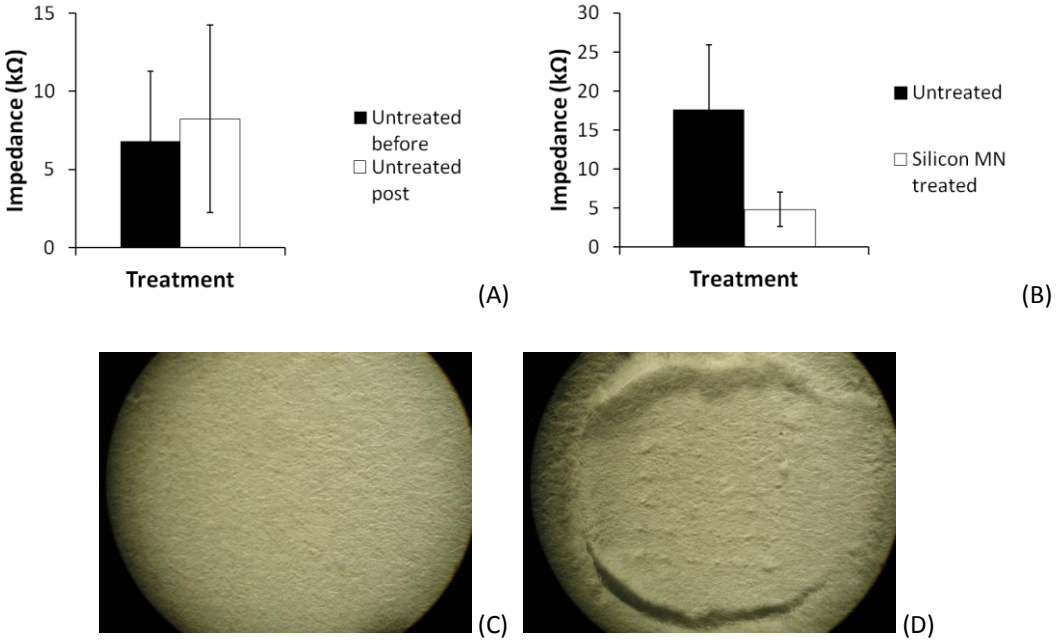

Figure 5.20 Estimation of epidermal membrane penetration.

The black bars represent electrical resistance measurement prior to treatment and the white bars represent data following (A) no treatment or (B) silicon MN treatment. Data presented as mean ± S.D. (n=6). (C) and (D) representative sections of filter paper supporting untreated and silicon MN treated membranes respectively.

It has been well characterised that silicon MN arrays reliably puncture human skin to facilitate drug delivery (Coulman et al. 2009; Henry et al. 1998; McAllister et al. 2003). In this study a significant increase in drug flux following MN treatment was not observed. It was speculated that this may have been due to inefficient puncture of the membrane, limitations of the experimental setup, or that ibuprofen was not the optimal model permeant due to high passive permeation of the molecule across skin.

5.4.5 Development and optimisation of static type Franz diffusion cells for microneedle facilitated penetration / permeation studies

Initial membrane screening studies, section 5.4.4, highlighted that the classical setup of Franz diffusion cells may not be optimal for assessing MN facilitated percutaneous drug delivery. Preliminary studies highlighted that without any support beneath the epidermal membrane within a diffusion cell, penetration of the barrier by MN arrays may be variable. Therefore, various adaptations of the classical setup were investigated to provide a platform for the assessment of SGMN arrays.

Three different modifications were investigated; the inverted method whereby the epidermal membrane was applied SC down on top of mounted MNs prior to cell assembly, the gauze method where a PTFE ring with a gauze section in the centre was fashioned and the PTFE disc method whereby small holes were drilled into the disc and clamped between the donor and receptor flanges. Sugar glass MN arrays were then applied *in situ* into the donor chamber. Each setup was investigated by the insertion of SGMN arrays into the SC side of the epidermal membrane. As Figure 5.21 shows, it was not visually obvious which setup provided the most reliable method for insertion of SGMN arrays.

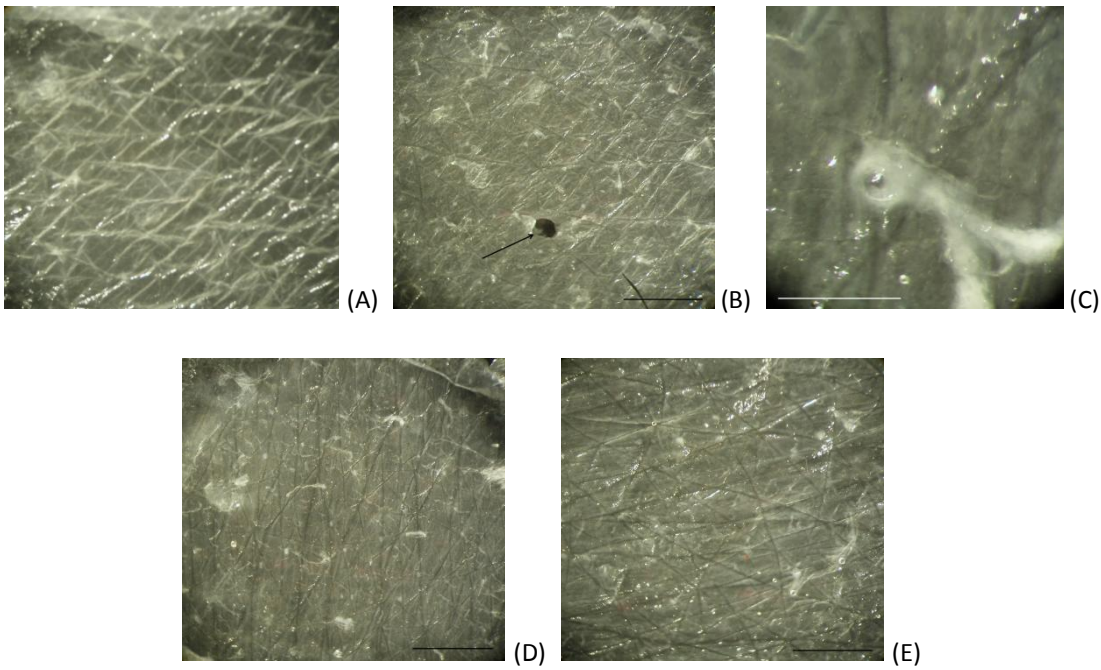

Figure 5.21 *En face* light photomicroscopy images of epidermal membranes.

(A) Untreated membrane and membrane following SGMN insertion using (B) and (C) inverted method, (D) gauze method, (E) PTFE ring method (representative of n=2). Bar = 1000 µm (black bar) or 500 µm (white bar).

Disregarding the large hole present in Figure 5.21 (B) (black arrow), reasoned to be an artefact formed during the dismantaling of the Franz cell process, and the remnants of hair follicles / sweat ducts, Figure 5.21 (C), there were no obvious signs of MN channels within any of the membranes. Various reasons for this outcome were proposed. It could have been that the SGMN arrays did not penetrate the membrane in any of the modified setups, or it could have been that the holes generated were too small to visualise at this magnification. Otherwise, it could have been that any microchannels formed simply resealed rapidly following MN insertion; although this seems unlikely as the treated areas were occluded during the study.

To probe the SGMN penetration properties of each method, MB dye solution was applied to the SC side of the membrane. The aim was to observe any channels created in the epidermis by the SGMN arrays. However, as the images in Figure 5.22 show, there was no evidence of discrete membrane puncture sites which would indicate that the SGMNs had inserted into the membrane. This result was even observed in positive control samples following silicon MN treatment of the membrane, Figure 5.22 (A).

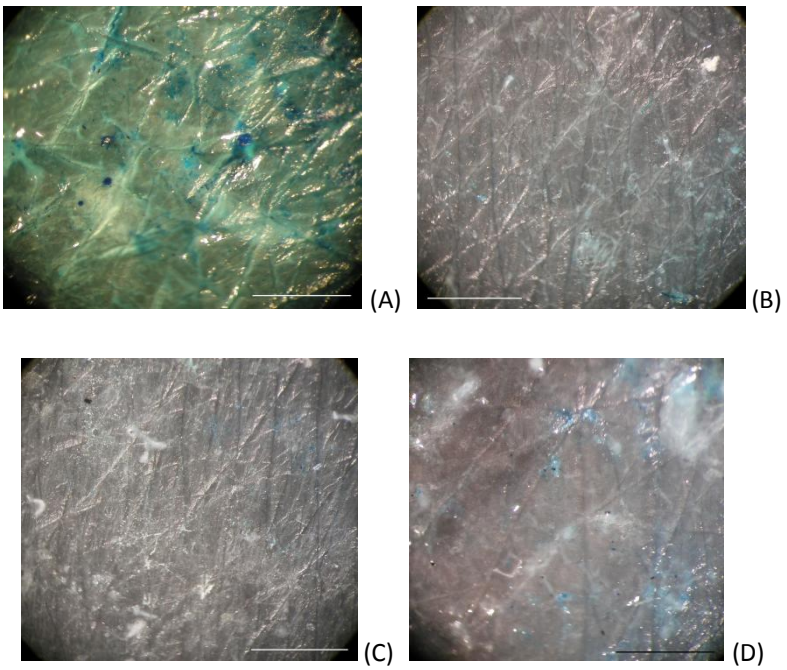

Figure 5.22 *En face* light photomicroscopy images of epidermal membranes following methylene blue dye staining.

The data show membrane following (A) silicon MN on corkboard treatment, (B) PTFE ring method, (C) inverted method and (D) gauze method (n=2) (Bar = 1000 µm).

These investigations demonstrated that it would not be possible to precisely assess the membrane penetration capabilities of MN arrays by membrane staining and light microscopy and therefore that more detailed analyses would be required.

A variety of strategies were used to investigate the penetration efficiency of epidermal membranes via MN arrays. These included fixing of treated membranes with glutaraldehyde solution and visualisation under fluorescence microscopy and environmental SEM imaging (data not shown). Both these techniques provided some evidence of membrane puncture, however there was still no obvious pattern of MN penetration. It was concluded that it would not be possible to observe a distinct penetration profile pattern within the membrane using MN arrays of these dimensions. Following a number of repeat experiments, it was determined that the gauze method, section 5.3.2.7 (2), provided the best Franz cell modification to assess SGMN epidermal membrane penetration. This conclusion was based on the relative ease of assembly of this modified cell and because the setup appeared to provide the best support for application of MNs *in situ*.

5.4.6 Assessment and validation of electrical resistance as a measure of epidermal barrier integrity

As the data in Figures 5.20 and 5.23 demonstrate, the methodology described in this work was appropriate for the assessment of ER of heat separated epidermis. However, it became apparent that some of the skin tissue used in early experiments was not fit for purpose and had impaired barrier function. This was demonstrated by some of the low initial ER measurements of intact membrane prior to MN insertion, for example Figures 5.20 (A) and 5.23. A correlation was observed between a low intact membrane resistance value and a tendency of the membrane to rapidly allow passage of the donor compartment NaCl solution into the receptor compartment. This "leaky" behaviour further suggested that the integrity of the membrane was poor and therefore visual inspection of the Franz cell became a secondary marker of skin barrier functionality. One possible reason for these observations may have been due to the duration of tissue storage under frozen conditions, as it is known that these conditions can disrupt barrier function if maintained for longer than 12 months (Davies et al. 2004).

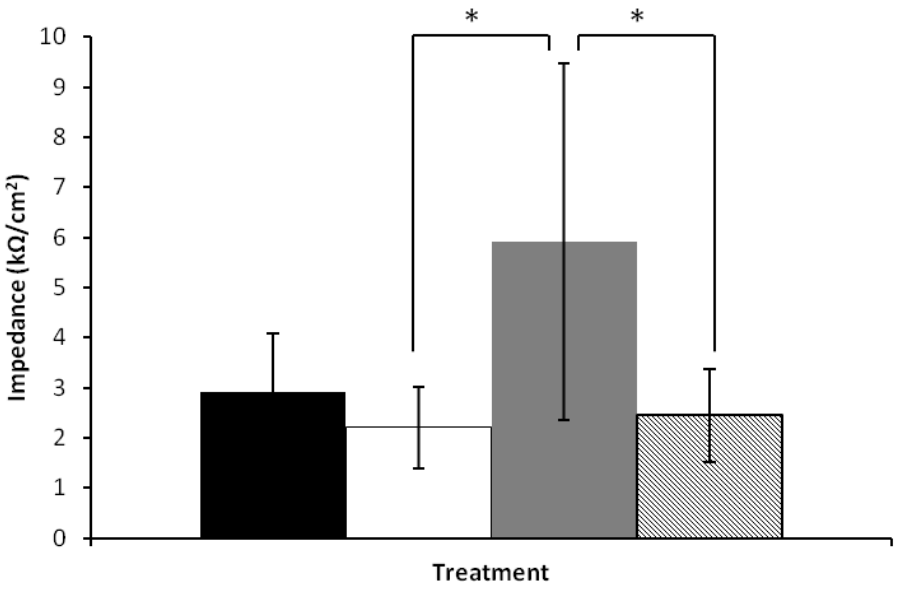

Figure 5.23 Electrical resistance measurement of epidermal membranes.

(Patient ages archived, 58 and 93 years). Treatments were as follows, intact skin (black bar, n=4), silicon MN treated (white bar, n=9), 5 $\%^{w}/_{w}$ IBU loaded SGs (grey bar, n=9) and 5 $\%^{w}/_{w}$ IBU loaded SGMN treated (hashed bar, n=11). Data presented as mean ± S.D., * denotes significance (P=0.0017).

It was noted that impedance measurements of membranes varied greatly between donors and also within samples from the same donor. For example, the impedance of membranes treated with flat SGs, Figure 5.23, were greater than intact membranes measured at the beginning of

the study, although they all came from the same donor population. Variation in ER measurement of untreated membrane has been noted previously by other workers (Fasano et al. 2002; Lawrence 1997) and therefore this was not unexpected. To address this issue, an initial screening methodology involving ER measurement combined with visual observation of test cells was developed to determine barrier integrity.

5.5 Conclusion

In summary, this chapter suggests that adhesive layers containing a variety of suspended model drug substances can be reliably produced. Subsequently, it has been shown that SGMN arrays fabricated with a thin base layer can be attached to a transdermal adhesive patch system for potential percutaneous drug delivery applications. Importantly, the morphology of the SGMNs appeared to be relatively stable when the array was attached to model drug loaded adhesive backings and stored under vacuum desiccation.

A range of model membranes were assessed for their applicability to SGMN penetration and diffusion studies. It was shown that human heat separated epidermis was superior to synthetic membranes in these studies. However, it was found that the classical setup of the Franz diffusion cell was not optimal for investigating MN facilitated transdermal drug delivery. Although not conclusive, modifications to the classical setup appeared to provide an enhancement of the application and penetration capabilities of MN arrays. In addition, a reliable methodology for assessing initial epidermal barrier integrity was developed utilising a combination of visual assessment and electrical resistance measurement. It was envisaged that these tools together would provide a robust platform for future investigation of SGMN array percutaneous drug delivery potential.

Chapter 6

Transdermal drug delivery using sugar glass microneedles

6 Transdermal drug delivery using sugar glass microneedles

6.1 Introduction

6.1.1 Microneedle facilitated transdermal drug delivery methods

As discussed previously, there are many examples of different biodegradable MN systems in the literature. The delivery of various drugs has been investigated utilising these systems and studies have been conducted to determine their potential for transdermal drug delivery. These studies have been conducted using both *in vitro* and *in vivo* models depending upon the properties of the drug under investigation. Accordingly, the main focus of this chapter was to investigate the drug delivery potential of SGMN arrays utilising an *in vitro* human skin model.

Early MN facilitated delivery studies conducted by Henry et al. utilised heat separated epidermal membrane as a model barrier (Henry et al. 1998) as it is known to provide the predominant mechanical barrier (Van Duzee 1978) to needle insertion. The epidermis was mounted within static Franz type diffusion cells with the SC facing the donor compartment and the lower epidermis facing the receptor compartment (Henry et al. 1998). Permeabilities for MN treated skin were determined for the surface area treated with the MN array only. This was justified as it was reasoned that, once treated with a MN array, drug transport of impermeable substances would only occur over the area where the needles have been inserted (Henry et al. 1998). Subsequently, this approach to permeation data analysis was utilised in all diffusion studies conducted in this chapter.

The work of McAllister et al. utilised heat separated epidermis which was removed from the diffusion cell and placed on a supported surface prior to MN application (McAllister et al. 2003). The rationale behind using epidermal membrane was further developed in this work as mathematical modelling was carried out by the authors. It was determined that removing the dermal barrier above the capillaries of the dermal-epidermal junction may overestimate skin permeability by a factor of 2, however the use of full thickness skin may underestimate permeability by a factor of 5 (McAllister et al. 2003) and hence this is why the epidermis alone was used. This rationale has been supported by others who have suggested that the dermis may provide an artefactual reservoir and binding site *in vitro* for drugs that would have been removed by capillaries in the dermal-epidermal layer *in vivo* (Amsden and Goosen 1995). Furthermore, shorter lag times across full thickness skin have been observed *in vivo* compared

to *in vitro* following MN insertion. It has been speculated that the increased lag time *in vitro* may be due to diffusion of the permeant through the entire thickness of the skin before detection in the receptor phase. *In vivo,* the drug is picked up by the microcirculation as soon as it traverses the epidermis (Kolli and Banga 2008) and hence displays a shorter lag time.

Park et al. utilised a similar methodology whereby cadaver heat separated epidermis was used as the barrier and was mounted onto layers of tissue paper to act as a mechanical support before polymer MN treatment. Once treated, the epidermis was placed onto a support mesh and loaded into the diffusion cells (Park et al. 2005). Coulman et al. used a similar approach in which separated epidermal sheets were replaced onto the dermis from which they had been separated. Silicon MN arrays were mounted onto metal applicators and applied to the membrane 5 times before they were mounted into Franz diffusion cells (Coulman et al. 2009). In both these experiments, donor solutions containing drug were applied following cell assemblage.

More recently, workers have investigated drug delivery from biodegradable MNs where the drug is incorporated within the MN structure itself. Solid state biodegradable microstructures (SSBMS) containing fluorescein isothiocyanate-tagged BSA (FITC-BSA) have been evaluated *in vitro* using split thickness human cadaver skin (Wendorf et al. 2011). Synthetic dissolving MNs containing insulin have been examined *in vitro* by analysing diffusion of the drug across dermatomed neonatal porcine skin using modified Franz diffusion cells. Here the skin was affixed to the donor flanges of the donor compartment before MNs were inserted (Migalska et al. 2011). In a similar set of experiments Donnelly et al. incorporated theophylline into polymeric MNs and assessed its permeation across dermatomed neonatal porcine skin. The skin was glued, SC side up, to the donor flanges and supported underneath by dental wax whilst MNs were inserted; the MN device was secured in place and the donor and receptor chambers were assembled (Donnelly et al. 2011).

In this work a novel adaptation of the classical Franz diffusion cell setup, as described in Chapter 5, was utilised to assess the drug delivery potential of SGMN arrays. To date there does not appear to be a single optimised methodology to investigate MN facilitated permeation of model substances across skin barrier *in vitro*. In this work a ring of PTFE was fashioned to fit between the flanges of the donor and receptor compartments of the Franz

cell. In the centre of the ring there was a 1 cm^2 hole with a section of steel gauze placed into it. In this way the cell could be greased and assembled, complete with the epidermal membrane, prior to SGMN insertion *in situ*. It was envisioned that this methodology may provide a promising alternative to evaluate the transdermal drug delivery potential of MN devices, and in particular rapidly dissolving biodegradable MNs containing drug. Previous methodologies have generally focussed on MN insertion prior to assembly of the Franz cell. This may lead to more complex assembly of the cell and give rise to the potential for MN devices to become dislodged during the process leading to inaccurate initial permeation measurements. To assess the efficacy of MNs to enhance permeation of a substance across skin the enhancement ratio has been calculated. In this study the enhancement ratio was based on the ratio of ibuprofen flux through SGMN treated skin compared to the flux across untreated skin, using the following equation (Donnelly et al. 2008; Stott et al. 1998).

Enhancement ratio = ibuprofen flux through SGMN treated skin / ibuprofen flux through untreated skin

Together, the studies detailed here highlight the different approaches to assessing the transdermal drug delivery efficiency of a number of MN enhancement techniques *in vitro*. In this work a novel methodology was developed, as described in Chapter 5, to investigate the transdermal drug delivery potential of SGMN arrays across human skin barrier.

6.1.2 Drug delivery from transdermal drug delivery systems

As discussed in Chapter 5, there are now a number of different TDDSs available. The benefit of delivering drugs transdermally across skin is that in certain systems zero-order drug kinetics may be achieved, that is, a constant amount of drug is delivered per unit time. This situation is most likely to lead to a stable level of drug in the plasma which is of benefit in treating chronic conditions. In contrast, first-order kinetics, whereby a fixed proportion of the total drug is delivered per unit time, as in conventional dosage forms, leads to initial peaks followed by potentially subtherapeutic troughs in drug concentration within the body (Lee and Robinson 2000). Reservoir patches are capable of providing zero-order delivery kinetics, whereas matrix patches are not designed to provide true zero-order release. In these systems, as drug closest to the skin is released, drug contained within the remainder of the patch must travel a further distance before permeation occurs. With time this gradually increases the diffusional pathway for drug within the patch and slows release (Hadgraft and Lane 2006). Well-designed matrix

patches circumvent this problem by minimising the reduction in release rate so that absorption is not affected (Hadgraft and Lane 2006). Typically this is achieved by high drug loading within the patch, and often 20 times the drug to be absorbed is contained within the patch to create a stable concentration gradient (Nitti et al. 2006).

Although drug release from matrix patches has potential limitations, in general these patches are the preferred formulation due to their enhanced clinical safety profile over the reservoir system (Margetts and Sawyer 2007). Accordingly, depending upon the adhesive polymer utilised and the physicochemical properties of the model drug within the patch, *in vitro* permeation has been shown to vary. For example, relatively high fluxes of primaquine base across human skin, approximately 57 μg/cm^2/h and 49 μg/cm^2/h, have been noted from two different acrylate adhesive matrices containing 10 mg/cm^2 (Jeans and Heard 1999). Alternatively, the permeation of fentanyl base across human skin from silicone-2920 and polyisobutylene adhesives, loaded at 2 %, were approximately 6 and 3 μg/cm^2/h, respectively (Roy et al. 1996). Duro-Tak® 2516 acrylate adhesive patches containing 1.5 % levonorgestrel and 21 % captopril, both stabilised by PVP, facilitated drug fluxes across hairless rat skin of approximately 0.6 and 105 μg/cm^2/h, respectively (Jain and Banga 2010). As these studies show, some variations in drug permeation from adhesive patches have been demonstrated *in vitro*; dependent upon the system under investigation. In general, maximal drug flux values are in the range of micrograms per centimetre squared per hour.

Accordingly, it was of interest in this chapter to investigate the permeation of large molecular weight model substances from integrated transdermal SGMN patches *in vitro*. Furthermore, it was an aim of this chapter to compare permeation of model substances across human epidermal membrane from drug loaded SGMN arrays and integrated SGMN patches.

6.2 Chapter objectives

1. Quantitative assessment of *in vitro* percutaneous drug delivery potential of SGMN arrays containing a small molecule across heat separated epidermis.

2. Quantitative assessment of *in vitro* percutaneous drug delivery potential of SGMN arrays containing larger molecular weight moieties across heat separated epidermis.

3. Investigate *in vitro* percutaneous drug delivery potential of integrated transdermal SGMN array patches containing model drug substance across heat separated epidermis.

4. Assess dissolution kinetics of SGMN arrays *in situ* in full thickness human skin *in vitro*.

6.3 Materials and methods

6.3.1 Materials

All reagents were obtained from Fisher Scientific Ltd. (Loughborough, UK) and were of analytical grade unless stated otherwise.

Human breast skin was obtained from the Aneurin Bevan Health Board Royal Gwent Hospital (Newport, Wales, UK) following mastectomy or breast reduction surgery with full ethical committee approval and informed patient consent.

6.3.2 Methods

6.3.2.1 Sugar glass microneedle facilitated diffusion studies across human epidermal membrane

6.3.2.1.1 SGMN arrays containing ibuprofen sodium

SGMN arrays containing 5 $\%^{w}/_{w}$ ibuprofen sodium (IBU) were prepared as described in section 4.3.2.1. Flat sections of blank SG and SG containing 5 $\%^{w}/_{w}$ IBU were prepared as described in section 5.3.2.4. Modified static type Franz diffusion cells were assembled (section 5.3.2.7.2) with heat separated epidermis from female donors aged 47, 80, 93 and 58 years and ER measurements were taken, as described in section 5.3.2.8. Drug loaded SGMNs and SGs were mounted onto the flattened end of syringe plunger and applied to the membrane as described in section 5.3.2.7.2. Control cells were assembled and the membrane was treated with a silicon MN array, applied in the same manner, before a section of SG was placed into the donor.

In this method the receptor compartment was filled with degassed PBS (pH 7.4) equilibrated to 37 ^{o}C only once the MNs had been applied to the membrane. Formulations were covered with a plasticised PVC film backing disc and cells were placed into a water bath on top of a magnetic plate as described in section 5.3.2.4. Cells were occluded and samples were taken as described in section 5.3.2.4. At the end of the study, the donor and receptor contents were removed and final ER measurement readings taken. Ibuprofen sample analysis was performed using reversed-phase HPLC as described in section 5.3.2.6. The flux of ibuprofen from SGMN arrays was compared to flat sections of SG and a mean enhancement ratio for SGMNs was obtained.

6.3.2.1.2 SGMN arrays containing sulforhodamine B sodium

SGMN arrays containing 5 $\%^{w}/_{w}$ SRB were prepared as described in section 4.3.2.1. Flat sections of SG containing 5 $\%^{w}/_{w}$ SRB were prepared as described in section 5.3.2.4. Initial ER measurements were taken, as described in section 5.3.2.8, before positive control membranes were treated with a single hypodermic needle puncture and a section of SG was placed into the donor chamber. 150 µL 5 $\%^{w}/_{w}$ drug loaded sugar solution was pipetted onto the surface of untreated skin sections as a negative control. Modified static Franz diffusion cells were assembled with heat separated epidermis from female donors aged 49 and 82 years, as described in section 6.3.2.1.1 and the same processes were carried out with these SGMNs. SRB sample analysis was performed by fluorescence spectrophotometry (Fluostar Optima™, BMG Labtech, Aylesbury, UK) using Greiner black polypropylene 96 well plates with excitation and emission filters set at 544 and 590 nm respectively. Sulforhodamine B quantities were estimated by linear regression and correlation analysis of the calibration curves generated (LOD 5 x 10^{-5} mM) in each method.

6.3.2.1.3 SGMN arrays containing fluorescein isothiocyanate conjugated bovine serum albumin

SGMN arrays containing 5 $\%^{w}/_{w}$ FITC-BSA were prepared as described in section 4.3.2.1. Flat sections of SG containing 5 $\%^{w}/_{w}$ IBU were prepared as described in section 5.3.2.4. Initial ER measurements were taken, as described in section 5.3.2.8, before positive and negative control membranes were treated as described in section 6.3.2.1.2. Modified static Franz diffusion cells were assembled with heat separated epidermis from female donors (archived tissue and those aged 49 and 82 years), as described in section 6.3.2.1.1, and the same processes were carried out with these SGMNs. FITC-BSA sample analysis was performed by fluorescence spectrophotometry (Fluostar Optima™, BMG Labtech, Aylesbury, UK) using Greiner black polypropylene 96 well plates with excitation and emission filters set at 485 and 520 nm respectively. FITC-BSA quantities were estimated by linear regression and correlation analysis of the calibration curves generated (LOD 5 x 10^{-5} mM) in each method.

6.3.2.2 SDS-PAGE electrophoresis

Running buffer concentrate (10x) was prepared with the following formula.

Glycine	144 g
Tris base	30.3 g
Sodium dodecyl sulphate (SDS)	10 g
(Biorad Laboratories Ltd., Hertfordshire, UK)	
dH_2O	up to 1000 mL

A 10 % resolving gel was prepared using the following components.

40 % Acrylamide/Bis-acrylamide (Sigma - Aldrich, Poole, UK)	5.0 mL
3M Tris base pH 8.8	2.5 mL
10 % SDS	0.2 mL
dH_2O	12.2 mL
Temed (Biorad Laboratories Ltd.)	15 µL (added just before pouring cassette)
Ammonium persulphate 10 % (Sigma - Aldrich, Poole, UK)	150 µL

The resolving gel was loaded into two 1.5 mm gel plate cassettes attached to a casting stand on the gasket of a casting clamp. Once loaded, the gel was kept moisturised with dH_2O and maintained at room temperature for approximately 40 mins until solidified.

A 4 % stack gel was prepared using the following components.

40 % Acrylamide/Bis-acrylamide	1.0 mL
1M Tris HCl pH 6.8	1.3 mL
10 % SDS	0.1 mL
dH_2O	7.6 mL
Temed	10 µL (added just before pouring cassette)
Ammonium persulphate 10 %	75 µL

Once the resolving gel had solidified, excess water was removed and the stacking gel was loaded into the cassette on top of the resolving gel. A comb was immediately inserted into the stacking gel and the gel was kept moisturised for approximately 40 mins until solidified. Once set, the comb was removed and 5 µL of molecular weight marker (GE Healthcare) was loaded into 2 wells. 20 µL aliquots of samples and BSA and FITC-BSA standards were loaded into

separate wells within the gel. The cassettes were then placed into an electrophoresis chamber filled with chilled diluted running buffer (1x). Electrophoresis of the samples was carried out at 110 V for approximately 60 mins to resolve samples.

6.3.2.3 Silver staining of gels

Once run, the gels were removed from the cassettes and rinsed twice in dH_2O for 10 mins each. They were then transferred into 10 % glutaraldehyde solution for 30 mins before being rinsed 3 times in dH_2O for 20 mins each. A staining solution was prepared as follows.

0.36 % NaOH	21 mL
dH_2O	74 mL
NH_4OH	1.4 mL
2 % silver nitrate solution	4 mL

The gel was transferred to a fresh container and the staining solution was added. The container was placed onto a flat bed rocker at 35 rpm and left for 30 mins. Following this, the gel was rinsed 3 times in dH_2O for 5 mins.

A developing solution was prepared as follows.

Formaldehyde	260 µL
1 % citric acid	2.5 mL
dH_2O	up to 500 mL

The developing solution was added and maintained at room temperature until the bands within the gel turned brown. Once the bands were well developed, the gels were transferred into stopping solution, consisting of the following.

Ethanol	40 mL
Acetic acid	10 mL
dH_2O	up to 100 mL

The gels were maintained in stopping solution until no further colour change was observed and then rinsed twice in dH_2O for 15 min each. Gels were analysed using Image Lab 3.0 (Bio-Rad Laboratories, Inc.) using the ChemiDoc™ XRS+ system software.

6.3.2.4 Bicinchoninic acid protein assay

A protein assay solution was prepared containing 49 parts bicinchoninic acid (BCA) (Sigma - Aldrich, Poole, UK) and 1 part copper sulphate solution. Fresh stock solutions of FITC-BSA in PBS (pH 7.4), concentration 1 mg/mL, were prepared and varying volumes from 2 – 20 µL were pipetted into 96 well plate wells. Standards were made up to 20 µL with PBS. 20 µL samples were taken from the 24 h time point samples of FITC-BSA studies and pipetted into the well plate. 200 µL protein assay solution was then added to all wells. Well contents were gently mixed and incubated at 37 ^{o}C for 30 mins before cooling to room temperature. Plates were analysed by UV spectrophotometer (Sunrise™, Tecan Group Ltd., Switzerland) with absorbance at 562 nm and BSA masses were estimated by linear regression and correlation analysis of the calibration curve generated.

6.3.2.5 Bradford protein assay

Fresh stock solutions of FITC-BSA in PBS (pH 7.4), concentration 1 mg/mL, were prepared and standards ranging between 0.05 – 1.0 mg/mL were formulated. 10 µL of standard or samples from the FITC-BSA 24 h time point studies were pipetted into 96 well plate wells. 200 µL of Bradford dye reagent (Sigma - Aldrich, Poole, UK) was then pipetted into each well and mixed thoroughly. Plates were maintained at room temperature for 45 mins before analysis by UV spectrophotometer (Sunrise™, Tecan Group Ltd., Germany) with absorbance at 595 nm. BSA quantities were estimated by linear regression and correlation analysis of the calibration curve generated.

6.3.2.6 Integrated transdermal sugar glass microneedle patch facilitated diffusion studies across human epidermal membrane

SRB was loaded into one of three backing layers at a concentraion of 5 $\%^{w}/_{w}$ as described in section 5.3.2.3. Backings included the adhesives Duro-Tak® 87202-A (an acrylate), BIO-PSA® 7-4302 (a pressure-sensitive silicone) and sugar glass (TRA:SUC 75:25 $\%^{w}/_{w}$). SGMN arrays with a thinner base were formed as described in section 5.3.2.3. SGMN patches with a diameter of 0.8 cm were formed by attaching the adhesive patch to the base of the microneedle array as detailed in section 5.3.2.3. Blank SGs were prepared from 40 µL sugar solution as described in section 5.3.2.4, and the same approach was utilised to fabricate patches without needles for control samples.

Modified static Franz diffusion cells were assembled with heat separated epidermis from female donors aged 49, 82 and 73 years and ER measurements were taken, as detailed in section 6.3.2.1.1. Positive control membranes were treated with 3 hypodermic needle punctures and patches were applied to the SC of each membrane by mounting them onto the flattened end of a syringe plunger and applying them for 10 secs each. Cells were occluded and samples were removed from each cell as described in section 5.3.2.4 up to 48 h. At the end of the study, the donor and receptor contents were removed and final ER measurement readings were taken as described in section 5.3.2.8.

6.3.2.7 Full thickness skin sugar glass microneedle dissolution study

A 20 $\%^{w}/_{v}$ solution of TRA and SUC 75:25 $\%^{w}/_{w}$ was prepared and MB powder was incorporated at 1 $\%^{w}/_{w}$ of final sugar glass weight. SGMN arrays and flat sheets of SG material were fabricated as described in section 3.3.2.5 and 5.3.2.4 respectively. Previously prepared frozen full thickness human skin sections (2 x 2 cm) from a female donor, age 73 years, with subcutaneous fat removed, were removed and equilibrated for approximately 1 h. Once defrosted, skin sections were pinned dermal side down onto curved corkboard covered in tin foil. SGMNs were applied onto the SC of the skin using the flattened end of a syringe plunger using a rolling motion. Arrays were applied for 10 secs and the skin was assembled into Franz diffusion cells, as described in section 5.3.2.5. A 0.8 cm diameter cling film disc was placed over the sugar formulations in the donor chamber to provide an occlusive backing. Cells were filled with equilibrated PBS and a section of Parafilm® was placed over the donor phase. A small magnetic bar was added to each cell and then placed into a water bath, as described in section 5.3.2.4, for 24 h. At 24 h, skin sections were removed from cells and the residual mass on the skin surface was weighed. Excess dye was removed with tissue paper soaked in ethanol prior to viewing under light microscopy. Finally, skin sections were snap frozen, cryosectioned and visualised under light microscopy, as described in section 3.3.2.11.

6.3.2.8 Statistical analysis

For direct comparisons, a one-tailed student's T-test was performed on the experimental data using the Microsoft Excel software package. For comparisons of multiple treatment groups, a one-way ANOVA with Bonferroni's multiple comparison *post hoc* test was performed on the experimental data using the GraphPad Prism 5 software package. In all cases, statistical significance was determined by a value of $P \leq 0.05$.

6.4 Results and discussion

6.4.1 Sugar glass microneedle facilitated diffusion studies across human epidermal membrane

6.4.1.1 SGMN arrays containing ibuprofen sodium

To assess the capability of SGMNs to facilitate transdermal drug delivery of model medicaments, a number of different molecules were incorporated within SGMN arrays. Ibuprofen was chosen as a model low molecular weight molecule due to its proven efficacy as a topically applied anti-inflammatory. The parent drug molecule has a MW of 206 and logP of around 4 (Herkenne et al. 2007) whereas the sodium salt has a MW of 229 and a lower logP of 0.92 (Patel et al. 2009) making it much more water soluble. In this work, ibuprofen sodium salt (IBU) was incorporated within SGMNs and flat sections of SG at a concentration of 5 $\%^{w}/_{w}$. The rationale behind this concentration was that topically applied ibuprofen is typically supplied as a 5 $\%^{w}/_{w}$ formulation and because it had been shown that increasing the mass of drug within a SGMN above 5 $\%^{w}/_{w}$ disrupted the robustness of the array, section 4.4.1. It was hypothesised that SGMNs would dissolve rapidly *in situ* to release incorporated drug cargo. Accordingly, a high initial permeation rate would be observed, followed by a gradual decrease in permeation as the sugar formulation depletes around the aqueous channels.

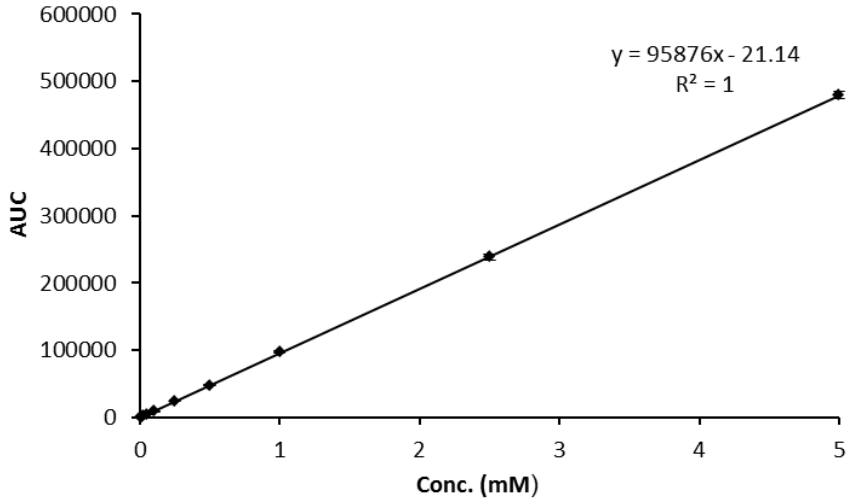

Figure 6.1 Exemplar standard curve used in quantitative determination of ibuprofen sodium flux across human epidermis.

Data presented as mean (n=2).

Using the standard curve generated in Figure 6.1, the quantity of ibuprofen permeated was estimated. As Figure 6.2 shows, there was a significant difference (P=0.03) in ibuprofen diffusion across epidermal membrane from loaded SGMNs at 24 h in comparison to flat SG sections. As observed previously, Figure 5.19, permeation of ibuprofen from a sugar formulation following MN treatment of epidermal membrane was initially rapid before reaching a plateau by 12 h. In both experiments, permeation reached a plateau at approximately 700 – 800 micrograms corresponding to approximately half of the total dose contained within the donor formulation (Figure 6.2). This further suggested that depletion of the donor phase, of greater than 10 % of the total dose, led to a reduction in concentration gradient across the membrane and hence violated sink conditions (Ng et al. 2010; Williams 2003).

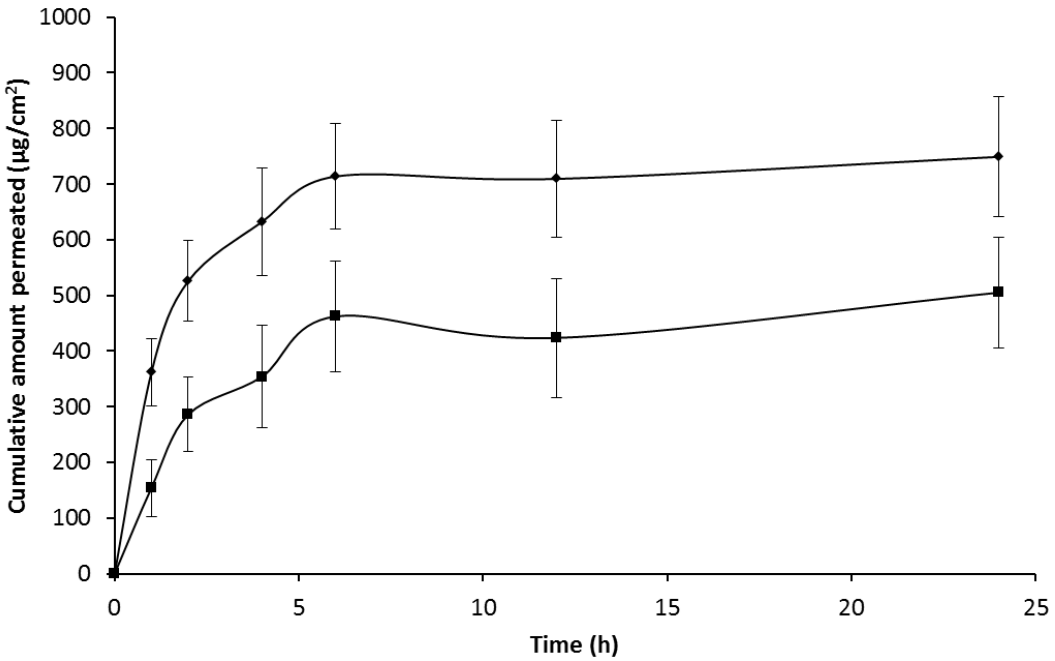

Treatment	Mean Q_6 (µg / cm^2) ± S.E.	Percentage formulation permeated at Q_6 (%) ± S.E.
SGMN array	713.9 ± 95.4	47.6 ± 6.4
SG section	462.3 ± 99.7	30.8 ± 6.6

Figure 6.2 Permeation profiles of ibuprofen from sugar glass formulations across human epidermal membrane.

Formulations included 5 $\%^{w}/_{w}$ SGMN arrays (diamonds) and flat sugar glasses (squares). Data presented as mean ± S.E. (n = 12).

This result was expected, as it was hypothesised that the SGMNs were able to puncture the stratum corneum (SC) to facilitate permeation of ibuprofen across the membrane. Accordingly, a large mean Q_6 of 713.9 ± 95.4 μg / cm^2 (Figure 6.2) was measured immediately following SGMN treatment of the membrane. Previous *in vitro* studies have shown that biodegradable polymer MNs demonstrate an initial burst release of approximately 50 % of the drug contained within the MNs (Migalska et al. 2011) which supports this data. However, in both treatment groups in this study, it was observed that only approximately half of the Franz cells contained residual sugar glass formulations within the donor chamber at 24 h. This suggested that water from the receptor phase may be causing dissolution of the entire dosage form during the study. This did not fit with our earlier hypothesis, and it was speculated that the results obtained may be due to formation of a concentrated sugar solution on the skin surface. This may have led to the generation of a hyperosmotic gradient across the membrane.

Furthermore, it appeared that ibuprofen permeated the membrane rapidly from SG formulations also. Subsequently, a small enhancement ratio of 1.4 was obtained. This was not expected and it was speculated that this could have been due to a number of reasons. It was shown in Chapter 5 that ibuprofen permeation across untreated epidermis from sugar solution was relatively high, (mean Q_6 = 716.9 ± 112.4 μg / cm^2), and that pre-treating membranes with a silicon MN array did not enhance permeation compared to untreated control, Figure 5.19. Therefore, it appeared that MN treatment of the membrane did not significantly enhance ibuprofen permeation. Alternatively, the high drug permeation observed from SG treated samples, Figure 6.2, could have been due to membrane damage caused by cracking of the brittle, glassy material under the force applied.

As a further control, cells were pre-treated with silicon MN arrays prior to application of ibuprofen loaded SGs to the donor chamber. Permeation of drug across these membranes showed an initial burst effect followed by a plateau from approximately 6 h onwards, (data not shown), which correlated with results observed previously (Figure 6.2). However, the results of this study were highly variable and hard to to draw definitive conclusions from. This behaviour was attributed to a high degree of experimental error due to lack of optimisation of the Franz diffusion cell setup for MN facilitated drug delivery prior to this study.

As the schematic in Figure 6.3 shows, it was speculated that following initial membrane penetration with silicon MNs the SG formulation was rapidly wetted and began dissolution, Figure 6.3 (A).

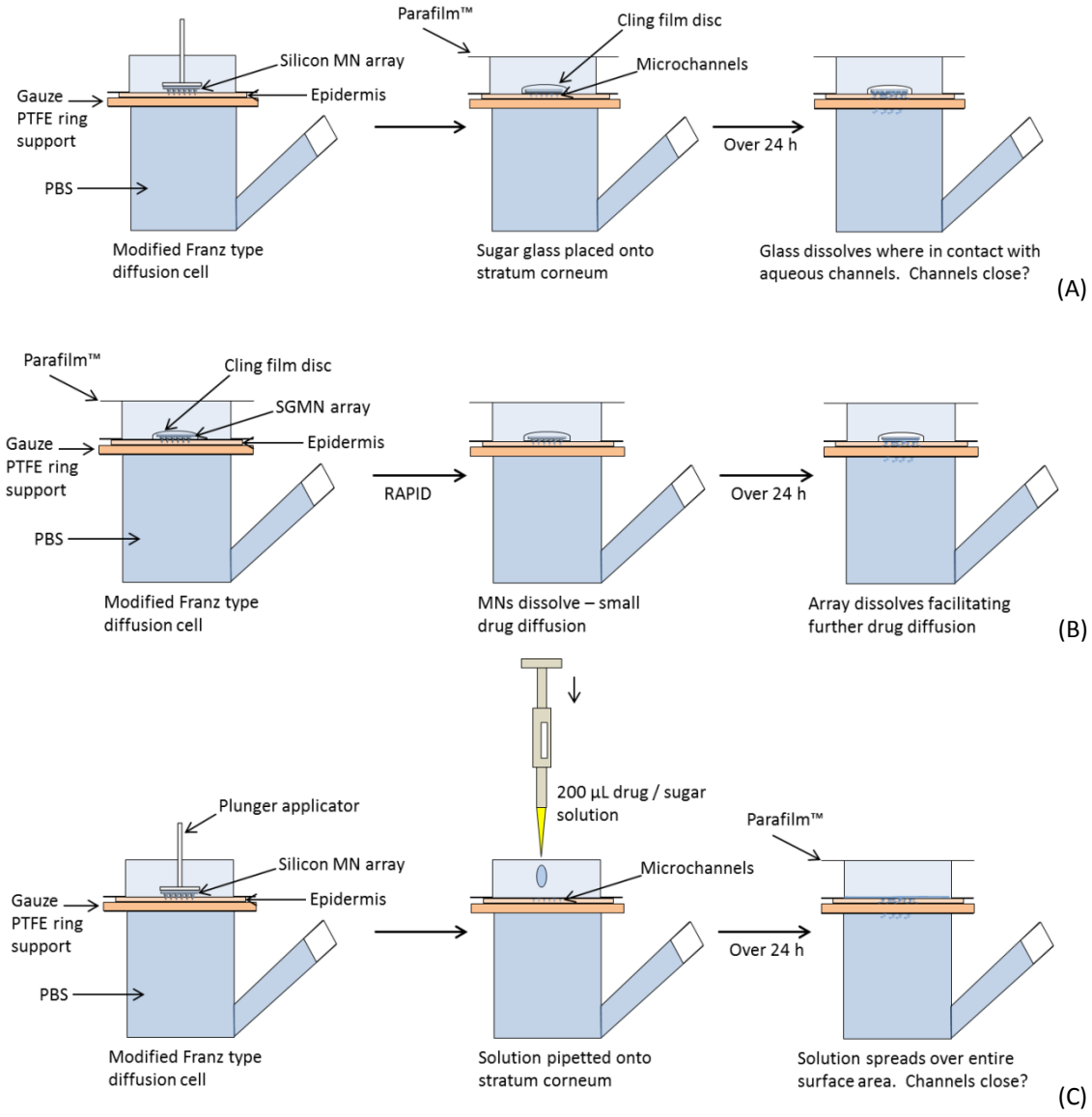

Figure 6.3 Schematic of ibuprofen diffusion from 5 %$^{w}/_{w}$ loaded sugar formulations across MN treated epidermis.

Formulations shown are (A) silicon MN application plus sugar glass, (B) SGMN array and (C) silicon MN application plus sugar solution.

Within 4 h this effect had become limited and little further ibuprofen permeated the membrane after this time. It was speculated that the microchannels formed may have re-sealed or become blocked with sugar or lipid during the study thereby preventing further drug permeation. Similar observations have been made by other workers where permeation from

biodegradable polymer MNs rapidly reached a plateau. The authors attributed this effect to blockage of microchannels by dissolved polymeric matrix material and pore closure (Migalska et al. 2011). Figures 6.3 (B) and (C) suggest explanations for the permeation profiles observed in SGMN, Figure 6.2, and control silicon MN / sugar solution treated cells.

Additionally, as stated, there was large variation in drug flux throughout the control study investigating silicon MN arrays, which suggested that membrane penetration may not have been uniform. This was supported by visual observation of MNs following the study which indicated extensive damage of individual MNs (data not shown). In combination, these studies demonstrated that ibuprofen flux across MN treated skin was not enhanced to a great extent. This was not surprising as the drug is found widely in many topically applied drug delivery systems, such as gels, and hence passively diffuses across the SC without significant barrier disruption. Therefore, the potential for enhanced ibuprofen permeation from SGMN arrays was potentially low, as it has been shown that the drug pentrates the SC well due to its high lipophilicity (Stott et al. 1998).

Alternative hypotheses for the similarity in data observed in this study was that there were inadequacies in the experimental set up or that epidermal barrier function was comprimised. Workers have found previously that a force of 0.1 – 3 N (Davis et al. 2004) is required for MN insertion into skin and hence this may not have been achieved in this study. Furthermore, skin samples used in this experiment had been frozen at -20 ^{o}C for over 3 years and therefore the barrier integrity of each may have been disrupted, as discussed in section 5.4.6. This will have influenced the flux of ibuprofen across each membrane and hence may account for the similarities in flux observed between SGs and SGMNs. This hypothesis was supported experimentally by electrical resistance measurement of the epidermal membranes at the end of the study, Figure 6.4.

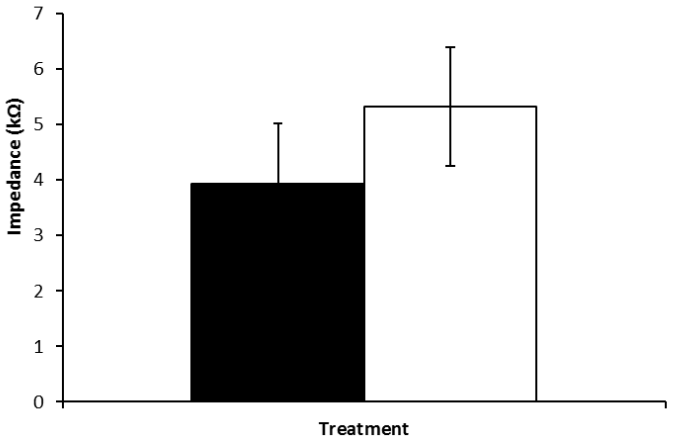

Figure 6.4 Electrical resistance measurement of epidermal membranes following treatment.

Membranes were treated with SGMN arrays (black bar) and flat SG sections (white bar). Data presented as mean ± S.D. (n = 6).

As Figure 6.4 shows, there was a small difference (P=0.03) between membranes treated by SGs and SGMN arrays. Although significantly different, all resistance measurements were very similar, and all relatively low, indicating that the barrier functionality in control samples may have been compromised. To attempt to overcome these deficiencies in experimental setup, enhanced membrane screening prior to diffusion study initiation was proposed, as described in section 5.4.6.

6.4.1.2 SGMN arrays containing sulforhodamine B sodium

As an alternative to ibuprofen, a model hydrophilic substance with a larger molecular weight, sulforhodamine B (SRB) was selected as a model permeant. Utilising the standard curve generated in Figure 6.5, it appeared that SRB permeation from various sugar formulations behaved quite differently to IBU loaded formulations, as shown in Figure 6.6.

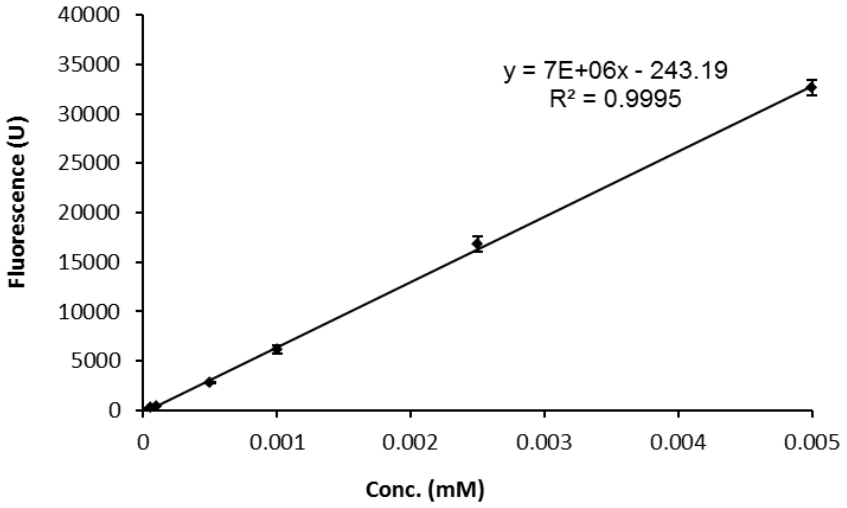

Figure 6.5 Exemplar standard curve used in quantitative determination of SRB sodium flux across human epidermis.

Data presented as mean ± S.D. (n=3).

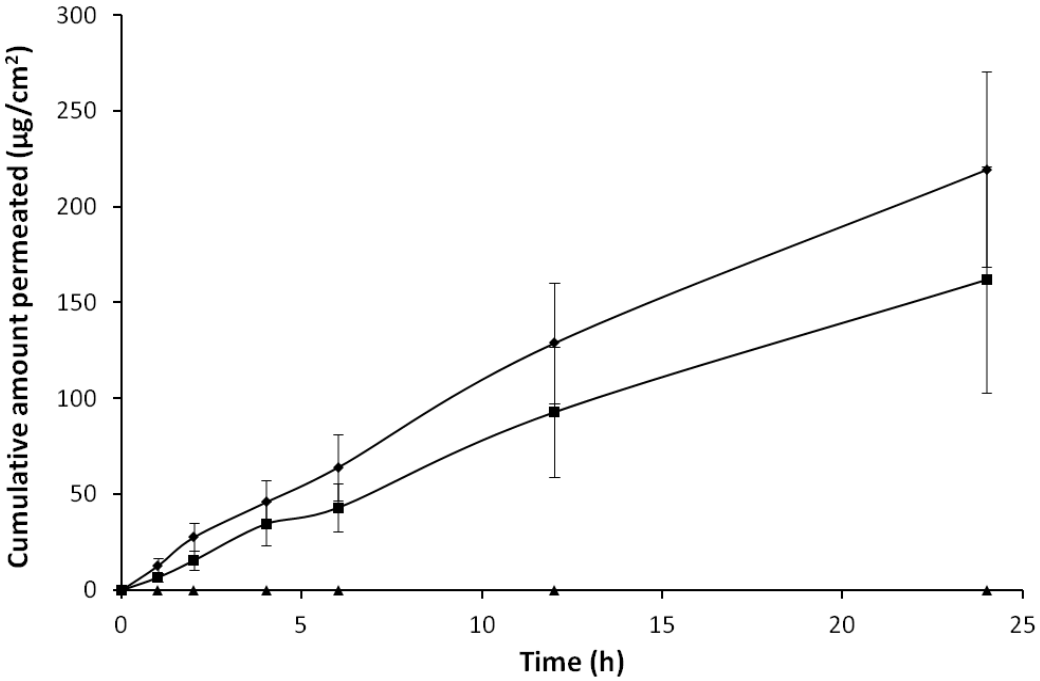

Treatment	Mean Q_6 (µg / cm^2) ± S.E.	Percentage formulation permeated at Q_6 (%) ± S.E.
SGMN array	64.1 ± 17.3	4.3 ± 1.2
Hypodermic + SG	43.0 ± 12.8	2.9 ± 0.9

Figure 6.6 Permeation profiles of SRB from sugar glass formulations across human epidermal membrane.

Treatments included glass sections loaded with 5 $\%^{w}/_{w}$ SRB across untreated (triangles) and hypodermic needle (26 G) treated (squares) or SGMN treated (diamonds) membranes. Data presented as mean ± S.E. (n=4).

To confirm that the SC of each membrane investigated was intact prior to the study, ER measurements were taken. The data in Figure 6.7 show how the membrane resistance changed throughout the study.

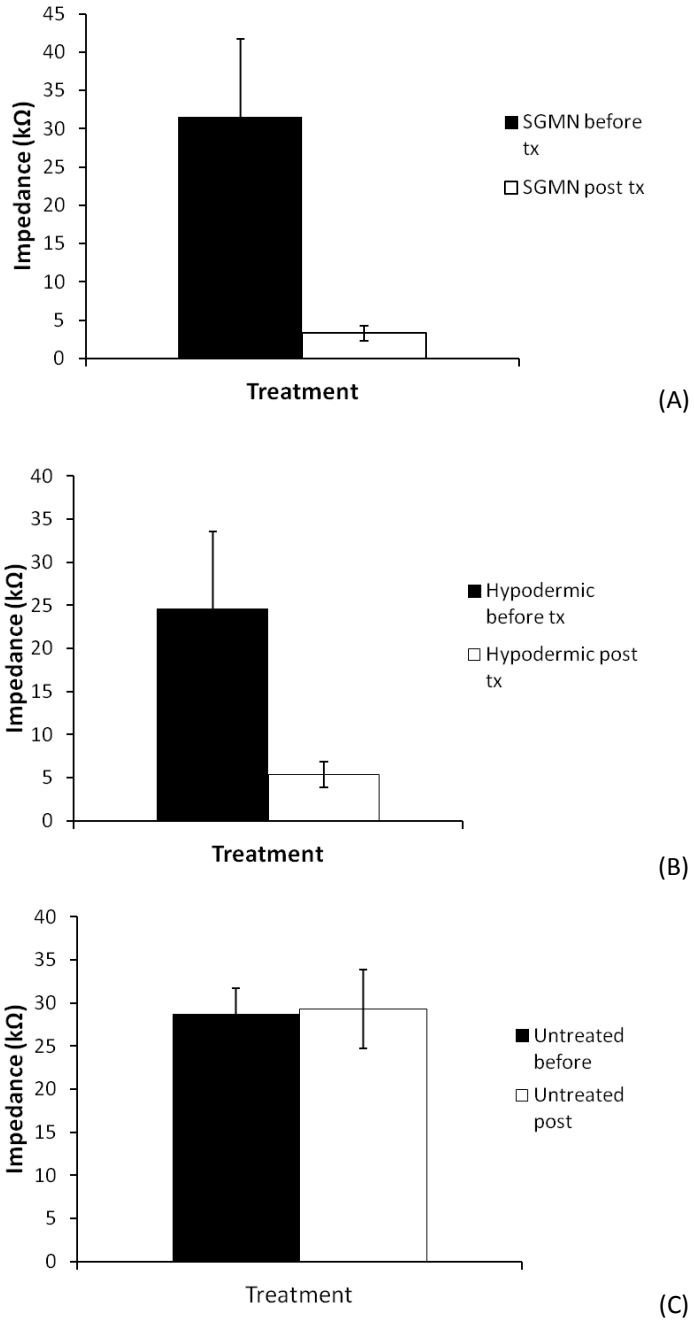

Figure 6.7 Electrical resistance measurement of epidermal membranes.

Bars denote resistance prior to treatment (black) and following (A) SGMN array treatment, (B) hypodermic needle (26 G) treatment or (C) no treatment (white). Data presented as mean ± S.D. (n=4).

In contrast to previous studies utilising IBU as a model permeant, it was apparent that no SRB permeated across untreated membrane when applied topically in a sugar solution, Figure 6.6. In support of this observation, ER measurement indicated that the SC remained intact throughout the study, Figure 6.7 (C), as there was no significant decrease in impedance (P=0.4). This result supported the hypothesis that due to its size and physicochemical properties, SRB would not passively permeate the SC. As with the IBU loaded formulation

studies, there was no lag phase shown in the permeation of SRB across either of the needle treated membranes. In support, it was suggested by ER measurement, Figures 6.7 (A) and (B), that SGMN arrays and hypodermic needles significantly decreased impedance of the epidermal barrier, P=0.0007 and 0.003 respectively. However, with this model substance there was no rapid plateau in permeation, as shown with ibuprofen permeation (Figure 6.2), and the percentage of permeant delivered by Q_6 was approximately 10 fold lower. This further suggested that ibuprofen passively permeated the membrane without enhancement.

Throughout the study there was a strong correlation between the permeation of SRB across membranes treated with a hypodermic needle or SGMN array. The mean Q_6 in each treatment arm were very similar (Figure 6.6) and this suggested that the SGMN array punctured the membrane with a similar efficacy to a hypodermic needle. Furthermore, by 24 h there was no significant difference between the cumulative amount permeated in each treatment arm (P=0.32). This suggested that microchannels generated within the epidermal membrane caused barrier disruption to a similar extent as hypodermic needle treated membranes. The permeation of SRB across SGMN treated membrane was also 2 orders of magnitude greater than across untreated membrane. These results confirmed the utility of a SGMN array to facilitate the delivery of a model hydrophilic substance across human SC. However, relatively large standard error values indicated that the rate of permeation continued to vary between diffusion cells. This effect has been noted by other workers where it was reasoned that the variability may be due to inconsistent penetration of the membrane by MNs and minor differences in the thickness of the separated membranes (Coulman et al. 2009).

It was observed that approximately 10 and 14 % of the theoretical total amount of drug (1500 µg) contained within SG and SGMN formulations respectively, permeated the membrane by 24 h. Therefore, much of the drug had not diffused across the membrane. In support of this, it was found that residual masses remained within each of the donor chambers at the conclusion of the study, Figure 6.8.

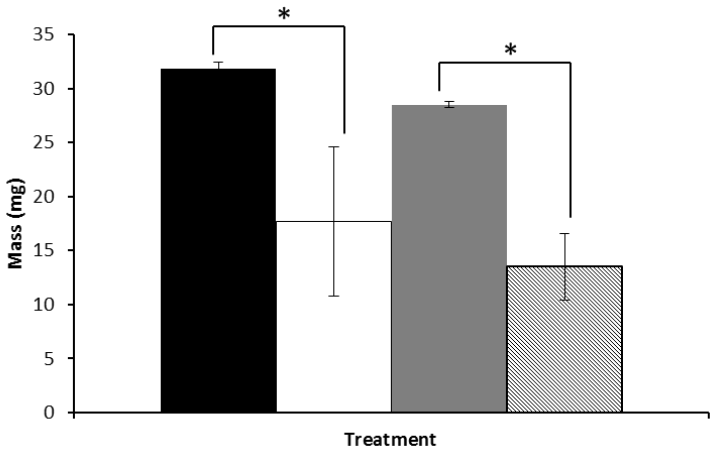

Figure 6.8 Mass of sugar glass formulations containing SRB during human epidermal study.

Bars denote mass of SG material before (black, n=3) and at 24 h (white, n=4) and SGMN array mass before (grey, n=3) and at 24 h (hashed, n=4). Data represented as mean ± S.D., * denotes significance (P=0.0005).

In contrast to the ibuprofen SGMN study, there was a residual mass of material left within each of the donor compartments at 24 h, Figure 6.8. Therefore, residual drug will have remained within the formulation at the end of the study, which suggests why no plateau was observed in permeation at 24 h in Figure 6.6. In addition, it was visually apparent that SRB had diffused into the epidermal membrane during the study, Figure 6.9.

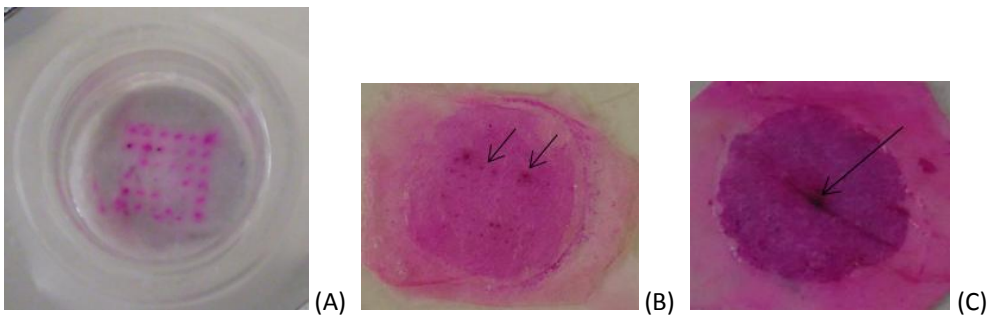

Figure 6.9 *En face* images of epidermal membranes during SRB diffusion study.

Images show membrane (A) immediately after SGMN application to donor chamber and (B) and (C) at 24 h following SGMN and hypodermic needle (26 G) application, respectively (figures representative of all treated membranes n=4).

As the arrows in Figure 6.9 (B) show, it was still possible to observe discrete SGMN channels created within the membrane at 24 h. However, in comparison to freshly treated membrane, Figure 6.9 (A), the channels were not as obvious due to partitioning of SRB throughout the

entire membrane. The same effect was observed in positive control membranes treated with a hypodermic needle, Figure 6.9 (C), where the needle channel (black arrow) stained more intensely than the surrounding tissue at 24 h. This suggested that channels created within the epidermis under these occluded patch formulations remained open throughout the study. Similar results have been observed by others investigating skin occlusion and MN channel lifetime (Kalluri and Banga 2011; Kalluri et al. 2011).

Taken together, the data in this section indicate the utility of SGMNs of these dimensions to incorporate a model hydrophilic drug molecule and to successfully deliver it across the SC barrier of human skin. Biodegradable MN structures have previously been shown to facilitate delivery of such molecules across porcine skin (Lee et al. 2008; Sullivan et al. 2008). However, Sullivan et al. investigated MNs of 750 µm length whilst Lee et al. utilised MNs measuring 600 µm; so the MNs used in this study were of a considerably shorter nature. As previously discussed, biodegradable MNs with a length of 500 µm have been shown to facilitate delivery of macromolecules more efficiently than 200 µm long needles, possibly due to ineffective skin penetration by the shorter needles (Li et al. 2009). Importantly, this study suggests that SGMNs with a pyramidal geometry and 250 µm length can successfully negate human skin barrier to facilitate cutaneous delivery of a model hydrophilic drug incorporated within the array matrix.

6.4.1.3 SGMN arrays containing fluorescein isothiocyanate conjugated bovine serum albumin

To further investigate the potential of SGMN arrays to facilitate transdermal delivery of model macromolecules, FITC-BSA was incorporated into the array matrix. Bovine serum albumin is a hydrophilic protein with a large molecular weight of approximately 66 kDa and it has widely been studied as a model macromolecular permeant in MN facilitated transdermal drug delivery studies (Lee et al. 2008; McAllister et al. 2003; Wendorf et al. 2011).

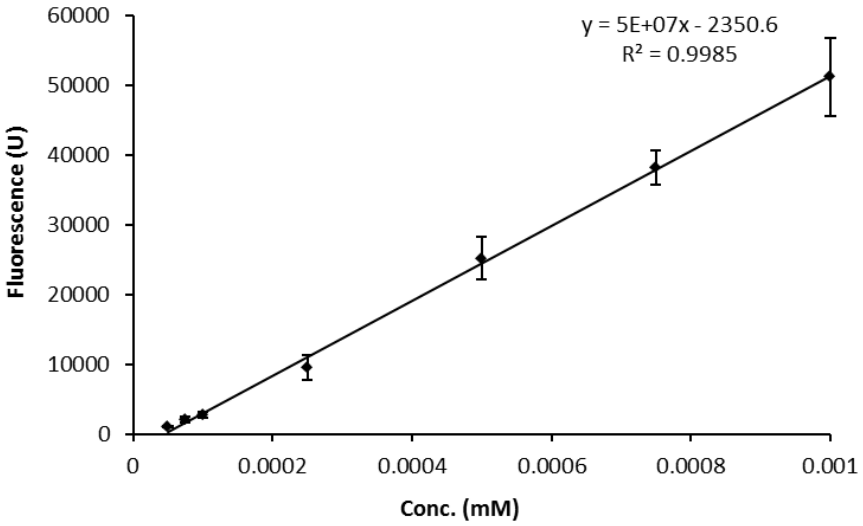

Figure 6.10 Exemplar standard curve used in quantitative determination of FITC-BSA flux across human epidermis.

Data presented as mean ± S.D. (n=3).

Utilising the standard curve in Figure 6.10, Figure 6.11 shows the estimated diffusion of FITC-BSA across epidermal membrane. As shown, two membranes in the untreated control group were discarded from the analysis. These membranes appeared to be compromised and demonstrated no initial lag phase. It was speculated that this may have been due to prolonged tissue storage at -20 ^{o}C, as discussed in section 5.4.6.

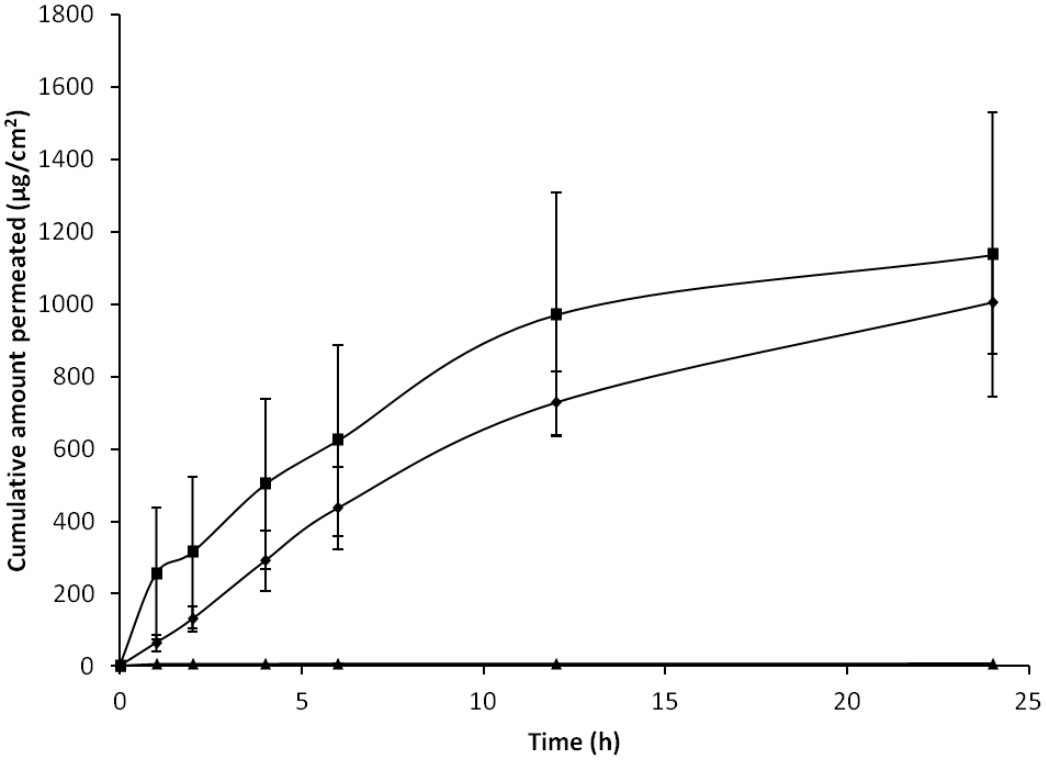

Treatment	Mean Q_6 (µg / cm^2) ± S.E.	Percentage formulation permeated at Q_6 (%) ± S.E.
SGMN array	436.1 ± 113.3	29.1 ± 8.6
Hypodermic + SG	623.3 ± 264.7	24.0 ± 16.2

Figure 6.11 Permeation profiles of FITC-BSA from 5 $\%^{w}/_{w}$ loaded sugar formulations across human epidermal membrane.

Membranes were left untreated with application of sugar solution containing FITC-BSA (triangles, n=2) or treated with a single hypodermic needle (26 G) puncture and solid SG application (squares, n=4) or SGMN array application (diamonds, n=4). Data presented as mean ± S.E.

The permeation profiles of these 2 membranes correlated with positive control data following hypodermic needle puncture of the membrane to completely negate the skin barrier, Figure 6.11. This observation was supported by SDS-PAGE which confirmed protein presence in the untreated samples (see Appendix 1). Even a small hydrophilic molecule would not be expected to permeate intact skin immediately and the diffusion profile would demonstrate an initial lag time, as demonstrated in Figure 6.12.

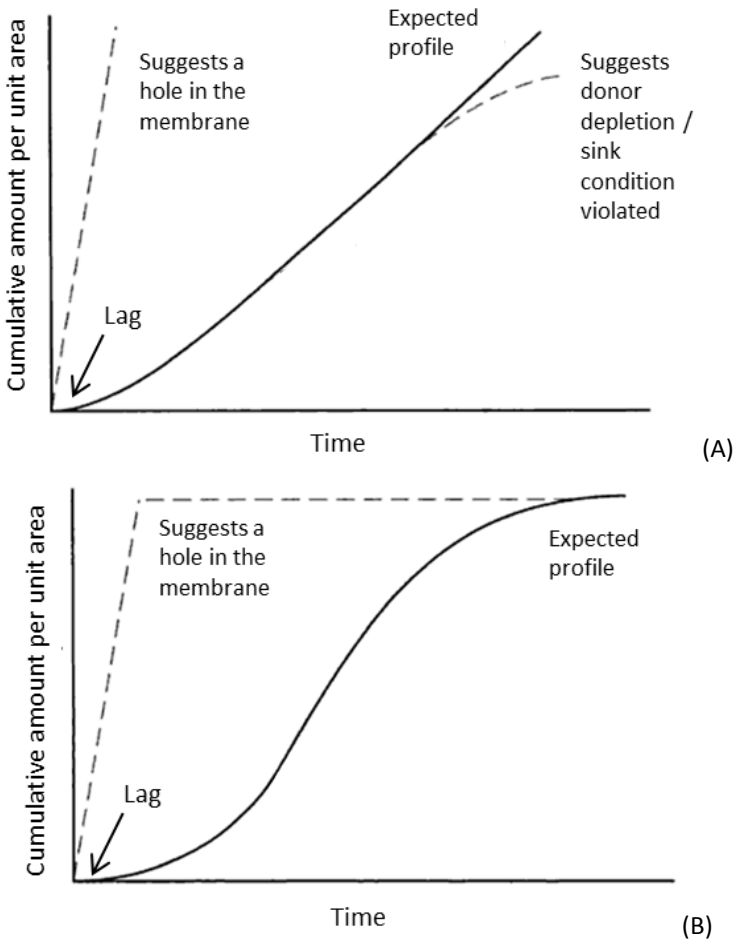

Figure 6.12 Exemplar permeation profiles obtained from (A) infinite dose and (B) finite dose application to human skin.

Adapted from source (Williams 2003).

Another feature of this experiment was that a large proportion of the total dose applied appeared to be delivered into the receptor compartment by 24 h following membrane treatment. This was a surprising result as typically 0 - 20 % of the applied dose is delivered utilising the classical Franz diffusion cell and a finite dose (Birchall et al. 2006; Coulman et al. 2009; Jeans and Heard 1999). It is generally accepted that permeation across intact skin occurs by passive diffusion (Scheuplein and Blank 1971) in accordance with Fick's Law (Flynn et al. 1974) as the permeant moves along its concentration gradient; as long as sink conditions are maintained. If the study duration permits, equal concentrations of the permeant will eventually be found in both the donor and receptor compartments, dependent upon their volume ratio. In this experiment however, a solid formulation was applied to the donor and it was found that approximately 30 % of the payload had permeated by 6 h increasing to approximately 66 % by 24 h, Figure 6.11. It was noted that permeation of FITC-BSA appeared to be reaching a plateau and hence that the amount of the permeant in the donor was

becoming depleted. This correlated well with the diffusion profile from a finite dosage form with holes created in the membrane, Figure 6.12 (B).

High levels of permeation from biodegradable MN structures *in vitro* have been found previously. For example, various workers have showed 100 % delivery of rhodamine from CMC and amylopectin MNs (Kim et al. 2012; Lee et al. 2008) following dissolution *in situ* and Donnelly et al. noted 83 % delivery of theophylline from polymer MNs (Donnelly et al. 2011). Hence, it appears that these observations are not entirely anomalous and it was speculated that there could have been a number of possible explanations for this result. Firstly, the drug loaded SGMN system is a novel transdermal drug delivery methodology with a finite dosage in a hydrophilic solid formulation maintained under an occlusive backing; a situation known to enhance the diffusion of drug through skin (Blank 1985). Also, it was hypothesised that once the SGMNs penetrated the SC they would dissolve rapidly within the epithelial cell layer creating aqueous channels, as shown in Figure 6.3 (B). This would allow "back diffusion" of water from the receptor compartment (Herkenne et al. 2007) to wet the main dosage reservoir of the SGMN array base. As the array was occluded, this could have created a highly concentrated environment on the skin surface therefore driving further drug diffusion from the base layer. Further studies in this chapter were conducted to observe whether the fate of SGMN arrays would be replicated in a full thickness skin model.

In a similar manner to the membranes investigated in Figure 6.4, it was noted from ER measurement, Figure 6.13, that the initial barrier properties of membranes appeared to vary greatly. Even though the same donor membrane was used in all treatment arms, it was apparent that the initial impedance in the SGMN and hypodermic treatment groups, Figure 6.13 (A) and (B) respectively, were lower than in the untreated group at the start of the study. This further highlighted the importance of establishing baseline membrane impedance prior to study initiation.

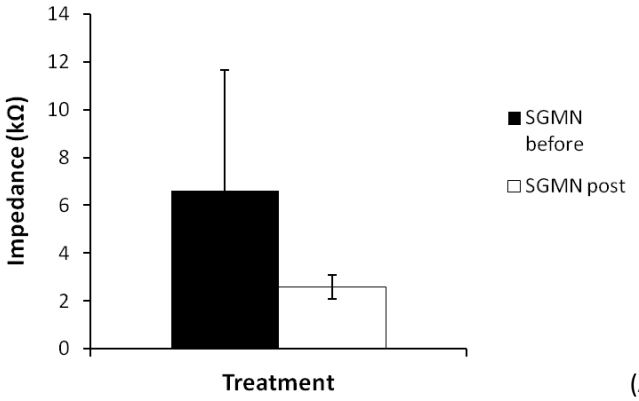

(A) (no significant difference P=0.08)

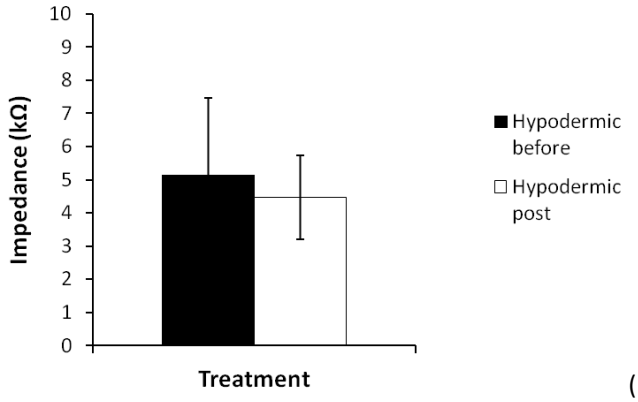

(B) (no significant difference P=0.32)

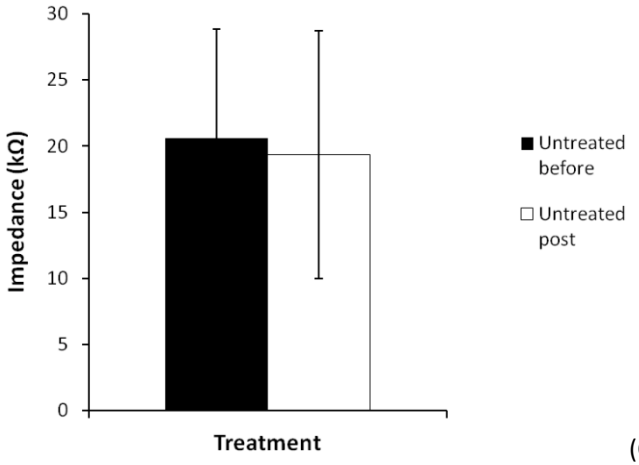

(C) (no significant difference P=0.44)

Figure 6.13 Electrical resistance measurement of epidermal membranes.

Bars denote resistance prior to treatment (black) and following (A) SGMN array treatment, (B) hypodermic needle (26 G) treatment or (C) no treatment (white). Data presented as mean ± S.D. (n=4).

Due to the unusual nature of these results, the experiment was repeated using skin tissue from different donors, Figure 6.14, combined with the standardised approach (section 5.4.6) to assessment of initial membrane barrier integrity, Figure 6.16.

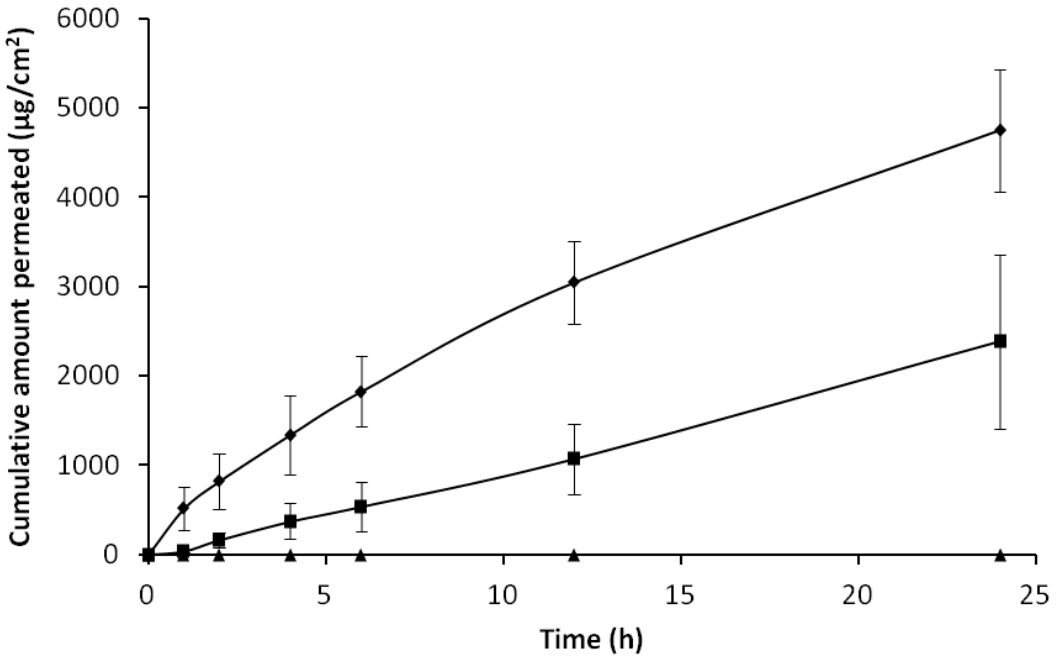

Figure 6.14 Permeation profiles of FITC-BSA from 5 $\%^{w}/_{w}$ loaded sugar formulations across human epidermal membrane.

Membranes were left untreated with application of stock sugar solution containing FITC-BSA (triangles) or treated with a single hypodermic needle (26 G) puncture and solid SG application (squares) or SGMN array application (diamonds). Data presented as mean ± S.E. (n=4).

As the data in Figure 6.14 show this experiment did not make the analysis any clearer. Immediately it appeared that the actual numerical data was not logical; the theoretical total dose of FITC-BSA contained within SGMN arrays was 1500 µg, therefore it would be impossible to deliver nearly three times this amount. The permeation profiles also appeared to be distinctly different to those shown in Figure 6.11. In this study there did not appear to be a pronounced plateau of the delivery of FITC-BSA from 12 h onwards, indicating that there was still excess drug in the donor compartment. The difference in permeation profile could be reasoned by utilisation of skin from different donors, however again the profile does not correlate with the numerical data obtained. As Figure 6.15 shows, the residual mass of formulation remaining in the donor chamber at the end of each study varied also.

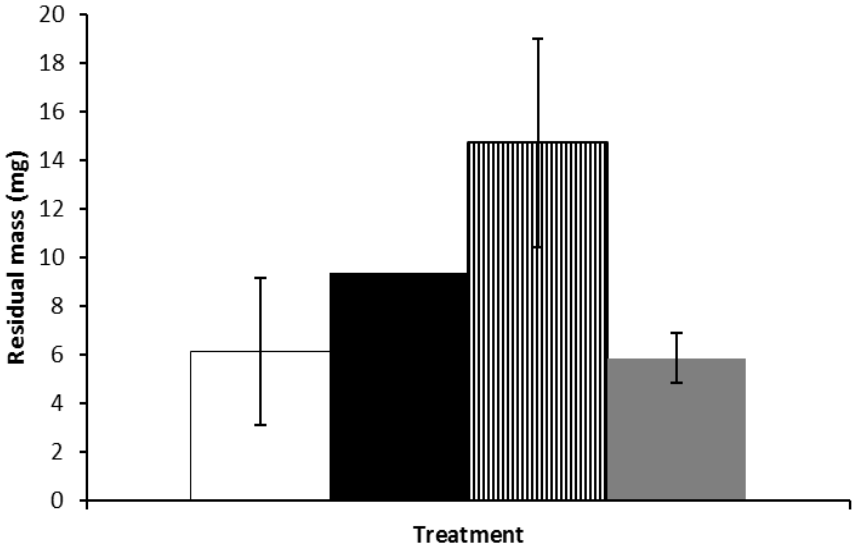

Figure 6.15 Residual mass of FITC-BSA formulation remaining in donor chamber at 24 h.

Bars indicate residues from 1st experiment; hypodermic (white bar, n=4), SGMN (black bar, n=1) and 2nd experiment; hypodermic (striped bar, n=4), SGMN (grey bar, n=2). Data presented as mean ± S.E.

As shown in Figure 6.15 there was considerable variation in the amount of residual formulation remaining in the donor chambers following 24 h. However, it was apparent that there were a greater number of residues remaining after the second experiment, and hence that it was likely that a greater proportion of FITC-BSA remained in the donor chamber. This evidence correlated with the permeation profiles observed in Figure 6.14, but further indicated that the numerical values were non-sensical.

From these observations it appeared that there must have been flaws in the experimental technique in this study. It was hypothesised that the FITC probe may have detached from the protein during the experiment and hence caused the spurious results observed. However, a positive outcome of this study was that no FITC-BSA permeated across untreated membranes, Figure 6.16. This correlated with the hypothesis that a protein would not passively diffuse across intact epidermal membrane. Electrical resistance data confirmed that the initial measurements of untreated membrane, Figure 6.16 (C), did not vary significantly from those in other treatment groups and that they remained intact throughout the study. Where membranes were treated with SGMNs or hypodermic needle, significant decreases in impedance were measured after the study, Figure 6.16 (A) and (B) respectively. This correlated with previous ER findings shown in Figure 6.7.

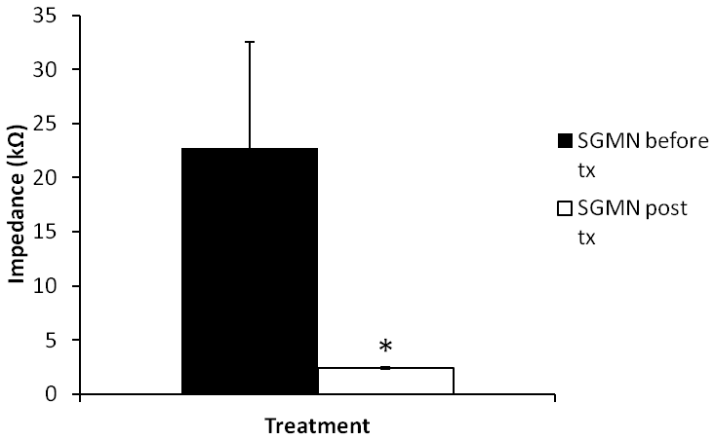

(A) (* denotes significance P=0.003)

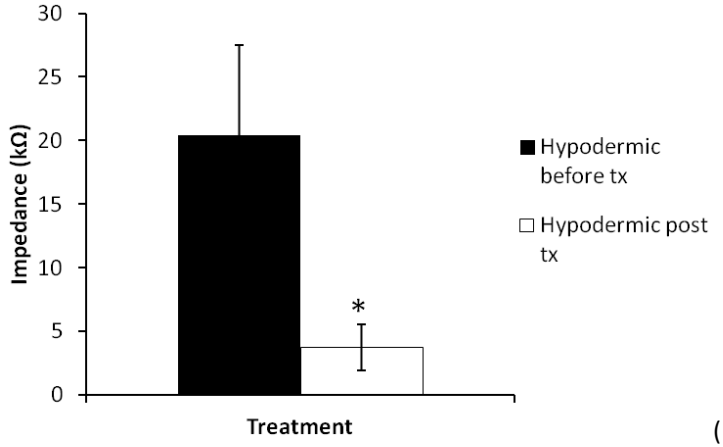

(B) (* denotes significance P=0.002)

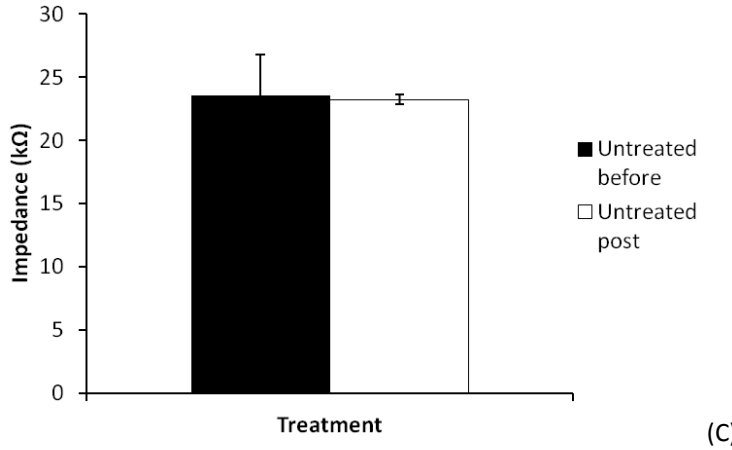

(C) (no significant difference P=0.42)

Figure 6.16 Electrical resistance measurement of epidermal membranes.

Bars denote resistance prior to treatment (black) and following (A) SGMN array treatment, (B) hypodermic needle (26 G) treatment or (C) no treatment (white). Data presented as mean ± S.D. (n=4).

To probe the spurious-looking results obtained in the FITC-BSA diffusion studies, analyses based on direct protein quantification were attempted. These studies relied upon interaction of protein and reagent and hence would not be affected by the fluorescent probe. Figure 6.18 shows the estimation of total protein in samples using the BCA assay using the standard curve

in Figure 6.17. Where the number of repeats is less than 4, the protein quantity was below the limit of quantification of the assay.

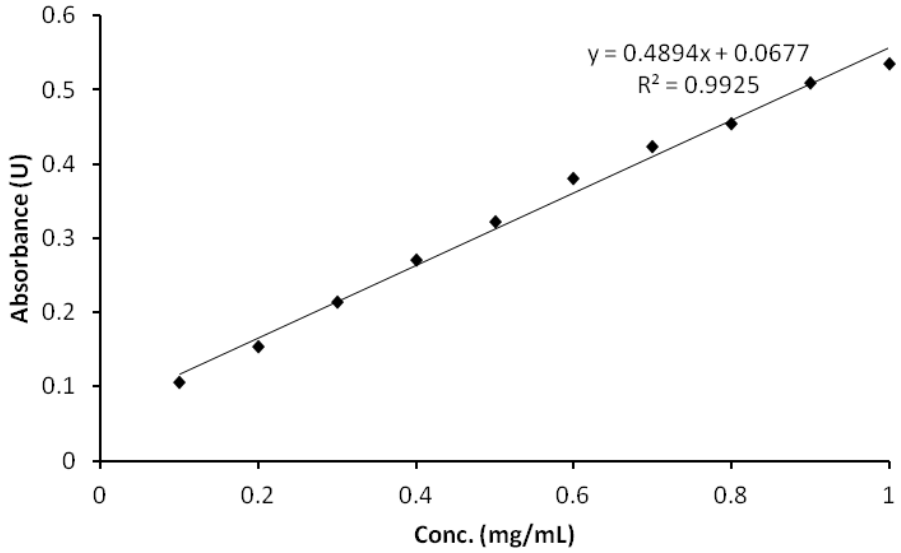

Figure 6.17 Exemplar standard curve used in quantitative determination of FITC-BSA by BCA assay. (n=1).

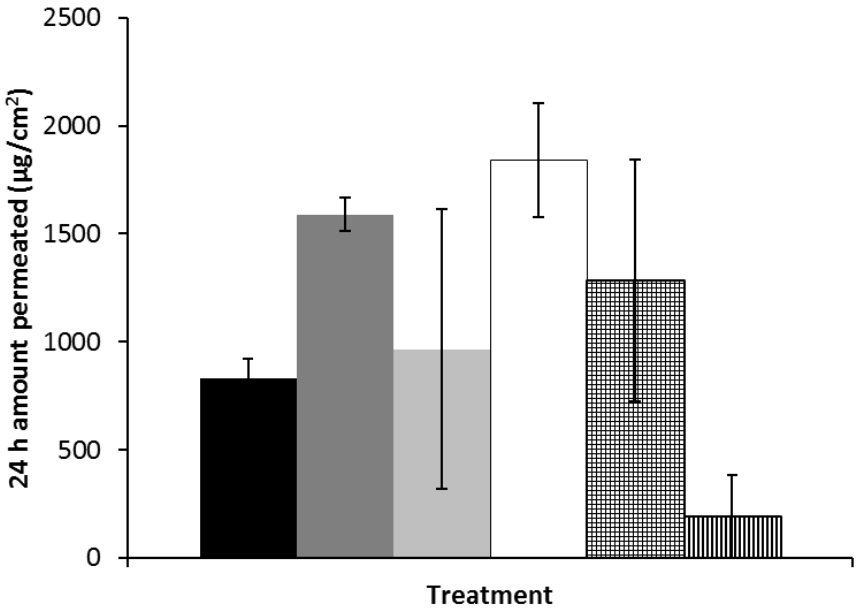

Figure 6.18 Bicinchoninic assay quantification of FITC-BSA permeated across human epidermis at 24 h.

Data from 1st experiment; hypodermic needle (26 G) treated (black bar, n=3), SGMN array treated (dark grey bar, n=3) and untreated (light grey bar, n=4). Data from 2nd experiment; SGMN array treated (white bar, n=4), hypodermic needle (26 G) treated (hatched bar, n=2) and untreated (striped bar, n=4). Data presented as mean ± S.E.

As Figure 6.18 shows, the total quantity of protein permeated in both experiments was much closer to the theoretical total amount of drug incorporated. This further indicated that the data obtained in Figure 6.14 were not logical. However, it was observed that the BCA assay was not sensitive enough to accurately quantify every treatment sample obtained. Therefore, the samples were further analysed using the Bradford assay, Figure 6.20.

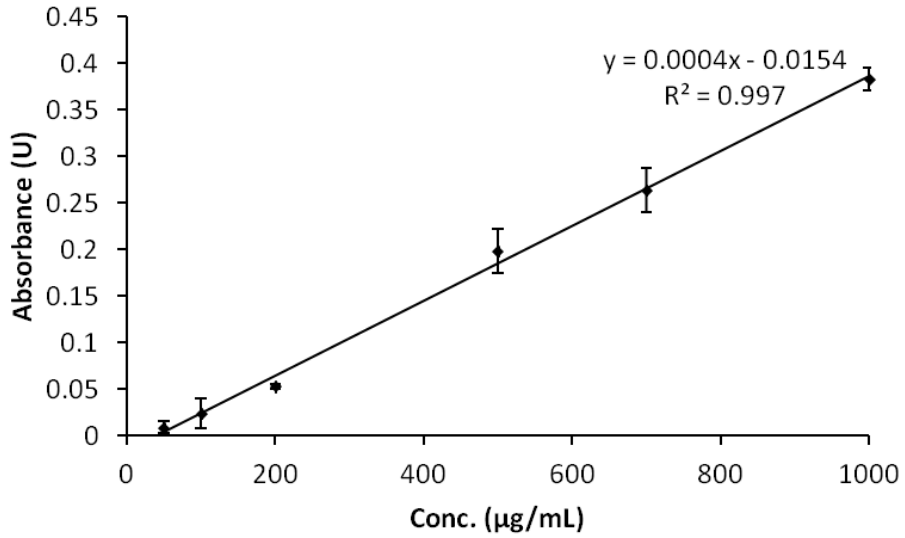

Figure 6.19 Exemplar standard curve used in quantitative determination of FITC-BSA by Bradford assay.

Data presented as mean ± S.D. (n=3).

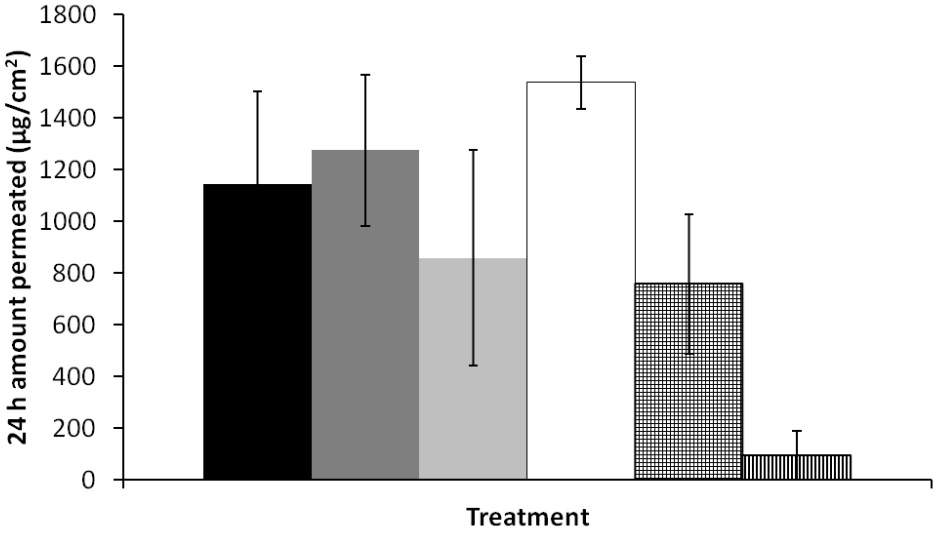

Figure 6.20 Bradford assay quantification of FITC-BSA permeated across human epidermis at 24 h.

Data from 1st experiment; hypodermic needle (26 G) treated (black bar), SGMN array treated (dark grey bar) and untreated (light grey bar). Data from 2nd experiment; SGMN array treated (white bar), hypodermic needle (26 G) treated (hatched bar) and untreated (hashed bar). Data presented as mean ± S.E. (n=4).

As shown, the Bradford assay was more sensitive than the BCA assay and all treated samples were quantifiable. Generally, it was observed that the results of the Bradford assay correlated with the BCA assay data, Figure 6.18. Importantly, both assays suggested that no more than approximately 1500 μg of protein was present within the receptor compartment at 24 h. Additionally, only a small amount of total protein was present in the untreated samples from the second experiment.

In summary, these data further suggest the utility of SGMN arrays of these dimensions to facilitate the delivery of a range of model substances, including hydrophilic macromolecular compounds, across human SC barrier.

6.4.2 Integrated transdermal sugar glass microneedle patch facilitated diffusion studies across human epidermal membrane

6.4.2.1 Acrylate adhesive backing

This section of the chapter aimed to assess the drug delivery potential of novel integrated transdermal SGMN patches fabricated in section 5.3.2.3. The basis for the design of these patches was a drug in adhesive, monolithic style (Tan and Pfister 1999) with a SGMN array attached to the adhesive layer. Previous data, section 6.4.1, demonstrated that large molecular weight hydrophilic drugs incorporated within the matrix of a SGMN array could successfully be delivered across human epidermal barrier. However, potential limitations of this device include the total amount of drug that can be loaded into the array matrix, the physical stability of the material, lack of controlled delivery and poor adhesion to skin. To attempt to overcome these issues it was conceived that SGMNs could be directly attached to adhesive backing layers containing drug.

Sulforhodamine B sodium was chosen as a model drug substance in this work due to the reasons stated in section 6.4.1.2 and due to its ease of assay. The delivery of SRB from an integrated Duro-Tak® (acrylate) adhesive SGMN patch is shown in Figure 6.21.

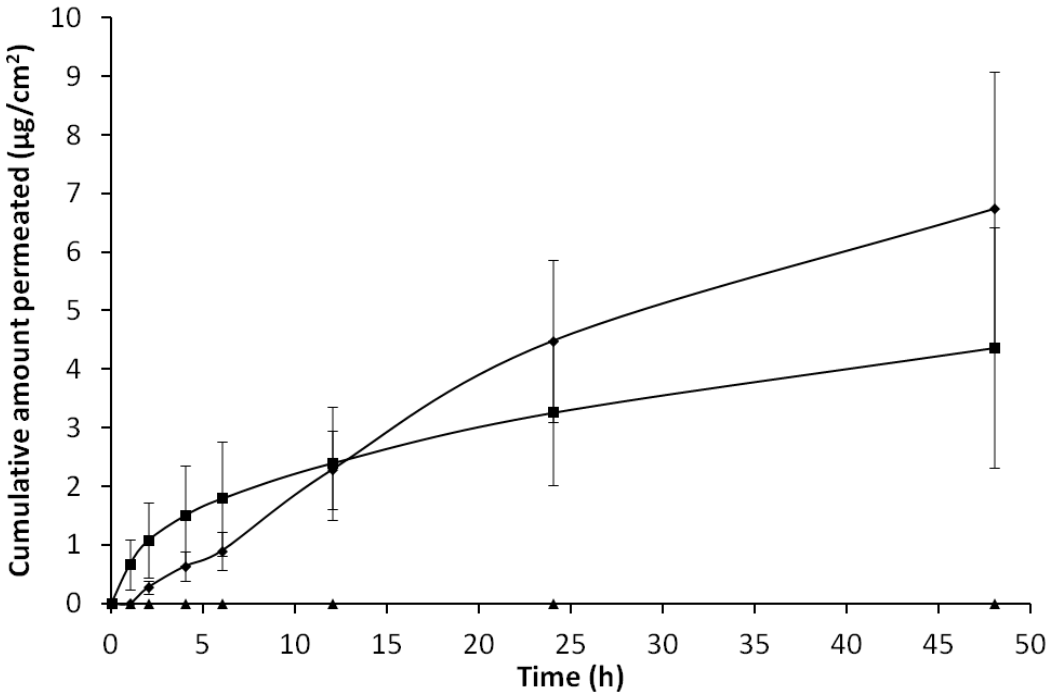

Treatment	Mean Q_{12} (µg / cm^2) ± S.E.	Percentage formulation permeated at Q_{12} (%) ± S.E.
Integrated SGMN adhesive patch	2.3 ± 0.7	0.9 ± 0.3
Hypodermic + patch	2.4 ± 1.0	1.0 ± 0.4

Figure 6.21 Permeation profiles of SRB from 5 $\%^{w}/_{w}$ loaded Duro-Tak® adhesive patches across human epidermal membrane.

Membranes were left untreated (triangles), or treated with 3 hypodermic needle (26 G) punctures (squares) or an integrated SGMN adhesive patch (diamonds). Data presented as mean ± S.E. (n=4).

As shown, the flux of SRB from an integrated SGMN adhesive patch was very different to that of the SGMN array alone, Figure 6.6. In contrast to the SRB loaded SGMN array, this patch system demonstrated a distinct lag phase, until 2 h, before a rapid increase in permeation up to 24 h. Lag times have been noted previously in passive transdermal adhesive systems (Jain and Banga 2010; Jeans and Heard 1999; Roy et al. 1996) before a steady-state flux was observed. In this sytem there was no permeant contained within the SGMNs and it was hypothesised that the lag time may have been due to the time required for needle and backing dissolution prior to wetting of the adhesive layer and SRB diffusion.

In this study, it was observed that the permeation profile obtained from an integrated SGMN adhesive patch correlated with a conventional transdermal patch that does not cause physical

disruption of the barrier (Jeans and Heard 1999). However, in this system, approximately 2 % of the total drug contained within the adhesive was delivered by 24 h, and only 3 % by 48 h. As stated, SRB appeared to be completely saturated within the adhesive matrix due to crystal presence, Figure 5.11. It has been found that if the solubility of a permeant is low in a particular vehicle this will increase its "leaving ability" via passive diffusion (Higuchi 1960). Hence, this should have provided maximal thermodynamic activity within the patch. However, it has been shown that increasing drug loading within adhesive patches above saturation does not significantly enhance flux across skin (Jain and Banga 2010; Roy et al. 1996). As the salt form of SRB was incorporated within the adhesive, the soluble drug concentration within the patch was likely to have been low. Other workers have incorporated drugs within acrylate adhesives in the free base form (Jain and Banga 2010; Jeans and Heard 1999; Roy et al. 1996) and hence this may explain the low total permeation of SRB from the integrated SGMN patch system over 48 h. Additionally, due to its size and physicochemical properties, SRB will only have diffused from the patch where it was in contact with an aqueous channel in the membrane. This hypothesis was supported by the permeation profile shown by hypodermic needle membrane treatment, Figure 6.21. In this treatment arm the drug flux up to 6 h was rapid, but began to decrease after this time point. This suggested that crystalline SRB in the patch immediately in contact with aqueous channels dissolved rapidly showing an initial burst effect, as noted in other similar adhesive systems (Guyot and Fawaz 2000; Roy et al. 1996). Following this initial burst, drug release slowed and followed a more linear profile, which could have been due to slow diffusion of SRB through the polymer (Guyot and Fawaz 2000). In contrast, the MNs and backing of the SGMN arrays, section 6.4.1, both consisted of sugar glass in which SRB was fully dissolved. Therefore, the base layer will have wetted rapidly once aqueous channels were created within the epidermis, as demonstrated in Figure 6.3 (B). This hypothesis would explain the higher flux value of SRB from SGMNs observed in 6.4.1 compared to the relatively low flux observed here, Figure 6.21.

To investigate epidermal membrane integrity, ER was measured prior to and following the study. In agreement with previous findings, section 6.4.1.3, membranes treated with a hypodermic needle or integrated transdermal SGMN patch demonstrated significant decreases in barrier impedance, $P = 0.02$ and 0.02 respectively. Membranes treated with an adhesive patch only did not show a significant change in ER throughout the study, $P=0.46$. This indicated the utility of integrated transdermal SGMN patches to effectively puncture the SC of human skin.

Upon conclusion of the study, transdermal patches were removed from the epidermal surface prior to *en face* observation, Figure 6.22. As shown, there were greater SRB residues found in the donor chambers of hypodermic and SGMN patch treated membranes, Figures 6.22 (A) and (B) respectively, compared to untreated membrane, Figure 6.22 (C). Although no discrete puncture sites were observed, this data further supported the hypothesis that SGMNs created aqueous pathways across the SC to facilitate wetting of the adhesive layer.

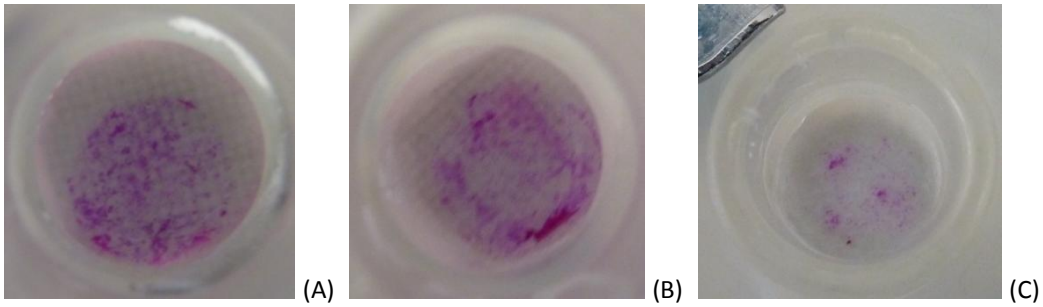

Figure 6.22 *En face* view of epidermal membranes from representative donor chambers at 48 h.

Cells were treated with (A) hypodermic (26 G) needle and patch, (B) integrated SGMN patch, (C) untreated and patch. (n=4).

6.4.2.2 Silicone adhesive backing

To investigate whether drug delivery from integrated transdermal SGMN patches could be enhanced a silicone adhesive, BIO-PSA® 7-4302, was utilised. In a manner analogous to the acrylate adhesive patch, the drug formed a solid suspension within the backing. However, the silicone is formulated to be amine-compatible and therefore it was thought that SRB may demonstrate a different release profile from the adhesive. The delivery of SRB from these adhesive patches is shown in Figure 6.23.

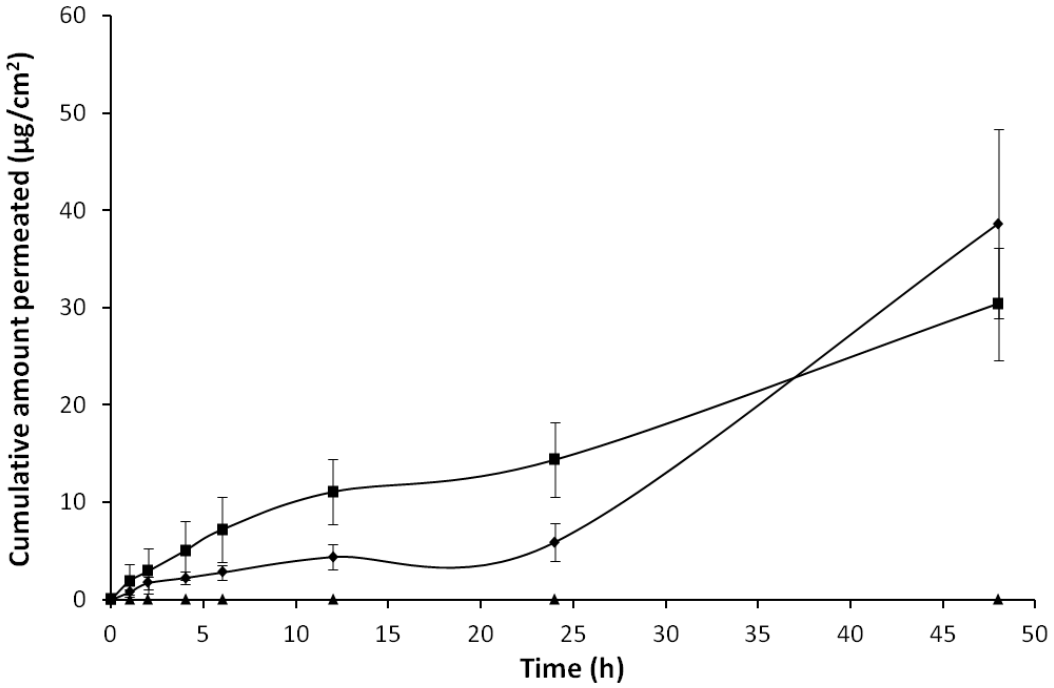

Treatment	Mean Q_{12} (µg / cm^2) ± S.E.	Percentage formulation permeated at Q_{12} (%) ± S.E.
Integrated SGMN adhesive patch	11.1 ± 3.4	4.4 ± 1.3
Hypodermic + patch	4.4 ± 1.3	1.8 ± 0.5

Figure 6.23 Permeation profiles of SRB from 5 $\%^{w}/_{w}$ loaded BIO-PSA® 7-4302 adhesive patches across human epidermal membrane.

Membranes were left untreated (triangles), or treated with 3 hypodermic needle (26 G) punctures (diamonds) or an integrated SGMN adhesive patch (squares). Data presented as mean ± S.E. (n=4).

As the data in Figure 6.23 show, permeation of SRB from silicone patches appeared to be biphasic. A sharp increase in permeation was observed at 24 h. This behaviour is unusual and suggests that the membrane may have deteriorated during the study. Additionally, by 24 h approximately 3 times the quantity of drug had permeated from the silicone adhesive patches compared to the acrylate adhesive, Figure 6.21. As the rate of drug release from an adhesive is determined by drug solubility and diffusion coefficient within the polymer (Roy et al. 1996), this data indicated that either SRB had a greater solubility limit in the silicone adhesive, or that the adhesive wetted better once the SGMNs had dissolved to allow more rapid drug release. Furthermore, it was noted that there was no lag phase shown in permeation of the drug from these SGMN patches. This suggested that the SGMNs penetrated the epidermal membrane and rapidly dissolved to allow drug diffusion from the patch backing. Logically, the SGMN array in the integrated acrylate adhesive patch will have dissolved rapidly too, therefore the

lag time observed with this patch, Figure 6.21, is likely to have been due to a lower solubility and poor diffusion of SRB within the adhesive. This suggested that the release of SRB from an acrylate backing was not optimal.

Electrical resistance measurement once again suggested that all epidermal membranes were intact prior to initiation of the study and that both hypodermic and SGMN array treatment caused significant decreases in impedance. The data in Figure 6.23 combined with ER measurement of untreated membranes suggested that there was no significant disruption of SC when patches without SGMNs were applied to the skin. Thus, there was no detectable permeation of SRB across these membranes throughout the study. This further suggested the utility of SGMNs to facilitate hydrophilic drug delivery across human skin.

6.4.2.3 Sugar glass backing

As a positive control study for the adhesive patch studies, a patch was designed with a hydrophilic backing layer composed of SG material. In this patch the drug was fully dissolved within the backing layer and no crystallisation was observed.

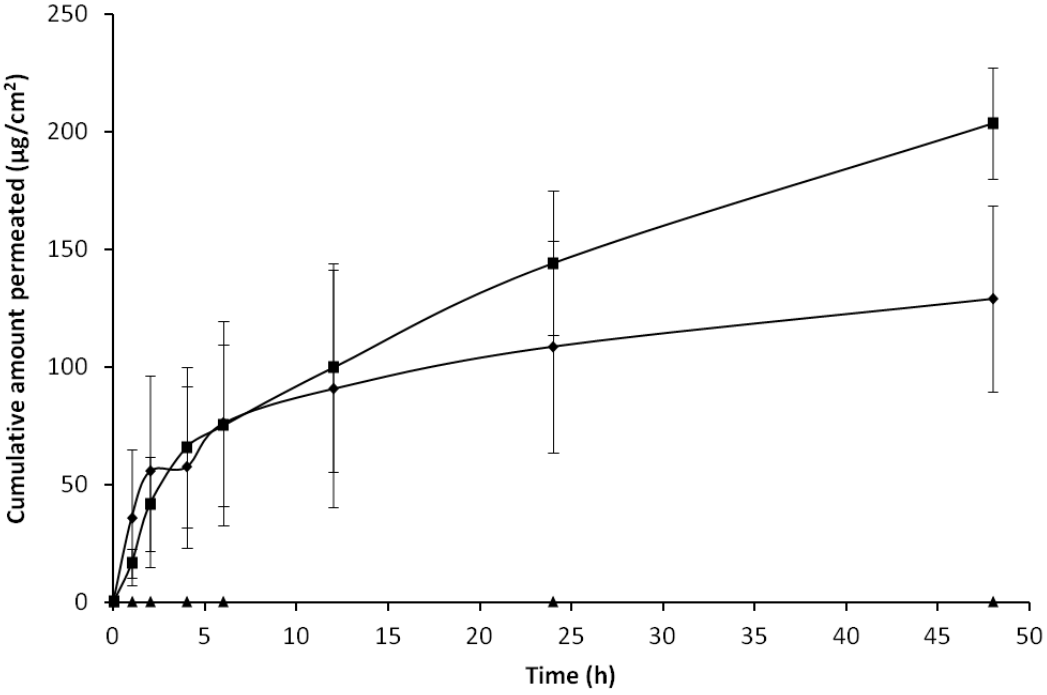

Treatment	Mean Q_{12} (µg / cm^2) ± S.E.	Percentage formulation permeated at Q_{12} (%) ± S.E.
Integrated SGMN adhesive patch	99.7 ± 44.1	39.9 ± 17.7
Hypodermic + patch	90.7 ± 50.4	36.3 ± 20.2

Figure 6.24 Permeation profiles of SRB from 5 $\%^{w}/_{w}$ loaded sugar glass patches across human epidermal membrane.

Membranes were left untreated (triangles), or treated with 3 hypodermic needle (26 G) punctures (diamonds) or an integrated SGMN adhesive patch (squares). Data presented as mean ± S.E. (n=4).

As Figure 6.24 demonstrates, when the drug was fully dissolved within a hydrophilic backing layer, permeation from the patch was much greater than from either of the more hydrophobic adhesive layers. There was no evidence of a lag phase in either of the needle treated groups in this study, and the amount of permeant delivered by 12 h was approximately 100 and 10 fold greater than with acrylate and silicone adhesive backing layers respectively. Electrical resistance measurement again suggested that hypodermic and SGMN array treatment of epidermal membranes significantly decreased impedance compared to untreated membrane. This data indicated that the SGMNs punctured the SC and dissolved rapidly to facilitate SRB permeation from the backing. This further suggested that the lag phase observed with the acrylate patch system was likely to be due to the poor solubility of SRB within the adhesive matrix. Furthermore, total permeation at 12 h was approximatley 40 %, rising to approximatley 80 **%** of the dose applied by 48 h. This was much greater than that observed

when using SGMNs with drug loaded throughout the entirety of the array, Figure 6.6. It was hypothesised that as a much smaller quantity of drug was contained within the integrated SGMN patch, this potentially provided a larger surface area to volume ratio for wetting and dissolution of the dosage formulation.

In summary, the combined data from the integrated transdermal SGMN patch diffusion studies is shown in Figure 6.25.

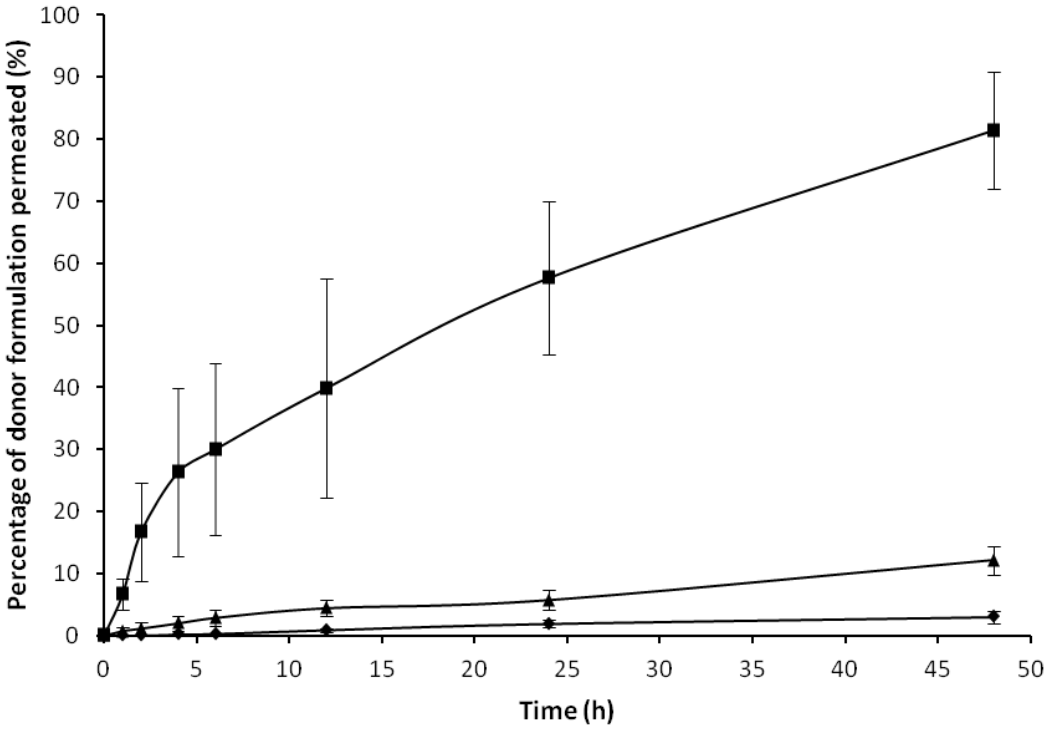

Figure 6.25 Permeation profiles of SRB from 5 $\%^{w}/_{w}$ loaded integrated SGMN patches across human epidermal membrane.

Profiles show diffusion from from BIO-PSA® 7-4302 (triangles), Duro-Tak® (diamonds) or SG (squares) backing layers. Data presented as mean ± S.E. (n=4).

As shown, the total permeation of SRB from both adhesive backing layers at 48 h was considerably less than from the SG backing layer. In clinical practice, a wafer of SG would not be the ideal backing layer as it is brittle and non-adhesive. However, the data suggested that varying the properties of the adhesive backing would alter the delivery of hydrophilic substances contained within the patch. Other workers have found that plasticisers, for example polyvinylpyrrolidone, can decrease the crystallisation tendency of drugs within adhesives and improve transdermal delivery (Jain and Banga 2010). Alternatively, more

hydrophilic adhesive layers have been utilised, for example hydroxypropylmethylcellulose (Guyot and Fawaz 2000), which may provide more stable incorporation of larger concentrations of hydrophilic drug entities. Therefore, with adhesive and drug loading optimisation, it is possible that the delivery of large molecular weight, hydrophilic drugs from integrated transdermal SGMN patches may be enhanced.

6.4.3 Full thickness skin sugar glass microneedle dissolution study

As stated in section 6.4.1.3, it was surprising that such a large quantity of the dose applied to the donor compartment permeated across the membrane during diffusion studies. It was speculated that this may be an artefact of the experimental set up and the epidermal membrane utilised. As epidermal membrane supported on filter paper was used as the model barrier membrane, and there was a large reservoir of PBS in the receptor chamber, it was hypothesised that this may be creating an unrealistically hydrated environment within the tissue. This may have accelerated the dissolution of SGMNs *in situ* and hence facilitated drug permeation from the drug reservoir.

To probe this theory further, a qualitative Franz diffusion cell study utilising full thickness human skin was designed. The aim of this study was to mimic the *in vivo* situation of human skin more closely.

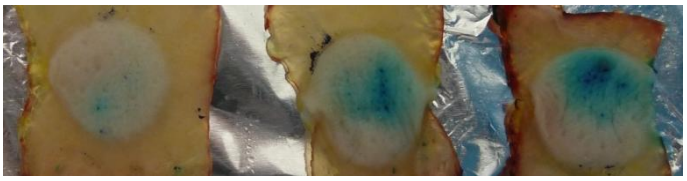

(A)

(B)

Figure 6.26 *En face* images of full thickness skin at 24 h following Franz diffusion cell study.

Skin samples were treated by (A) SGMN arrays and (B) flat SG sections, both containing 1 $\%^{w}/_{w}$ MB.

As Figure 6.26 (A) shows, all the SGMN arrays punctured the SC to permit delivery of MB dye into the epidermal layer. This was demonstrated by a square shaped delivery pattern which

correlated precisely with the area treated by the MNs. Delivery and diffusion of the dye was confirmed by subsequent transverse section of the skin tissue, Figure 6.27, where all skin sections demonstrated penetration of the SC and deposition of blue dye into the epidermis. Once again, it was apparent that these MNs did not penetrate deep into the epidermal layer and that delivery varied between samples. However, it further confirmed that SGMNs of these dimensions are robust enough to reliably disrupt the SC to provide an aqueous pathway across the barrier. It was speculated that these issues may be addressed by increasing the length of SGMNs and standardising the method and force of MN application in future work.

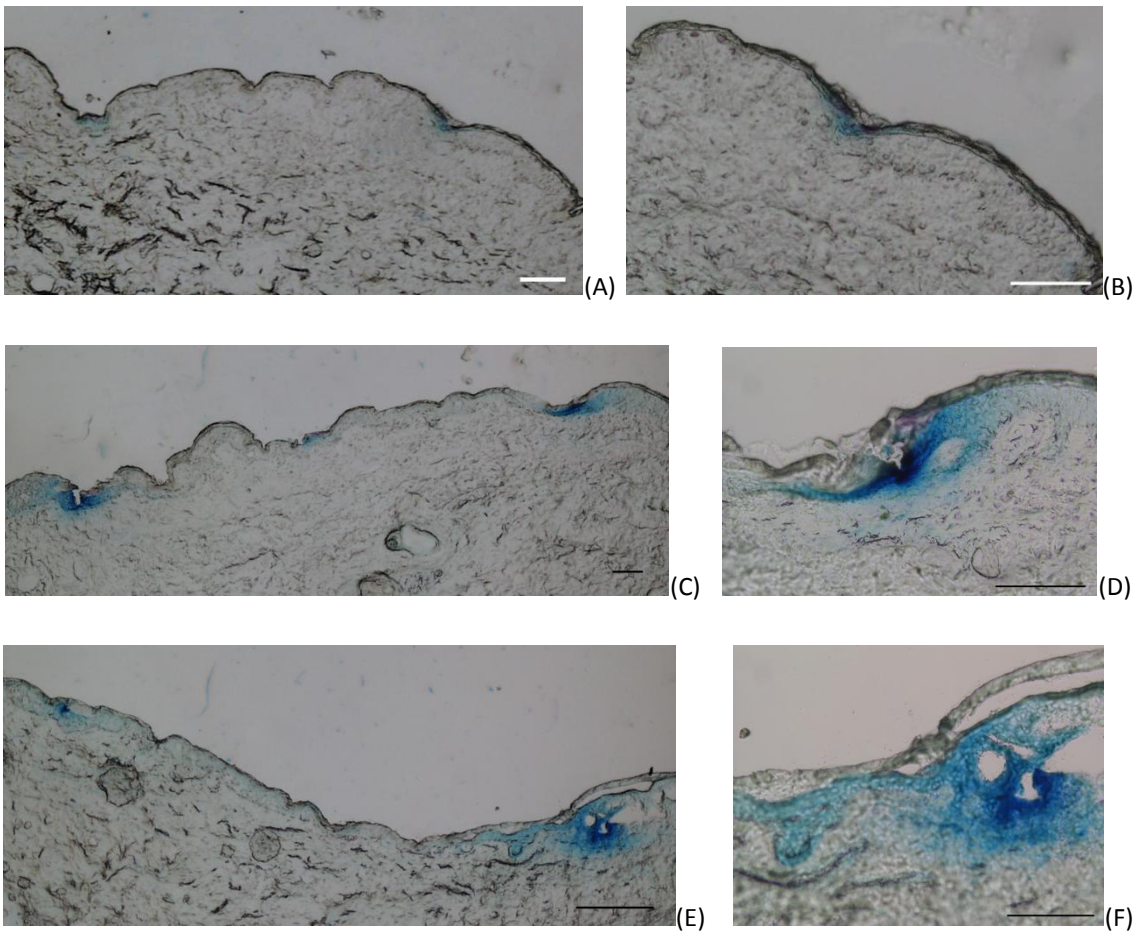

Figure 6.27 Transverse sections of skin samples shown in Figure 6.27 (A).

Sites stained blue indicate SGMN penetration of the membrane (Bar = 100 µm).

Importantly, it was noted that flat SG sections were capable of puncturing the SC when applied in this manner, Figure 6.26 (B). Two of the SG treated samples appeared to show evidence of SC penetration, although this was not present in every repeat and appeared to be a random occurrence. This result demonstrated that the rigid but brittle nature of the glassy material may potentially disrupt skin barrier properties when applied under force. However, it was

visually apparent that SGMN arrays penetrated the skin more reliably when applied in the same manner.

To explore whether the permeation efficacy observed in the FITC-BSA SGMN and SG-backed patch diffusion studies were artefactual, the mass of residues remaining in the donor chamber were recorded at the end of the study, Figure 6.28.

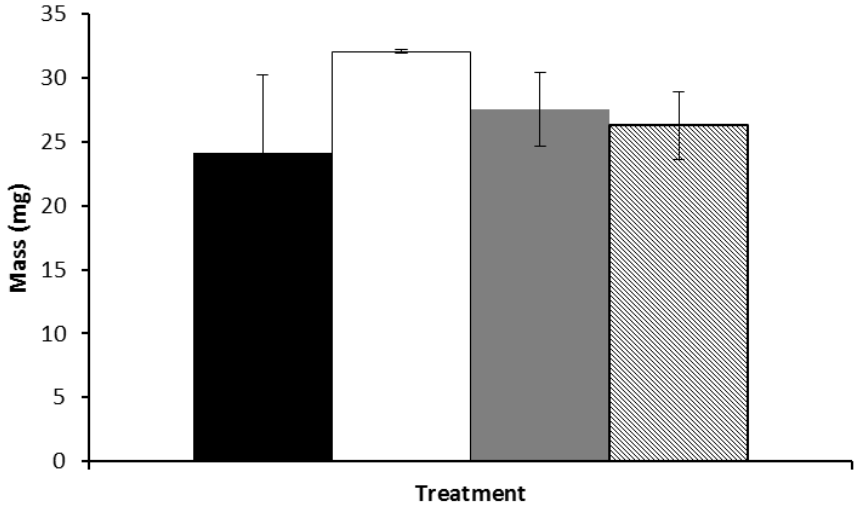

Figure 6.28 Mass of sugar formulations during full thickness skin study.

Bars represent mass of SGMN (black bar) and SG (white bar) prior to the study and at 24 h, SGMN (grey bar), SG (hashed bar). Data presented as mean ± S.D. (n=3).

As Figure 6.28 shows, there was very little change in weight of the SG formulations following the study. This indicated that when using full thickness human skin as the model barrier *in vitro*, the formulations did not wet as well in comparison to using epidermal membrane, and hence did not dissolve so rapidly. It was shown that SGMNs penetrated the barrier in this experiment, Figure 6.27, to create aqueous channels in the SC. However, it appeared that hydration of the membrane was lower in this setup due to the increased tissue depth provided by the dermis. As McAllister et al. predicted, the use of full thickness skin in diffusion studies may underestimate permeability by a factor of 5, whereas use of epidermal membrane may overestimate delivery by a factor of 2 (McAllister et al. 2003). Therefore, it is likely that the actual delivery of medicaments via SGMN arrays *in vivo* may be up to two times less than predicted in these diffusion studies, but would certainly be greater than that observed in this final study. Further *in vivo* experiments would be useful to determine the transdermal delivery potential of SGMN arrays.

6.5 Conclusion

The focus of this chapter was to quantitatively assess the transdermal drug delivery potential of biodegradable SGMN array devices. It has been demonstrated that various model molecules with differing physicochemical properties can successfully be loaded into these devices and delivered across human skin at therapeutically relevant doses. However, limitations of the modified *in vitro* Franz cell methodology developed in Chapter 5 appear likely to have caused an overestimation of the drug delivery potential of SGMNs. Due to experimental limitations it would not be appropriate to extrapolate these findings to delivery of medicaments *in vivo* as it appears that the actual permeation *in vivo* would be smaller than that observed in these diffusion studies. However, it has been shown that a range of model substances can successfully be delivered across human skin barrier using SGMN arrays. Importantly, it has been demonstrated that large molecular weight molecules, that would not normally permeate the skin passively, can be delivered across the SC barrier. This suggests that molecules such as peptides, antibodies, proteins and DNA may be delivered via the transdermal route using these devices.

In pursuit of developing a more commercially viable device, it has been shown that SGMN arrays can be successfully integrated into a transdermal patch type system to facilitate delivery of a hydrophilic molecule from the adhesive backing layer. Once more, it was shown that the molecule would not permeate the skin barrier passively from the adhesive layer unless the SC was disrupted. Slower rates of delivery from these patches were observed, but they provided the potential for controlled drug release, optimisation of drug thermodynamic activity within the patch and skin adhesion. Therefore, it is speculated that these devices may provide a realistic, patient-friendly drug delivery system. Additionally, it appears that if the drug molecule is incorporated within a hydrophilic adhesive type matrix, then delivery from the patch may be enhanced due to improved wetting of the drug layer. Hence, these studies suggest the utility of biodegradable SGMN arrays to facilitate transdermal drug delivery of a range of molecules, potentially including macromolecules, from integrated adhesive systems.

Chapter 7

General discussion

7 General discussion

Despite the many perceived benefits of MNs for transdermal drug delivery applications, the number of clinical trials conducted with these devices to date has been limited. Although MNs have demonstrated efficacy at increasing the permeation of model drug molecules across skin within the laboratory, there may be significant hurdles to translating this into clinical practice. Issues surrounding which medicines are appropriate for MN facilitated delivery, chemical stability of medicaments within devices, safety of MN materials, reliability of dosing and practical patient application of the device are all potential barriers to this form of drug delivery. These problems have often been associated with solid MN devices and it is envisaged that biodegradable MNs may provide solutions to many of these. Subsequently, this study was motivated by the opportunity to develop an optimised system for stable drug delivery utilising dissolvable biodegradable MNs.

The aim of this thesis was to evaluate the feasibility of creating biodegradable MN arrays from amorphous sugar glass material. It was envisaged that sugar glasses may be a suitable material for MN fabrication due to the many different routes to formation of a molecular glass (Surana et al. 2004) providing flexibility in formulation and micromoulding fabrication. To date, a variety of biodegradable MN permutations have been reported which have been fabricated from a number of different materials. These materials have included natural substances, for example the disaccharides maltose (Lee et al. 2011b; Miyano et al. 2005) and galactose (Donnelly et al. 2009a), the polymeric carbohydrates carboxymethylcellulose (Lee et al. 2011a; Lee et al. 2008) and amylopectin (Lee et al. 2008) and thread-forming polymers including chondroitin sulphate, dextrin and albumin (Ito et al. 2006). Alternatively, others have investigated synthetic materials for biodegradable MN fabrication, such as polyvinylpyrrolidone (Sullivan et al. 2008), poly lactic acid (Chu et al. 2010; Park et al. 2005), poly lactide-co-glycolic acid (Park et al. 2005) and polyvinyl alcohol (Chu et al. 2010). Fabrication of these MN arrays has often focused upon a micromoulding methodology coupled with a variety of techniques to load material into the moulds. Initial efforts frequently concentrated on the use of elevated temperature to aid filling of micromoulds which often resulted in inactivation of delicate molecules, such as proteins (Donnelly et al. 2009a; Park et al. 2006), incorporated within the matrix. Subsequently, this led to a scenario involving insertion of solid biodegradable MN structures followed by application of a drug formulation in a two-step process (Kolli and Banga 2008; Miyano et al. 2005; Park et al. 2005). This methodology was similar to the original “poke and apply” methodology utilised in early solid

MN studies (Donnelly et al. 2008; Henry et al. 1998; McAllister et al. 2003) and was undesirable.

To overcome these limitations there has been significant interest in fabrication of biodegradable MN structures utilising low temperature methodologies. These have included drying of viscous drug formulations under centrifugation and low temperature (Lee et al. 2011a; Lee et al. 2008) or the pressure of a metallic plate (Fukushima et al. 2011; Ito Y. et al. 2010a). Alternatively, liquid pre-polymer solutions have been formed into micromoulds and polymerised *in situ*, for example vinyl pyrrolidone (Sullivan et al. 2008) and eShell 200 monomer (Gittard et al. 2009). These efforts have facilitated the stable incorporation of a range of macromolecules within MN structures for percutaneous delivery. Macromolecular drugs now represent an increasing proportion of all new medicines on the market, although it is widely accepted that their stable delivery to the body is associated with significant challenges (Brown et al. 2006).

Accordingly, the utilisation of sugar glasses to fabricate biodegradable MNs for labile medicament incorporation and stabilisation appeared attractive. Sugar glasses are utilised in nature to protect delicate biological molecules in the dehydrated state (Potts 1994). Subsequently, it was realised that these materials may find utility in the pharmaceutical sciences to stabilise biomolecules during processing and storage (Uritani et al. 1995). To date, there have been many reports of different methodologies utilised to formulate amorphous sugar glasses. Typically, the route to amorphisation has been chosen based upon the intended application of the glass. Many of these techniques have involved the use of mechanical processes, involving elevated temperature or shear force, to vitrify the sugar (Willart et al. 2001). However, other techniques have involved utilisation of solution evaporation (Wright et al. 2002) and it was speculated that these methodologies may be suitable for SGMN fabrication and stable molecule incorporation. In Chapter 2 a number of different solutions containing individual sugars and sugar alcohols, and binary combinations of these, were examined during a low temperature dehydration process. Subsequently, it was shown that non-crystalline sugars could be produced from solutions containing a combination of the disaccharides trehalose and sucrose. This finding was vital to the future utility of sugar glasses to fabricate MN arrays utilising a micromould based filling technique. Physical characterisation of the material suggested that although these sugars appeared to be non-crystalline they had a

complex nature, which may have been due to the low temperature (non-thermal) methodology utilised to form them (Willart et al. 2002).

The critical question arising over many biodegradable MN structures is whether the material is robust enough for reliable skin insertion. In comparison to silicon or metal, biodegradable materials, by their nature, tend to have poorer structural rigidity and hence may be prone to failure upon insertion (Lee et al. 2008). Sugar glasses, in particular, are an amorphous solid generally exhibiting decreased physical stability (Zhou et al. 2007) compared to the crystalline state. Furthermore, it has been shown that maltose MNs with a length of 500 μm are more effective at penetrating human skin than those with a shorter length of 200 μm (Li et al. 2009). Therefore, it was an important aspect of this work to investigate the stability and skin penetration capabilities of SGMNs of the dimensions fabricated in this study.

Due to restrictions imposed by the geometry of silicon MN master structures, it was important to investigate and establish the skin puncture capacity of SGMNs with the same pyramidal-shaped dimensions, and small aspect ratio, early in this work. As demonstrated in Chapter 3, SGMNs formed by a novel low temperature vacuum-forming technique had suitable structural robustness to reliably insert into human skin. This was a critical finding which suggested the utility of SGMN arrays as a platform for facilitating transdermal drug delivery. In addition, it was found throughout Chapters 3 to 6 that it was possible to incorporate a range of different model substances within SGMN arrays and to deliver them across the human SC barrier. These model substances included small molecular weight entities, such as methylene blue dye and ibuprofen, a larger hydrophilic moiety, sulforhodamine B, and the macromolecules FITC-BSA and β-galactosidase. Significant increases in permeation of these model substances across human skin were noted following SGMN facilitated delivery. However, due to the short length of these MNs, it was found that they only punctured the epidermis superficially and penetrated only a short way into the viable tissue. It is speculated that SGMNs with a longer needle shaft, and an increased aspect ratio, may penetrate deeper into the aqueous skin layers which may be advantageous for needle dissolution and drug delivery *in vivo*.

As discussed previously, the physical stability of sugar glasses is a key issue regarding their utilisation as pharmaceuticals. Accordingly, it was an important aspect of this work to assess both the stability of the SGMNs themselves and also model substances incorporated within the

MN matrix. In Chapter 4 it was found that a functional protein, β-galactosidase, retained activity over a period of months following dehydration and inclusion within a glassy matrix; when stored under desiccated conditions. However, significant reductions in enzyme activity were found during the dehydration process compared to freshly prepared enzyme solutions. In this system, it appeared that once a vitrified solid had been produced, and annealed at room temperature, the protein remained stable throughout a 3 month storage period. It is now well characterised that sugar glass material becomes unstable when stored under elevated humidity (Hageman 1992) or temperature (Zhou et al. 2007) conditions due to its hygroscopic (Dittmar 1935) and meta-stable (Zhou et al. 2007) nature, which was supported in this study. Surprisingly, it was found that SGMNs appeared to be most stable when maintained within a low moisture environment at ambient temperature rather than under a completely desiccated environment however. This was not expected and suggested that an equilibrium relationship may be involved between the residual water content contained within the sugar glass material and the moisture in the environment. From a practical perspective, it was found that manipulation and utilisation of SGMNs under humid environmental conditions was problematic and led to rapid MN degradation. Once again, this may limit the use of this material for MN fabrication and utilisation in practice.

To investigate the delivery of model substances from SGMN arrays *in vitro* a modified arrangement of the well described Franz diffusion cell set up was developed. Many groups investigating MN facilitated drug delivery have utilised human skin membranes and have treated the tissue prior to loading within the diffusion cell (Coulman et al. 2009; McAllister et al. 2003). The modification proposed in Chapter 5 allowed SGMNs to be applied *in situ* within the donor chamber, which was of particular benefit due to the rapid dissolution kinetics of sugar glass. It is perceived that this set up may provide a robust platform for the assessment of biodegradable MN devices by others in future studies. However, a potential limitation of this arrangement may be that dissolution of MNs and drug delivery are overestimated when utilising epidermal membrane as a model barrier. In this instance an artificially aqueous environment may be created leading to more rapid dissolution of MNs than would occur *in vivo*. It was speculated that it may be possible to circumvent this issue through the use of dermatomed or split thickness skin in future. Furthermore, future studies should be conducted *in vivo* to assess the dissolution kinetics of SGMNs in living organisms.

A feature of the SGMN arrays developed in this work was that drug incorporated within the MN structure was released rapidly upon dissolution in a bolus dose manner. In some instances this may be advantageous, for example in osteoporosis treatment with parathyroid hormone, where it has been shown that rapid high concentrations followed by a short drug half-life are most effective at increasing bone density (Cosman et al. 2010). However, often it is desirable to deliver a drug over a prolonged period of time for maximum therapeutic benefit and increased patient compliance. In an attempt to address this issue, it was shown in Chapters 5 and 6 that a model hydrophilic drug substance could be incorporated within adhesive backing layers to control its rate of release following SGMN microporation. In this embodiment, it was speculated that the SGMNs created channels within the SC and rapidly dissolved to leave aqueous pathways for wetting of the adhesive layer. Drug suspended within the adhesive was then free to permeate across the skin as occurs in a conventional transdermal patch system. In this study it was found that only a small proportion of the total quantity of drug contained within the adhesive permeated across SGMN treated skin by 48 h. It was speculated that this was due to a combination of the physical characteristics of the adhesive and the physicochemical properties of the permeant. Both these factors can be optimised in a conventional transdermal patch system to maximise the thermodynamic potential of the substance within the adhesive matrix. Consequently, it is envisaged that future studies could lead to production of viable integrated SGMN transdermal patches for controlled release of medicaments.

7.1 Future work

The results presented throughout this thesis demonstrate the principle that sugar glasses may be a suitable material for biodegradable MN manufacture. However, due to time restraints it was not possible to conduct all the experiments desired to fully characterise the SGMN array system. One of the most important areas to investigate would be the behaviour of SGMNs applied to an *in vivo* skin model. *In vitro* studies conducted in this work have shown that SGMNs may facilitate transdermal drug delivery as a proof of principle. To fully probe this potential, the delivery of medicaments to *in vivo* models, along with the study of pharmacokinetic profiles, would be desirable to fully examine the utility of SGMNs as a transdermal drug delivery device. In this way, it would be possible to examine the therapeutic potential of SGMNs prior to clinical trials of the device.

Furthermore, it would be desirable to fabricate SGMNs with differing geometries and dimensions to probe the optimal utility of these MNs. A significant constraint of this work was the silicon MN master structures that were used for micromoulding SGMNs. It was hypothesised that SGMNs with a greater aspect ratio and length would facilitate more reliable skin penetration thereby leading to more consistent delivery of model substances. Alongside such studies, it would be important to probe the long-term stability of SGMN arrays further. A more extensive range of storage conditions could be explored over longer time periods to fully characterise optimal storage for SGMNs and maintenance of MN morphology and viability. Such studies could also be designed to probe the stability of model medicaments incorporated within the matrix of SGMN arrays.

Finally, it would be of interest to investigate the potential utility of integrated SGMN transdermal patches further. This novel design provides many exciting opportunities for controlled transdermal drug delivery of medicaments that are currently challenging to deliver across skin barrier. Investigation of parameters such as drug solubilisation and stabilisation within adhesive layers may provide improved delivery kinetics from these systems. Similarly, it would be desirable to examine the behaviour of these devices *in vivo* to fully characterise their transdermal drug delivery potential.

7.2 General conclusion

In summary, this work is significant in that it demonstrates for the first time the utility of amorphous sugar glass material to formulate biodegradable MN structures via a low temperature process. The SGMN arrays developed in this paper have shown reliable penetration of human skin for cutaneous drug delivery applications. Furthermore, SGMNs formed by this process have demonstrated potential for the incorporation of a range of model compounds. This suggests that SGMNs may be capable of facilitating the delivery of macromolecular medicaments, such as insulin and growth hormone, via the transdermal route. Furthermore, a novel integrated SGMN adhesive patch system has been presented which may enable the controlled and prolonged delivery of molecules across skin. It is envisaged that such a system may offer real opportunity for patient controlled transdermal drug delivery to treat a variety of chronic conditions in a safe and convenient manner.

Bibliography

8 Bibliography

Akomeah, F. K. et al. 2009. Short-term iontophoretic and post-iontophoretic transport of model penetrants across excised human epidermis. *International Journal of Pharmaceutics* 367(1-2), pp. 162-168.

Al-Qallaf, B. and Das, D. B. 2008. Optimization of square microneedle arrays for increasing drug permeability in skin. *Chemical Engineering Science* 63, pp. 2523-2535.

Al-Saidan, S. M. 2004. Transdermal self-permeation enhancement of ibuprofen. *Journal of Controlled Release* 100, pp. 199-209.

Allison, S. D. et al. 1999. Hydrogen bonding between sugar and protein is responsible for inhibition of dehydration-induced protein unfolding. *Archives of Biochemistry and Biophysics* 365(2), pp. 289-298.

Allison, S. D. et al. 2000. Stabilization of lipid/DNA complexes during the freezing step of the lyophilization process: The particle isolation hypothesis. *Biochimica et Biophysica Acta (BBA) - Biomembranes* 1468(1–2), pp. 127-138.

Amsden, B. G. and Goosen, M. F. A. 1995. Transdermal delivery of peptide and protein drugs: An overview. *America Institute of Chemical Engineers Journal* 41(8), pp. 1972-1997.

Anderson, R. L. and Cassidy, J. M. 1973. Variations in physical dimensions and chemical composition of human stratum corneum. *Journal of Investigative Dermatology* 61(1), pp. 30-32.

Aso, Y. et al. 2001. Feasibility of using isothermal microcalorimetry to evaluate the physical stability of amorphous nifedipine and phenobarbital. *Thermochimica Acta* 380(2), pp. 199-204.

Audet, M.-C. et al. 2001. Evaluation of contraceptive efficacy and cycle control of a transdermal contraceptive patch vs an oral contraceptive. *The Journal of the American Medical Association* 285(18), pp. 2347-2354.

Badkar, A. V. and Banga, A. K. 2002. Electrically enhanced transdermal delivery of a macromolecule. *Journal of Pharmacy and Pharmacology* 54(7), pp. 907-912.

Bal, S. M. et al. 2008. In vivo assessment of safety of microneedle arrays in human skin. *European Journal of Pharmaceutical Sciences* 35(3), pp. 193-202.

Banga, A. K. et al. 1999. Iontophoresis and electroporation: Comparisons and contrasts. *International Journal of Pharmaceutics* 179(1), pp. 1-19.

Banks, S. et al. 2011. Diclofenac enables prolonged delivery of naltrexone through microneedle-treated skin. *Pharmaceutical Research*, pp. 1-9.

Barry, B. W. 1983. *Dermatological formulation: Percutaneous absorption*. New York: Marcel Dekker, p. 480.

Barry, B. W. 2001. Novel mechanisms and devices to enable successful transdermal drug delivery. *European Journal of Pharmaceutical Sciences* 14(2), pp. 101-114.

Belton, P. S. and Gil, A. M. 1994. IR and Raman spectroscopic studies of the interaction of trehalose with hen egg white lysozyme. *Biopolymers* 34(7), pp. 957-961.

Benet, L. Z. et al. 1996. Intestinal drug metabolism and antitransport processes: A potential paradigm shift in oral drug delivery. *Journal of Controlled Release* 39(2–3), pp. 139-143.

Bhugra, C. et al. 2006. Predictions of onset of crystallization from experimental relaxation times I-Correlation of molecular mobility from temperatures above the glass transition to temperatures below the glass transition. *Pharmaceutical Research* 23(10), pp. 2277-2290.

Bieganski, R. M. et al. 1998. Stabilization of active recombinant retroviruses in an amorphous dry state with trehalose. *Biotechnology Progress* 14(4), pp. 615-620.

Birchall, J. et al. 2006. Cutaneous gene expression of plasmid DNA in excised human skin following delivery via microchannels created by radio frequency ablation. *International Journal of Pharmaceutics* 312(1-2), pp. 15-23.

Blank, I. H. 1985. *Percutaneous absorption. Mechanisms - Methodology - Drug Delivery*. New York: Marcel Dekker.

Bommannan, D. et al. 1992a. Sonophoresis. II. Examination of the mechanism(s) of ultrasound-enhanced transdermal drug delivery. *Pharmaceutical Research* 9(8), pp. 1043-1047.

Bommannan, D. et al. 1992b. Sonophoresis. I. The use of high-frequency ultrasound to enhance transdermal drug delivery. *Pharmaceutical Research* 9(4), pp. 559-564.

Bos, J. D. and Meinardi, M. M. H. M. 2000. The 500 Dalton rule for the skin penetration of chemical compounds and drugs. *Experimental Dermatology* 9(3), pp. 165-169.

Briggaman, R. A. and Wheeler, C. E. 1975. The epidermal-dermal junction. *Journal of Investigative Dermatology* 65(1), pp. 71-84.

Bronaugh, R. L. and Maibach, H. I. eds. 1999. *Percutaneous absorption: Drugs-cosmetics-mechanisms-methodology.* 3rd ed. New York: Marcel Dekker, Inc.

Bronaugh, R. L. et al. 1982. Methods for in vitro percutaneous absorption studies II. Animal models for human skin. *Toxicology and Applied Pharmacology* 62(3), pp. 481-488.

Brown, L. and Langer, R. 1988. Transdermal delivery of drugs. *Annual Review of Medicine* 39(1), pp. 221-229.

Brown, M. B. et al. 2006. Dermal and transdermal drug delivery systems: Current and future prospects. *Drug Delivery* 13(3), pp. 175-187.

Brown, M. B. et al. 2008. Transdermal Drug Delivery Systems: Skin Perturbation Devices. Vol. 437. pp. 119-139.

Buitink, J. and Leprince, O. 2004. Glass formation in plant anhydrobiotes: Survival in the dry state. *Cryobiology* 48(3), pp. 215-228.

Buitink, J. et al. 2000. High critical temperature above Tg may contribute to the stability of biological systems. *Biophysical Journal* 79(2), pp. 1119-1128.

Bundgaard, H. 1992. The utility of the prodrug approach to improve peptide absorption. *Journal of Controlled Release* 21(1–3), pp. 63-72.

Burnette, R. R. and Ongpipattanakul, B. 1988. Characterization of the pore transport properties and tissue alteration of excised human skin during iontophoresis. *Journal of Pharmaceutical Sciences* 77(2), pp. 132-137.

Cardona, S. et al. 1997. Thermal stability of invertase in reduced-moisture amorphous matrices in relation to glassy state and trehalose crystallization. *Journal of Food Science* 62(1), pp. 105-112.

Carpenter, J. F. and Crowe, J. H. 1988. Modes of stabilization of a protein by organic solutes during desiccation. *Cryobiology* 25(5), pp. 459-470.

Carpenter, J. F. and Crowe, J. H. 1989. An infrared spectroscopic study of the interactions of carbohydrates with dried proteins. *Biochemistry* 28(9), pp. 3916-3922.

Carpenter, J. F. et al. 1987a. Stabilization of phosphofructokinase with sugars during freeze-drying: Characterization of enhanced protection in the presence of divalent cations. *Biochimica et Biophysica Acta (BBA) - General Subjects* 923(1), pp. 109-115.

Carpenter, J. F. et al. 1987b. Stabilization of phosphofructokinase during air-drying with sugars and sugar/transition metal mixtures. *Cryobiology* 24(5), pp. 455-464.

Chabri, F. et al. 2004. Microfabricated silicon microneedles for nonviral cutaneous gene delivery. *British Journal of Dermatology* 150(5), pp. 869-877.

Chilcott, R. P. et al. 1996. A rapid technique to identify structurally non-viable epidermal membranes during in vitro percutaneous penetration studies. *Human and Experimental Toxicology* 15, p. 161.

Chong, S. and Fung, H. L. eds. 1989. *Transdermal drug delivery systems: pharmacokinetics, clinical efficacy, and tolerance development.* New York: Marcel Dekker, pp. 135-153.

Christophers, E. 1971. Cellular architecture of the stratum corneum. *Journal of Investigative Dermatology* 56(3), pp. 165-169.

Chu, L. Y. et al. 2010. Fabrication of dissolving polymer microneedles for controlled drug encapsulation and delivery: Bubble and pedestal microneedle designs. *Journal of Pharmaceutical Sciences* 99(10), pp. 4228-4238.

Cicerone, M. T. and Soles, C. L. 2004. Fast dynamics and stabilization of proteins: Binary glasses of trehalose and glycerol. *Biophysical Journal* 86, pp. 3836-3845.

Cinti, S. 2005. The adipose organ. *Prostaglandins, Leukotrienes and Essential Fatty Acids* 73(1), pp. 9-15.

Cordone, L. et al. 1999. Harmonic behavior of trehalose-coated carbon-monoxy-myoglobin at high temperature. *Biophysical Journal* 76(2), pp. 1043-1047.

Cormier, M. et al. 2004. Transdermal delivery of desmopressin using a coated microneedle array patch system. *Journal of Controlled Release* 97(3), pp. 503-511.

Cosman, F. et al. 2010. Effect of transdermal teriparatide administration on bone mineral density in postmenopausal women. *Journal of Clinical Endocrinology & Metabolism* 95(1), pp. 151-158.

Coulman, S. A. et al. 2009. Microneedle mediated delivery of nanoparticles into human skin. *International Journal of Pharmaceutics* 366(1-2), pp. 190-200.

Crowe, J. H. et al. 1998. The role of vitrification in anhydrobiosis. *Annual Review of Physiology* 60, pp. 73-103.

Crowe, J. H. and Clegg, J. S. 1973. *Anhydrobiosis*. Stroudsburg, PA: Dowden, Hutchinson and Ross.

Crowe, J. H. et al. 1992. Anhydrobiosis. *Annual Review of Physiology* 54, pp. 579-599.

Crowe, L. M. et al. 1985. Preservation of freeze-dried liposomes by trehalose. *Archives of Biochemistry and Biophysics* 242(1), pp. 240-247.

Curtis, J. E. et al. 2006. Inertial suppression of protein dynamics in a binary glycerol-trehalose glass. *The Journal of Physical Chemistry* 110, pp. 22953-22956.

Dale, B. A. et al. 1985. Filaggrin: A keratin filament associated protein. *Annals of the New York Academy of Sciences* 455(1), pp. 330-342.

Davies, D. J. et al. 2004. Multi-species assessment of electrical resistance as a skin integrity marker for in vitro percutaneous absorption studies. *Toxicology in Vitro* 18(3), pp. 351-358.

Davis, S. P. et al. 2004. Insertion of microneedles into skin: Measurement and prediction of insertion force and needle fracture force. *Journal of Biomechanics* 37(8), pp. 1155-1163.

Davis, S. P. et al. 2005. Hollow metal microneedles for insulin delivery to diabetic rats. *IEEE Transactions on Biomedical Engineering* 52(5), pp. 909-915.

de Jonge, J. et al. 2007. Inulin sugar glasses preserve the structural integrity and biological activity of influenza virosomes during freeze-drying and storage. *European Journal of Pharmaceutical Sciences* 32(1), pp. 33-44.

Ding, Z. et al. 2009. Microneedle arrays for the transcutaneous immunization of diphtheria and influenza in BALB/c mice. *Journal of Controlled Release* 136(1), pp. 71-78.

Dittmar, J. H. 1935. Hygroscopicity of sugars and sugar mixtures. *Industrial and Engineering Chemistry* 27(3), pp. 333-335.

Donnelly, R. F. et al. 2011. Design, optimization and characterisation of polymeric microneedle arrays prepared by a novel laser-based micromoulding technique. *Pharmaceutical Research* 28(1), pp. 41-57.

Donnelly, R. F. et al. 2008. Microneedle-mediated intradermal delivery of 5-aminolevulinic acid: Potential for enhanced topical photodynamic therapy. *Journal of Controlled Release* 129(3), pp. 154-162.

Donnelly, R. F. et al. 2009a. Processing difficulties and instability of carbohydrate microneedle arrays. *Drug Development and Industrial Pharmacy* 35(10), pp. 1242-1254.

Donnelly, R. F. et al. 2009b. Microneedle arrays allow lower microbial penetration than hypodermic needles in vitro. *Pharmaceutical Research* 26(11), pp. 2513-2522.

Duddu, S. P. and DalMonte, P. R. 1997. Effect of glass transition temperature on the stability of lyophilized formulations containing a chimeric therapeutic monoclonal antibody. *Pharmaceutical Research* 14(5), pp. 591-595.

Dugard, P. H. et al. 1984. Absorption of some glycol ethers through human skin in vitro. *Environmental Health Perspectives* 57.

Eckert, R. L. 1989. Structure, function, and differentiation of the keratinocyte. *Physiological Reviews* 69(4), pp. 1316-1346.

El Adib, M. et al. 1989. X-Ray kinetic study of glassy crystal formation in adamantane derivatives: TTT curves and crystal size effect. *Phase Transitions* 14(1-4), pp. 85-96.

Elias, P. M. 1981. Lipids and the epidermal permeability barrier. *Archives of Dermatological Research* 270(1), pp. 95-117.

Elias, P. M. 1983. Epidermal lipids, barrier function, and desquamation. *Journal of Investigative Dermatology* 80(Supplement), pp. S44-S49.

Elias, P. M. et al. 1988. Membrane structural alterations in murine stratum corneum: Relationship to the localization of polar lipids and phospholipases *Journal of Investigative Dermatology* 91(1), pp. 3-10.

Elliott, S. R. 1990. *Physics of amorphous materials*. 2nd ed. Harlow, Essex: Longman Scientific & Technical, p. 404.

Escobar-Chavez, J. J. et al. 2009. Electroporation as an efficient physical enhancer for skin drug delivery. *The Journal of Clinical Pharmacology* 49(11), pp. 1262-1283.

Fasano, W. J. et al. 2002. Rapid integrity assessment of rat and human epidermal membranes for in vitro dermal regulatory testing: Correlation of electrical resistance with tritiated water permeability. *Toxicology in Vitro* 16(6), pp. 731-740.

Fendler, J. H. and Romero, A. 1977. Liposomes as drug carriers. *Life Sciences* 20(7), pp. 1109-1120.

Flynn, G. L. et al. 1974. Mass transport phenomena and models: Theoretical concepts. *Journal of Pharmaceutical Sciences* 63(4), pp. 479-510.

Fraenkel, L. et al. 2006. Patient treatment preferences for osteoporosis. *Arthritis Care & Research* 55(5), pp. 729-735.

Franks, F. 1997. Phase changes and chemical reactions in solid aqueous solutions: Science and technology. *Pure and Applied Chemistry* 69(5), pp. 915-920.

Franks, F. 2003. Scientific and technological aspects of aqueous glasses. *Biophysical Chemistry* 105, pp. 251-261.

Fukushima, K. et al. 2011. Two-layered dissolving microneedles for percutaneous delivery of peptide/protein drugs in rats. *Pharmaceutical Research* 28(1), pp. 7-21.

Gawkrodger, D. J. 2008. *Dermatology 4th ed.* Edinburgh, London, New York, Sydney, Toronto: Churchill Livingstone Elsevier.

Gerstel, M. S. and Place, V. A. 1976. Drug delivery device.US3,964,482.

Gill, H. S. and Prausnitz, M. R. 2007. Coating formulations for microneedles. *Pharmaceutical Research* 24(7), pp. 1369-1380.

Gittard, S. D. et al. 2009. Fabrication of polymer microneedles using a two-photon polymerization and micromolding process. *Journal of Diabetes Science and Technology* 3(2), pp. 304–311.

Gray, G. M. et al. 1982. Lipid composition of the superficial stratum corneum cells of pig epidermis. *British Journal of Dermatology* 106(1), pp. 59-63.

Green, J. L. and Angell, C. A. 1989. Phase relations and vitrification in saccharide-water solutions and the trehalose anomaly. *The Journal of Physical Chemistry* 93(8), pp. 2880-2882.

Grigera, J. R. and Bolzicco, V. 2008. Molecular mobility and ageing of sugar glasses. *Food Chemistry* 106(4), pp. 1314-1317.

Guo, N. et al. 2000. Trehalose expression confers desiccation tolerance on human cells. *Nature Biotechnology* 18(2), pp. 168-171.

Guy, R. H. et al. 1987. Transdermal drug delivery and cutaneous metabolism. *Xenobiotica* 17(3), pp. 325-343.

Guyot, M. and Fawaz, F. 2000. Design and in vitro evaluation of adhesive matrix for transdermal delivery of propranolol. *International Journal of Pharmaceutics* 204(1–2), pp. 171-182.

Hadgraft, J. and Lane, M. E. 2006. Passive transdermal drug delivery systems: Recent considerations and advances. *American Journal of Drug Delivery* 4, pp. 153-160.

Hageman, M. J. 1992. *Water sorption and solid-state stability of proteins*. New York: Plenum, pp. 273-309.

Han, M. et al. 2009. Improvement in antigen-delivery using fabrication of a grooves-embedded microneedle array. *Sensors and Actuators B-Chemical* 137(1), pp. 274-280.

Hancock, B. C. et al. 1995. Molecular mobility of amorphous pharmaceutical solids below their glass transition temperatures. *Pharmaceutical Research* 12(6), pp. 799-806.

Haq, M. I. et al. 2009. Clinical administration of microneedles: Skin puncture, pain and sensation. *Biomedical Microdevices* 11(1), pp. 35-47.

Henry, S. et al. 1998. Microfabricated microneedles: A novel approach to transdermal drug delivery. *Journal of Pharmaceutical Sciences* 87(8), pp. 922-925.

Herkenne, C. et al. 2007. Ibuprofen transport into and through skin from topical formulations: in vitro–in vivo comparison. *Journal of Investigative Dermatology* 127, pp. 135-142.

Heylings, J. R. et al. 2003. A prevalidation study on the in vitro skin irritation function test (SIFT) for prediction of acute skin irritation in vivo: Results and evaluation of ECVAM Phase III. *Toxicology in Vitro* 17(2), pp. 123-138.

Higashiyama, T. 2002. Novel functions and applications of trehalose. *Pure and Applied Chemistry* 74(7), pp. 1263–1269.

Higuchi, T. 1960. Physical chemical analysis of percutaneous absorption process from creams and ointments. *Journal of The Society of Cosmetic Chemists* 11(11), pp. 85-97.

Hincha, D. K. et al. 2002. Specific effects of fructo- and gluco-oligosaccharides in the preservation of liposomes during drying. *Glycobiology* 12(2), pp. 103-110.

Hirvonen, J. et al. 1993. Transdermal penetration enhancers in rabbit pinna skin: Duration of action, skin irritation, and in vivo/in vitro comparison. *International Journal of Pharmaceutics* 99(2–3), pp. 253-261.

Iervolino, M. et al. 2000. Membrane penetration enhancement of ibuprofen using supersaturation. *International Journal of Pharmaceutics* 198(2), pp. 229-238.

Ito, Y. et al. 2007. Sustained-release self-dissolving micropiles for percutaneous absorption of insulin in mice. *Journal of Drug Targeting* 15(5), pp. 323-326.

Ito, Y. et al. 2010. Self-dissolving micropile array tips for percutaneous administration of insulin. *Journal of Materials Science : Materials in Medicine* 21(2), pp. 835-841.

Ito, Y. et al. 2006. Self-dissolving microneedles for the percutaneous absorption of EPO in mice. *Journal of Drug Targeting* 14(5), pp. 255-261.

Ito Y. et al. 2010a. Self-dissolving micropile array chip as percutaneous delivery system of protein drug. *Biological & Pharmaceutical Bulletin* 33(4), pp. 683-690.

Ito Y. et al. 2010b. Permeation enhancement of ascorbic acid by self-dissolving micropile array tip through rat skin. *Chemical & Pharmaceutical Bulletin* 58(4), pp. 458-463.

Izutsu, K. et al. 1994. Effect of mannitol crystallinity on the stabilization of enzymes during freeze-drying. *Chemical and Pharmaceutical Bulletin* 42(1), pp. 5-8.

Jain, P. and Banga, A. K. 2010. Inhibition of crystallization in drug-in-adhesive-type transdermal patches. *International Journal of Pharmaceutics* 394(1-2), pp. 68-74.

Jeans, C. W. and Heard, C. M. 1999. A therapeutic dose of primaquine can be delivered across excised human skin from simple transdermal patches. *International Journal of Pharmaceutics* 189(1), pp. 1-6.

Ji, J. et al. 2006. Microfabricated silicon microneedle array for transdermal drug delivery. *Journal of Physics: Conference Series* 34, pp. 1127-1131.

Kalluri, H. and Banga, A. 2011. Formation and closure of microchannels in skin following microporation. *Pharmaceutical Research* 28(1), pp. 82-94.

Kalluri, H. et al. 2011. Characterization of microchannels created by metal microneedles: Formation and closure. *The AAPS Journal* 13(3), pp. 473-481.

Karande, P. et al. 2005. Design principles of chemical penetration enhancers for transdermal drug delivery. *Proceedings of the National Academy of Sciences of the USA* 102(13), pp. 4688-4693.

Karande, P. et al. 2006. Relationships between skin's electrical impedance and permeability in the presence of chemical enhancers. *Journal of Controlled Release* 110(2), pp. 307-313.

Kauzmann, W. 1948. The nature of the glassy state and the behavior of liquids at low temperatures. *Chemical Reviews* 43(2), pp. 219-256.

Kermici, M. et al. 1977. Measurement of biochemical parameters in the stratum corneum. *Society of Cosmetic Chemists* 28(4), pp. 151-164.

Kim, M. et al. 2012. Hydrogel swelling as a trigger to release biodegradable polymer microneedles in skin. *Biomaterials* 33(2), pp. 668-678.

Kim, Y.-C. et al. 2011. Stability kinetics of influenza vaccine coated onto microneedles during drying and storage. *Pharmaceutical Research* 28(1), pp. 135-144.

Kleinknecht, R. A. 1994. Acquisition of blood, injury, and needle fears and phobias. *Behaviour Research and Therapy* 32(8), pp. 817-823.

Kolli, C. S. and Banga, A. K. 2008. Characterization of solid maltose microneedles and their use for transdermal delivery. *Pharmaceutical Research* 25(1), pp. 104-113.

Kost, J. 1993. Ultrasound induced delivery of peptides. *Journal of Controlled Release* 24(1–3), pp. 247-255.

Koster, K. L. and Leopold, A. C. 1988. Sugars and desiccation tolerance in seeds. *Plant Physiology* 88, pp. 829-832.

Kripke, M. et al. 1990. Evidence that cutaneous antigen-presenting cells migrate to regional lymph nodes during contact sensitization. *The Journal of Immunology* 145(9), pp. 2833-2838.

Kushner, J. I. V. et al. 2007. Dual-channel two-photon microscopy study of transdermal transport in skin treated with low-frequency ultrasound and a chemical enhancer. *Journal of Investigative Dermatology* 127(12), pp. 2832-2846.

Lackermeier, A. H. et al. 1999. In vivo ac impedance spectroscopy of human skin: Theory and problems in monitoring of passive percutaneous drug delivery. *Annals of the New York Academy of Sciences* 873(1), pp. 197-213.

Ladero, M. et al. 2006. Thermal and pH inactivation of an immobilized thermostable beta-galactosidase from Thermus sp strain T2: Comparison to the free enzyme. *Biochemical Engineering Journal* 31(1), pp. 14-24.

Lai, M. C. et al. 1999. Chemical stability of peptides in polymers. 1. Effect of water on peptide deamidation in poly(vinyl alcohol) and poly(vinyl pyrrolidone) matrixes. *Journal of Pharmaceutical Sciences* 88(10), pp. 1073-1080.

Langer, R. 1998. Drug delivery and targeting. *Nature* 392, pp. 5-10.

Laurent, P. E. et al. 2007. Evaluation of the clinical performance of a new intradermal vaccine administration technique and associated delivery system. *Vaccine* 25(52), pp. 8833-8842.

Lavon, I. and Kost, J. 2004. Ultrasound and transdermal drug delivery. *Drug Discovery Today* 9(15), pp. 670-676.

Lawrence, J. N. 1997. Electrical resistance and tritiated water permeability as indicators of barrier integrity of in vitro human skin. *Toxicology in Vitro* 11(3), pp. 241-249.

Lee, J. W. et al. 2011a. Dissolving microneedle patch for transdermal delivery of human growth hormone. *Small* 7(4), pp. 531-539.

Lee, J. W. et al. 2008. Dissolving microneedles for transdermal drug delivery. *Biomaterials* 29(13), pp. 2113-2124.

Lee, K. et al. 2011b. Dissolving microneedles for transdermal drug administration prepared by stepwise controlled drawing of maltose. *Biomaterials* 32(11), pp. 3134-3140.

Lee, T. W. and Robinson, J. R. 2000. *Controlled-release drug-delivery systems*. Baltimore: Lippincott Williams & Wilkins, pp. 903-929.

Lee, W.-R. et al. 2003. Lasers and microdermabrasion enhance and control topical delivery of vitamin C. *Journal of Investigative Dermatology* 121(5), pp. 1118-1125.

Leopold, A. C. et al. 1994. The glassy state in seeds: Analysis and function. *Seed Science Research* 4(3), pp. 267-274.

Leslie, S. B. et al. 1995. Trehalose and sucrose protect both membranes and proteins in intact bacteria during drying. *Applied and Environmental Microbiology* 61(10), pp. 3592-3597.

Levy, J. A. and Fieldsteel, A. H. 1982. Freeze-drying is an effective method for preserving infectious type C retroviruses. *Journal of Virological Methods* 5(3-4), pp. 165-171.

Li, G. et al. 2010. Microchannels created by sugar and metal microneedles: Characterization by microscopy, macromolecular flux and other techniques. *Journal of Pharmaceutical Sciences* 99(4), pp. 1931-1941.

Li, G. et al. 2008. In vitro transdermal delivery of therapeutic antibodies using maltose microneedles. *International Journal of Pharmaceutics* 368, pp. 109-115.

Li, G. et al. 2009. In vitro transdermal delivery of therapeutic antibodies using maltose microneedles. *International Journal of Pharmaceutics* 368(1-2), pp. 109-115.

Lin, W. et al. 2001. Transdermal delivery of antisense oligonucleotides with microprojection patch (Macroflux®) technology. *Pharmaceutical Research* 18(12), pp. 1789-1793.

Liu, J. et al. 2002. Dynamics of pharmaceutical amorphous solids: The study of enthalpy relaxation by isothermal microcalorimetry. *Journal of Pharmaceutical Sciences* 91(8), pp. 1853-1862.

Longbridge, D. J. et al. eds. 1998. *Effects of particle size and cylinder pressure on dermal Powderject® delivery of testosterone to conscious rabbits* Proceedings of the International Symposium of Controlled Release Bioactive Materials.

Luthra, S. A. et al. 2008. Investigation of the impact of annealing on global molecular mobility in glasses: Optimization for stabilization of amorphous pharmaceuticals. *Journal of Pharmaceutical Sciences* 97(9), pp. 3865-3882.

Lv, Y.-G. et al. 2006. Modeling of transdermal drug delivery with a microneedle array. *Journal of Micromechanics and Microengineering* 16, pp. 2492–2501.

MacLaughlin, J. et al. 1982. Spectral character of sunlight modulates photosynthesis of previtamin D3 and its photoisomers in human skin. *Science* 216(4549), pp. 1001-1003.

Margetts, L. and Sawyer, R. 2007. Transdermal drug delivery: Principles and opioid therapy. *Continuing Education in Anaesthesia, Critical Care & Pain* 7(5), pp. 171-176.

Martanto, W. et al. 2004. Transdermal delivery of insulin using microneedles in vivo. *Pharmaceutical Research* 21(6), pp. 947-952.

Martanto, W. et al. 2006. Microinfusion using hollow microneedles. *Pharmaceutical Research* 23(1), pp. 104-113.

Matriano, J. A. et al. 2002. Macroflux® microprojection array patch technology: A new and efficient approach for intracutaneous immunization. *Pharmaceutical Research* 19(1), pp. 63-70.

May, D. J. and Allen, J. S. 2002. Dynamics and fragmentation of thick-shelled microbubbles. *IEEE Transactions on Ultrasonics, Ferroelectrics, and Frequency Control* 49(10), pp. 1400-1409.

McAllister, D. V. et al. 2003. Microfabricated needles for transdermal delivery of macromolecules and nanoparticles: Fabrication methods and transport studies. *Proceedings of the National Academy of Sciences USA* 100(24), pp. 13755-13760.

Megrab, N. A. et al. 1995. Oestradiol permeation through human skin and silastic membrane: Effects of propylene glycol and supersaturation. *Journal of Controlled Release* 36(3), pp. 277-294.

Mezei, M. and Gulasekharam, V. 1980. Liposomes - a selective drug delivery system for the topical route of administration I. Lotion dosage form. *Life Sciences* 26(18), pp. 1473-1477.

Migalska, K. et al. 2011. Laser-engineered dissolving microneedle arrays for transdermal macromolecular drug delivery. *Pharmaceutical Research* 28(8), pp. 1919-1930.

Mikszta, J. A. et al. 2002. Improved genetic immunization via micromechanical disruption of skin-barrier function and targeted epidermal delivery *Nature Medicine* 8, pp. 415-419.

Mikszta, J. A. et al. 2003. Topical delivery of vaccines.US6,595,947.

Miyano, T. et al. 2005. Sugar micro needles as transdermic drug delivery system. *Biomedical Microdevices* 7(3), pp. 185-188.

Moon, S. J. and Lee, S. S. 2005. A novel fabrication method of a microneedle array using inclined deep x-ray exposure. *Journal of Micromechanics and Microengineering* 15, pp. 903-911.

Møss, J. and Bundgaard, H. 1990. Prodrugs of peptides. 7. Transdermal delivery of thyrotropin-releasing hormone (TRH) via prodrugs. *International Journal of Pharmaceutics* 66(1–3), pp. 39-45.

Murthy, S. N. 1999. Magnetophoresis: An approach to enhance transdermal drug diffusion. *Pharmazie* 54(5), pp. 377-379.

Nagahama, M. and Suga, H. 2002. Molecular alloys formed by solid-state vitrification. *Journal of Molecular Liquids* 95, pp. 261-284.

Naik, A. et al. 2000. Transdermal drug delivery: Overcoming the skin's barrier function. *Pharmaceutical Science & Technology Today* 3(9), pp. 318-326.

Nakano, M. and Patel, N. K. 1970. Release, uptake, and permeation behavior of salicylic acid in ointment bases. *Journal of Pharmaceutical Sciences* 59(7), pp. 985-988.

Ng, S.-F. et al. 2010. Validation of a static Franz diffusion cell system for in vitro permeation studies. *AAPS PharmSciTech* 11(3), pp. 1432-1441.

Nitti, V. W. et al. 2006. Transdermal delivery of drugs for urologic applications: Basic principles and applications. *Urology* 67(4), pp. 657-664.

Noel, T. R. et al. 2005. Physical aging of starch, maltodextrin, and maltose. *Journal of Agricultural and Food Chemistry* 53(22), pp. 8580-8585.

Nowakowski, C. M. and Hartel, R. W. 2002. Moisture sorption of amorphous sugar products. *Journal of Food Science* 67(4), pp. 1419-1425.

Obland, G. F. 1958. The fine structure of the interrelationship of cells in the human epidermis. *The Journal of Biophysical and Biochemical Cytology* 4(5), pp. 529-538.

Oh, S. Y. et al. 1993. Effect of current, ionic strength and temperature on the electrical properties of skin. *Journal of Controlled Release* 27(2), pp. 115-125.

Oliver, G. J. A. et al. 1988. An in vitro model for identifying skin-corrosive chemicals. I. Initial validation. *Toxicology in Vitro* 2(1), pp. 7-17.

Öst, L.-G. 1992. Blood and injection phobia: Background and cognitive, physiological, and behavioral variables. *Journal of Abnormal Psychology* 101(1), pp. 68-74.

Park, J. H. et al. 2005. Biodegradable polymer microneedles: Fabrication, mechanics and transdermal drug delivery. *Journal of Controlled Release* 104(1), pp. 51-66.

Park, J. H. et al. 2006. Polymer microneedles for controlled-release drug delivery. *Pharmaceutical Research* 23(5), pp. 1008-1019.

Park, J. H. et al. 2007. Polymer particle-based micromolding to fabricate novel microstructures. *Biomedical Microdevices* 9(2), pp. 223-234.

Patel, A. et al. 2009. Pharmaceutical salts: a formulation trick or a clinical conundrum? *The British Journal of Cardiology* 16(6), pp. 281-286.

Pathan, I. B. and Setty, C. M. 2009. Chemical penetration enhancers for transdermal drug delivery systems. *Tropical Journal of Pharmaceutical Research* 8(2), pp. 173-179.

PDR, T. 2005. *Physicians' Desk Reference*. Montvale, NJ.

Pellett, M. A. et al. 1994. Effect of supersaturation on membrane transport: 2. Piroxicam. *International Journal of Pharmaceutics* 111(1), pp. 1-6.

Pellett, M. A. et al. 1997. Supersaturated solutions evaluated with an in vitro stratum corneum tape stripping technique. *International Journal of Pharmaceutics* 151(1), pp. 91-98.

Pikal, M. J. et al. 1978. Quantitative crystallinity determinations for β-lactam antibiotics by solution calorimetry: Correlations with stability. *Journal of Pharmaceutical Sciences* 67(6), pp. 767-773.

Potts, M. 1994. Desiccation tolerance of prokaryotes. *Microbiological Reviews* 58(4), pp. 755-805.

Potts, R. O. and Francoeur, M. L. 1991. The influence of stratum corneum morphology on water permeability. *Journal of Investigative Dermatology* 96(4), pp. 495-499.

Potts, R. O. and Guy, R. H. 1992. Predicting skin permeability. *Pharmaceutical Research* 9(5), pp. 663-669.

Prausnitz, M. R. 2001. Analysis: Overcoming skin's barrier: The search for effective and user-friendly drug delivery. *Diabetes Technology & Therapeutics* 3(2), pp. 233-236.

Prausnitz, M. R. 2004. Microneedles for transdermal drug delivery. *Advanced Drug Delivery Reviews* 56(5), pp. 581-587.

Prausnitz, M. R. et al. 1993. Electroporation of mammalian skin: A mechanism to enhance transdermal drug delivery. *Proceedings of the National Academy of Sciences USA* 90(22), pp. 10504-10508.

Prestrelski, S. J. et al. 1993. Dehydration-induced conformational transitions in proteins and their inhibition by stabilizers. *Biophysical Journal* 65(2), pp. 661-671.

Roe, R.-J. 1968. Surface tension of polymer liquids. *The Journal of Physical Chemistry* 72(6), pp. 2013-2017.

Roos, Y. and Karel, M. 1991a. Phase transitions of mixtures of amorphous polysaccharides and sugars. *Biotechnology Progress* 7(1), pp. 49-53.

Roos, Y. and Karel, M. 1991b. Plasticizing effect of water on thermal behavior and crystallization of amorphous food models. *Journal of Food Science* 56(1), pp. 38-43.

Roy, S. D. et al. 1996. Controlled transdermal delivery of fentanyl: Characterizations of pressure-sensitive adhesives for matrix patch design. *Journal of Pharmaceutical Sciences* 85(5), pp. 491-495.

Sampedro, J. and Uribe, S. 2004. Trehalose-enzyme interactions result in structure stabilization and activity inhibition. The role of viscosity. *Molecular and Cellular Biochemistry* 256-257(1), pp. 319-327.

Sasaki, H. et al. 1990. Transdermal delivery of 5-fluorouracil and its alkylcarbamoyl derivatives. *International Journal of Pharmaceutics* 60(1), pp. 1-9.

Schebor, C. et al. 1996. Glassy state in relation to the thermal inactivation of the enzyme invertase in amorphous dried matrices of trehalose, maltodextrin and PVP. *Journal of Food Engineering* 30(3-4), pp. 269-282.

Schebor, C. et al. 1997. Glassy state and thermal inactivation of invertase and lactase in dried amorphous matrices. *Biotechnology Progress* 13(6), pp. 857-863.

Scheuplein, R. J. 1976. Percutaneous absorption after twenty-five years: Or "old wine in new wineskins". *Journal of Investigative Dermatology* 67(1), pp. 31-38.

Scheuplein, R. J. and Blank, I. H. 1971. Permeability of the skin. *Physiological Reviews* 51(4), pp. 702-747.

Schreier, H. and Bouwstra, J. 1994. Liposomes and niosomes as topical drug carriers: Dermal and transdermal drug delivery. *Journal of Controlled Release* 30(1), pp. 1-15.

Schulz, M. et al. 2010. Drug release and adhesive properties of crospovidone-containing matrix patches based on polyisobutene and acrylic adhesives. *European Journal of Pharmaceutical Sciences* 41(5), pp. 675-684.

Scott, R. C. et al. 1991. The influence of skin structure on permeability: An intersite and interspecies comparison with hydrophilic penetrants. *Journal of Investigative Dermatology* 96(6), pp. 921-925.

Seo, J.-A. et al. 2006. The glass transition temperatures of sugar mixtures. *Carbohydrate Research* 341, pp. 2516-2520.

Shalaev, E. Y. and Zografi, G. eds. 2002. *The concept of "structure" in amorphous solids from the perspective of the pharmaceutical sciences.* Cambridge, UK: The Royal Society of Chemistry, pp. 11-30.

Shamblin, S. L. et al. 2006. Coupling between chemical reactivity and structural relaxation in pharmaceutical glasses. *Pharmaceutical Research* 23(10), pp. 2254-2268.

Shamblin, S. L. et al. 2000. Interpretation of relaxation time constants for amorphous pharmaceutical systems. *Journal of Pharmaceutical Sciences* 89(3), pp. 417-427.

Shaw, J. E. et al. 1976. Percutaneous absorption: Controlled drug delivery for topical or systemic delivery *Journal of Investigative Dermatology* 67, pp. 677-678.

Sintov, A. C. and Botner, S. 2006. Transdermal drug delivery using microemulsion and aqueous systems: Influence of skin storage conditions on the in vitro permeability of diclofenac from aqueous vehicle systems. *International Journal of Pharmaceutics* 311(1–2), pp. 55-62.

Sintov, A. C. et al. 2003. Radiofrequency-driven skin microchanneling as a new way for electrically assisted transdermal delivery of hydrophilic drugs. *Journal of Controlled Release* 89(2), pp. 311-320.

Slade, L. and Levine, H. 1988. Non-equilibrium behavior of small carbohydrate water systems. *Pure and Applied Chemistry* 60(12), pp. 1841-1864.

Stoeber, B. and Liepmann, D. eds. 2000. *Fluid injection through out-of-plane microneedles*. Microtechnologies in Medicine and Biology, 1st Annual International Conference On.

Stott, P. W. et al. 1998. Transdermal delivery from eutectic systems: Enhanced permeation of a model drug, ibuprofen. *Journal of Controlled Release* 50(1-3), pp. 297-308.

Streefland, L. et al. 1998. Bond cleavage reactions in solid aqueous carbohydrate solutions. *Pharmaceutical Research* 15(6), pp. 843-849.

Struik, L. C. E. ed. 1978. *Physical aging in amorphous polymers and other materials.* Amsterdam, New York: Elsevier Scientific Pub. Co., p. 229.

Sullivan, S. P. et al. 2010. Dissolving polymer microneedle patches for influenza vaccination. *Nature Medicine* 16, pp. 915–920.

Sullivan, S. P. et al. 2008. Minimally invasive protein delivery with rapidly dissolving polymer microneedles. *Advanced Materials* 20(5), pp. 933-938.

Surana, R. et al. 2004. Effect of preparation method on physical properties of amorphous trehalose. *Pharmaceutical Research* 21(7), pp. 1167-1176.

Tachibana, K. and Tachibana, S. 1991. Transdermal delivery of insulin by ultrasonic vibration. *Journal of Pharmacy and Pharmacology* 43(4), pp. 270-271.

Takano, N. et al. 2009. Insertion testing of polyethylene glycol microneedle array into cultured human skin with biaxial tension. *Journal of Solid Mechanics and Materials Engineering* 3(3), pp. 604-612.

Tan, H. S. and Pfister, W. R. 1999. Pressure-sensitive adhesives for transdermal drug delivery systems. *Pharmaceutical Science & Technology Today* 2(2), pp. 60-69.

Touitou, E. et al. 1994. Modulation of caffeine skin delivery by carrier design: Liposomes versus permeation enhancers. *International Journal of Pharmaceutics* 103(2), pp. 131-136.

Uritani, M. et al. 1995. Protective effect of disaccharides on restriction endonucleases during drying under vacuum. *Journal of Biochemistry* 117(4), pp. 774-779.

Van Damme, P. et al. 2009. Safety and efficacy of a novel microneedle device for dose sparing intradermal influenza vaccination in healthy adults. *Vaccine* 27(3), pp. 454-459.

van den Berg, C. et al. 1995. Molecular mobilities around the glass transition in sugar water systems. In: Belton, P.S. et al. eds. *Magnetic Resonance in Food Science*. Cambridge, UK: The Royal Society of Chemistry, pp. 93-101.

Van Duzee, B. F. 1978. The Influence of Water Content, Chemical Treatment and Temperature on the Rheological Properties of Stratum Corneum. *Journal of Investigative Dermatology* 71(2), pp. 140-144.

Verbaan, F. J. et al. 2008. Improved piercing of microneedle arrays in dermatomed human skin by an impact insertion method. *Journal of Controlled Release* 128(1), pp. 80-88.

Verbaan, F. J. et al. 2007. Assembled microneedle arrays enhance the transport of compounds varying over a large range of molecular weight across human dermatomed skin. *Journal of Controlled Release* 117(2), pp. 238-245.

Wang, P. M. et al. 2006. Precise microinjection into skin using hollow microneedles. *Journal of Investigative Dermatology* 126(5), pp. 1080-1087.

Wang, Y. et al. 1993. Iontophoresis of hydrocortisone across hairless mouse skin: Investigation of skin alteration. *Journal of Pharmaceutical Sciences* 82(11), pp. 1140-1144.

Weaver, J. C. et al. 1999. Theory of electrical creation of aqueous pathways across skin transport barriers. *Advanced Drug Delivery Reviews* 35, pp. 21-39.

Weinstein, J. et al. 1979. Liposomes and local hyperthermia: Selective delivery of methotrexate to heated tumors. *Science* 204(4389), pp. 188-191.

Wendorf, J. et al. 2011. Transdermal delivery of macromolecules using solid-state biodegradable microstructures. *Pharmaceutical Research* 28(1), pp. 22-30.

Wester, R. C. and Maibach, H. I. 1983. *In vivo percutaneous absorption*. New York: Hemisphere.

Wickett, R. R. and Visscher, M. O. 2006. Structure and function of the epidermal barrier. *American Journal of Infection Control* 34(10, Supplement 1), pp. S98-S110.

Widera, G. et al. 2006. Effect of delivery parameters on immunization to ovalbumin following intracutaneous administration by a coated microneedle array patch system. *Vaccine* 24(10), pp. 1653-1664.

Wilke, N. et al. 2005. Process optimization and characterization of silicon microneedles fabricated by wet etch technology. *Microelectronics Journal* 36(7), pp. 650-656.

Wilkes, G. L. et al. 1973. The biomechanical properties of skin. *CRC Critical Reviews in Bioengineering* 1(4), pp. 453-495.

Willart, J. F. et al. 2002. Vitrification and polymorphism of trehalose induced by dehydration of trehalose dihydrate. *Journal of Physical Chemistry B* 106(13), pp. 3365-3370.

Willart, J. F. et al. 2001. Direct crystal to glass transformation of trehalose induced by ball milling. *Solid State Communications* 119(8-9), pp. 501-505.

Willart, J. F. and Descamps, M. 2008. Solid state amorphization of pharmaceuticals. *Molecular Pharmaceutics* 5(6), pp. 905-920.

Willart, J. F. et al. 2006. Formation of lactose-mannitol molecular alloys by solid state vitrification. *Solid State Communications* 138(4), pp. 194-199.

Williams, A. C. 2003. *Transdermal and topical drug delivery*. London and Grayslake: Pharmaceutical Press.

Williams, I. R. and Kupper, T. S. 1996. Immunity at the surface: Homeostatic mechanisms of the skin immune system. *Life Sciences* 58(18), pp. 1485-1507.

Wright, W. W. et al. 2002. Mixed trehalose/sucrose glasses used for protein incorporation as studied by infrared and optical spectroscopy. *Analytical Biochemistry* 307(1), pp. 167-172.

Wright, W. W. et al. 2003. Protein in sugar films and in glycerol/water as examined by infrared spectroscopy and by the fluorescence and phosphorescence of tryptophan. *Biophysical Journal* 85(3), pp. 1980-1995.

Wu, Y. et al. 2008. Microneedle-based drug delivery: Studies on delivery parameters and biocompatibility. *Biomedical Microdevices* 10(5), pp. 601-610.

Xueqiu, Y. et al. eds. 2010. *Rapidly dissolving silk protein microneedles for transdermal drug delivery*. Nano/Molecular Medicine and Engineering (NANOMED), 2010 IEEE 4th International Conference on.

Yan Jin, C. et al. 2009. Mass producible and biocompatible microneedle patch and functional verification of its usefulness for transdermal drug delivery *Biomedical Microdevices* 11(6), pp. 1195-1203.

Yoshioka, S. et al. 2003. Inactivation and aggregation of β-galactosidase in lyophilized formulation described by Kohlrausch-Williams-Watts stretched exponential function. *Pharmaceutical Research* 20(10), pp. 1655-1660.

Zhang, L. et al. 2002. Enhanced delivery of naked DNA to the skin by non-invasive in vivo electroporation. *Biochimica et Biophysica Acta (BBA) - General Subjects* 1572(1), pp. 1-9.

Zhao, K. and Singh, J. 1999. In vitro percutaneous absorption enhancement of propranolol hydrochloride through porcine epidermis by terpenes/ethanol. *Journal of Controlled Release* 62(3), pp. 359-366.

Zhou, D. et al. 2007. A calorimetric investigation of thermodynamic and molecular mobility contributions to the physical stability of two pharmaceutical glasses. *Journal of Pharmaceutical Sciences* 96(1), pp. 71-83.

Zhu, Q. Y. et al. 2009. Immunization by vaccine-coated microneedle arrays protects against lethal influenza virus challenge. *Proceedings of the National Academy of Sciences of the USA* 106(19), pp. 7968-7973.

Appendix

9 Appendix

9.1 Appendix 1

To qualitatively confirm the presence of protein within the samples obtained in the FITC-BSA diffusion study, a polyacrylamide gel was run to examine the samples (Figure 1).

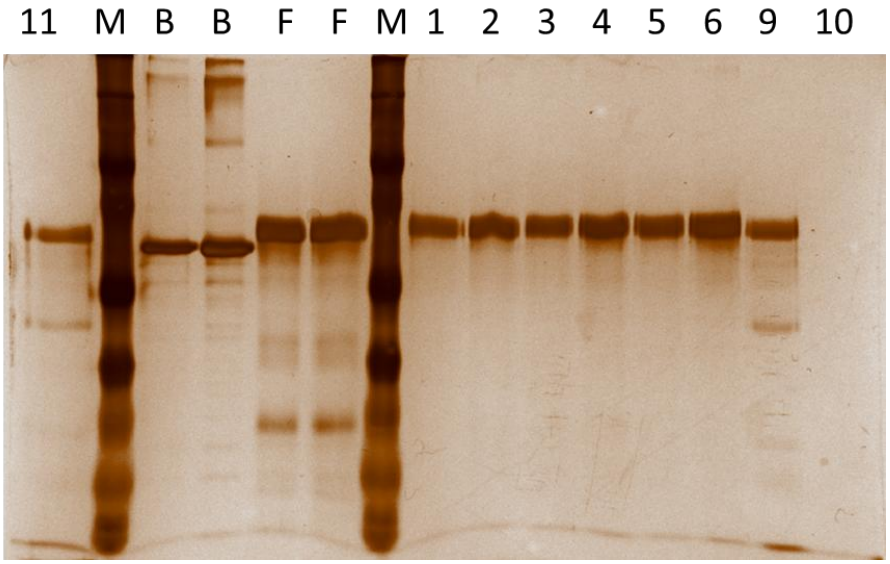

Figure 1 **Polyacrylamide gel of samples obtained from FITC-BSA diffusion study.** Lanes marked as follows, M = marker, B = BSA control, F = FITC-BSA control, 1-3 = hypodermic treated membranes, 4-6 = SGMN treated membranes, 9 & 11 = untreated membrane controls where fluorescence observed in receptor and 10 = untreated membrane controls where fluorescence not observed in receptor (n=2).

As Figure 1 shows, all samples investigated, except sample 10, showed the presence of FITC-BSA in the receptor solution. It had been noted during the diffusion study that the receptor solution at 24 h in cells 10 and 12 remained visually transparent and hence cell 10 was chosen as a representative sample. The gel confirmed that protein did permeate the untreated membranes in cells 9 and 11 and therefore further suggested that the barrier integrity of these membranes was compromised prior to the study.

9.2 Appendix 2

Journal of Controlled Release 158 (2012) 93–101

Contents lists available at SciVerse ScienceDirect

Journal of Controlled Release

journal homepage: www.elsevier.com/locate/jconrel

Low temperature fabrication of biodegradable sugar glass microneedles for transdermal drug delivery applications

C.J. Martin [a], C.J. Allender [a], K.R. Brain [a], A. Morrissey [b], J.C. Birchall [a,*]

[a] Welsh School of Pharmacy, Cardiff University, Cardiff, CF10 3NB, UK
[b] Biomedical Microsystems Team, Tyndall National Institute, Cork, Ireland

article info

Article history:
Received 6 July 2011
Accepted 21 October 2011
Available online 29 October 2011

Keywords:
Microneedle
Sugar glass
Biodegradable
Transdermal
Vacuum

abstract

Transdermal drug delivery is limited by the barrier properties of the outer skin layer. Microneedles (MNs) effectively circumvent the skin barrier to offer this route as a potential alternative to oral and parenteral delivery of therapeutics. Biodegradable microneedles offer particular advantages however processing commonly requires elevated temperatures that may adversely affect heat-labile molecules and macromolecules. In this study, solid amorphous sugar glasses containing low residual quantities of water were created by dehydration of trehalose and sucrose sugar combination solutions. Biodegradable sugar glass MNs were fabricated following optimisation of a simple and novel low temperature vacuum deposition micromoulding methodology. These had absolute morphological fidelity to silicon master structures and demonstrated sufficient structural rigidity to efficiently penetrate excised human breast skin. Sugar glass MNs incorporating a marker compound dissolved rapidly and completely in situ releasing dye into deeper skin layers. The biological activity of a model macromolecule was partially retained over extended storage following incorporation into sugar glass. This is the first demonstration that MNs created from amorphous sugar glasses can be used for incorporating and delivering molecules, and potentially biologically active macromolecules, via the transdermal route.

1. Introduction

Microneedles (MNs) offer an innovative approach to transdermal drug delivery. MNs transiently puncture the outermost skin barrier layer, the stratum corneum (SC), facilitating efficient delivery of therapeutics and vaccines in a manner similar to injections whilst retaining the convenience of the transdermal patch [1,2]. MNs have been shown to increase skin permeability by orders of magnitude for compounds ranging from low molecular weight molecules [3] to proteins [4,5], nanoparticles [6] nucleic acids [7,8] and vaccines [9,10].

MNs prepared from silicon [4,11], metal [12,13] and glass [14,15] are typically used to facilitate drug delivery through depositing a dried surface-coating of active into the skin or enabling injection of a liquid formulation through multiple hollow channels. As an alternative polymer MNs can be manufactured from biocompatible materials using moulding processes that lend themselves to inexpensive and robust mass production [6]. Importantly, polymer MNs can be designed to degrade within biological tissues to release an incorporated medicament cargo. To date biodegradable MNs have been fashioned from a range of synthetic and natural materials including poly-lactide-co-glycolide [16], polyvinylpyrrolidone [2], carboxymethylcellulose [17], amylopectin [17], dextrin [18], galactose [19] and maltose [13], [20]. A number of model compounds of various size, for example, sodium salicylate, calcein, [20] sulforhodamine, bovine serum albumin and β-galactosidase enzyme [2] have been successfully incorporated into biodegradable MNs.

Whilst biodegradable MNs have been shown to facilitate permeation of a drug formulation [21], loading of drug into the MN itself can be problematic due to the high processing temperatures usually required to produce MNs. For example, Park et al. observed extensive denaturation of bovine serum albumin (BSA) incorporated within poly-lactide-co-glycolide MNs [16] and BSA and 5-aminolevulinic acid were degraded upon incorporation into galactose MNs [19]. The production of sugar MNs utilising a simple process that does not require high processing temperatures would allow the incorporation of heat-labile medicaments including biologically active macromolecules such as proteins and peptides, molecules that represent an increasingly significant proportion of new medicinal products [22]. Whilst oral delivery would be desirable the bioavailability of proteins and peptides via this route is often restrictive [1,23] and they are commonly administered by hypodermic injection, a procedure that, whilst effective, causes pain, apprehension [24,25] and inconvenience and requires medical training and expertise [26]. This can be particularly problematic when the treatment needs to be regularly administered over prolonged periods.

* Corresponding author at: Welsh School of Pharmacy, Redwood Building, King Edward VII Avenue, Cardiff, CF10 3NB, UK. Tel.: + 44 29 20875815; fax: + 44 29 29874149.
E-mail address: birchalljc@cf.ac.uk (J.C. Birchall).

0168-3659/$ – see front matter © 2011 Elsevier B.V. All rights reserved.
doi:10.1016/j.jconrel.2011.10.024

Carbohydrates play an essential role in the stabilisation of biological components under water stress [27]. In nature, anhydrobiotic organisms are able to survive extreme dehydration due to their ability to accumulate high levels of disaccharides, such as sucrose or trehalose. These sugars protect and preserve sensitive biological structures via a synergistic mechanism involving direct interactions with biomolecules and formation of sugar glasses [28]. Sugar glasses are formed by rubber to glass transitions that can be generated by cooling or drying processes applied to many amorphous compounds. These transitions signify the behavioural change of a carbohydrate from a viscous liquid-like material to a vitreous solid-like state [29]. In theory, the molecular mobility in glassy state systems is many orders of magnitude lower than in liquid systems [30] and this facilitates the stabilisation of delicate biological structures within glasses.

The focus of this study was to investigate the feasibility of using a low temperature processing method to produce biodegradable MNs from sugar glasses, to demonstrate that they have sufficient physical strength for skin puncture, proffer improved stability of a model protein and are able to deposit an incorporated model compound into skin through biodegradation.

2. Materials and methods

2.1. Materials

All reagents were obtained from Fisher Scientific Ltd. (Loughborough, UK) and were of analytical grade unless stated otherwise.

Master silicon MN arrays used in this study were fabricated by the Microsystems Centre, Tyndall National Institute, University College Cork, Ireland using a previously reported wet-etching process and subsequent coating with a 0.3 μm layer of platinum [11]. The master MN structures were octagonal pyramid in morphology being approximately 250 μm in length and 200 μm at base width.

2.2. Methods

2.2.1. Preparation of sugar glasses

Dehydrated sugar formulations were prepared using trehalose anhydrous (TRA), trehalose dihydrate (TRD), sucrose (SUC), maltose (MAL), mannitol (MAN) and xylitol (XYL). Four hundred milligrams of sugar (either individual sugars or binary mixtures) was dissolved in 2 mL of deionised water to give a 16.7% w/v solution. These solutions were added to 100 mL beakers and allowed to dehydrate in a fume cupboard, flow rate 0.53 m/s, at room temperature (RT) for 24 h followed by 24 h at 50 °C.

2.2.2. Preparation and scanning electron microscopy of sugar glass films

Polydimethylsiloxane (PDMS) pre-polymer (Sylgard 184 silicone; RW Greef, Glasgow) and catalyst were combined in a 10:1 ratio, mixed and degassed for 30 min under 900 mbar vacuum at RT. A PDMS mould of a glass slide was prepared by covering the slide with PDMS solution, degassing under vacuum (RT 30 min 900 mbar), and curing at 100 °C for 1 h. This formed a PDMS well of approximately 1 × 25 × 75 mm into which sugar solutions were pipetted and dehydrated for 48 h to form sheets of sugar glass. Samples were stored under vacuum desiccation before analysis. The samples were manually sectioned transversely and sputter coated with gold prior to visualisation using scanning electron microscopy (SEM; Philips XL-20, Philips, Eindhoven, The Netherlands).

2.2.3. Thermal characterisation of sugars

Unprocessed sugars and solid sugar films of 100% TRA, 100% SUC, TRA/SUC 75:25% and TRD/SUC 75:25% w/w (prepared as described in Section 2.2.2) were analysed by differential scanning calorimetry (DSC; Perkin-Elmer Series 7). Samples (approximately 10 mg) in crimped aluminium pans were heated between 20 and 220 °C at a rate of 10 °C min^{-1}. Samples of 5 mg were further analysed by thermogravimetric analysis (TGA; Perkin-Elmer Series 7) in a platinum pan between 20 and 220 °C at a heating rate of 10 °C min^{-1}.

2.2.4. Determination of residual water content of sugar glasses

Three sugar solutions, (TRA/SUC 75:25% w/w, TRD/SUC 75:25% w/w, MAL/TRA 75:25% w/w) were dehydrated for 48 h (as described in Section 2.2.1). Following the initial 48 h of drying, samples were maintained at 50 °C under ambient humidity. Thereafter samples were placed under ambient temperature and humidity conditions and stored up to 360 h. Sample weight was recorded throughout the dehydration step, at the end of the raised temperature storage and throughout storage under ambient conditions. Residual water content was inferred by subtracting the initial powder mass from sample weight.

2.2.5. Assessment of macromolecule stability within sugar glasses

A 16.7% w/v solution of TRA/SUC (75:25% w/w) was prepared by dissolving the sugars in 1 mL sodium phosphate buffer (PB). β-Galactosidase enzyme (β-gal; Sigma-Aldrich, Poole, UK) was added to a final concentration of 5 IU/mL. To form sugar glasses, 200 μL samples of solution were dehydrated, as described in Section 2.2.1, within 24-well polystyrene plates. Following dehydration, samples were re-hydrated with 200 μL deionised water and left for 10 min to dissolve. Enzyme was quantified by adding 100 μL of sample to a reaction vessel containing 100 μL 2-nitrophenyl β-D-galactopyranoside (ONPG) substrate, equilibrated to 37 °C, and incubated at 37 °C for 90 min. The reaction was stopped with 1 M sodium carbonate solution and samples were analysed by a UV spectrophotometer (Fluostar Optima™, BMG Labtech, Aylesbury, UK), with absorbance at 405 nm. Further samples were stored under vacuum desiccation at 20 ± 2 °C or desiccation at 4 ± 2 °C for up to 3 months. Samples were re-hydrated as stated previously and residual enzyme activity was determined at 7, 35 and 95 days following sugar glass formation. A one-way ANOVA with Bonferroni's multiple comparison post hoc test was performed on the experimental data using the GraphPad Prism 5 software package. In all cases, statistical significance was determined by a value of $p < 0.05$.

2.2.6. Polydimethylsiloxane micromoulding

PDMS micromoulds were created from master silicon MNs. PDMS was added to a well containing the master array, prior to degassing for 30 min and curing (Section 2.2.2) to form the mould. The master array was subsequently removed to yield the MN mould.

2.2.7. Fabrication of sugar glass MNs incorporating powdered methylene blue

2.2.7.1. Standard deposition method. A 16.7% w/v solution of TRA/SUC 75:25 w/w was prepared as in Section 2.2.1. Methylene blue (MB) powder was incorporated at 5% w/w of final sugar glass weight. Two hundred microlitres of a sugar solution containing 5% w/w MB was pipetted onto the surface of a micromould and viewed by a digital camera, (Nikon, Coolpix 5600, Japan), and a light microscope (Olympus BH-2, Japan). The micromould was then placed into a vacuum oven at 300 mbar for 60 min to form MNs. The solution was dehydrated (Section 2.2.1) with the mould being viewed with time to show MN formation. Once formed, sugar glass arrays were removed by hand and stored in a vacuum desiccator at room temperature.

2.2.7.2. Vacuum deposition method. Sugar glass MNs containing 2% w/w MB were fabricated using an improved vacuum-loading methodology. A micromould was placed into a 100 mL conical

vacuum flask. The flask was sealed and held under a vacuum of approximately 100 mbar for 30 min. Two hundred microlitres of a 20% w/v solution of TRA/SUC 75:25 w/w was injected onto the mould surface and the vacuum was then released immediately. The micromould was removed from the vacuum chamber and dehydrated as described in Section 2.2.1. Once formed, sugar glass arrays were removed by hand and stored in a vacuum desiccator at RT.

2.2.8. Scanning electron microscopy of sugar glass MN arrays

SEM was used to characterise the shape and morphology of sugar glass MN arrays. The arrays were mounted onto aluminium stubs, sputter coated with gold and imaged as in Section 2.2.2.

2.2.9. Sugar glass MN penetration of human skin

Human breast skin was obtained from surgical procedures under ethical approval and informed patient consent. A previously frozen full-thickness skin sample was defrosted for 60 min. Subcutaneous fat was removed by blunt dissection and the sample pinned onto a semicircular cork board. The skin surface was patted dry with tissue paper. Sugar glass MN arrays (not loaded with any model compounds) and silicon MN arrays were mounted onto flattened 2.0 mL syringe plungers using double-sided adhesive tape. Plungers were applied to the skin in a rolling fashion with downward pressure being applied for 10 s and the array being rolled off in the same direction as the application. Following application, the MNs were viewed under light microscopy (Zeiss Stemi 2000-C, Hertfordshire, UK) to observe structural integrity. Ten microlitres of a 2% w/v MB staining solution was pipetted onto the treated skin area and left to air dry for 10 min. Excess dye was removed with tissue paper soaked in ethanol prior to viewing under light microscopy.

2.2.10. Human skin sectioning and staining

Samples of MN treated skin were mounted transversely onto cork sections and covered with OCT embedding media (RA Lamb, Thermo Fisher Scientific) before snap freezing in hexane and storage at − 80 °C. Skin samples removed from the freezer were maintained on dry ice before cryosectioning (Leica CM3050s, Wolf Laboratories Limited). Sections (10 μm) were mounted onto glass slides, rinsed in phosphate buffered saline and fixed in acetone. Slides were stained with eosin and counterstained with hematoxylin, rapidly dehydrated in an ethanol gradient and then xylene before permanently mounting in Histomount (National Diagnostics, GA, USA).

2.2.11. Measurement of transepidermal water loss (TEWL)

TEWL readings were taken immediately prior to and following MN array application to skin using a Dermalab® open chamber TEWL apparatus (Cortex Technology, Smedevaenget, DK). A one-way ANOVA with Dunnett's multiple comparison post hoc test was performed on the experimental data using the GraphPad Prism 5 software package. In all cases, statistical significance was determined by a value of p b 0.05.

2.2.12. Dissolution of sugar glass MNs in situ

Ex vivo human skin was defrosted and prepared as in Section 2.2.9. Sugar glass MN arrays containing 2% w/w MB powder were mounted onto syringe barrels and rolled onto the skin. The plunger was pressed down for 10 s before being secured in place with adhesive plaster (Fastaid, Robinson Healthcare, Nottinghamshire, UK). The arrays were left in situ, under ambient conditions, for time periods up to 5 h before removal. Arrays were viewed before and after application under a light microscope (Olympus BH-2, Japan). Residual MB was removed (Section 2.2.9) prior to visualisation of the skin under light microscopy.

3. Results

3.1. Sugar glass fabrication

Solutions of individual sugars and sugar alcohols, and binary combinations of these, were dehydrated to determine those that formed solid sugar glasses and those that crystallised. Table S1 provides a full list of the 32 different sugar formulations investigated and the nature of the products formed following dehydration. Each of the solutions containing single sugars crystallised upon dehydration; Fig. 1A shows the crystalline nature of dehydrated sucrose as an example. Certain combinations of sugars and sugar alcohols also crystallised upon dehydration; Fig. 1B shows one such example (TRA/MAN 50:50% w/w). Where a sugar combination consisted of two sugar molecules of approximately the same molecular weight however, for example two disaccharides, a stable solid sugar glass could be formed at certain composite ratios; for example TRD/SUC 75:25% w/w (Table S1), TRA/SUC 75:25% w/w Fig. 1C and TRA/SUC 50:50% w/w Fig. 1D. It was speculated that sugar combinations containing molecules of different relative molecular sizes did not interact during dehydration and therefore co-crystallised. Sugar combinations containing xylitol did not form a stable solid product by the end of the dehydration period, this behaviour being attributed to the hygroscopic nature and extremely low glass transition temperature (Tg) of xylitol, 247 K, making the glass unstable at RT.

To support the data obtained in Fig. 1 the solid sugar products were further examined using SEM. Transverse sections of the solid mass formed from dehydrated single sugars suggested an ordered structure of crystalline nature (Fig. 1E, F). SEM images of transverse sections of sugar solid formed from combinations of sugars shown to form a non-crystalline mass, e.g. TRA/SUC 75:25% w/w (Fig. 1G), provided no evidence of order. It was not clear whether the material formed by the sugar combination was less ordered through its amorphous nature or was more prone to melting under the electron beam. Nevertheless, these data suggest the utility of this simple dehydration methodology to form sugar glasses from selected sugar combination solutions.

3.2. Thermal characterisation of sugars

Individual sugars and promising sugar glass forming combinations were further analysed by DSC and TGA. The DSC scan of a 100% TRA dehydrated film is characterised by two sharp endotherms with peaks at 101 and 214 °C with a third more poorly defined

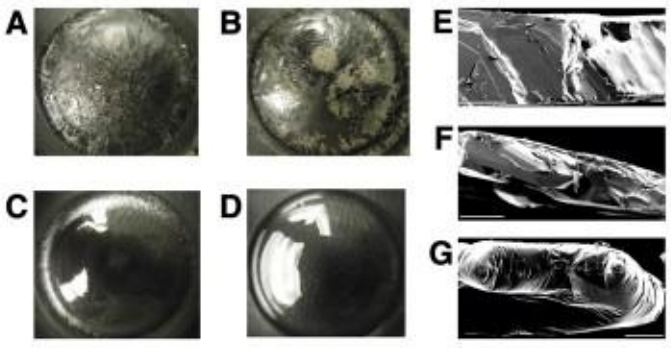

Fig. 1. Images of dehydrated solid sugar products. Macro photographic images of sugars following dehydration. (A) D (+) - sucrose (SUC) 100%, (B) D (+) - trehalose dihydrate (TRD) / D-mannitol (MAN) 50:50% w/w, (C) D-trehalose anhydrous (TRA) / SUC 75:25% w/w, (D) TRA / SUC 50:50% w/w. Scanning electron micrographs of transverse sections of dehydrated sugar films: (E) TRA 100%, (F) SUC 100%, (G) TRA/SUC 75:25% w/w (Bar = 500 μm).

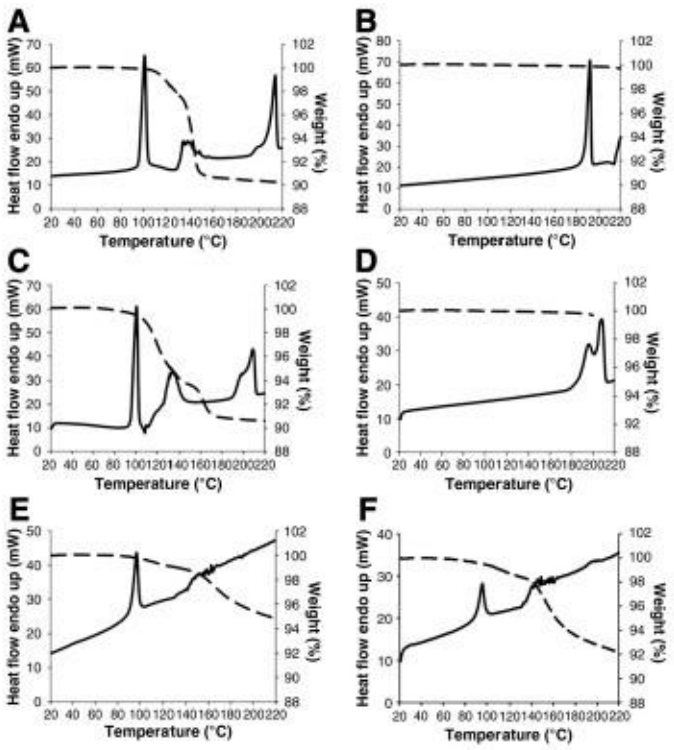

Fig. 2. Thermal characterisation of solid sugar films. Differential scanning calorimetry (DSC; solid line) and thermogravimetric analysis (TGA; dashed line) profiles of unprocessed and dehydrated sugars. (A) 100% TRA dehydrated sugar film, (B) 100% SUC dehydrated sugar film, (C) unprocessed TRD powder, (D) unprocessed TRA powder, (E) TRA/SUC 75:25% w/w (F) TRD/SUC 75:25% w/w dehydrated sugar film. Unprocessed powders were analysed once and dehydrated sugar films were analysed in triplicate. Representative thermograms are shown.

endothermic region between 130 and 150 °C (Fig. 2A). The weight loss profile with temperature (TGA) for the same material is superimposed in Fig. 2A and shows a total weight loss of approximately 10% w/w over the heating range. This water loss was greatest over the temperature range 90–140 °C and hence the endothermic peaks observed over this range correspond to dehydration of the dihydrate crystal. This suggests that the hydrated form of the sugar was formed during the process and that residual water remained within the glass following dehydration.

Fig. 2C and D show the DSC and TGA scans of unprocessed TRD and TRA powder respectively. Unprocessed TRA (Fig. 2D) shows a distinctly different thermal profile to the dehydrated TRA film (Fig. 2A), showing only a single melting endotherm at approximately 200 °C, corresponding to melting of the trehalose crystal. No weight loss was observed through the temperature range, indicating that no water was present in the sample. Fig. 2C however, displays endothermic peaks and respective weight losses at approximately the same temperatures as the dehydrated TRA film, further indicating that TRD was formed following dehydration of aqueous TRA solution. The thermal profile of 100% SUC dehydrated film (Fig. 2B) suggests no residual water content as demonstrated by the single endothermic peak observed at 191 °C attributed to melting of pure SUC crystal, and no evidence of weight loss. Fig. 2E shows DSC and TGA scans of a TRA/SUC 75:25% w/w dehydrated film. This film appeared to have a more complex nature than the individual sugar films. A sharp endothermic peak was observed at 97 °C, corresponding with the loss of water from the sample, but no other discrete thermal events were observed. A poorly defined endothermic region was shown between 130 and 170 °C and a gradual weight loss of the sample was observed from approximately 80 to 220 °C. The thermal behaviour of the TRD/SUC 75:25% w/w dehydrated film (Fig. 2F) was shown to be very similar to the TRA/SUC 75:25% w/w dehydrated film (Fig. 2E), supporting the similar apparent nature of the dehydrated products (Table S1). In replicate samples, the endothermic peak at 97 °C was not always observed (data not shown), correlating with the duration of storage under desiccation following formation of the glass. However, the key feature in all replicate samples was the absence of endothermic peaks at elevated temperatures indicating that the samples were non-crystalline in nature.

3.3. Determination of residual water content in sugar glasses

The degree of residual water content in dehydrated samples was further explored by measuring the sample weight of three binary sugar combinations following initial dehydration over 48 h to form solid glasses. Fig. 3 depicts the change in water content of three different sugar solutions with dehydration time. For all sugar solutions the majority of water loss occurred during the first 24 h. A further 24 h of dehydration at elevated temperature removed the remaining water to leave a solid glass. The TRA/SUC 75:25% w/w sugar glass retained approximately 9% w/w water in its structure at 48 h. The reason why this value appears higher than the TRD/SUC 75:25% w/w sample relates to the fact that there was no bound water in TRA powder at the beginning of the study. The MAL/TRA 75:25% w/w sample contained less TRA and therefore retained less water.

The weight of all of the sugar glasses decreased slightly between 48 and 192 h whilst maintained at 50 °C (Fig. 3). However, following re-introduction into ambient conditions, the weight of each of the sugar glasses increased marginally, returning to the levels observed at 48 h. This was expected as sugar glasses have a hygroscopic nature [31].

3.4. Assessment of macromolecule stability within sugar glasses

To investigate whether a heat-labile macromolecule could be loaded into a solid sugar glass using the novel methodology, a model protein macromolecule, β-galactosidase (β-gal) enzyme, was incorporated into dehydrated TRA/SUC (75:25% w/w) sugar glasses. Fig. 4 shows that whilst β-gal enzyme activity diminished over the

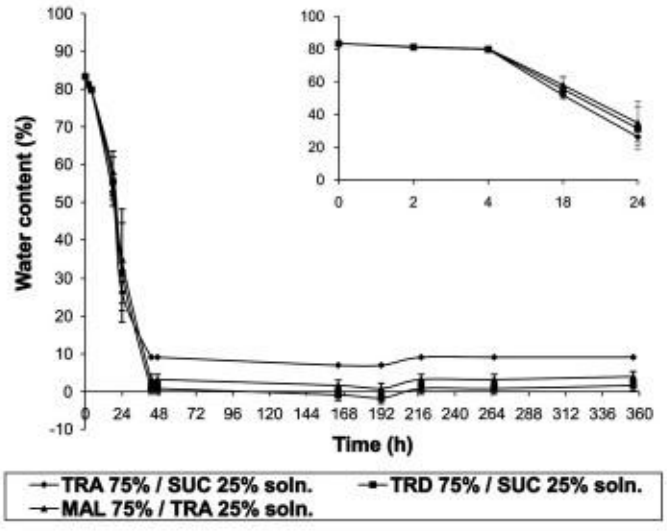

Fig. 3. Analysis of water content in sugar solutions. Sugar solutions were dehydrated at ambient temperature for 24 h then at 50 °C until 192 h. After 192 h solid sugar glasses were maintained under ambient conditions until 356 h. Changes in sample weight upon dehydration and storage were used to determine water content. Data represented as mean ± SD (n = 3).

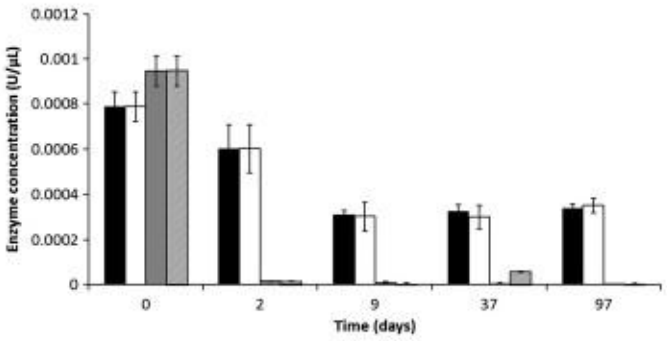

Fig. 4. Assessment of biomolecule stability within sugar glasses. β-galactosidase enzyme was incorporated within solid sugar glasses (black and white bars) or dehydrated PB only (grey and stripped bars) as a control. Samples were stored under vacuum desiccation at 20 ± 2 °C (white and stripped bars) or desiccation at 4 ± 2 °C (black and grey bars) for a period of 3 months. Residual enzyme activity was quantified at time points by 2-nitrophenyl β-D-galactopyranoside assay. Data represented as mean ± SD (n = 3).

first week of storage the activity was significantly (p b 0.0001) higher when the enzyme was stored within a sugar glass matrix when compared to storage in PB alone. Whilst the enzyme was almost completely denatured following dehydration in PB alone, enzyme activity was retained above 40% for over 3 months storage under vacuum or refridgeration.

As a result of these initial characterisation studies the TRA/SUC 75:25% w/w sugar combination was selected for microneedle fabrication studies. This material was chosen on the basis of reliable and reproducible non-crystalline sugar glass formation and partial stabilisation of a model protein cargo.

3.5. Polydimethylsiloxane micromoulding and fabrication of sugar glass MNs

The SEM in Fig. 5A shows a silicon master array prepared at Tyndall National Institute by wet-etch fabrication. A single silicon MN is shown in Fig. 5B displaying the octagonal pyramidal geometry of the master structure with base width of approximately 200 µm and needle length of approximately 250 µm. To form a micromould, prepolymerised PDMS was poured over the surface of the MN array. Due to the low surface tension of the polymer [32] it easily conformed to the high aspect ratio structure of the master arrays producing an inverse mould of the master array that had a strong correlation to the geometry of the master array; an example of a single channel created within the cured PDMS micromould being shown in Fig. 5D.

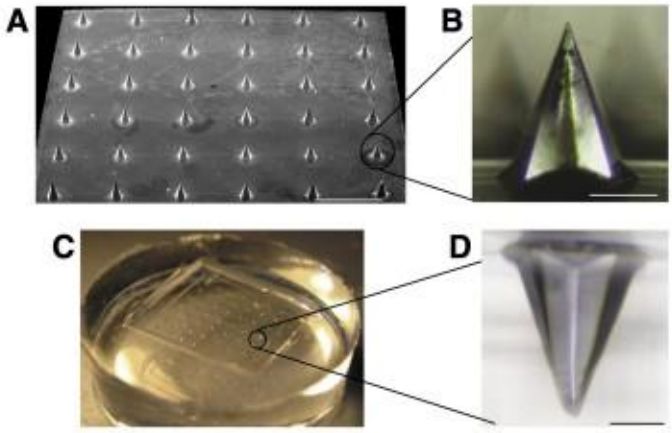

Fig. 5. Micromoulding silicon MN templates. Polydimethylsiloxane (PDMS) micromoulds were prepared against a master silicon MN array, fabricated by collaborators at Tyndall National Institute, Ireland. (A) Scanning electron micrograph of master silicon MN array following micromoulding (Bar = 1 mm), (B) light photomicrograph of an individual silicon MN (Bar = 100 µm), (C) PDMS micromould and (D) light photomicrograph of a transverse section through the micromould showing an individual mould channel (Bar = 100 µm).

The initial stages involved in sugar glass MN manufacture were studied using MNs incorporating methylene blue dye and created using the simple methodology described in Section 2.2.7.1. When the sugar solution was placed onto the mould it initially remained on the mould surface forming a large droplet with a high contact angle (Fig. 6A). None of the micromould invaginations contained any solution at this stage, which would be expected as PDMS is a hydrophobic material and the sugar solution is hydrophilic. After the moulds had been placed under vacuum for 1 h however, the sugar solution was observed to have filled the micromould invaginations (Fig. 6B). The height and contact angle of the solution droplet had also decreased following vacuum exposure. It is apparent from Fig. 6B that not all of the PDMS micromould invaginations were filled with sugar solution (black arrow) at this stage. After 48 h dehydration however the sugar glass material appeared to have filled the micromould entirely as confirmed by light microscopy (Fig. 6C).

To confirm successful formation of sugar glass MNs, the newly formed MN arrays were removed from the PDMS moulds and individual MNs viewed by light microscopy. Fig. 6D shows that sugar glass MNs that were fully formed had a strong morphological correlation to the master structure, as shown in Fig. 5B. However, in this first prototype only 22 sugar glass MNs were exact replicas of the 36 silicon MN master needles with the remainder being incompletely formed (Fig. 6E). In subsequent studies (at least 6 repeats were performed) the number of completely formed sugar glass MNs varied widely and it was never possible to produce a complete array of 36 needles. Whilst it was unknown at this stage whether the MNs were incompletely formed in the mould or damaged upon removal from the mould, the processing method was clearly sub-optimal.

3.6. Optimised fabrication of sugar glass MN arrays

To overcome the deficiencies in formation of a complete biodegradable sugar glass MN array a novel vacuum-forming methodology was developed (Fig. 7). In the original vacuum oven method (Section 2.2.7.1) vacuum pressure could not be applied before the sugar solution was placed on the mould surface. Subsequently when the droplet of sugar solution was applied air was entrapped within the micromould invaginations. An optimised method (Section 2.2.7.2) was developed whereby a vacuum was produced within an enclosed chamber before the sugar solution was applied to the mould surface (Fig. 7).

As a corollary no air was entrapped within the micromould during application of the sugar solution. The individual sugar glass MNs formed using this improved methodology (Fig. 8A) had an identical morphological fidelity to the master structure (Fig. 5B). More importantly this process development enabled the precise fabrication of a complete sugar glass MN array, i.e. 36 out of 36 replicate structures (Fig. 8B). As we used the same procedure to extract the microneedles from the PDMS mould this suggests that the incompletely formed microneedles produced using the previous fabrication process (Fig. 6E) were as a result of incomplete filling of the mould rather than fracture of the microneedle upon removal from the mould. Replicate studies (at least 6 repeats) have showed this revised process to be reliable in forming sugar glass MN arrays of 36 needles that do not contain any entrapped air. Sugar glass MNs fabricated using this novel vacuum-forming methodology were used in all subsequent studies.

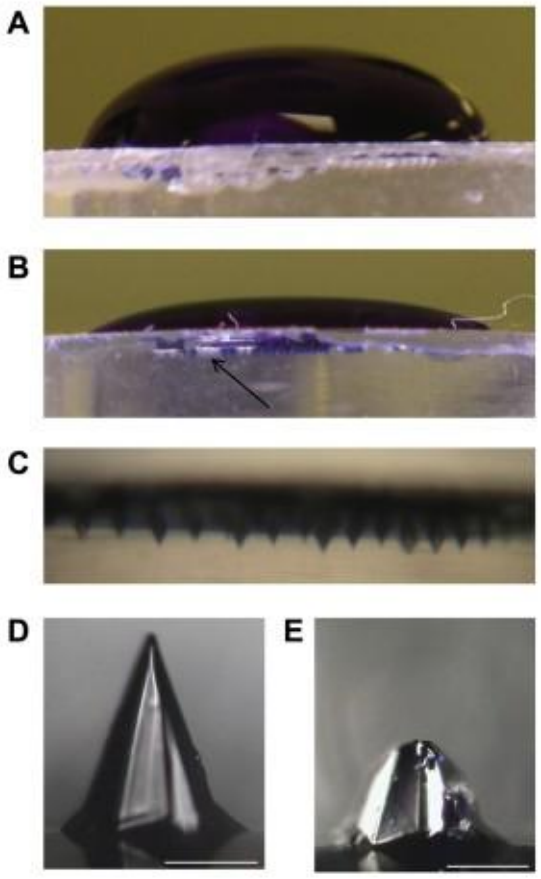

Fig. 6. Initial process of sugar glass MN fabrication. Macro images of a PDMS micromould showing (A) sugar solution containing 5% w/w methylene blue powder on mould surface (prior to vacuum), (B) mould following processing under 300 mBar vacuum for 60 min (arrow indicates empty mould invaginations), (C) light photomicrograph of a sugar glass MN array within the micromould following 48 h dehydration. (D) and (E) representative light photomicrographs of two 'MNs' formed by this process (Bar = 100 μm).

3.7. Human skin penetration study

To investigate the structural rigidity and skin puncture performance of sugar glass MNs the arrays were inserted into excised human skin obtained from surgical procedures. Methylene blue post-staining of the punctures generated in skin following MN array application for 10 s showed that sugar glass MNs (Fig. 9B) appeared to puncture human skin with the same efficacy as silicon MNs (Fig. 9A). Transverse skin sections further confirmed that sugar glass MNs effectively punctured human SC to facilitate diffusion of methylene blue dye, applied post-application, into the epidermal layer (Fig. 9D) in a manner analogous to silicon MNs (Fig. 9C). Whilst the master silicon MNs were largely unaffected by the skin application process (Fig. 9E), sugar glass MNs were physically altered following 10 second insertion into human skin; Fig. 9F shows a representative sugar glass MN following skin application.

Skin puncture performance was further assessed by measurement of transepidermal water loss (TEWL) from skin following MN application. TEWL data confirmed that human skin insertion of both silicon and sugar glass MNs significantly ($p < 0.05$) increased water loss over that of intact non-treated skin (Fig. 9G).

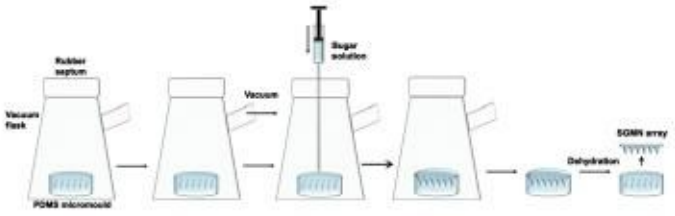

Fig. 7. Schematic of novel vacuum deposition methodology for sugar glass MN fabrication. A PDMS micromould was placed within a vacuum flask held under vacuum (approximately 100 mBar for 30 min). Sugar solution was injected through the septum onto the micromould surface. The vacuum was released immediately and the mould removed prior to dehydration at room temperature for 24 h followed by 24 h at 50 °C. SGMN = sugar glass MN array.

3.8. Dissolution kinetics of sugar glass MNs in skin

The sugar glass MNs were designed to dissolve rapidly and completely within skin to deposit the incorporated drug cargo. To test this, sugar MNs incorporating 2% w/w methylene blue powder were inserted into ex vivo human skin and left in situ for various time periods. Fig. 10 shows the dissolution status of the MNs, with complete dissolution being evident between 10 min (Fig. 10B) and 20 min (Fig. 10C) after skin insertion.

Sugar glass MNs were shown to penetrate the SC and to dissolve in situ (Fig. 10D). Fig. 10E and F show the degree of skin staining arising from dissolution of MNs containing methylene blue within the needle structure at 10 and 20 min respectively. These images generally support the dissolution kinetics detailed above and further confirm the utility of these MNs for creating microchannels within skin and releasing material incorporated within the matrix of the array.

4. Discussion

The aim of this work was to manufacture novel biodegradable sugar glass MNs for transdermal drug delivery. Glass forming sugars are used in nature to protect biological tissues in the dehydrated state [33]. These protective properties are exploited pharmaceutically to stabilise biological molecules including proteins [34,35], liposomes and lipoplexes [36,37] and viruses [38,39] during lyophilisation and subsequent product storage. It was therefore anticipated that sugar glass MNs may be advantageous for the incorporation of thermolabile macromolecular drugs within their matrices, our long-term aim.

A glass is an amorphous solid in which the molecules form a non-periodic and non-symmetric network as a result of rubber to glass phase transitions generated by cooling or drying processes [29]. This behaviour was exploited in this study to produce solid sugar glasses at low processing temperatures. Dehydration of solutions comprising a single sugar, namely trehalose anhydrous (TRA), trehalose dihydrate (TRD), sucrose (SUC), mannitol (MAN) and xylitol (XYL) did not result in the formation of sugar glasses. This was unsurprising given that crystallisation occurs when sugar solutions of pure sugars are evaporated slowly at low or ambient temperatures [40]. Calorimetric analysis suggested that dehydrated pure TRA films retained water from solution to form hydrated trehalose as demonstrated by the loss of approximately 10% w/w water between 100 and 150 °C and the endotherm at 100 °C in the DSC profile. We speculate that this water was bound to the trehalose molecule to form the dihydrate form of the sugar and hence that it would not adversely affect the stability of any incorporated medicaments. Following water loss, TRA showed a clear endotherm at approximately 214 °C, correlating with literature values for the melting point of the anhydrous trehalose crystal at 210.5 °C [41]. Dehydrated SUC alone was shown to recrystallise without incorporating water, as demonstrated by the single endothermic peak observed at 191 °C.

Dehydration of binary mixtures consisting of two sugar molecules of similar molecular weight, for example two disaccharides, appeared to result in sugar glass formation. Similar observations have been

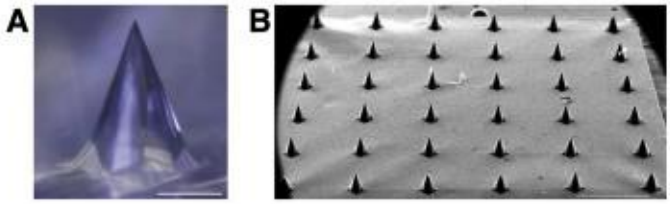

Fig. 8. Sugar glass MN array formed by the vacuum deposition method. (A) Light photomicrograph of an individual sugar glass MN (Bar = 100 μm), (B) scanning electron micrograph of entire sugar glass MN array (Bar = 1 mm).

noted by Wright et al. who reported that using a mixture of disaccharides circumvented crystallisation of sugar solutions evaporated slowly at low or ambient temperatures [40,42]. Whilst Wright et al. utilised 1/1 mixtures of trehalose and sucrose, in this study we found that 75:25% w/w combinations were better at forming sugar glasses. Calorimetry data demonstrated an absence of anhydrous crystalline melting endotherms for the TRA/SUC 75:25% w/w sugar glass with SEM images also reflecting the non-ordered nature of this material. We speculate that this phenomenon was due to the interaction between two different sugar molecules in solution to hinder the formation of individual sugar crystals during dehydration. Mixtures containing disaccharides and sugar alcohols failed to form sugar glasses under the same processing conditions. It was speculated that the low Tg of MAN and XYL, 303 and 247 K respectively, hindered the formation of a solid glass under these conditions. The Tg of these two sugar alcohols is close to ambient temperature and therefore sugar combinations containing these sugars will have lower Tgs [43] and hence are less likely to form a stable amorphous state under ambient conditions.

The presence of water can affect the chemical stability of solid protein formulations in at least three ways: (i) as a solvent, (ii) as a substrate in a reaction such as hydrolysis, and (iii) as a plasticiser, inducing a physical transition from a brittle, dynamically constrained glassy state to a more mobile, less viscous, rubbery state at the glass transition temperature [44]. The amount of water present in a sugar glass will therefore be a key determinant in governing thermodynamic properties and stability. Monitoring the weight of dehydrated samples suggests that TRA/SUC 75:25% w/w sugar glasses formed at low processing temperatures retain 9% w/w water. Previous studies showing that trehalose may associate with two molecules of water, which account for approximately 10% w/w of the crystal [45], supports this finding. Sugar glasses containing TRA increased in water content marginally upon storage under ambient conditions, which was expected as sugar glasses are known to have a hygroscopic nature [31], a factor that will require consideration when defining optimal packaging and storage requirements for sugar glass MNs.

A more detailed discussion of the macromolecular stabilisation capacity of this material will be discussed in a future paper; here we

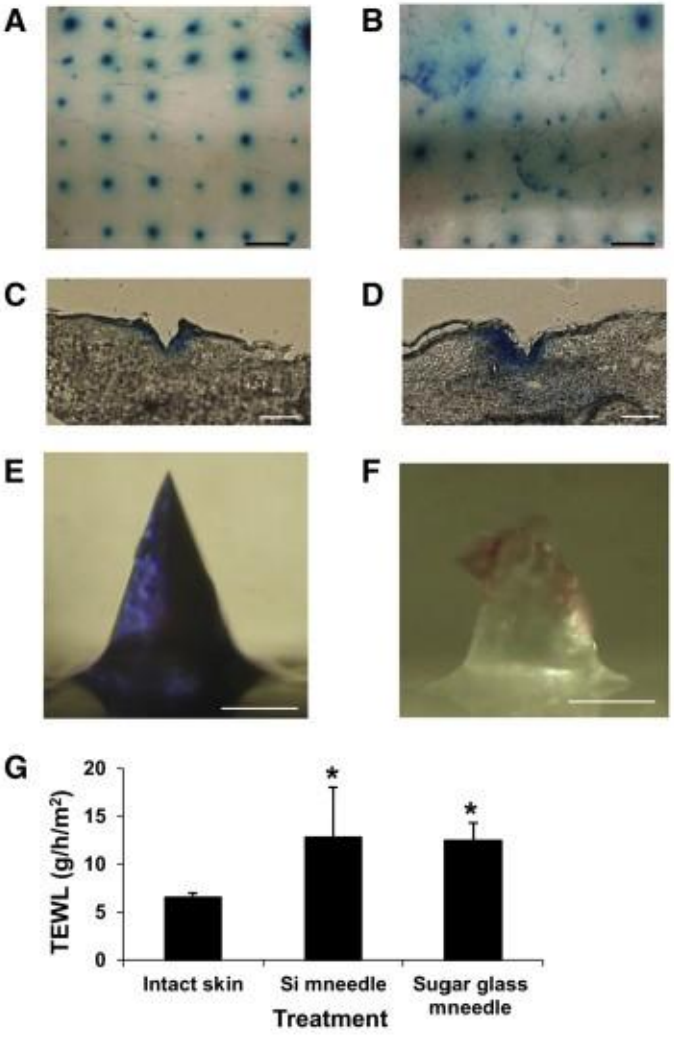

Fig. 9. Human skin penetration capability of sugar glass MNs. MNs were inserted into excised human skin and removed prior to staining with 2% w/v methylene blue dye. En face images of microchannels following insertion of (A) silicon and (B) sugar glass MN arrays (Bar = 1 mm). Light photomicrographs of transverse skin sections taken from skin shown in (A) (silicon MNs, panel C) and (B) (sugar glass MNs, panel D) respectively (Bar = 100 μm). Light photomicrographs of representative silicon (E) and sugar glass (F) MNs following rapid (10 seconds) skin insertion (Bar = 100 μm). (G) Trans-epidermal water loss (TEWL) measurement across human skin following microneedle treatment. Both sugar glass (n = 3) and silicon MN treatments (n = 4) were shown to significantly increase TEWL versus intact skin (n = 3). Data presented as mean ± SEM. * denotes statistical significance at p b 0.05.

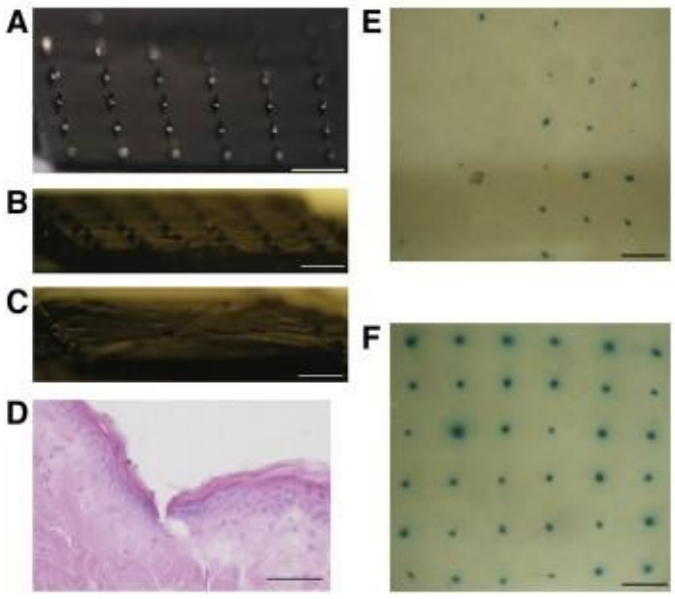

Fig. 10. In situ dissolution kinetics of sugar glass MNs incorporating 2% w/w methylene blue. Representative light photomicrographs of sugar glass MNs: (A) after formation, (B) following 10 min insertion into ex vivo human skin and (C) following 20 min insertion into ex vivo human skin (n = 4) (Bar = 1 mm). (D) 10 μm hematoxylin and eosin stained transverse tissue section of skin showing a single microneedle puncture site following 20 min insertion (Bar = 100 μm). En face images of skin after removal of sugar glass MNs incorporating dye at 10 min (E) and 20 min (F) insertion time (Bar = 1 mm).

have shown that biologically active protein can successfully be incorporated into sugar glasses and retain some activity throughout the SGMN production conditions and subsequent medium-term storage. Whilst the model enzyme was shown to initially lose some activity following dehydration of the sugar solution, enzyme activity remained 100% stable thereafter throughout 3 months of storage at both room temperature and 4 °C. Therefore whilst further optimisation of both the formulation components and the dehydration conditions may be required to reduce or abolish the initial adverse effects on the incorporated macromolecule the data suggests that macromolecules will be very well preserved once they are embedded with the fully formed sugar glass. As such this preliminary study provides early evidence that an amorphous sugar combination can offer protection to biological macromolecules and that such materials can be loaded into, stored within and thereafter delivered from, sugar glass MNs.

Our early studies showed that whilst a PDMS micromould can be created with precise morphological fidelity to master MN structures, sugar solutions did not completely fill the micromould invaginations due to the high surface tension of the solution, as demonstrated by the initial high contact angle of the solution on the mould surface. It was postulated that the applied vacuum was insufficient to release all of the air bubbles trapped beneath the solution, or the vacuum was not applied for a sufficient duration to evacuate all the air trapped within the micromould indentations. To improve filling of the micromould, a novel processing method was developed to maintain vacuum during loading of the sugar solution onto the mould. Following optimisation of processing conditions this new method was able to reproducibly fabricate complete arrays of 36 sugar glass MNs.

The resulting sugar glass MNs possess suitable structural rigidity and sharpness to efficiently penetrate the SC of human skin as demonstrated by external application of a marker dye following MN array insertion and removal. The sugar glass MNs were damaged or partially dissolved during this process rendering their re-use for skin puncturing purposes unlikely. More importantly, as these MNs are designed for in situ deposition of incorporated drug, a further study showed that the sugar glass MNs dissolved completely in human skin to efficiently release a model marker compound. It is anticipated that the MNs developed in this study will be appropriate for the stable incorporation of macromolecular drugs to enable rapid and painless delivery to human skin leaving behind no hazardous waste.

Previous studies that have developed MNs to dissolve or degrade in skin have generally focussed on melting polymers into a mould at temperatures that are potentially deleterious to the incorporated drug [16,6,20]. Another approach involves hand assembly of individual needles of millimetre dimensions [18], which could be a poorly controlled and non-scalable process [17]. The methodology we use to prepare novel sugar glass MNs in this study provides another alternative for making biodegradable microneedles at low temperatures and it is anticipated that such systems could be inexpensively produced on a mass scale as neither the materials nor the processing conditions are costly or complex. As the sugar glass MNs can be produced at a temperature of 50 °C and have been shown to partially preserve macromolecular enzyme functionality, it is speculated that the processing conditions would be favourable for the inclusion and preservation of a range of molecules and macromolecules, including proteins, peptides and nucleic acids, for intradermal and transdermal drug delivery applications.

5. Conclusion

This study has shown for the first time that sugar glass MNs can be fabricated from sugar combination solutions using a low temperature vacuum-forming methodology. The MNs possess suitable structural rigidity to effectively puncture human skin. The prompt and complete dissolution of sugar glass MNs within skin suggests that they may find utility in the transdermal delivery of potent therapeutics, potentially including hydrophilic macromolecules. Further studies, using therapeutically relevant molecules and macromolecules, are currently underway to improve the loading and stabilisation capacity of the sugar glass materials and the temporal and spatial distribution of delivered material.

Supplementary materials related to this article can be found online at doi:10.1016/j.jconrel.2011.10.024.

References

[1] K. Fukushima, A. Ise, H. Morita, R. Hasegawa, Y. Ito, N. Sugioka, K. Takada, Two-layered dissolving microneedles for percutaneous delivery of peptide/protein drugs in rats, Pharm. Res. 28 (1) (2011) 7–21.
[2] S.P. Sullivan, N. Murthy, M.R. Prausnitz, Minimally invasive protein delivery with rapidly dissolving polymer microneedles, Adv. Mater. 20 (5) (2008) 933–938.
[3] R.K. Sivamani, B. Stoeber, G.C. Wu, H. Zhai, D. Liepmann, H. Maibach, Clinical microneedle injection of methyl nicotinate: stratum corneum penetration, Skin Res. Technol. 11 (2) (2005) 152–156.
[4] D.V. McAllister, P.M. Wang, S.P. Davis, J.H. Park, P.J. Canatella, M.G. Allen, M.R. Prausnitz, Microfabricated needles for transdermal delivery of macromolecules and nanoparticles: fabrication methods and transport studies, Proc. Natl. Acad. Sci. U.S.A. 100 (24) (2003) 13755–13760.
[5] S.P. Davis, W. Martanto, M.G. Allen, M.R. Prausnitz, Hollow metal microneedles for insulin delivery to diabetic rats, IEEE Trans. Biomed. Eng. 52 (5) (2005) 909–915.
[6] J.H. Park, M.G. Allen, M.R. Prausnitz, Biodegradable polymer microneedles: fabrication, mechanics and transdermal drug delivery, J. Control. Release 104 (1) (2005) 51–66.
[7] M. Pearton, C. Allender, K. Brain, A. Anstey, C. Gateley, N. Wilke, A. Morrissey, J. Birchall, Gene delivery to the epidermal cells of human skin explants using microfabricated microneedles and hydrogel formulations, Pharm. Res. 25 (2) (2008) 407–416.
[8] F. Chabri, K. Bouris, T. Jones, D. Barrow, A. Hann, C. Allender, K. Brain, J. Birchall, Microfabricated silicon microneedles for nonviral cutaneous gene delivery, Br. J. Dermatol. 150 (5) (2004) 869–877.
[9] J.A. Mikszta, J.P. Dekker III, N.G. Harvey, C.H. Dean, J.M. Brittingham, J. Huang, V.J. Sullivan, B. Dyas, C.J. Roy, R.G. Ulrich, Microneedle-based intradermal delivery of the anthrax recombinant protective antigen vaccine, Infect. Immun. 74 (12) (2006) 6806–6810.
[10] S.P. Sullivan, D.G. Koutsonanos, M.d.P. Martin, J.W. Lee, V. Zarnitsyn, S.-O. Choi, N. Murthy, R.W. Compans, I. Skountzou, M.R. Prausnitz, Dissolving polymer microneedle patches for influenza vaccination, Nat. Med. 16 (2010) 915–920.
[11] N. Wilke, A. Mulcahy, S.R. Ye, A. Morrissey, Process optimization and characterization of silicon microneedles fabricated by wet etch technology, Microelectron. J. 36 (7) (2005) 650–656.
[12] W. Martanto, S.P. Davis, N.R. Holiday, J. Wang, H.S. Gill, M.R. Prausnitz, Transdermal delivery of insulin using microneedles in vivo, Pharm. Res. 21 (6) (2004) 947–952.
[13] G. Li, A. Badkar, H. Kalluri, A.K. Banga, Microchannels created by sugar and metal microneedles: characterization by microscopy, macromolecular flux and other techniques, J. Pharm. Sci. 99 (4) (2010) 1931–1941.
[14] P.M. Wang, M. Cornwell, J. Hill, M.R. Prausnitz, Precise microinjection into skin using hollow microneedles, J. Invest. Dermatol. 126 (5) (2006) 1080–1087.
[15] W. Martanto, J.S. Moore, O. Kashlan, R. Kamath, P.M. Wang, J.M. O'Neal, M.R. Prausnitz, Microinfusion using hollow microneedles, Pharm. Res. 23 (1) (2006) 104–113.
[16] J.H. Park, M.G. Allen, M.R. Prausnitz, Polymer microneedles for controlled-release drug delivery, Pharm. Res. 23 (5) (2006) 1008–1019.
[17] J.W. Lee, J.H. Park, M.R. Prausnitz, Dissolving microneedles for transdermal drug delivery, Biomaterials 29 (13) (2008) 2113–2124.
[18] Y. Ito, J. Yoshimitsu, K. Shiroyama, N. Sugioka, K. Takada, Self-dissolving microneedles for the percutaneous absorption of EPO in mice, J. Drug Target. 14 (5) (2006) 255–261.
[19] R.F. Donnelly, D.I.J. Morrow, T.R.R. Singh, K. Migalska, P.A. McCarron, C. O'Mahony, A.D. Woolfson, Processing difficulties and instability of carbohydrate microneedle arrays, Drug Dev. Ind. Pharm. 35 (10) (2009) 1242–1254.
[20] T. Miyano, Y. Tobinaga, T. Kanno, Y. Matsuzaki, H. Tkaeda, M. Wakui, K. Hanada, Sugar micro needles as transdermic drug delivery system, Biomed. Microdevices 7 (3) (2005) 185–188.
[21] G. Li, A. Badkar, S. Nema, C.S. Kolli, A.K. Banga, In vitro transdermal delivery of therapeutic antibodies using maltose microneedles, Int. J. Pharm. 368 (1–2) (2009) 109–115.
[22] N. Shibata, Y. Ito, K. Takada, Pharmacokinetics, Wiley-Interscience, MA, 2007.
[23] R. Langer, Drug delivery and targeting, Nature 392 (1998) 5–10.
[24] L.-G. Öst, Blood and injection phobia: background and cognitive, physiological, and behavioral variables, J. Abnorm. Psychol. 101 (1) (1992) 68–74.
[25] R.A. Kleinknecht, Acquisition of blood, injury, and needle fears and phobias, Behav. Res. Ther. 32 (8) (1994) 817–823.
[26] S.P. Davis, B.J. Landis, Z.H. Adams, M.G. Allen, M.R. Prausnitz, Insertion of microneedles into skin: measurement and prediction of insertion force and needle fracture force, J. Biomech. 37 (8) (2004) 1155–1163.
[27] J.R. Grigera, V. Bolzicco, Molecular mobility and ageing of sugar glasses, Food Chem. 106 (4) (2008) 1314–1317.

[28] A.E. Oliver, E.L. Kendall, M.C. Howland, B. Sanii, A.P. Shreve, A.N. Parikh, Protecting, patterning, and scaffolding supported lipid membranes using carbohydrate glasses, Lab Chip 8 (6) (2008) 892–897.
[29] C. van den Berg, I. van den Dries, M.A. Hemminga, Magnetic Resonance in Food Science, in: P.S. Belton, I. Delgadillo, A.M. Gil, G.A. Webb (Eds.), The Royal Society of Chemistry, Cambridge, UK, 1995, pp. 93–101.
[30] S.R. Elliott, Physics of Amorphous Materials, Longman Scientific & Technical, Harlow, Essex, 1990.
[31] J.H. Dittmar, Hygroscopicity of sugars and sugar mixtures, Ind. Eng. Chem. 27 (3) (1935) 333–335.
[32] R.-J. Roe, Surface tension of polymer liquids, J. Phys. Chem. 72 (6) (1968) 2013–2017.
[33] J.-A. Seo, S.J. Kim, H.-J. Kwon, Y.S. Yang, H.K. Kim, Y.-H. Hwang, The glass transition temperatures of sugar mixtures, Carbohydr. Res. 341 (15) (2006) 2516–2520.
[34] M. Uritani, M. Takai, K. Yoshinaga, Protective effect of disaccharides on restriction endonucleases during drying under vacuum, J. Biochem. 117 (4) (1995) 774–779.
[35] C. Schebor, L. Burin, M.P. Buera, J.M. Aguilera, J. Chirife, Glassy state and thermal inactivation of invertase and lactase in dried amorphous matrices, Biotechnol. Prog. 13 (6) (1997) 857–863.
[36] D.K. Hincha, E. Zuther, E.M. Hellwege, A.G. Heyer, Specific effects of fructo- and gluco-oligosaccharides in the preservation of liposomes during drying, Glycobiology 12 (2) (2002) 103–110.
[37] L.M. Crowe, J.H. Crowe, A. Rudolph, C. Womersley, L. Appel, Preservation of freeze-dried liposomes by trehalose, Arch. Biochem. Biophys. 242 (1) (1985) 240–247.
[38] R.M. Bieganski, A. Fowler, J.R. Morgan, M. Toner, Stabilization of active recombinant retroviruses in an amorphous dry state with trehalose, Biotechnol. Prog. 14 (4) (1998) 615–620.
[39] J.A. Levy, A.H. Fieldsteel, Freeze-drying is an effective method for preserving infectious type C retroviruses, J. Virol. Methods 5 (3–4) (1982) 165–171.
[40] W.W. Wright, J.C. Baez, J.M. Vanderkooi, Mixed trehalose/sucrose glasses used fo protein incorporation as studied by infrared and optical spectroscopy, Anal. Biochem. 307 (1) (2002) 167–172.
[41] T. Higashiyama, Novel functions and applications of trehalose, Pure Appl. Chem. 74 (7) (2002) 1263–1269.
[42] W.W. Wright, G.T. Guffanti, J.M. Vanderkooi, Protein in sugar films and in glycerol/water as examined by infrared spectroscopy and by the fluorescence and phosphorescence of tryptophan, Biophys. J. 85 (3) (2003) 1980–1995.
[43] J.F. Willart, N. Descamps, V. Caron, F. Capet, F. Danede, M. Descamps, Formation lactose–mannitol molecular alloys by solid state vitrification, Solid State Commun. 138 (4) (2006) 194–199.
[44] M.C. Lai, M.J. Hageman, R.L. Schowen, R.T. Borchardt, E.M. Topp, Chemical stabi peptides in polymers. 1. Effect of water on peptide deamidation in poly(vinyl alcohol) and poly(vinyl pyrrolidone) matrixes, J. Pharm. Sci. 88 (10) (1999) 1073–1080.
[45] L.S. Taylor, P. York, Characterization of the phase transitions of trehalose dihydrate on heating and subsequent dehydration, J. Pharm. Sci. 87 (3) (1998) 347–355.